

University of Nottingham
UK | CHINA | MALAYSIA

Evaluating and Improving Thermal and Energy Performance of 3D-Printed and Conventional Residential Buildings in Saudi Arabia

A Thesis submitted to the University of Nottingham in fulfilment for the degree of Doctor of Philosophy

July 2025

Khalid Abdulrauof A Mirza, B. Arch., MS in Sustainable Design

20261410

Supervisor: Dr Mohamed B Gadi

Department of Architecture and Built Environment, Faculty of Engineering

University of Nottingham



In the Name of Allah, the Most Gracious, the Most Merciful.

ABSTRACT

Saudi Arabia is one of the world's largest energy producers, with high rates of energy consumption and carbon emissions. The domestic demand for energy is on the rise despite governmental efforts to promote sustainability and improve energy efficiency. Among all sectors, the building and construction industry contributes significantly to this high demand, with approximately half of the KSA's electricity being consumed by residential buildings. Statistics suggest that about 65% of existing houses lack thermal insulation, leading to poor thermal performance and heavy reliance on active cooling systems, which account for 70% of total energy use. Given the severe local climate conditions, coupled with a fast-growing population (at an annual rate of 2.5%) and a corresponding surge in housing demand, improving the thermal performance of modern residential buildings is becoming increasingly urgent. This is particularly critical as modern construction technologies and materials, including large-scale 3-dimensional concrete construction techniques, are being adopted without evaluating their thermal performance and suitability for the local climate.

To foster sustainable development in KSA's residential sector, this study explores the thermal performance of contemporary dwellings. The study selected two distinct houses as case studies, each constructed with a different construction method: 3D concrete printing and conventional construction techniques. The investigation of these two cases helped determine the current performance of modern Saudi dwellings (both conventional and 3D printed) and identify parameters that require further improvements. Additionally, the study goes on to explore various solutions learned from vernacular architecture and modern sustainable building technology and to assess their effectiveness through simulations.

To assess the indoor thermal environment of the selected cases, two primary methods were used in this study: field monitoring and computer energy simulation. Field monitoring was conducted with specific scientific instruments used to monitor environmental parameters during the summer. For computer energy modelling and simulations, Integrated Environmental Solutions Virtual Environment computer simulation software was utilized. Findings from both methods were compared and analysed. The thermal performance of the simulated models was validated by comparing the predicted indoor temperatures against actual in-situ measurements for each house over the same period and under identical conditions, at hourly intervals.

Dynamic thermal simulations revealed that external heat gain through the building envelope was the most influential factor affecting the indoor thermal environment and cooling requirements. Upon identifying key areas of the building envelope for potential improvements, various improvement measures were proposed and simulated to enhance the buildings' thermal performance and reduce energy consumption and associated carbon emissions. From these simulations, a combination of the proposed measures was suggested to construct the improved model for each house.

The findings indicated that applying the proposed measures could reduce cooling load by up to 68.5% for the 3D-printed house and 57.7% for the conventionally constructed house. Furthermore, an additional 10% saving in cooling load is possible by allowing natural ventilation, resulting in a total savings of 77.5% and 67.4%, respectively. Consequently, this achieved a total reduction in electricity consumption and associated carbon emissions of 45.5% in the 3D-printed house and 34.1% in the conventionally constructed house, with annual electricity consumptions of 104.47 kWh/m^2 and 81.49 kWh/m^2, respectively. The study demonstrates that adopting simple design strategies can offer significant benefits to improve energy efficiency and thermal performance of KSA's residential buildings.

The study concludes that while the 3D-printed house demonstrated superior thermal behaviour in terms of inner surface temperatures and indoor thermal comfort hours, the conventional house achieved lower energy consumption per square meter. The research findings are based on two case studies in Riyadh that differ in design, construction methods, and urban context. Additionally, the simulations relied on simplified modelling of the 3D-printed walls, historical weather data, and typical occupancy and load profiles derived from older datasets, which may not fully reflect actual behaviour, operational patterns, or recent climate trends.

DECLARATION

I, the author, certify that this thesis titled '*Evaluating and Improving Thermal and Energy Performance of 3D-Printed and Conventional Residential Buildings in Saudi Arabia*' and the work presented in it are my own, except where otherwise stated; all sources of help have been acknowledged.

I confirm that this thesis is the result of my own work, which has been mainly undertaken during my period of registration for this degree at the University of Nottingham, and that it has not previously been submitted for a degree or any other qualification to this university or any other institution.

Signed: Khalid Abdulrauof A Mirza **Date:** 1 July 2025

DEDICATION

I dedicate this work to my dear aunt, Foziyah Kamal (may she rest in peace), who departed this world on 29 October 2022 (4 Rabi al-Thani 1444 AH), leaving a void that can never be filled. Though you are no longer with us, your presence continues to be felt in every precious, cherished memory you left behind. Dearly loved and sadly missed, your love and prayers remain a constant source of strength, and you will always be remembered and held close to my heart. May Allah grant you eternal peace and mercy, and may we be reunited with you in Jannat al-Firdaws, Ameen.

Your beloved nephew,
Khalid Abdulrauof A Mirza
1 July 2025

ACKNOWLEDGMENTS

First and foremost, I am always thankful to Allah for granting me the knowledge, strength, and health to undertake this work and enabling me to its completion. I bear witness that there is no true guidance but the guidance from Allah. *Alhamdulillah*.

I would like to express my deepest gratitude and sincere thanks to Dr. Mohamed Gadi, my main research supervisor, for his continuous support, stimulating suggestions, and generous guidance throughout my PhD journey at the University of Nottingham, with all its challenges. This thesis would not have been possible without Dr. Gadi's guidance, patience, and encouragement.

I am also grateful to Dr. Jie Zhu for his invaluable comments and insightful feedback during the first and second annual reviews. My sincere appreciation is further extended to my thesis examiners, Professor Li Show and Dr. John Calautit, for their time, thoughtful review, and constructive suggestions. Their critiques of my thesis were incredibly helpful and insightful and have significantly strengthened its quality and clarity.

I would also like to thank Daniel Serotsky for his kind assistance, continuous support, and for always being approachable and responsive whenever help, guidance, or advice was needed from the PGR office.

I am also thankful to my colleagues at the Building, Energy and Environment Research Group, especially Dr. Abdullah Bagasi, Dr. Azzam Alosaimi, Dr. Hiatham Alrasbi, Dr. Abdulaziz Alkelani, and Dr. Turki Alosaimi—who, at the time of preparing this thesis for final submission, had already completed their PhDs—for their valuable discussions, feedback, and shared knowledge. A special thanks to my colleagues: Ali Alzahrani, Anas Mahjoob, Amjad Alsawaf, and Hani Baeissa for their constant support and assistance throughout my academic journey.

I would like to express my appreciation to the Saudi Cultural Bureau (SACB) and the University of Umm Al-Qura for granting me the opportunity to pursue this PhD and for their financial support throughout this journey. Special thanks to Dr. Ibraheem Albukhari and Dr. Omar Osra for their support, concern, and flexible approach.

I also extend my gratitude to CyBe Construction, the Ministry of Housing, and the National Housing Company for their cooperation during the data collection processes. I am deeply

thankful to Mashaan Alotaibi and Fahad Alnassar for their invaluable assistance in providing access to the houses on which this study is based, ensuring smooth field data monitoring.

I would also like to acknowledge Scribendi for their professional proofreading services, which helped improve the clarity and presentation of this thesis. The content, interpretations, and conclusions presented here remain entirely my own.

Finally, and most importantly, I am deeply grateful to my family for their unfailing love, support, and encouragement: my wonderful parents (Abdulrauof Mirza and Faiqah Kamal), my great brothers (Dr. Ahmad Mirza and Dr. Abdulrahim Mirza), my beloved wife (Lujain Hafiz), and my lovely little queen (Elin), whose magical positive energy—felt in every hug and joyful presence—has kept me optimistic despite all challenges. No words can truly express my gratitude for their continuous support throughout my postgraduate studies in the USA and UK, and in my life in general.

TABLE OF CONTENTS

ABSTRACT ..... **ii**

DECLARATION ..... **iv**

DEDICATION ..... **v**

ACKNOWLEDGMENTS ..... **vi**

TABLE OF CONTENTS ..... **viii**

LIST OF FIGURES ..... **xiii**

LIST OF TABLES ..... **xxiv**

LIST OF EQUATIONS ..... **xxvi**

LIST OF ACRONYMS ..... **xxvii**

Chapter 1: INTRODUCTION AND RESEARCH JUSTIFICATION **2**

1.1 Introduction 2
1.2 Research problem 3
1.3 Aim and objectives 5
1.4 Research questions 5
1.5 Methodology 6
1.6 Novelty of the research 7
1.7 Thesis structure 7

Chapter 2: SAUDI ARABIA: BUILDING AND CLIMATE **12**

2.1 Introduction 12
2.2 Background of the Kingdom of Saudi Arabia 12
2.3 Climate of Saudi Arabia 13
2.4 Trends of energy and CO_2 emissions in Saudi Arabia 18
2.5 The construction and building sector in Saudi Arabia 21
2.6 Past and current buildings in Saudi Arabia 23
2.6.1 Traditional buildings in KSA 23
2.6.2 Contemporary buildings in Saudi Arabia 28
2.6.3 Conventional construction methods and materials in KSA: 29
2.6.4 Typologies of residential buildings in KSA 30
2.7 Initiatives and programs towards energy-efficient built environments 31
2.7.1 The Saudi Energy Efficiency Centre 32
2.7.2 Building code 33
2.8 SBC 602 for low-rise residential buildings 34
2.9 The Building Technology Stimulus Initiative 35
2.10 Summary 37

Chapter 3: ENVELOPE DESIGN AND THERMAL COMFORT **40**

3.1 Introduction 40
3.2 The building envelope 40
3.3 Thermal transmission and heat gain control 42

3.3.1 Solar heat gain....44
3.3.2 Solar reflectivity....48
3.3.3 Internal heat gain....49
3.3.4 Ventilation and infiltration gains....50
3.4 Thermal comfort....50
3.4.1 Thermal comfort factors and models (indices)....52
3.5 Passive cooling....60
3.5.1 Thermal mass....60
3.5.2 Natural ventilation....62
3.6 Research on thermal performance and energy efficiency measures....63
3.7 Summary....67

Chapter 4: DIGITAL FABRICATION IN THE CONSTRUCTION INDUSTRY....70
4.1 Introduction....70
4.2 Innovative technology in building design and construction....70
4.3 Digital fabrication of concrete....71
4.4 Categories of digital fabrication for concrete....72
4.4.1 Subtractive....72
4.4.2 Formative manufacturing....74
4.4.3 Additive manufacturing....75
4.5 Development of 3D concrete printing....76
4.6 Feasibility of 3D printing in the construction industry....78
4.6.1 Constructability benefits....79
4.6.2 Sustainability benefits....81
4.6.3 Examples of large-scale 3D-printed structures....81
4.7 3D printing of concrete and thermal performance....86
4.8 Summary....91

Chapter 5: RESEARCH METHODOLOGY....94
5.1 Introduction....94
5.2 The selected methodology and tools....94
5.3 Case study....95
5.3.1 The selection of Riyadh City....95
5.3.2 Local climate consideration in Riyadh....96
5.3.3 The selection of the case study buildings in Riyadh....99
5.3.4 Description of case studies....101
5.4 Field monitoring of building thermal performance....107
5.4.1 Selection of instruments....107
5.4.2 Limitations....110
5.5 Building energy simulation software....110
5.5.1 Integrated Environmental Solution-Virtual Environment (IES-VE)....113
5.6 Obtaining the weather data file for simulation....114
5.7 Energy model validation....115
5.8 Determining the baseline model....116
5.8.1 Operational schedules....116

5.8.2 HVAC system and cooling set point temperature....119
5.8.3 Power density and internal heat gain....119
5.9 Proposed enhancement measures....120
5.10 Summary....123

Chapter 6: INDOOR THERMAL ENVIRONMENT (MONITORED)....126
6.1 Introduction....126
6.2 Logger calibration....127
6.3 Placing the data loggers (setting up)....127
6.4 Data analysis....130
6.4.1 Outdoor measurements....130
6.4.2 Indoor field monitoring (steady state)....132
6.4.3 Investigating the potential of natural ventilation....136
6.5 Summary....141

Chapter 7: BUILDING MODEL DEVELOPMENT....144
7.1 Introduction....144
7.2 Constructing the energy model....144
7.2.1 Defining the buildings' geometry....144
7.2.2 Building envelopes and construction materials (thermal and physical properties)....146
7.2.3 Infiltration....148
7.2.4 Ground temperature....150
7.3 Model validation....153
7.4 Incident solar radiation rate....156
7.5 Summary....158

Chapter 8: ANALYSIS OF INDOOR THERMAL ENVIRONMENT USING COMPUTER SIMULATION SOFTWARE....160
8.1 Introduction....160
8.2 Indoor air temperature results....160
8.3 Heat gain through the building fabric....169
8.4 Cooling load....177
8.5 Baseline energy consumption and CO_2 emissions....180
8.6 Summary....184

Chapter 9: PARAMETRIC STUDY AND OPTIMIZATION USING ENERGY SIMULATION SOFTWARE....187
9.1 Introduction....187
9.2 External walls....188
9.2.1 Air temperature....189
9.2.2 Cooling load....193
9.2.3 Conclusion....194
9.3 Roof....195
9.3.1 Air temperature....195
9.3.2 Cooling load....201

9.3.3 Conclusion 202
9.4 Ground floor insulation 202
9.4.1 Air temperature 203
9.4.2 Cooling load 207
9.4.3 Conclusion 208
9.5 Air infiltration 208
9.5.1 Air temperature 209
9.5.2 Cooling load: 212
9.5.3 Conclusion 212
9.6 Window shading 213
9.6.1 External shading assessment 213
9.6.2 Applying the proposed shading devices to both case study buildings in Riyadh 219
9.7 Proposed combination of best building fabric alternatives 223
9.7.1 Indoor temperatures 223
9.7.2 Heat gain 227
9.7.3 Cooling load 228
9.7.4 Energy consumption and CO_2 emissions 231
9.8 Summary 234

Chapter 10: CONCLUSION 236
10.1 Introduction 236
10.2 Research conclusions 237
10.2.1 How can the performance of the selected cases be effectively simulated while ensuring that the predicted outcomes accurately reflect the actual physical conditions? 237
10.2.2 What are the current thermal performance and energy consumption rates for a 3D concrete house and a conventionally constructed house in the hot climate of Riyadh, KSA? 237
10.2.3 What is the role of the building envelope in improving the thermal behaviour of KSA's modern houses? 239
10.2.4 How can design strategies learned from vernacular architecture and modern sustainable building technology improve the thermal performance of residential buildings in Riyadh, KSA? 239
10.2.5 To what extent can applying the proposed passive strategies reduce cooling load (and associated energy consumption and CO_2 emissions) in a 3D-printed house and a conventionally constructed house in KSA? 241
10.3 Research key findings and implementation 242
10.4 Contributions to knowledge 245
10.5 Research limitations 246
10.6 Recommendations for future research 248
10.7 Summary 250

REFERENCES 252

APPENDICES 266

Appendix A 266
A-A: Research validation of energy simulation software for residential buildings in Riyadh 266
A-B: Specification sheet of data loggers 269
A-C: Hourly Tout in relation to comfort identified limits 272
A-D: Example of hourly air temperature measurements 272
Appendix B 273
B-A: Correlation between Ta and To in tested rooms 273
B-B: Summary of indoor air temperature predictions for selected zones in both case studies in Riyadh 274
B-C: A comparison between existing construction and uninsulated models 276
B-D: A comparison between predicted energy consumptions (EUI) and consumption reported consumptions in relevant literature 279
Appendix C 280
C-A: External wall options 280
C-B: Roof options 281
C-C: Ground floor options 282
C-D: Air infiltration 283
C-E: External shading analysis 284
C-F: Summary of tested improvement measures of the building fabric components 286
Appendix D 287
D-A: Air temperature results (baseline versus improved building fabric) 287
D-B: Heat gain analysis: Improved models VS Baselines 288
D-C: Monthly cooling load 289
D-D: Energy consumption predictions 291

LIST OF FIGURES

Figure 1-1 Electricity Consumption in the Kingdom of Saudi Arabia in 2020 by sector. Total energy consumed is 289,330 gigawatts per hour. Based on data from GAS (2023) and Statista (2022). 3
Figure 1-2 Summary of thesis procedures 7
Figure 1-3 Structural outline of the thesis 10
Figure 2-1 World Map of Koppen-Geiger Climate Classification. Note that the Gulf Region is located within the yellow classification of BWh (arid desert hot climate) (Kottek, Grieser, Beck, Rudolf, & Rubel, 2006). 14
Figure 2-2 The climatic zones of Saudi Arabia (Alrashed & Asif, 2015b). 14
Figure 2-3 Historical monthly air temperature averages for Saudi Arabia (2003–2023). Based on data from WorldData.info (2023). 15
Figure 2-4 Average annual daily solar radiation in Saudi Arabia (Baig, Sellami, Bahaidarah, & Mallick, 2013) 16
Figure 2-5 Historical monthly averages of relative humidity in Saudi Arabia (2003–2023). Based on data from WorldData.info (2023). 16
Figure 2-6 Climate zones of Saudi Arabia according to the energy conservation code. Adapted from SBC 602 (2018). 17
Figure 2-7 Per capita electricity consumption and total annual population in Saudi Arabia from 1990 to 2020. Data obtained from GAS (2023), Saudi Central Bank (2023), and The World Bank Group (2022a). 19
Figure 2-8 Per capita CO_2 emissions in Saudi Arabia compared with global trends between 1990 and 2019. Based on data from The World Bank Group (2023). 19
Figure 2-9 Sold electricity and peak load in KSA from 1990 to 2020. Data obtained from Saudi Central Bank (2023) and Saudi Electricity Company (2023). 20
Figure 2-10 Average electricity consumption distribution in KSA between 2015 and 2020. Based on data from Saudi Central Bank (2023). 20
Figure 2-11 Number of constructions permits in Saudi Arabia between 1990 and 2019. Based on data from GAS (2023). 22
Figure 2-12 The distribution of construction permits by building sector issued in 2019 in Saudi Arabia. Based on data from GAS (2023). 22
Figure 2-13 Illustrations of traditional dwellings in the Riyadh region: (A) A typical floor plan (Facey, 2015); (B) External view (HCDR, 2023). 25

Figure 2-14 Traditional buildings in the western region (Hariri-Rifai & Hariri-Rifai, 1990). 26
Figure 2-15 Traditional building features in the eastern region (Talib, 1984). 26
Figure 2-16 Different styles of traditional buildings in the southern region (Alobailan & Alawad, 2022; Talib, 1984). 27
Figure 2-17 Traditional buildings in Buraidah with small and protected openings on the external façade along with shaded, narrow streets (Talib, 1984). 28
Figure 2-18 Villa design introduced by ARAMCO and applied in the new housing development in Al-Malaz district, Riyadh: (A) External view; (B) Floor plan (Al-Hathloul, 1996). 28
Figure 2-19 Examples of residential buildings during the construction phase (images taken by author). 30
Figure 2-20 Housing types in Saudi Arabia. Based on data from GAS (2023). 30
Figure 2-21 Housing types in Riyadh City. Based on data from GAS (2023). 30
Figure 2-22 Example of energy efficiency label for household appliances (Abuhussain, 2020). 32
Figure 3-1 Representation of the heat balance equation (Parsons, 2014). 41
Figure 3-2 The time lag effect of a massive wall at various times of the day during the overheating season in hot and dry climates. Adapted from Lechner (2014). 43
Figure 3-3 Solar radiation received by envelope elements in Riyadh City, Saudi Arabia. Note that the preferred orientation is along the east and west axis to maximize northern and southern exposure. Reproduced from Autodesk Rivet (2022).....45
Figure 3-4 External shading devices and their shading masks. Adapted from Szokolay (2004). 47
Figure 3-5 Sources of heat gain in indoor environments. Adapted from Lechner (2014). 50
Figure 3-6 The comfort zone plotted on the psychrometric chart with different types of discomfort (Lechner, 2014). 52
Figure 3-7 PPD as a function of PMV (note that a minimum of 5% dissatisfaction is found under ideal conditions). Adapted from Auliciems and Szokolay (2007).....58
Figure 3-8 Applying thermal mass helps stabilize temperature fluctuations within a building across its diurnal cycle. Adapted from Saulles (2019). 61
Figure 4-1 The fabrication process of the Zollhof Tower's reinforced concrete panels using CNC-milled moulds: (A–B) CNC milling of the moulds; (C–D) Concrete casting into the moulds; (E) On-site assembly of the precast concrete panels. Adapted from Kolarevic (2005). 73

Figure 4-2 TialorCrete project by Gramazio Kohler Research at ETH Zurich: (A) Flexible mould; (B) Final concrete element with wax inlay. Adapted from Gramazio Kohler Research (2023). 74
Figure 4-3 The fabrication process of a free-form structure using a robotic slip-forming technique: (A) A square formwork that rotates as it moves vertically; (B) Applying a flexible formwork with four actuators. Adapted from Lloret-Fritschi (2016). 75
Figure 4-4 Illustration of concrete 3D printing process: (A) Preparing the digital model; (B) Slicing the model into layers; (C) Depositing the concrete layer by layer; (D) Final product. Adapted from Pessoa et al. (2021). 76
Figure 4-5 3D printing process of Contour Crafting. Adapted from Khoshnevis (2004)..... 77
Figure 4-6 Onsite 3D printing of insulating foam: (A) View of the successfully printed formwork; (B) Top view showing an open section of the form for the mobile robotic arm to enter and leave the construction site. Adapted from Keating (2016). 77
Figure 4-7 Images of the produced concrete slab: (A) On-site assembly; (B) Internal view after assembling the concrete slab segments (Meibodi et al., 2018). 78
Figure 4-8 Conventional construction process versus 3D concrete printing (Nithesh, 2018) . 79
Figure 4-9 A comparison between different construction methods: (A) Conventional construction; (B) 3D printing (Pessoa et al., 2021). 80
Figure 4-10 YhanovaTM house: (A) Wall cross-section; (B) External view of the 3D-printed house without coating; (C) The final finished product (Pessoa et al., 2021). 82
Figure 4-11 Apis Cor produced the first on-site 3D-printed house in Russia within 24 hours: (A) External view of the house; (B) Apis Cor 3D printer in action (Nithesh, 2018)..... 82
Figure 4-12 The world's first 3D-printed concrete office building by Winsun in Dubai: (A) View after construction (Camacho et al., 2018); (B) During on-site assembly (Ibrahim et al., 2022). 83
Figure 4-13 Apis Core printed the building using a robotic printer, which was moved around the site using a crane (Block, 2019). 84
Figure 4-14 3D-printed 6-story building by Winsun (Urbanist, 2023)..... 84
Figure 4-15 3D-printed house in Sharjah utilising the CyBe robotic arm (Ibrahim et al., 2022) 85
Figure 4-16 A 3-story residential building was fabricated on-site using COBOD's gantry-based 3D concrete printer (COBOD, 2022). 85

Figure 4-17 Examples of typical 3D-printed wall cross sections: (A) Luyten (Kelly, 2025); (B) Apis Cor (Harrouk, 2019); (C) COBOD (Aerts, 2025); (D) CyBe (CyBe Construction, 2023); (E) WinSun (E.Construct, 2016). 87
Figure 5-1 The overall methodological approach of this study 95
Figure 5-2 Monthly average temperatures for Riyadh based on 30-year historical data. Based on data from World Meteorological Organization (2022). 97
Figure 5-3 Relative humidity averages in Riyadh. Based on data from Weatherbase (2022). 97
Figure 5-4 Average precipitation in Riyadh. Based on data from World Meteorological Organization (2022). 97
Figure 5-5 Average daylengths in Riyadh. Based on data from Weather Atlas (2022). 98
Figure 5-6 Sun path diagram for Riyadh with summer and winter solstices (GAISMA, 2023). 98
Figure 5-7 Psychrometric chart for Riyadh showing that only 12% of the year falls within the predicted comfort zone (Plotted using Climate Consultant 6.0). 99
Figure 5-8 Aerial view of the case studies' location: (A) Map of Riyadh City; (B) Location of Case Study 1; (C) Location of Case Study 2. Adapted from Google (2023)..... 101
Figure 5-9 Photos of the 3D-printed house (Case Study 1) taken by the author: (A) South-west view; (B) North-east view 102
Figure 5-10 Construction process of the 3D-printed case study building: (A) Preparation of the foundation prior to concrete casting; (B) Layer-by-layer 3D-printed wall system with integrated structural steel and service conduits. Adapted from Consolidated Contractors Group (2018). 103
Figure 5-11 Floor plan of the house: As-built drawing produced using Autodesk Revit 2022 104
Figure 5-12 External view of Case Study 2 (photo taken by the author) 106
Figure 5-13 Floor plans of Case Study 2, produced using Autodesk Revit 2022 (highlighted selected rooms): (A) Ground floor layout; (B) First floor layout; (C) Upstairs annexe layout 106
Figure 5-14 Instruments employed during fieldwork 108
Figure 5-15 Summary of IES simulation process 114
Figure 5-16 Workflow for building energy modelling software. Adapted from Mahgoub and Saber (2022). 114

Figure 5-17 Typical daily profiles for occupancy, lighting, and equipment for the four main zones in Saudi dwellings: living, guests, kitchen, and sleeping. Adapted from Monawar (2001). 118
Figure 5-18 Illustration of overhang projection factor ratio. Created based on SBC-602 122
Figure 5-19 Proposed AC and window control scheme 123
Figure 6-1 Temperature data logger calibration 127
Figure 6-2 Installation process of the outdoor data logger with the protective screen 128
Figure 6-3 Locations of data loggers in selected zones in Case 1 (3D-printed house): (A) Selected rooms for analysis and measured parameters; (B) Images of the rooms after placing data loggers. 129
Figure 6-4 Locations of data loggers in Case 2: (A) Selected room in first floor (R1); (B) Selected room in upper floor (R2); (C) Images of the rooms after being equipped with data loggers. 129
Figure 6-5 (A) Readings of outdoor and indoor air temperatures for the selected rooms in Case 1 (3D-printed house) from 11–19 August 2022; (B) A truncated graph provides a clearer indication of the daily temperature profile. 132
Figure 6-6 Correlation between measurements of indoor air temperature (Ta) and globe temperature (Tg) for the three selected zones in Case 1: (A) Living room; (B) Bedroom; (C) Dining room 133
Figure 6-7 Highlighted measured surfaces orientation of the 3D-printed house 134
Figure 6-8 Surface temperatures of external walls on a typical summer day (19 August 2022): (A) External surface temperatures; (B) Internal surface temperatures 135
Figure 6-9 (A) Readings of indoor air temperatures for the selected rooms in Case 2 from 11–19 August 2022 in relation to the outdoor temperatures; (B) A truncated graph provides a clearer indication of the daily temperature profile. 136
Figure 6-10 Readings of outdoor and indoor air temperatures for bedroom and dining room on 21 August with daytime ventilation strategy (06:00 to 18:00). 138
Figure 6-11 Frequency of air velocity measurements for the bedroom on 21 August. 138
Figure 6-12 Correlation between Tg and Ta readings for the bedroom (with DTV strategy). 138
Figure 6-13 Readings of outdoor and indoor air temperatures for bedroom and dining room after employing NV (from 23 Aug at 06:00 to 24 Aug at 06:00). 139
Figure 6-14 Frequency of air velocity measurements for the dining room on 23 August. 140
Figure 6-15 Correlation between Tg and Ta readings for the dining room with NV. 140

Figure 6-16 Indoor air temperature readings from selected rooms in Case 2: (A) Data gathered on 18 August (with closed windows); (B) Data gathered on 22 August (with open windows). 141
Figure 7-1 The constructed IES models: (A) A 3D view of Case Study 1; (B) A 3D view of Case Study 2 145
Figure 7-2 Sensitivity analysis of air infiltration impacts on indoor air temperature 150
Figure 7-3 Sensitivity analysis of ground temperature impacts on indoor air temperatures for a typical summer day and a winter day in both case studies 151
Figure 7-4 Measured and predicted air temperature for selected rooms in the 3D-printed house (Case Study 1) from 13 August to17 August: (A) Bedroom; (B) Dining room. 153
Figure 7-5 Measured and predicted air temperatures for selected rooms in the conventional house (Case Study 2): (A) Room 1 (first floor); (B) Room 2 (top floor). 154
Figure 7-6 Incident solar radiation on external surfaces (in W/m^2) for both houses during a typical summer day and a winter day 157
Figure 8-1 Hourly simulation results for selected rooms in each house: (A) Predicted indoor air temperature frequencies for Case 1 and Case 2; (B) Predicted hourly indoor temperatures for both houses in Riyadh 161
Figure 8-2 Hourly Ta predictions for the selected rooms in Case 1 during a typical summer day and a typical winter day 164
Figure 8-3 Hourly Ta predictions for the selected rooms in Case 2 during a typical summer day and a typical winter day 164
Figure 8-4 Comparison of maximum, minimum, and mean indoor temperatures for selected rooms in both houses: (A) Simulation results for a typical summer day; (B) Simulation results for a typical winter day 165
Figure 8-5 Thermal comfort analysis for selected zones in Case 1 and Case 2 165
Figure 8-6 Assessing the impact of proposed natural ventilation strategies on improving the indoor thermal environments of selected rooms in Case 1 (3D-printed house) during a typical summer day. Note that results shown are before and after applying NV. 166
Figure 8-7 Assessing the impact of proposed natural ventilation strategies for selected rooms in Case 2 (conventional house) during a typical summer day. Note that the results shown are before and after applying NV. 167
Figure 8-8 Evaluation of the percentage of overheating hours (above 28.6 °C) for the tested rooms in both buildings over the course of the year under various ventilation strategies 168

Figure 8-9 Heat gain/loss analysis for both case study buildings in summer and winter. Note the significant heat flow per m^3 in Case 1 compared to Case 2 170
Figure 8-10 Breakdown of total external heat gain/loss by source for both case study buildings during a typical summer day and a typical winter day 173
Figure 8-11 Heat gain/loss through the building envelope for selected case study buildings in Riyadh. Note that the results shown are in kWh per unit volume of each house. 174
Figure 8-12 Predicted inner surface temperatures of external walls for the selected rooms in Case 1 176
Figure 8-13 Predicted inner surface temperatures of the external walls for selected rooms in Case 2 176
Figure 8-14 Predictions of total cooling load with various setpoint temperatures: (A) Simulation results for Case Study 1; (B) Simulation results for Case Study 2 178
Figure 8-15 Predicted cooling and heating load hours for both case study buildings in Riyadh 179
Figure 8-16 Monthly cooling load analysis by element (in kWh): (A) Simulation results for Case 1; (B) Simulation results for Case 2 180
Figure 8-17 Energy consumption per unit area for residential buildings in Riyadh, KSA.... 181
Figure 8-18 Baseline energy consumption predictions for Case 1: (A) Monthly energy consumption in relation to outdoor temperature; (B) Distribution of annual energy consumption (in MWh). 182
Figure 8-19 Baseline energy consumption predictions for Case 2: (A) Monthly energy consumption in relation to outdoor temperature; (B) Distribution of annual energy consumption (in MWh). 182
Figure 8-20 Monthly predictions of CO_2 emissions for selected case study buildings in Riyadh: (A) Simulation results for Case 1; (B) Simulation results for Case 2. 183
Figure 9-1 Indoor temperature predictions for Case 1 with varying insulation thicknesses and locations: (A) Results for a typical summer day; (B) Results for a typical winter day 190
Figure 9-2 Indoor temperature predictions for Case 2 with varying insulation thicknesses and locations: (A) Results for a typical summer day; (B) Simulation results for a typical winter day 190
Figure 9-3 Hourly air temperature profile for Case 1 with different insulation locations: (A) Simulation results for a typical summer day; (B) Simulation results for a typical winter day 191

Figure 9-4 Hourly air temperature profile for Case 2 with different insulation locations: (A) Simulation results for a typical summer day; (B) Simulation results for a typical winter day 191
Figure 9-5 Hourly indoor air temperature predictions for selected rooms after applying proposed natural ventilation on a typical summer day: (A) Simulation results for Case 1; (B) Simulation results for Case 2. Note the reduction in indoor temperatures during peak outdoor temperature periods for the external insulation option. 192
Figure 9-6 Indoor thermal comfort analysis with various thermal insulation locations while maintaining same U-value: (A) Case 1 (bedroom); (B) Case 2 (upper room).....193
Figure 9-7 Indoor thermal comfort analysis with various thermal insulation locations while maintaining same U-value after applying NV: (A) Case 1 (bedroom); (B) Case 2 (upper room).....193
Figure 9-8 Total annual cooling load predictions for selected rooms with various insulation locations: (A) Case 1 (bedroom); (B) Case 2 (upper room) 194
Figure 9-9 Indoor temperature predictions for Case 1 with varying roof insulation thicknesses: (A) Simulation results for a typical summer day; (B) Simulation results for a typical winter day.....196
Figure 9-10 Indoor temperature predictions for Case 2 with varying roof insulation thicknesses: (A) Simulation results for a typical summer day; (B) Simulation results for a typical winter day.....196
Figure 9-11 Hourly air temperature profile for Case 1 after applying various roof types: (A) Simulation results for a typical summer day; (B) Simulation results for a typical winter day 198
Figure 9-12 Hourly air temperature profile for Case 2 after applying various roof types: (A) Simulation results for a typical summer day; (B) Simulation results for a typical winter day 198
Figure 9-13 Indoor thermal comfort analysis with various proposed roof options: (A) Simulation results for Case 1 (bedroom); (B) Simulation results for Case 2 (upper room) ..200
Figure 9-14 Indoor thermal comfort analysis with various proposed roof options after applying natural ventilation: (A) Simulation results for Case 1 (bedroom); (B) Simulation results for Case 2 (R2) 200
Figure 9-15 Total annual cooling load predictions for selected rooms with various roof improvement strategies: (A) Case 1 (bedroom); (B) Case 2 (upper room) 202

Figure 9-16 Indoor temperature predictions for Case 1 with varying ground floor insulation thicknesses: (A) Simulation results for a typical summer day; (B) Simulation results for a typical winter day.....204
Figure 9-17 Indoor temperature predictions for Case 2 (ground floor dining room) with varying ground floor insulation thicknesses: (A) Simulation results for a typical summer day; (B) Simulation results for a typical winter day.....204
Figure 9-18 Hourly air temperature profile for Case 1 with and without SBC ground floor insulation: (A) Simulation results for a typical summer day; (B) Simulation results for a typical winter day.....205
Figure 9-19 Hourly air temperature profile for Case 2 (ground floor dining room) with and without SBC ground floor insulation requirements: (A) Simulation results for a typical summer day; (B) Simulation results for a typical winter day.....205
Figure 9-20 Indoor thermal comfort analysis before and after applying SBC ground floor insulation requirements without natural ventilation: (A) Case 1 (bedroom); (B) Case 2 (ground floor dining room).....206
Figure 9-21 Indoor thermal comfort analysis before and after applying SBC ground floor insulation requirements with proposed NV strategy: (A) Case 1 (bedroom); (B) Case 2 (ground floor dining room).....206
Figure 9-22 Annual cooling load predictions for selected rooms with varying ground floor options: (A) Simulation results for Case 1 (bedroom); (B) Simulation results for Case 2 (ground floor dining room).....207
Figure 9-23 Indoor temperature results for Case 1 with various infiltration rates: (A) Simulation results for a typical summer day; (B). Simulation results for a typical winter day 209
Figure 9-24 Indoor temperature results for Case 2 with various infiltration rates: (A) Simulation results for a typical summer day; (B) Simulation results for a typical winter day 209
Figure 9-25 Indoor thermal comfort analysis with various air infiltration values: (A) Simulation results for Case 1 (bedroom); (B) Simulation results for Case 2 (upper room) ..211
Figure 9-26 Indoor thermal comfort analysis with various air infiltration values after applying natural ventilation strategy: (A) Simulation results for Case 1 (bedroom); (B) Simulation results for Case 2 (upper room). Note that the potential of a free-running period increases when controlled airflow is reduced.....211

Figure 9-27 A comparison of different air infiltration values versus controlled ventilation for selected rooms: (A) Simulation results for Case 1; (B) Simulation results for Case 2.....211
Figure 9-28 Annual cooling load predictions for selected rooms with various uncontrolled infiltration rates: (A) Simulation results for Case 1 (bedroom); (B) Simulation results for Case 2 (upper room). Note that the baseline infiltration rate varies for each house.....212
Figure 9-29 Illustrations of the proposed external shading devices: (A) Overhang (PF = 0.50); (B) Egg-crate shadings (PF = 0.5); (C) Louvers (25 cm depth) 214
Figure 9-30 Solar gain results for the tested room with various shading techniques under different orientation scenarios during a typical summer day: (A) Simulation results for Case 1; (B) Simulation results for Case 2.....215
Figure 9-31 Indoor temperature predictions for a typical summer day for both rooms under various orientations and different shading options: (A) Simulation results for bedroom in Case 1; (B) Simulation results for upper room (R2) in Case 2.....216
Figure 9-32 Annual cooling load predictions for tested rooms: (A) Simulation results for the bedroom in Case 1; (B) Simulation results for the upper room in Case 2.....218
Figure 9-33 Images of the constructed energy models after the implementation of external shading devices: (A) Case Study 1; (B) Case Study 2.....219
Figure 9-34 Indoor temperature predictions for Case 1 after applying proposed shading devices integrated with different glazing types: (A) Simulation results for a typical summer day; (B) Simulation results for a typical winter day.....220
Figure 9-35 Indoor temperature predictions for Case 2 after applying proposed shading devices integrated with different glazing types: (A) Simulation results for a typical summer day; (B) Simulation results for a typical winter day.....220
Figure 9-36 Indoor thermal comfort analysis with various window shading cases: (A) Simulation results for Case 1 (bedroom); (B) Simulation results for Case 2 (upper room) ..221
Figure 9-37 Indoor thermal comfort analysis with various window shading cases after applying natural ventilation: (A) Simulation results for Case 1 (bedroom); (B) Simulation results for Case 2 (Room 2) 221
Figure 9-38 Annual cooling load predictions for selected rooms with the integration of various window shading options: (A) Simulation results for Case 1 (bedroom); (B) Simulation results for Case 2 (upper room).....222
Figure 9-39 Indoor air temperature predictions for Case 1 (bedroom) after the implementation of the proposed building fabric alternatives: (A) Simulation results for a typical summer day; (B) Simulation results for a typical winter day.....224

Figure 9-40 Indoor air temperature predictions for Case 2 (upper room) after the implementation of the proposed building fabric alternatives: (A) Simulation results for a typical summer day; (B) Simulation results for a typical winter day 224
Figure 9-41 Indoor air temperature predictions for selected rooms after applying natural ventilation during a typical summer day: (A) Simulation results for Case 1 (bedroom); (B) Simulation results for Case 2 (upper room).....225
Figure 9-42 Indoor thermal comfort analysis before and after applying the proposed building enhancement alternatives: (A) Case 1 (bedroom); (B) Case 2 (upper room) 226
Figure 9-43 Indoor thermal comfort analysis before and after applying the proposed building enhancement alternatives with the implementation of natural ventilation: (A) Case 1 (bedroom); (B) Case 2 (upper room) 226
Figure 9-44 A comparison of external heat gain (external walls, roof, ground, infiltration, and windows) between baseline and improved model for a typical summer and a typical winter day (in kW): (A) Simulation results for Case Study 1 (3D-printed house); (B) Simulation results for Case Study 2 (conventional house).....227
Figure 9-45 Total annual cooling load predictions for residential buildings in Riyadh: (A) Case 1 (3D-printed house); (B) Case 2 (conventional house) 228
Figure 9-46 A comparison of monthly cooling loads between baseline and improved models for both houses in Riyadh: (A) Case 1 (3D-printed house); (B) Case 2 (conventional house) 229
Figure 9-47 Predicted cooling and heating hours for the improved models (after applying proposed building fabric enhancements and mixed-mode ventilation strategy) of both houses in Riyadh.....231
Figure 9-48 Predicted energy consumption and CO_2 emissions for Case Study 1 and Case Study 2 232
Figure 9-49 Potential energy savings for residential buildings in Riyadh, KSA, in comparison with the estimated savings in this study.....233

LIST OF TABLES

Table 2-1 Climatic features of the identified climatic zones in Saudi Arabia. Adapted from Alrashed and Asif (2015b) 15
Table 2-2 Residential electricity tariffs before and after reforms. Adapted from Al Dubyan and Gasim (2020) and AlGhamdi (2019). 32
Table 2-3 Envelope thermal requirements of the Saudi energy conservation code. Adapted from SBC 602 (2018) 35
Table 3-1 Solar absorptance for commonly applied materials and surface finishes. Adapted from (IES-VE, 2023). 49
Table 3-2 Subjective reaction to air movement. Adapted from Szokolay (2004). 53
Table 3-3 Metabolic rates for typical household tasks. Adapted from ASHRAE (2017). 56
Table 3-4 Thermal sensation scale for the PMV. Adapted from Asimakopoulos (1996). 57
Table 3-5 Thermal properties of commonly used building materials. Adapted from Saulles (2019). 61
Table 3-6 Summary of previous studies on the potential impact of various design strategies on the thermal and energy performance of residential buildings 67
Table 4-1 Summary of previous studies on the thermal and energy performance of 3D concrete printing 91
Table 5-1 Adaptive comfort temperatures for Riyadh 98
Table 5-2 Window types and properties used in the 3D-printed house 104
Table 5-3 Details of window types and physical properties for selected rooms in Case Study 2 106
Table 5-4 Instruments used in this study and their specifications 108
Table 5-5 Comparison of selected building energy simulation tools. Adapted from Solmaz (2019) 112
Table 5-6 Description of HVAC systems in a typical house in Saudi Arabia. 119
Table 5-7 Energy model thermal parameters 120
Table 5-8 Heat gain from occupants 120
Table 5-9 Characteristics of proposed window glazing cases for both dwellings in Riyadh 123
Table 6-1 Summary of monitored outdoor air temperature and relative humidity 131
Table 6-2 Outer surface temperature measurements recorded on a typical summer day (19 August) 134
Table 7-1 Mean features of external façade for Case 1 145

Table 7-2 Mean features of external façade for Case 2 145
Table 7-3 Description of Case 1's construction elements and their thermal properties 146
Table 7-4 Description of Case 2's construction elements and their thermal properties 147
Table 7-5 Average monthly ground temperatures in Riyadh (Abdel-Ghany et al., 2022). ... 152
Table 7-6 Validation results of the statistical analysis for the selected rooms in Case 1 and Case 2 156
Table 7-7 Daily average incident solar radiation rate (W/m^2) of external surfaces (external walls and roofs) for typical summer and winter days 158
Table 9-1 Characteristics of the proposed external wall options for Case Study 1 and Case Study 2 189
Table 9-2 Proposed and simulated roof alternatives for the selected case study buildings in Riyadh 197
Table 9-3 Description of proposed insulated ground floor types for both case study buildings 203
Table 9-4 Proposed and tested window shading cases 219
Table 9-5 Summary of thermal analysis results of proposed combination of the building fabric and proposed mix-mode ventilation strategy in comparison with baseline models 230
Table 9-6 Summary of baseline, improved model, and the proposed ventilation strategy 232

LIST OF EQUATIONS

(3-1).....41
(3-2).....53
(3-3).....55
(3-4).....55
(3-5).....55
(3-6).....59
(3-7).....59
(7-1).....154
(7-2).....155
(7-3).....155
(7-4).....155

LIST OF ACRONYMS

3DCP	Three-dimensional concrete printing
AC	Air conditioning
ACH	Air changes per hour
ASHRAE	American Society of Heating, Refrigerating and Air-Conditioning Engineers
AM	Additive manufacturing
Av	Air velocity
Ave	Average
BR	Bedroom (south-facing bedroom in Case 1)
BTSI	Building Technology Stimulus Initiative
CAD	Computer-aided design
CC	Contour Crafting
CMA	Computer-aided manufacturing
CDD	Cooling Degree Days
CNC	Computer numerically control
CO_2	Carbon dioxide emissions
DR	Dining room (west-facing dining room in Case 1)
DTV	Daytime ventilation
EUI	Energy usage intensity (energy consumption per unit area)
GAS	General Authority for Statistics
GHG	Greenhouse gas emissions
HSA	Horizontal shadow angle
HVAC	Heating, ventilation, and air-conditioning
IEA	International Energy Agency
IES-VE	Integrated Environmental Solutions-Virtual Environment
IST	Inner surface temperature of external walls
KSA	Kingdom of Saudi Arabia
M	Metabolic rate
Max	Maximum
Min	Minimum

MRT	Mean radiant temperature
NTV	Nighttime ventilation
NURBS	Non-uniform rational basis splines
PF	Projection factor
PMV	Predicted mean vote
PPD	Predicted percentage of discomfort
R1	Room 1 (first floor bedroom room in Case 2)
R2	Room 2 (top floor bedroom in Case 2)
RH	Relative humidity
R-value	Thermal resistance
SAR	Saudi riyal
SBC	Saudi building code
SBC 602	Saudi energy conservation code for residential buildings
SDC	Smart dynamic casting
SEEC	Saudi Energy Efficiency Centre
SHGC	Solar heat gain coefficient for window glazing
SV2030	Saudi Vision 2030
Ta	Indoor air temperature
Tc	Comfort temperature
Tg	Globe temperature
To	Operative temperature
Tout	Outdoor temperature
UAE	United Arab of Emirates
U-value	Thermal transmittance
VSA	Vertical shadow angle
WWR	Window-to-wall area ratio

CHAPTER 1

INTRODUCTION AND RESEARCH JUSTIFICATION

- Research introduction
- Problem statement
- Research aim, objectives, and questions
- Methodology
- Thesis structure

Chapter 1: INTRODUCTION AND RESEARCH JUSTIFICATION

1.1 Introduction

The world is facing severe energy and environmental challenges. Over the past half-century, global demand for energy has grown continuously. Between 2010 and 2022, global electricity consumption is reported to have increased by more than 37% (Statista, 2024). According to a report by the International Energy Agency (IEA) (2024), global energy consumption is forecast to increase even further over the next three years, at an average annual rate of 3.4% through 2026. Fossil fuel, the primary source of CO_2 emissions, remains the primary source of global energy as it accounted for 80% of global energy consumption in 2019 (Alrashed, 2015; Edie, 2021).

The continuously increasing concentration of CO_2 and other greenhouse gas emissions in the atmosphere has contributed to the rise in global temperatures over the past century. In 2020, the global average temperature was about 1.02 °C warmer than the 1951–1980 mean (NASA, 2021). Since the signing of the Paris Agreement in 2015, the number of countries announcing ambitious plans to achieve net-zero emissions over the next few years has continued to grow. If fully achieved, such a pledge could reduce global carbon emissions by about 70% (BP-p.l.c., 2021).

The building and construction sector plays a crucial role in global energy consumption and greenhouse gas (GHG) emissions. The sector is responsible for more than one-third of global energy use, with further increases anticipated (Friess & Rakhshan, 2017; Pérez-Lombard, Ortiz, & Pout, 2008; Shehata & Waheeb, 2018), and nearly 40% of global energy-related CO_2 emissions (Abergel, Dean, & Dulac, 2017). Overall, buildings' energy consumption is driven by numerous factors, including climatological factors, occupants' behaviour, and building configuration (Friess & Rakhshan, 2017). In 2018, energy demand in buildings increased by 7% from 2010, putting the sector off track with the level of action required to address recently raised climatic concerns (IEA, 2019). Given these statistics, the building sector can contribute significantly towards addressing energy and environmental concerns.

Buildings' energy demand is most significant in extreme climatic conditions, in which achieving indoor thermal comfort requirements contributes to a high portion of overall building energy requirements. This is the case in hot and arid climates, such as Saudi Arabia, where energy-intensive active cooling systems have become essential to maintain occupants' comfort. The high demand for space cooling has a significant impact on peak energy loads,

especially during overheating periods when active cooling is used in full capacity to satisfy indoor thermal requirements. According to the *Net Zero Roadmap* report by IEA (2023), under current policies and trends, global energy requirements for space cooling are set to more than double by 2025.

It is more than likely that improving building systems and equipment efficiency alone will not be sufficient to address worsening environmental and energy issues. Encouraging climate-friendly buildings through building design, configuration and passive techniques is a must to reduce active cooling consumption.

1.2 Research problem

Saudi Arabia has for many years maintained its global role as the largest exporter of crude oil. It produces more than 10 million barrels per day, which contributes to more than half of the Kingdom's revenue. However, the country is also one of the largest oil consumers in the Middle East, consuming nearly 3 million barrels per day (25% of its produced oil) (Alrashed, 2015; EIA, 2021). According to the World Bank Group (2022a), the average energy consumption in Saudi Arabia is about 45% higher than the global average. The KSA is among the world's top countries in terms of per capita energy consumption; it was ranked twelfth in 2019 (EIA, 2021).

The demand for electricity in KSA is experiencing rapid growth, with the building sector being the largest consumer. In 2020, KSA's total national energy consumption exceeded 289,000 GWh, with the residential sector alone accounting for 47.5% of this amount (Almushaikah & Almasri, 2020; Alrashed, 2015; GAS, 2023; Statista, 2022). Figure 1-1 shows energy consumption in KSA by sector.

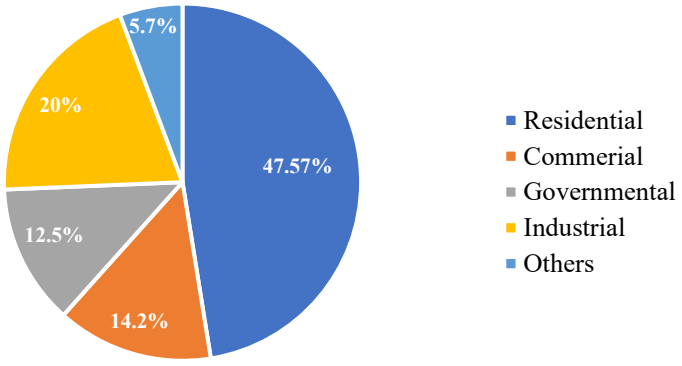


Figure 1-1 Electricity Consumption in the Kingdom of Saudi Arabia in 2020 by sector. Total energy consumed is 289,330 gigawatts per hour. Based on data from GAS (2023) and Statista (2022).

Contemporary buildings in Saudi Arabia are generally not designed for the local climate, often exhibiting poor thermal performance. Additionally, the abandonment of vernacular strategies and architectural elements has left these buildings heavily reliant on energy-intensive cooling systems to maintain indoor thermal comfort, particularly during overheating seasons. Consequently, a significant share of total energy consumption in the residential sector is attributed to cooling (Ahmed & Asif, 2020; Al-Homoud & Krarti, 2021; Alaidroos & Krarti, 2015; Almushaikah & Almasri, 2020).

In 2016, KSA launched Vision 2030, an ambitious plan to diversify the country's economy, end its heavy dependency on oil, and improve public services such as education, health, infrastructure, recreation, and tourism (Vision 2030, 2022a). Promoting sustainability across all sectors, and the building and construction sector in particular, is a key aim of this ambitious plan; thus, improving the energy efficiency of residential buildings has become a national goal (Balabel & Alwetaishi, 2021). To achieve these objectives, several initiatives, standards, and regulations have recently been introduced, such as the Saudi Building Code (SBC), which intends to improve building thermal performance and reduce energy consumption.

The rapid urban population growth and development that the country has witnessed over the past few decades—growth and development driven by economic growth in KSA—has not only contributed to increased energy demand and associated CO_2 emissions but has also caused a significant housing shortage (Ghabra, 2018; Obaid & Mufti, 2008). According to the *Housing Program Delivery Plan* published by Vision 2030 (2022a), the country aspires to increase homeownership from 60% (reported in 2020) to 70% by 2030, adding to the existing housing shortage a deficit of 1.5 million units and increasing the already high demands for energy. To achieve these goals, the adoption of modern and sustainable construction technology and methods have become essential (Ministry of Municipal Rural Affairs and Housing, 2022).

To address these challenges, the Building Technology Stimulus Initiative (BTSI) was introduced to transform the local building construction market by encouraging the use of intelligent and sustainable construction methods and novel construction techniques, including digital fabrication and robotic technologies (Alabbasi, Chen, & Agkathidis, 2021; Vision 2030, 2022a).

Given the severe climate conditions of KSA, it is critical to investigate the thermal performance of emerging construction technologies and their suitability for maintaining adequate indoor thermal environments. This research is driven by the need to address the challenges facing the Saudi residential sector by exploring how modern constructions can foster a sustainable future in KSA. The following sections outline the main aim, objectives, and questions relating to the research.

1.3 Aim and objectives

This research aims to investigate the thermal performance of residential buildings constructed with two distinct construction methods (large-scale 3D concrete printing and conventional construction techniques) and to learn from vernacular architecture in the region and advances in modern building technology to propose and test (through computer simulation) more sustainable solutions for residential buildings to foster a sustainable future in Saudi Arabia. To achieve the stated aim, the following key objectives were developed:

1- To review current energy consumption rates, building characteristics, regulations, and recent energy efficiency related to initiatives within the residential sector.
2- To review the literature on 3D concrete printing techniques for building construction and the thermal performance of these buildings in hot climates.
3- To determine the factors that contribute to high energy demands and CO_2 emissions in Saudi Arabia's residential buildings through an examination of selected cases.
4- To identify a range of passive strategies—from vernacular building principles and modern strategies—for improving the thermal and energy performance of contemporary residential buildings in the hot climate of KSA.
5- To evaluate the indoor thermal environments of a 3D-printed house and a conventionally constructed house through field monitoring and computer energy simulations.
6- To investigate the effectiveness of the proposed measures in improving the thermal and energy performance of the selected cases through simulation while maintaining indoor thermal comfort.

1.4 Research questions

1- How can the performance of the selected case studies be effectively simulated while ensuring that the predicted outcomes accurately reflect the actual physical conditions?

2- What are the current thermal performance and energy consumption rates for a 3D-printed concrete house and a conventionally constructed house in the hot climate of Riyadh, KSA?
3- What is the role of the building envelope in improving the thermal behaviour of KSA's contemporary houses?
4- How can design strategies learned from vernacular architecture and modern sustainable building technology improve the thermal performance of residential buildings in Riyadh, KSA?
5- To what extent can applying the proposed passive strategies reduce cooling load (and associated energy consumption and CO_2 emissions) in a 3D-printed house and a conventionally constructed house?

1.5 Methodology

This research focuses on the thermal performance of residential buildings constructed with different construction methods, mainly 3D concrete printing (3DCP) and conventional construction methods, in a hot and arid climate context, particularly in Saudi Arabia. In this respect, the methodology of this research revolves around a case study approach. Two existing houses were identified and used as case study buildings to predict their current performance and investigate the impact of implementing improvement measures and strategies to enhance indoor thermal environments and reduce cooling consumption.

The use of computer energy simulation has been suggested by a number of published studies, including successfully completed PhD theses by Abuhussain (2020), Alaboud (2021), Alkhalifah (2024), Alosaimi (2023), and Alyami (2022). This work facilitated the exploration of the selected cases to determine their current thermal and energy performance and identify potential areas for improvement. The methods employed in this study involved actual field measurements and computer energy simulations. For more details, see Chapter 5. The overall research workflow is summarized in Figure 1-2, which illustrates the steps undertaken from the literature review to simulation and performance evaluation of the selected case studies.

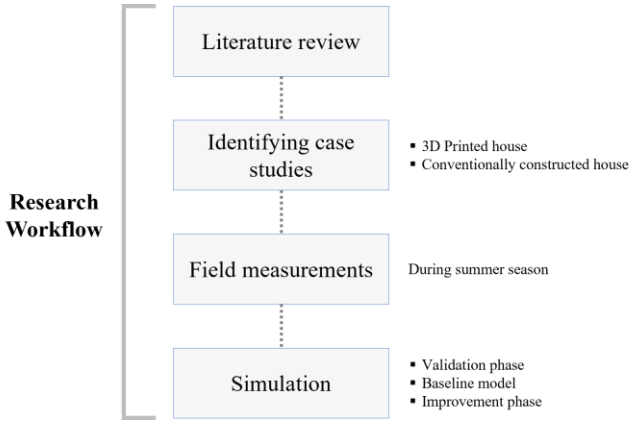


Figure 1-2 Summary of thesis procedures

1.6 Novelty of the research

The novelty of this research lies in providing the first comprehensive thermal assessment of a 3D-printed residential building compared with a conventionally constructed house in the hot and arid climate of Riyadh, Saudi Arabia. While several studies have investigated the thermal and energy performance of typical Saudi dwellings, very few have evaluated full-scale 3D-printed buildings, particularly in hot and dry regions (Pessoa, Guimarães, Lucas, & Simões, 2021; Sovetova & Kaiser Calautit, 2024).

Unlike previous efforts, this research integrates empirical field measurements with validated dynamic simulation to assess current performance and explores potential improvements through passive design measures and cooling strategies inspired by vernacular architecture and modern technologies. The employed methodological approach offers new insights into thermal and energy performance of 3D-printed compared with conventionally constructed residential buildings in hot and arid contexts.

Additionally, the study aligns with current regulations and initiatives, using actual construction systems implemented in Riyadh. In doing so, it evaluates the effectiveness of the Saudi Building Energy Conservation Code for Residential Buildings (SBC 602) when applied to emerging construction technologies such as 3D concrete printing and identifies practical opportunities to reduce cooling demand and enhance energy performance while maintaining indoor thermal comfort requirements.

1.7 Thesis structure

This thesis comprises ten chapters and is divided into three main sections. The first section provides background information and a literature review, the second section explains in detail

the research methodology, and the last section contains the main body of the research and the research conclusions. Figure 1-3 shows a brief overview of the thesis structure.

Chapter 1: INTRODUCTION AND RESEARCH JUSTIFICATION

This chapter presents an overview of the study, relevant background information, and a description of the rationale for this research in the form of a problem statement. It also highlights the study's objectives and research questions, offers a brief description of the research methodology, and provides a brief overview of each chapter. See pp.1–10.

Chapter 2: SAUDI ARABIA: BUILDING AND CLIMATE

This chapter explores the study location, Saudi Arabia, through a broad review of relevant literature. It provides a picture of the current energy and environmental challenges facing the building sector in general and residential buildings in particular, along with the significantly growing demand for housing. Furthermore, it describes past and modern trends in the Saudi building sector from both architectural and structural points of view and a review of recent initiatives and governmental efforts towards energy efficiency and more sustainable building developments. See pp. 11–38.

Chapter 3: ENVELOPE DESIGN AND THERMAL COMFORT

This chapter includes a literature review of the impact of building envelope on thermal environment. It explores the role of the building envelope and explains the physics, function, and methods that can be applied to mitigate environmental impacts. It also discusses the concept of thermal comfort, including factors influencing indoor thermal comfort, methods to evaluate the indoor thermal environment, and adaptive strategies in hot climates. See pp. 39–67.

Chapter 4: DIGITAL FABRICATION IN THE CONSTRUCTION INDUSTRY

This chapter discusses the application of digital fabrication techniques in the building industry, with a particular focus on additive manufacturing (3D printing). The chapter explores the feasibility of 3DCP technique in the building industry and provides a review of the thermal and energy performance of 3D-printed buildings with a focus on hot and arid regions. See pp. 69–91.

Chapter 5: RESEARCH METHODOLOGY

This chapter describes the methodology adopted to achieve the research aim and objectives. It also presents a methodology flowchart to provide a clear visualization of the research steps and their sequential stages. Additionally, it provides a review of the study location and the

selected case study buildings, including architectural drawings, and discusses the employed tools and equipment for thermal analysis and inputs for the simulation software. The chapter ends with a brief discussion of the proposed improvement measures and strategies. See pp. 93–123.

Chapter 6: INDOOR THERMAL ENVIRONMENT (MONITORED)

This chapter focuses on field data collection. It contains the objectives of conducting field measurements and selected zones in each house. It presents field measurement results and analysis of indoor thermal performance for selected zones in both the 3D-printed house and the conventionally constructed house. See pp. 125–141.

Chapter 7: BUILDING MODEL DEVELOPMENT

This chapter is divided into two main sections, the first of which describes the process of modelling the two case study buildings using the selected simulation tool, Integrated Environmental Solutions Virtual Environment (IES-VE). It provides the required details, including specifications of baseline construction material. The second section discusses the validation stage of the two energy models by comparing field measurements against predicted data. See pp. 143–157.

Chapter 8: ANALYSIS OF INDOOR THERMAL ENVIRONMENT USING COMPUTER SIMULATION SOFTWARE

This chapter provides a comprehensive analysis of baseline models. It explores the thermal environment of the selected buildings in terms of indoor air temperature, comfort performance, surface temperatures, and heat gain analysis under specified conditions. Following this analysis, the chapter attempts to predict annual cooling load, energy consumption, and carbon emissions for both case study buildings. See pp. 159–184.

Chapter 9: PARAMETRIC STUDY AND OPTIMIZATION USING ENERGY SIMULATION SOFTWARE

This chapter applies proposed improvement measures and strategies (learned from vernacular architecture and modern building technology) separately for each house and evaluates their impacts on building thermal performance by altering one variable at a time. The resulting data are presented and discussed in terms of potential improvement on indoor thermal environment and reduction in cooling load.

Following this step, the impact of combining the best performing alternative for each parameter is investigated, and the final improved model is compared to the baseline simulations. See pp. 186–233.

Chapter 10: CONCLUSION

The final chapter provides a summary of the key findings of the research in relation to the stated aim and research questions. It highlights the research contributions, explains the research limitations, and provides recommendations for future research. See pp. 235–249.



Figure 1-3 Structural outline of the thesis

CHAPTER 2

SAUDI ARABIA: BUILDING AND CLIMATE

- Introduction
- Climate of Saudi Arabia
- Trends of energy and CO_2 emissions in Saudi Arabia
- Past and current buildings in Saudi Arabia
- Initiatives and programs towards energy efficient built environment
- Saudi Building code (SBC 602)

Chapter 2: SAUDI ARABIA: BUILDING AND CLIMATE

2.1 Introduction

Reflecting upon energy and environmental concerns in KSA, particularly within the residential sector, and the nation's rapidly growing housing demand, this chapter sets out the context of the research. It begins with a brief overview of Saudi Arabia in terms of geographic location and climate features, followed by an examination of the country's growing energy demands and CO_2 emissions on one hand, and on the other hand the rapidly growing demand for new housing development. These are discussed in Sections 2.2 to 2.5. The second half of the chapter explores past and current trends in residential buildings (see Section 2.6), and reviews new initiatives and programs towards energy efficiency in general and sustainable building developments in particular (Sections 2.7 to 2.9).

2.2 Background of the Kingdom of Saudi Arabia

Saudi Arabia is known for its rapid social and economic development. According to the Saudi Census 2022 published by the General Authority for Statistics (GAS), the total population of the Kingdom increased by more than 30% between 2010 and 2022, reaching 32,175,224, with a 4.5% population growth rate compared to 2021. Additionally, it is predicted that the population will surpass 39 million by 2026 (O'Neill, 2021).

Saudi Arabia occupies an important place among the nations of the world for at least two reasons. First, it is an important oil producer, holding up to one quarter of the world's proven oil reserves. Since the 1930s, when oil was discovered in abundant quantities in the Kingdom, the country has become a major global oil exporter. Despite ongoing economic diversification efforts, the economy still heavily relies on oil. In addition, the country has religious significance for Muslims around the world as the two most recognized and sacred mosques are located in Saudi Arabia, which is also known as 'the Land of the Two Holy Mosques'. Thus, Saudi Arabia plays significant economic and political roles in the Middle East.

The Kingdom of Saudi Arabia (KSA) is the second-largest Arab state and occupies a great portion of the Arabian Peninsula. It is located between 16° and 30º N latitude (in the Tropic of Cancer) and has a land area of 2,149,690 km^2, which is nine times larger than the United Kingdom (The World Bank Group, 2022b). The country is bordered by the Arabian Gulf on the east and the Red Sea on the west and is located north of Yemen and Oman. In the east, the

country shares borders with the United Arab Emirates, Qatar, and Bahrain, with Kuwait, Jordan, and Iraq in the north.

The Kingdom is divided into thirteen administrative provinces, or regions. Each region is unique in many respects, including culture, climate, and soil. Riyadh, located in the Central Province, is the capital city and the country's largest urban centre. Jeddah is another major city and is the gateway to the sacred cities and the country's main seaport to the Red Sea. Makkah and Al Madinah are the two sacred cities and are held in great esteem by Muslims around the world. Other important cities in Saudi Arabia include Dammam, Abha, Hail, and Najran.

2.3 Climate of Saudi Arabia

Climate has always been a major factor influencing human behaviour and the design of buildings. Due to the profound impact of external factors on the indoor thermal environment and occupants' comfort, it is necessary to consider them when designing buildings (Al-Oraier, 2005).

As it is situated in a desert area lacking water bodies, Saudi Arabia is characterized by a dry desert and semi-arid climate with prevailing high temperatures and low humidity levels (Dwidar, 2019; National Center for Meteorology, 2023). The geography of Saudi Arabia, with vast desert areas, mountain chains, and rocky plateaus, is among the major factors that influence the local climate, resulting in various microclimates (WorldData.info, 2023). Owing to topographic variations, the climate in Saudi Arabia varies from one zone to another. Additionally, as Saudi Arabia is surrounded by the Red Sea in the west and the Arabian Gulf in the east, the nation's climate is affected by nearby moisture sources.

It is also close to large water bodies: the Indian Ocean and the Mediterranean Sea are south and northwest of the Arabian Peninsula, respectively. The temperature difference between the land and water surfaces, aside from their distinct thermal properties (e.g. heat gain and loss), causes different regional pressure zones throughout the year, while air mass movements affect the country's climate from different sides (Al-Ahmadi & Al-Ahmadi, 2013; National Center for Meteorology, 2023). According to Köppen-Geiger's climate classification (see Figure 2-1), Saudi Arabia is categorized as a hot, arid desert (BWh).

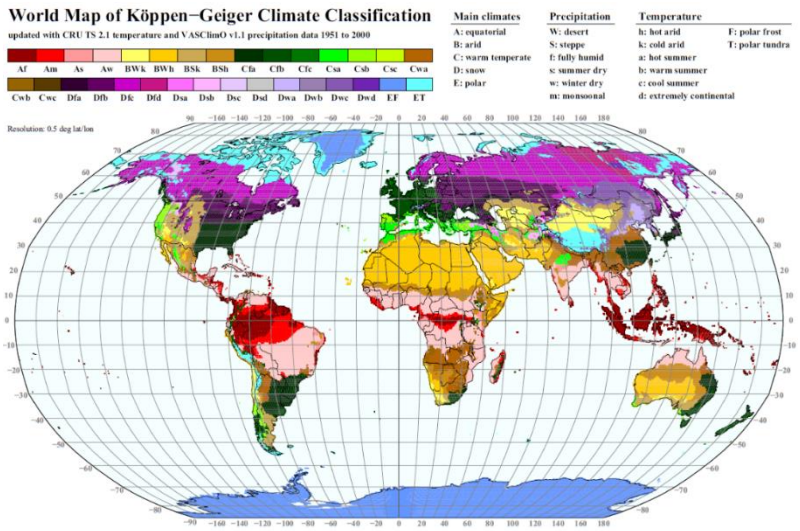


Figure 2-1 World Map of Koppen-Geiger Climate Classification. Note that the Gulf Region is located within the yellow classification of BWh (arid desert hot climate) (Kottek, Grieser, Beck, Rudolf, & Rubel, 2006).

One clear effect of the country's topography on its climate variation is seen in temperature and precipitation. The mountainous areas of Asir, located in the southwest of the Kingdom, have moderate temperatures and high annual precipitation rates compared to the rest of the country (Al-Ahmadi & Al-Ahmadi, 2013). Bagasi (2022) noted that the Western Highlands restrict winds from the west and southwest from travelling deeply into the rest of the country. Moreover, major differences in Saudi Arabia's climate can be found between internal areas and coastal regions (National Center for Meteorology, 2023).

A notable study undertaken by Alrashed and Asif (2015b) to identify different climate zones in Saudi Arabia classified the Kingdom into five distinct inhabited climatic zones (in addition to the Empty Quarter, an uninhabited region). Each of the five inhabited zones was represented by a city selected from each zone, as shown in Figure 2-2. The main climatic features of each of the five cities are shown in Table 2-1.

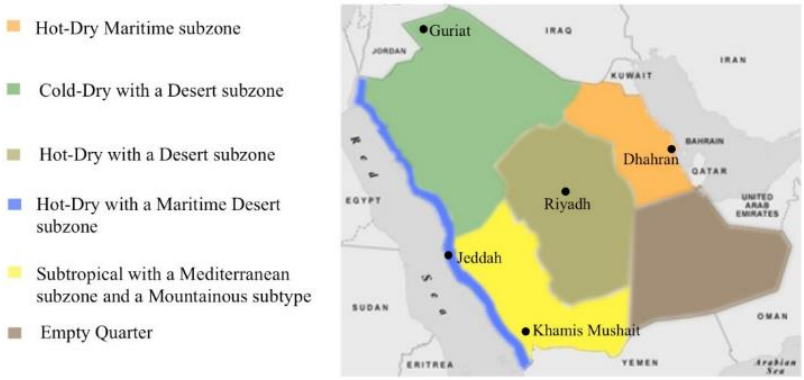


Figure 2-2 The climatic zones of Saudi Arabia (Alrashed & Asif, 2015b).

Table 2-1 Climatic features of the identified climatic zones in Saudi Arabia. Adapted from Alrashed and Asif (2015b)

	Air temperature (°C)			Relative humidity (%)			Air velocity (m/s)			Global solar radiation (W/m²)		
	Min	Max	Ave	Min	Max	Ave	Min	Max	Ave	Min	Max	Ave
Dhahran	5.0	45.7	25.8	19	99	57	0	5.7	0.9	0	990	195
Guriat	−3.3	43.9	19.8	12	100	40	0	16.3	4.2	0	1053	235
Riyadh	2.2	43.7	25.1	10	91	32	0	11.9	3.1	0	1049	252
Jeddah	13.9	41.7	27.9	37	100	65	0	11.2	2.6	0	1035	257
Khamis Mushait	2.7	34.3	18.9	17	100	51	0	12.4	3.1	0	1127	289

Saudi Arabia is one of the hottest countries in the world. Most of its regions tend to experience extremely high temperatures in the summer, except for the mountainous areas, and mild winters. The average daily temperatures range between 23 °C and 41 °C, exceeding 45 °C on some days in hot and dry regions. Depending on the region, winter temperatures can drop to 11 °C and fall below freezing in some parts of the northern regions. Historical monthly daytime and nighttime temperature averages for the last 20 years (from 2003 to 2023) are shown in Figure 2-3.

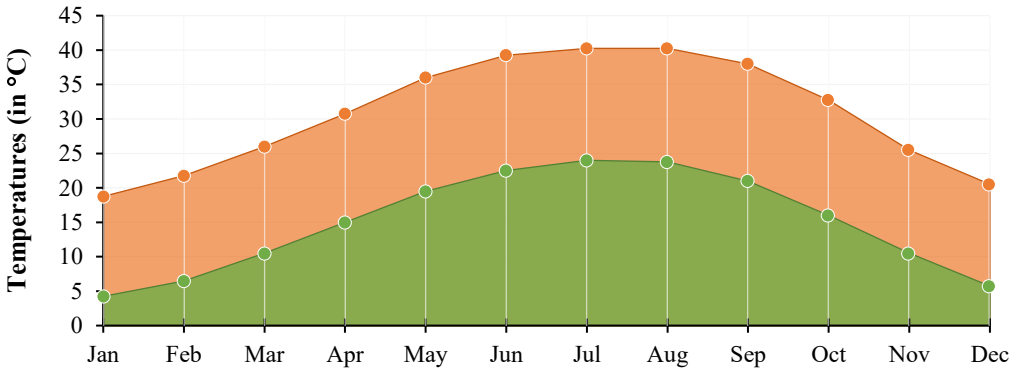


Figure 2-3 Historical monthly air temperature averages for Saudi Arabia (2003–2023). Based on data from WorldData.info (2023).

Note that the red zone shows the monthly maximum averages and the green zone shows the minimum monthly averages.

As it is located on the so-called sunbelt, which lies between 40°N and 40°S, Saudi Arabia receives high amounts of solar radiation with long periods of daylight. The amount of daily solar radiation in the country varies depending on geographical location, from a minimum of 4.479 kW/m^2 in Tabuk to a maximum daily value of 7.004 kW/m^2 in Bisha. Thus, horizontal surfaces in Saudi Arabia receive an average of more than 5.5 kW/m^2 of solar radiation each day.

As shown in Figure 2-4, the southern areas receive more solar radiation than the rest of the country, while lower amounts are observed in the northern areas. The estimated average of sunlight duration in Saudi Arabia is 8.89 hours per day, or 3,245 hours per year (Almasoud & Gandayh, 2015).

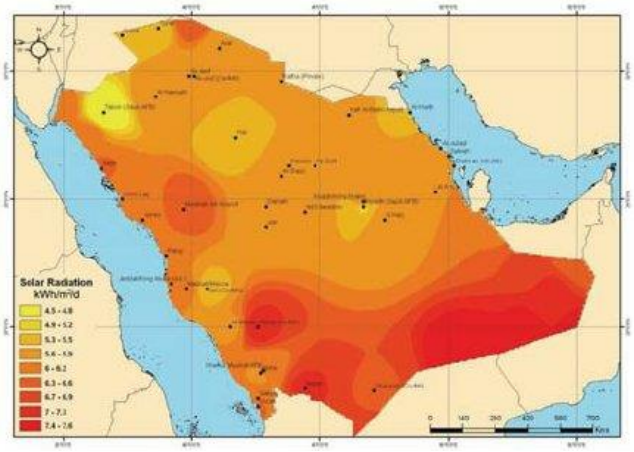


Figure 2-4 Average annual daily solar radiation in Saudi Arabia (Baig, Sellami, Bahaidarah, & Mallick, 2013)

Saudi Arabia is also one of the driest countries in the world. The average annual precipitation in most parts of the country is very low, except in the Asir Mountains of the southern region, which receives around 300 mm of rainfall throughout the year as it is impacted by summer monsoons and north-westerly air masses originating in the Mediterranean during the winter season (Al-Ahmadi & Al-Ahmadi, 2013; National Center for Meteorology, 2023). The average amount of rainfall in the rest of the country is generally low and is characterized by seasonality and variation in amounts and periods.

Relative humidity (RH) in Saudi Arabia varies from one region to another and is impacted by proximity to sources of moisture such as water bodies, as previously indicated, along with the location of agricultural areas and the moist sea air masses that blow over the country. Except for some parts of the coastal areas, most of the country is characterized by low humidity levels (National Center for Meteorology, 2023). RH is lowest in the central parts of the country, which are dominated by the arid desert landscape and low vegetation cover. Nevertheless, high temperatures in Saudi Arabia mean that the RH falls within an acceptable range (between 30% and 60%), as shown in Figure 2-5 (WorldData.info, 2023).

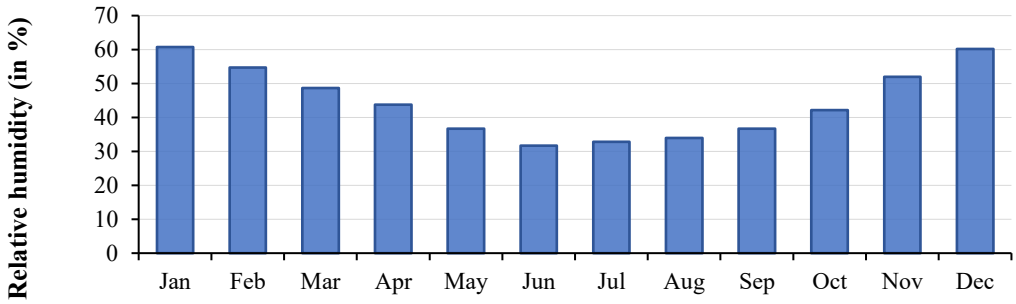


Figure 2-5 Historical monthly averages of relative humidity in Saudi Arabia (2003–2023). Based on data from WorldData.info (2023).

The different climatic conditions in Saudi Arabia are reflected in the *Saudi Building Code* (SBC). SBC 602 categorizes the country into three climatic zones based on Cooling Degree Days (CDD) values, which indicate how much energy is needed to heat and cool a building according to weather conditions (i.e. how hot or cold a given location is). CDD values are used to compare mean outdoor temperatures for a given location against a standard temperature. CDD values increase as the outdoor temperature becomes more extreme. A higher number of Degree Days generally means that more energy is required for space heating or cooling. The SBC prescribes a fixed and relatively low base temperature of 10 °C to estimate the CDD. Accordingly, the climate of Saudi Arabia is classified into three zones:

- Zone 1: extremely hot climate with CDD 10 °C higher than 5,000.
- Zone 2: very hot climate with CDD 10 °C higher than 3,500.
- Zone 3: hot climate for the remaining cities.

The climate zones of Saudi Arabia and the selected 28 major cities are shown in Figure 2-6, where Zone 1 is highlighted in white, Zone 2 in yellow, and Zone 3 in red. As can be seen in the figure, about 70% of the Kingdom's area is covered by Zone 1, including most of the major cities, such as Riyadh. The extreme climatic conditions in Zone 1, where the temperature can be as high as 50 °C, necessitate investigating building thermal performance as it is considered a crucial challenge to the country. An analysis of the climate data for Riyadh, the selected case study city for this thesis, is provided in Chapter 5.

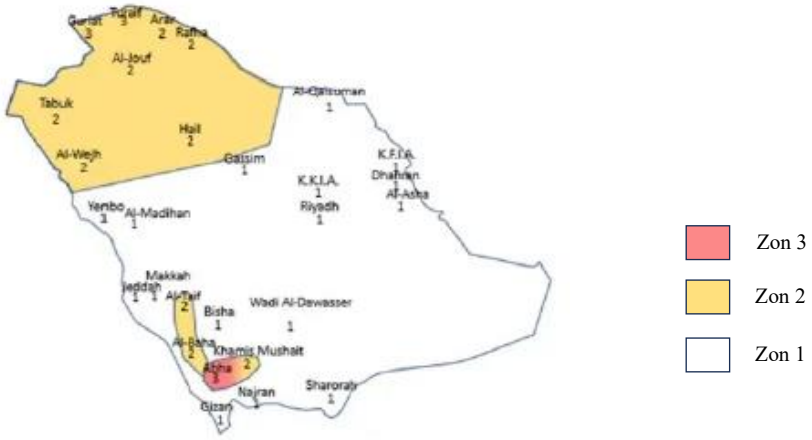


Figure 2-6 Climate zones of Saudi Arabia according to the energy conservation code. Adapted from SBC 602 (2018).

2.4 Trends of energy and CO_2 emissions in Saudi Arabia

Demands for energy:

Saudi Arabia is a fast-growing country with an annual economic growth rate of 6.8% (Abuhussain, 2020). However, the country's energy sector is experiencing considerable energy and environmental challenges. Owing to factors such as rapid urban development, a swelling population, and subsidized energy tariffs, Saudi Arabia's energy demand is on a steep rise, with annual per capita electricity consumption increasing at a fast rate over the past three decades (from 1990 to 2021), from an estimated 4 kWh per capita to 8.9 kWh per capita, as shown in Figure 2-7 (Al Harbi & Csala, 2019; IEA, 2021). Abuhussain (2020) indicated that electricity consumption per capita in Saudi Arabia is 'extremely inefficient' in relation to population growth, making it necessary to develop solutions to reduce kWh per capita. In 1992, the country recorded a consumption of 4.3 kWh/capita; demand rose to 8.5 kWh/capita in 2012 (i.e. twice the amount recorded in 1992) and continued to increase, rising to 9.5 kWh/capita in 2015. However, per capita consumption was reduced to 9.1 kWh in 2017, which may be the results of initiatives and governmental efforts to promote energy efficiency nationwide, as will be discussed in subsequent sections (GAS, 2023; The World Bank Group, 2022a).

CO_2 emissions:

Carbon dioxide emissions in Saudi Arabia are dominated by fossil fuel consumption (i.e. oil and natural gas) for energy generation and industrial purposes, with oil being responsible for the majority of the Kingdom's CO_2 emissions from fossil fuels (Climate Transparency, 2022; Ritchie, Roser, & Rosado, 2020). Carbon dioxide emissions per capita significantly increased over the past two decades (between 1990 to 2020) compared to global averages, as shown in Figure 2-8. Thus, the Kingdom is one of the nations with the highest per capita CO_2 emissions, with 17.3 metric tons per capita recorded in 2015. This was more than twice the CO_2 emissions generated in the European Union, which recorded 6.5 metric tons per person (The World Bank Group, 2023). Despite the country's efforts to reduce its CO_2 emissions, they remain higher than global averages. Considering the fact that oil is not a renewable source of energy, combined with a potential reduction in consumption in the future due to climate change agreements, it is crucial for Saudi Arabia to consider measures and design strategies to improve building efficiency and reduce energy-related carbon emissions.

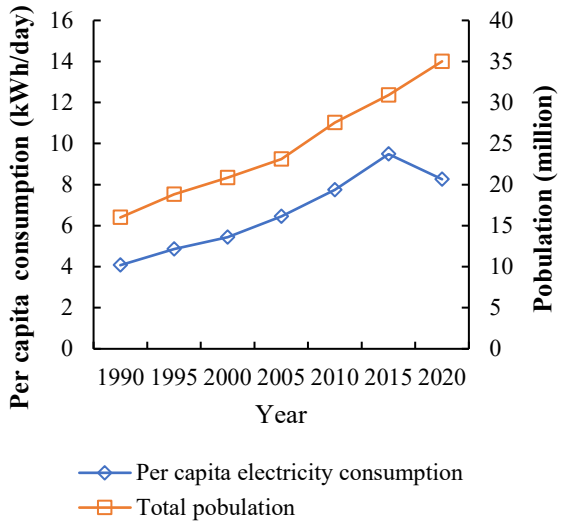


Figure 2-7 Per capita electricity consumption and total annual population in Saudi Arabia from 1990 to 2020. Data obtained from GAS (2023), Saudi Central Bank (2023), and The World Bank Group (2022a).

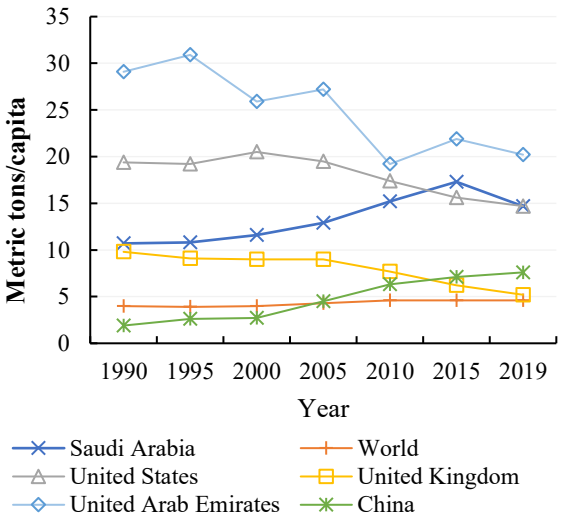


Figure 2-8 Per capita CO_2 emissions in Saudi Arabia compared with global trends between 1990 and 2019. Based on data from The World Bank Group (2023).

Energy consumption and the building sector in KSA:

Saudi Arabia relies mainly on fossil fuels (i.e. oil and natural gas) to generate electricity for domestic use, with a negligible amount of energy produced from renewable resources (Climate Transparency, 2022; IEA, 2021). On average, about half a million barrels of crude oil are consumed every day for power generation, with such consumption peaking in the summer (from June to August) (IEA, 2021). According to the Saudi Electric Company's annual report (2023), the total electricity produced in 2022 reached 362 TWH, or the equivalent of 348 million barrels of oil, which is and 50% more than the electricity produced in 2010.

The country is experiencing swift growth in electricity demand (IEA, 2021). In 2015, the maximum peak load reached 63.6GW, rising by 10% from 2014's peak load, with the highest peak load recorded over the period 1990–2020, as illustrated in Figure 2-9. Saudi Arabia produces most of its electricity from oil and natural gas, which account for about 40% and 60%, respectively (Climate Transparency, 2022; IEA, 2021), with annual electricity consumption exceeding 280 TWH in 2020, compared to nearly 60GW in 1990, as shown in Figure 2-9. The Kingdom thus plans to increase its total power generation capacity to 120GW by 2032 to meet the country's rapidly growing electricity demand (IEA, 2021). According to the Saudi Electricity Company's report, the highest recorded peak load took place in August at 13:00.

The building sector (commercial, governmental, and residential buildings) consumed an average of 75% of the country's entire provision of electricity, with an annual growth rate of 7% (Abuhussain, 2020; Al Harbi & Csala, 2019). Among all types of buildings, the residential sector contributes the most to total electricity consumption in Saudi Arabia. Over the past half-decade (between 2015 and 2020), the residential sector averaged nearly 50% of total electricity consumption, followed by the industrial and commercial sectors at 18% and 17%, respectively (see Figure 2-10). Within a decade, electricity consumption in the residential sector in Saudi Arabia increased by 45%, from about 89,000 GWh in 2007 to 130,000 GWh in 2018, with the highest consumption of 144,000 GWh reported in 2015 (Al Dubyan & Gasim, 2020).

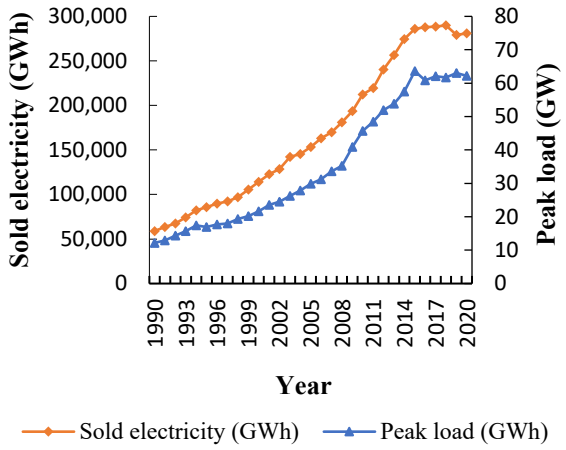


Figure 2-9 Sold electricity and peak load in KSA from 1990 to 2020. Data obtained from Saudi Central Bank (2023) and Saudi Electricity Company (2023).

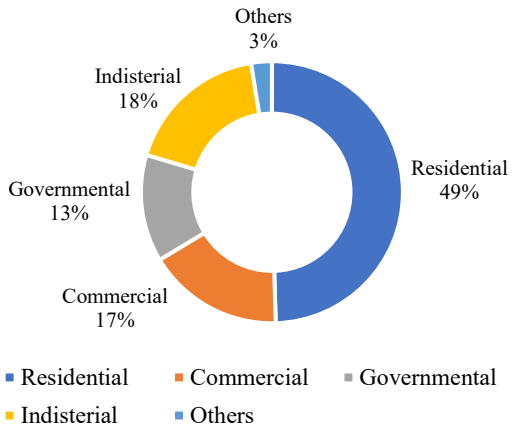


Figure 2-10 Average electricity consumption distribution in KSA between 2015 and 2020. Based on data from Saudi Central Bank (2023).

The hot climate of Saudi Arabia demands significant reliance on cooling systems to maintain indoor thermal comfort, especially during summer (from April to October) (Al Harbi & Csala, 2019). Accordingly, air conditioning systems account for 70% of the country's total electricity consumption, a rate that is double the consumption in winter. The high consumption of energy in the residential sector could be attributed to poor thermal performance. According to GAS's 2021 *Household Energy Statistics* report, about 65% of Saudi Arabia's residential buildings lack thermal insulation. As a result, the residential sector is a major contributor to the country's growing power demand, which, along with cooling demand, peaks in the summer. Abuhussain (2020) stated that most new buildings are developed to meet the client's needs, without attention being paid to local climates or efforts made to improve energy efficiency.

Moreover, Monawar (2001) stated that the subsidized electricity tariff in Saudi Arabia is a major factor contributing to significantly increased electricity demand in recent years due to the 'uneconomic electricity consumption' that resulted from the low prices policy. Alrashed (2015) pointed out that the subsidized electricity policy resulted in electricity prices that were lower than production costs. The average electricity price in 2014 was reported to be about 0.14 Saudi riyals (SAR) per kWh compared to 0.31 SAR per kWh in the USA (i.e. 50% less than the USA's average).

However, a number of initiatives and plans have been announced since 2016 to improve energy efficiency and reduce greenhouse gas emissions in Saudi Arabia (these will be discussed in the next section). Al Dubyan and Gasim (2020) highlighted the impact of these efforts on the recent decline in the residential sector's energy consumption in Saudi Arabia. Nevertheless, electricity demand from the building sector is expected to continue to grow over the next few years owing to contributing factors such as population growth and economic development (Abuhussain, 2020; Alrashed & Asif, 2015a; Belaid & Al Dubyan, 2021). Furthermore, the residential sector, the largest energy consumer in Saudi Arabia, is experiencing rapid growth. The following section will discuss the construction market and the significant housing demand in Saudi Arabia, followed by governmental programs and initiatives aimed at improving the sector's energy efficiency.

2.5 The construction and building sector in Saudi Arabia

Saudi Arabia is experiencing growing infrastructure developments that are driven by the oil boom, making its construction market among the most active in the world (Alrashed, 2015; Saudi Infrastructure EXPO). Among Gulf Cooperation Council (GCC) countries, the Kingdom has the largest and fastest-growing construction sector, with a greater than 60% share of the region's planned projects for the next years (Arab News, 2022; DC HUB, 2022; Statista, 2023). Considering the continuously growing demand for industrial, commercial, and residential buildings nationwide, the Saudi construction industry has great potential for growth. Based on construction permit statistics provided by the Ministry of Municipal and Rural Affairs, the GAS (2023) indicated that the total number of construction permits issued by regional municipalities grew significantly in recent years (Figure 2-11). Among all types of buildings, residential and commercial buildings make up most of these permits, accounting for 95% of the total issued construction permits in 2019 (see Figure 2-12).

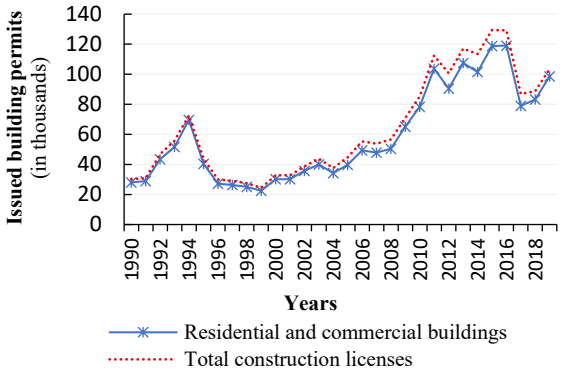


Figure 2-11 Number of constructions permits in Saudi Arabia between 1990 and 2019. Based on data from GAS (2023).

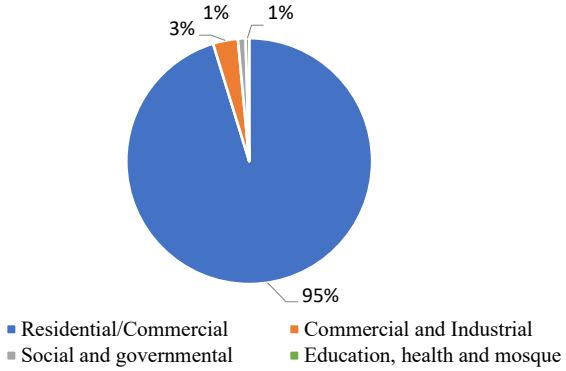


Figure 2-12 The distribution of construction permits by building sector issued in 2019 in Saudi Arabia. Based on data from GAS (2023).

In 2018, Saudi Arabia announced its ambition to increase home-ownership levels from the 47% reported in 2016 to 70% by 2030 as a part of Vision 2030 (Vision 2030, 2022b). Estimates suggested that the country would need to construct about 2.3 million houses by 2020 to fulfil the rising housing demand of the continuously growing population (Alrashed & Asif, 2015a). Accordingly, the Housing Program rapidly increased home ownership from 47% to 60% within a short time (2016–2020) by enhancing regulations, boarding financing access, and introducing advanced and modern construction technologies (Vision 2030, 2022b). The total number of units constructed in 2020 alone reached 344,550, a 4.3% growth rate compared to the 330,350 units built in 2019 (Ministry of Municipal Rural Affairs and Housing, 2023). Experts believe that the Kingdom will need to build about 1.2 million units by 2030, with an average of 124,000 units needed every year (Arabian Business, 2022; Shahrouri, Moghazy, & Awad, 2022; Zawya, 2022).

Significant housing demand and a rapidly growing population have resulted in a crucial need for dwelling construction at an urgent pace. In addition to the continual rise in energy consumption, this rapidly growing housing demand is expected to push the country to adopt advanced construction methods and materials, as conventional techniques may not be sufficiently efficient to satisfy the market's growing dwelling demand. The following sections provide an overview of the past and current status of the building sector in Saudi Arabia's different regions to understand the shift between vernacular and contemporary buildings and new initiatives in the building and construction sectors to address increasing energy and housing demands. Advances in construction methods will be discussed in detail in Chapter 4.

2.6 Past and current buildings in Saudi Arabia

2.6.1 Traditional buildings in KSA

Varying climatic conditions influence the design of buildings in KSA, motivating building typology and orientation (Elseragy, 2003). Saudi Arabia's climatic variability and topographic differences have resulted in the emergence of different architectural variations of traditional buildings. In addition to climatic influences, the Kingdom's geographical location affected the traditional style of architecture via the influence of neighbouring regions. Geographically, Saudi Arabia is divided into five different regions: central, western, eastern, southern, and northern. Traditional buildings are thus characterized by their uniqueness and diversity from one region to another in terms of design, typology, and materials, and have been influenced by the different environmental and climatic conditions of each region as well as adjacent neighbouring countries (Dwidar, 2019).

Various vernacular features—such as courtyards, water fountains, wind towers, and *mashrabiya*—were employed in traditional buildings to promote indoor thermal comfort and provide daylight. High thermal mass is another strategy that characterizes traditional buildings in hot and dry climate regions and is achieved by constructing thick walls using heavy materials such as mud, stones, and adobe (Mohamed, 2010). A discussion of design strategies in arid regions and their impacts on indoor thermal behaviour, energy performance, and user comfort will be provided in Chapter 3.

Local materials, such as clay, coral, and stone, were used in construction. The combination of adobe, sun-dried mud bricks, and mortar is considered the oldest and most widely recognized form of vernacular human-made construction material in the world and was used for more than a thousand years in arid regions such as the Middle East and Egypt (Dabaieh, 2011). It is basically created from clay, sand, and silt mixed with water, which is then cast into the desired shape. A small amount of straw, in many cases, is added to the mixture (Illampas, Ioannou, & Charmpis, 2009). To take advantage of thermal mass, the thickness of the adobe wall must be around 500 mm (Alrashed, 2015). Adobe was widely used as the main construction material in traditional buildings in Saudi Arabia due to its abundant availability and ability to moderate the harsh climate.

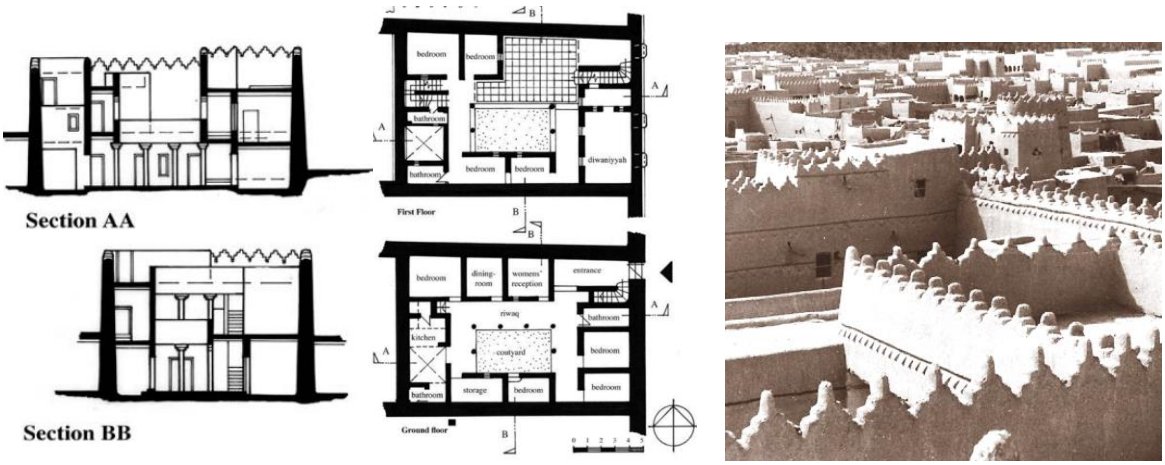
According to Abdulmajeed, Agkathidis, Dounas, and Lombardi (2022), Saudi Arabia's dwellings have historically undergone significant changes in response to society's changing needs, material availability, and advances in construction technologies. The use of adobe for

construction virtually disappeared with the introduction of steel and concrete in the construction industry during the late nineteenth century, despite adobe's superior thermal properties (Abdulmajeed et al., 2022; Saleh, 1990). In addition to the replacement of traditional construction materials, the vernacular elements of traditional building no longer appear in contemporary Saudi Arabian architecture. Undoubtedly, the emergence of new construction materials and systems introduced by foreign firms and architects, coupled with factors such as rapid urban development, a fast-growing population, and abundant and affordable air-conditioning systems and energy, have paved the way for drastic changes in the building and construction industry in Saudi Arabia.

For demonstration purposes, the following subsections present examples and analyses of traditional buildings from the five geographical regions of Saudi Arabia.

2.6.1.1 Tradition buildings of the central region (Najd):

The central region is the home of the capital city of Saudi Arabia, Riyadh, and has a hot and dry climate. Traditional buildings in the central region were constructed adjacent to each other, sharing two or more walls to make one large form. Most of the buildings in this hot climate were protected from outdoor conditions, especially through the use of narrow, shaded streets and pathways (Talib, 1984). The internal courtyard, which keeps the house shaded for most of the day, is one of the most important vernacular elements found in traditional buildings in this region. As shown in Figure 2-13, all rooms are arranged around a central courtyard open to the sky; this is the main source of natural ventilation and daylight, with limited and narrow openings on the external walls protecting the house from the heat and providing privacy. In some cases, wetlands (e.g. a water fountain) can be found in the courtyard to provide natural cooling by evaporation. To moderate the harsh climate, buildings in this region were built with thick adobe walls as the main construction material of the envelope. Such walls offer up to a 12-hour time lag and keep the house cool in the summer and warm in the winter (Dwidar, 2019; Facey, 2015; Taleb, 2011; Talib, 1984).



(A) (B)

Figure 2-13 Illustrations of traditional dwellings in the Riyadh region: (A) A typical floor plan (Facey, 2015); (B) External view (HCDR, 2023).

2.6.1.2 Traditional buildings of the western region (Hijaz style)

The western region of Saudi Arabia is situated along the western coast of the Red Sea. It contains several important cities, such as Jeddah, and is home to the sacred cities of Makkah and Al-Madinah. The architectural design and building techniques of Hijaz were influenced by the Ottoman Empire, which ruled the region centuries ago. Additionally, the significant role of Jeddah as a trading port, which allowed for cultural and commercial exchange between the region and other countries, along with the movement of pilgrims, have affected building technology in the region (Talib, 1984). Traditional buildings in this region were made of coral and mud blocks and wood. Stones were also commonly used in Hijazi dwellings. A thick layer of lime plaster was used for decoration purposes and to provide thermal comfort (Taleb, 2011).

The *mashrabiya* is one the most distinctive vernacular elements of traditional buildings in the Hijaz region (see Figure 2-14). It is a projected enclosed balcony or window covered with carved wooden screen and sometimes extends over several stories. Depending on its design, *mashrabiya* can perform several functions, such as controlling daylight, facilitating airflow, and ensuring occupants' privacy needs, in addition to adding aesthetic value to the building. In many cases, traditional clay water jars were placed in the *mashrabiya* to cool the air as it passed through the slots, providing an evaporative cooling effect in hot dry cities such as Makkah (Fathy, 1986; Talib, 1984).



Figure 2-14 Traditional buildings in the western region (Hariri-Rifai & Hariri-Rifai, 1990).

2.6.1.3 Traditional buildings of the eastern region (Arabian Gulf Coast)

The eastern region is situated between the coast of the Arabian Gulf to the east and the central region in the west and has a hot and dry climate. Traditional buildings in this region were influenced by neighbouring countries such as Bahrain and Kuwait. Locally available materials, such as mud and stone, were used to construct traditional buildings in the eastern region (Alrashed, 2015; Dwidar, 2019). Locals had to deal with excessive humidity and high temperatures. Some traditional buildings comprised an internal courtyard with deep entrances and colonnaded corridors around the courtyard to provide shade. Moreover, wind catchers (*badgirs*) were used to induce natural ventilation and control the amount of airflow entering the house through sliding boards, which can be closed during sandstorms. These wind catchers, with this specific design, are considered the main feature of vernacular building design in the eastern region as air movement during the humid period is required. As shown in Figure 2-15, window openings were provided on the covered corridor surrounding the courtyard, while external windows are limited and mostly provided on the upper floor to allow cross ventilation during the hot-humid season (Talib, 1984).

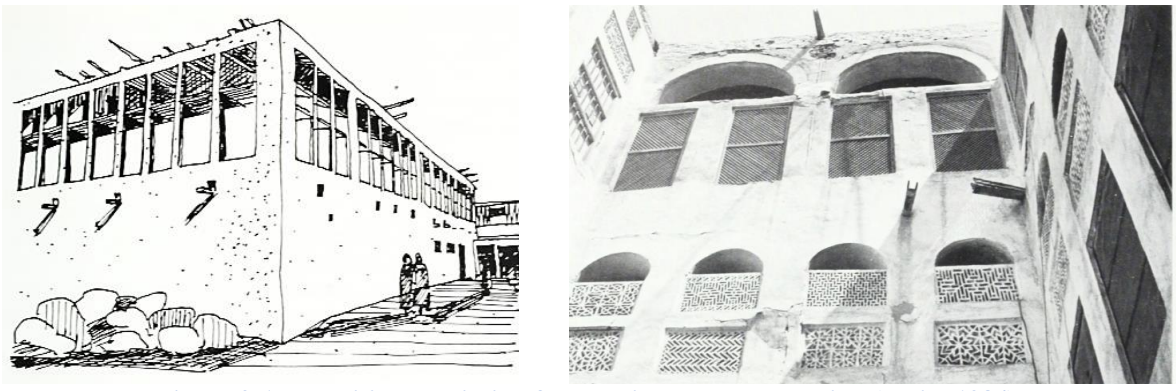


Figure 2-15 Traditional building features in the eastern region (Talib, 1984).

2.6.1.4 Traditional buildings of the southern region (Asir style)

The southern region extends from the Hijaz region, the western region, to the Yemen border in the south. The climate of the southern region varies from relatively cold in the hill and mountainous areas, the highest in Saudi Arabia, to hot and humid along the Red Sea Coast. Traditional buildings in this region are characterized by their diversity and were influenced by the region's variety of climatic conditions, topography, and natural resources. Different construction methods and materials were used in traditional buildings in this region, resulting in significantly different architectural styles (Alobailan & Alawad, 2022; Marzoq, 2010). For instance, straw houses were developed in coastal areas of the southern region known as Tihama Plains. These conical, hut-like houses were constructed using straw and mud. The design of these houses is meant to maximize indoor thermal comfort in the hot humid climate of this part of the southern region. The curved surfaces of these vernacular buildings minimized exposure of the external walls to solar radiation. In mountainous areas, traditional buildings were constructed from mud and stone. Plate stone layers were placed between the mud bricks, forming projecting slates from the wall, to provide protection against heavy rains. Traditional houses in the southern region were between three and four stories. Moving east towards the inner plateaus, the mud building style is dominant due to the lack of stone and an abundance of mud for construction (Alobailan & Alawad, 2022; Dwidar, 2019; Marzoq, 2010). The different styles of vernacular buildings in the southern region are shown in Figure 2-16.



Figure 2-16 Different styles of traditional buildings in the southern region (Alobailan & Alawad, 2022; Talib, 1984).

2.6.1.5 Traditional buildings of the northern region

Traditional buildings in the northern region are remarkably similar to those in the central region. Using the most effective passive solutions, traditional buildings were built to be adaptable to the local environment and achieve thermal comfort (Dwidar, 2019). Like vernacular houses in the central region, traditional buildings in the northern region were constructed from adobe, while stones were also sometimes used for construction. Design strategies include thick walls and courtyards. Streets were designed to be narrow to maximize

shading, and in many cases a suspended or bridging room can be found in two-story buildings to provide additional shade. Figure 2-17 shows images of traditional buildings in the northern region, illustrating their similarity to those in the central region (Talib, 1984).



Figure 2-17 Traditional buildings in Buraidah with small and protected openings on the external façade along with shaded, narrow streets (Talib, 1984).

2.6.2 Contemporary buildings in Saudi Arabia

The first attempt to revolutionize the built-up environment in Saudi Arabia and utilize reinforced concrete in the construction industry, instead of adobe bricks or stone walls and wood roofs, was in the Arab American Oil Company (Aramco) housing projects of the early '50s (Al-Hathloul, 1996). According to Al-Naim (2008), Aramco's housing projects in the eastern province sparked contemporary residential settlements in the country, introducing a new home image. The produced house was adopted for various projects in the country, such as the Al-Malaz residential district in Riyadh, as shown in Figure 2-18. Many sources have emphasized the social and economic developments the country underwent as a result of oil wealth, due to which the country experienced rapid development and modernisation in various sectors, including construction. Further, the rapidly growing population, along with changes in living standards, rendered traditional building materials inefficient in fulfilling and keeping up with significant demand (Abuhussain, 2020; Almehrej, 2015).

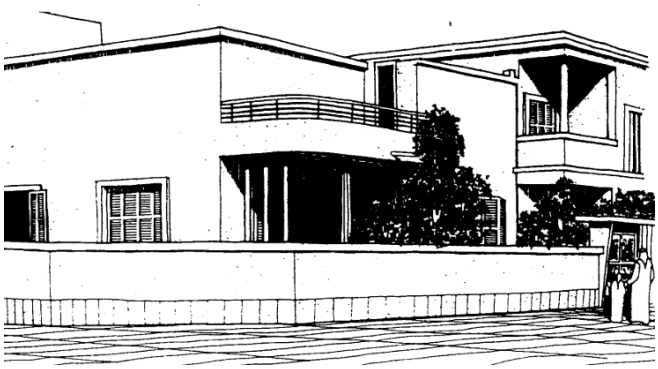
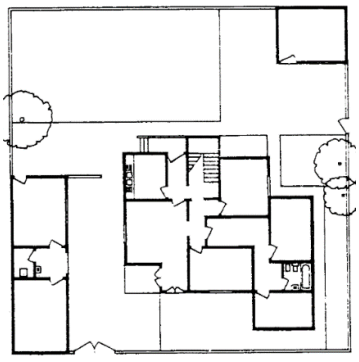
(A)  (B) 

Figure 2-18 Villa design introduced by ARAMCO and applied in the new housing development in Al-Malaz district, Riyadh: (A) External view; (B) Floor plan (Al-Hathloul, 1996).

Clearly, this shift towards modern architecture has increased reliance on imported modern materials, designs, and building techniques developed overseas. Almost all new buildings were constructed using reinforced concrete, which contributed significantly to expanding the imported and new building styles of the foreign architects. Thus, traditional building construction swiftly declined in the '70s. In addition, Al-Hathloul (1996) noted that during this modernisation period in the built environment of Saudi Arabia, a significant number of traditional buildings were demolished to make room for modern ones and planned settlements.

Unlike vernacular buildings, contemporary buildings do not reflect the climatic diversification of the country; rather, they share similar styles, typologies, and materials that are influenced by the market's needs, with little to no consideration for climatic conditions (Dwidar, 2019). The use of reinforced concrete in contemporary houses in Saudi Arabia not only quickened the construction process but also offered considerable potential for various volumes and greater spans, thus providing larger indoor spaces compared with the limited spaces in traditional homes built with thick load-bearing walls. The new methods of construction benefited from the mass production of concrete blocks, accelerating the building process and thus fulfilling the rapidly growing demand for new houses (Abuhussain, 2020; Almehrej, 2015).

The use of reinforced concrete has revolutionized the construction industry as far as building flexibility and durability are concerned. However, when it comes to thermal performance, this material lacks the thermal properties of traditional materials. Monawar (2001) indicated that reinforced concrete buildings have poor thermal behaviour in hot areas owing to their low resistance to heat flow, making them inadequate in such climates. In this context, Alrashed (2015) added that the use of air-conditioning systems is one of the main reasons for 'moving away' from the vernacular elements and bioclimatic features utilized in traditional buildings centuries ago to maintain indoor thermal comfort. All architectural knowledge developed over previous years seems to be ignored. As a result, these buildings rely mainly on energy-intensive cooling systems to maintain indoor thermal comfort.

2.6.3 Conventional construction methods and materials in KSA:

In Saudi Arabia, the reinforced concrete frame structure is the dominant conventional system for home construction and is commonly applied to various types of buildings (Abuhussain, 2020; Monawar, 2001). According to an analysis performed by GAS (2023), more than 85%

of existing residential buildings throughout the country were constructed from reinforced concrete. This structural system comprises cast in-situ reinforced concrete columns and beams, which are then infilled with concrete blocks or bricks to form external and internal walls. Floors and roofs are typically constructed using reinforced concrete slabs. Figure 2-19 shows images of residential buildings during their construction phase, illustrating the materials and construction methods of modern houses in Saudi Arabia.



Figure 2-19 Examples of residential buildings during the construction phase (images taken by author).

2.6.4 Typologies of residential buildings in KSA

Four major types of dwellings can be found in Saudi Arabia: villas, apartment units, traditional houses, and single floors in a villa. The distribution of these types varies across the country. According to statistical reports by GAS (2023), the dominant housing types in the country are apartment units (flats) and villas (detached/semidetached houses), which made up respective shares of almost 44% and 30% of the total residential units occupied by Saudi households in 2019. These are followed by traditional houses, which are typically occupied by low-income families, and other housing types, including annexes, at 18% and 8%, respectively (see Figure 2-20).

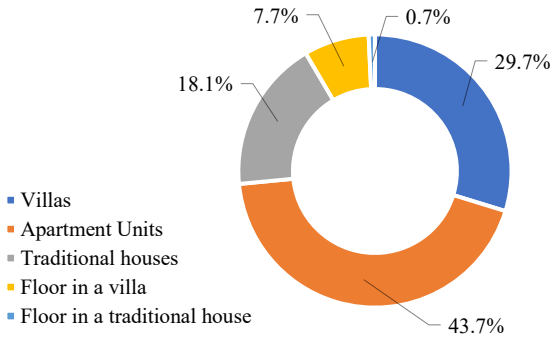


Figure 2-20 Housing types in Saudi Arabia. Based on data from GAS (2023).

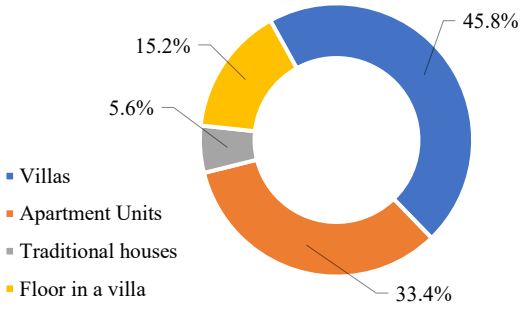


Figure 2-21 Housing types in Riyadh City. Based on data from GAS (2023).

As of 2019, Riyadh Province had one of the highest numbers of housing units, with a total of 865,390 units, representing nearly 24% of the total residential units in Saudi Arabia. As shown in Figure 2-21, the favoured housing type in Riyadh is the villa, which made up over

45% of the total units in the region, followed by apartment units and a floor in a villa (e.g. annex) at shares of 33% and 15%, respectively.

2.7 Initiatives and programs towards energy-efficient built environments

Saudi Arabia implemented a new long-term strategy for Vision 2030, which was announced in 2016, to promote the concept of sustainability and highlight the challenges of meeting the future's growing requirements. Saudi Vision 2030 (SV2030) is a broad privatization and economic reform program aimed towards shifting the country's economy away from oil revenues and improving government spending efficiency (Al Surf & Mostafa, 2017). It comprises 13 executive programs, known as Vision Realization Programs, targeting 96 strategic objectives, with the energy sector being among the most significant areas of reform. The scheme involves implementing reforms and reducing subsidies in several industries, including the energy sector, to bring domestic prices closer to the global market (Al Dubyan & Gasim, 2020; Al Harbi & Csala, 2019).

As mentioned in Section 2.4, electricity consumption is experiencing swift growth, with peak load anticipated to rise at an annual rate of about 7% over the next few years. As discussed by Al Harbi and Csala (2019), the country's energy plans include preventing oil spillage, reducing subsidies by gradually rising energy tariffs in multiple phases over the next few years, and conducting massive energy reforms to reassess all sources of energy. Moreover, Saudi Arabia intends to develop energy consumption control in the country with greater efficiency by concentrating on minimizing consumption during peak demand periods.

In 2016, Saudi Arabia launched its plan to reform energy costs as the initial phase of a policy that aims to rationalize the consumption of energy and improve energy efficiency. Energy prices rose from an extremely low base level and were still far below global market levels (APICORP, 2018). Early in 2018, domestic electricity tariffs were revised by applying only two consumption brackets instead of the four categories established in 2016, in addition to the implementation of a Value-Added Tax (VAT) (AlGhamdi, 2019). Thus, electricity prices for the low consumption brackets were increased significantly from 0.05 SAR per kWh to 0.18 SAR per kWh, whereas monthly household electricity consumption levels above 6,000 kWh were unaffected during the second wave of reforms (see Table 2-2).

Table 2-2 Residential electricity tariffs before and after reforms. Adapted from Al Dubyan and Gasim (2020) and AlGhamdi (2019).

Consumption (kWh)	Prices before price reform (2000–2015)		First wave of price reform (2016–2017)		Percentage change	Second wave of price reform (2018–present)		Percentage change
Residential	SAR/kWh	US$/kWh	SAR/kWh	US$/kWh	%	SAR/kWh	US$/kWh	%
≤ 2,000	0.05	0.01	0.05	0.01	0%	0.18	0.05	+260%
2,001–4,000	0.10	0.03	0.10	0.03	0%	0.18	0.05	+80%
4,001–6,000	0.12	0.03	0.20	0.05	+67%	0.18	0.05	−10%
> 6,000	0.15 to 0.26	0.04 to 0.07	0.30	0.08	50% to 1%	0.30	0.08	0%

2.7.1 The Saudi Energy Efficiency Centre

As part of the country's efforts to control domestic energy consumption and improve energy management, several organizations and programs were introduced. The Saudi Energy Efficiency Centre (SEEC) was established in 2010 to improve energy consumption efficiency, unify the efforts of all relevant partners in public and private sectors in this field, and raise awareness and capabilities about rationalization and energy management (Al-Tamimi, 2017; SEEC, 2023). By supporting and preserving the abundance of local energy sources, these efforts contribute to strengthening development and the national economy as well as helping minimize consumption levels in the building, industrial, and transportation sectors. Al-Tamimi (2017) summarized SEEC's achievements in the building sector as follows:

- Initiating technical regulations concerning buildings' thermal insulation.
- Developing the Saudi Building Code's Energy Conservation Requirements (SBC 602).
- Updating specifications for household appliances and monitoring products such as air-conditioners, refrigerators, lamps, etc.
- Enforcing the use of energy efficiency labels for all household appliances to inform consumers about their energy consumption rates (see Figure 2-22).

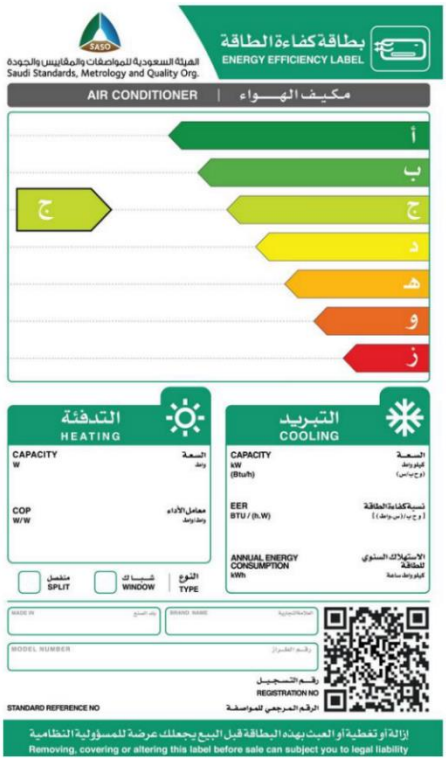


Figure 2-22 Example of energy efficiency label for household appliances (Abuhussain, 2020).

Furthermore, significant awareness campaigns were implemented through various media outlets, social media, brochures, and workshops as part of SEEC's efforts to educate the public about methods of reducing energy consumption (Al Harbi & Csala, 2019; SEEC, 2023). These energy insight solutions include, in addition to a set of recommendations, using highly efficient equipment and improving consumption patterns. For example, SEEC recommends that all users set their air conditioning to no lower than 24 °C and their water heater temperature to a maximum of 60 °C to reduce energy requirements for cooling and domestic hot water.

2.7.2 Building code

Among the initiatives carried out over the past few years was developing the Saudi Building Code (SBC). The code was established as early as 2000, and its initial version was made publicly accessible in 2007 (Al-Tamimi, 2017). The SBC outlines the minimum standards and specifications of building construction through a set of legal, technical, and administrative requirements and guidelines to ensure the safety and health of the public. The initial version of the code incorporates requirements from various sectors such as structural, architectural, mechanical, electrical, fire protection, and sanitary.

As energy consumption was at relatively low levels and no serious threats were anticipated from peak loads, the initial version of SBC neglected buildings' energy efficiency performance (Alaidroos & Krarti, 2015). As previously discussed, Saudi Arabia experienced a sharp increase in electricity consumption from both industrial and building sectors, driven by swift population growth and rapid economic development. Alaidroos and Krarti (2015) indicated that a lack of standards and regulations concerning energy efficiency exaggerated the increase in domestic energy consumption in recent years, resulting in an urgent need for the building energy code to be redeveloped to specify minimum requirements for buildings and to advocate energy-efficient and high-performance building construction.

The SBC for 'Energy Conservation Requirements' was developed based on the International Energy Conservation Code (IECC) and ASHRAE standard 90.1. It provides energy conservation requirements for residential and commercial buildings, which comprises general requirements, mechanical systems and equipment, building envelope requirements, electrical power and lighting systems, domestic water heating systems, and total building performance (Al-Tamimi, 2017; Alaidroos & Krarti, 2015). Notably, initial application of the building energy conservation code in 2009 was on a voluntary basis, becoming mandatory for

governmental buildings in 2010; however, it was not yet enforced for other building types, such as residential buildings. Nevertheless, it was not until 2014 that the application of thermal insulation on walls and roofs became a mandatory requirement for all new constructions as a prerequisite to connecting new buildings to electrical services provided by the Saudi Electricity Company (Asif, 2016; Krarti, Dubey, & Howarth, 2017). By the end of 2018, an updated version of the energy conservation code was released; SBC 602 for low-rise residential buildings was enforced in 2020 for all new residential buildings. This code will be adopted and investigated within the interests of this research. All thermal performance-related requirements for the building envelope outlined in BSC 602 will be described and discussed in the following section.

2.8 SBC 602 for low-rise residential buildings

SBC 602 provides basic standards and minimum energy efficiency-related requirements for low-rise residential buildings in Saudi Arabia. This code applies to all new low-rise and residential buildings that are specified for residential purposes, with a maximum height of 3 stories above ground level (e.g. single-family dwellings). To enhance residential buildings' thermal performance and energy efficiency, the standard defines the required thermal transmittance value for such buildings. It excludes existing buildings unless renovation or modification processes are undertaken.

As discussed in Section 2.3, Saudi Arabia was climatically categorized into three distinct climatic zones by the Energy Conservation Code based on CDD. Accordingly, SBC 602 (2018) regulates maximum acceptable levels of thermal transmittance (U-value) for building envelope components (i.e. walls, roofs, fenestrations, and doors) for each climate zone. The SBC 602 thermal requirements for low-rise residential buildings are shown in Table 2-3.

Thermal transmittance (U-value), also known as the coefficient of heat transfer, is the time rate of heat transfer through the skin of the building per unit temperature difference between indoor and outdoor environments. It is measured in units of Watts per square meter per Kelvin ($W/m^2 \cdot K$). For a multi-level element, such as a wall, the U-value is calculated as the inverse of the sum of the thermal resistance (R-value) of each material making up the element. Thermal resistance (R-value) is the ability of a material to resist heat flow and is measured in $m^2 \cdot K/W$. It is described by the material thickness divided by the thermal conductivity of the material. Thermal conductivity is the heat flux through a unit thickness of a material, with a unit temperature difference between the two surfaces of the material and is

measured in units of W/m·K. Materials with lower thermal conductivity have higher thermal resistance and vice versa.

As shown in Table 2-3, the SBC 602 limits the Window-to-Wall ratio (WWR) to a maximum of 25% in all three zones. WWR is the ratio between the glazed surface areas of an external wall to the gross area of the wall. For external glazing, the code outlines two performance regulations for all climate zones: a maximum 2.67 U-value and 0.25 SHGC. Solar heat gain coefficient (SHGC) is the fraction of solar energy transmitted through glazing, with a rate between 0 and 1. Windows with lower SHGC values admit less solar energy and have greater shading ability. The 0.25 SHGC requirement can be met by using highly efficient window glazing types. Alternatively, the code credits the application of suitable shading devices (e.g. overhangs). To apply this credit, overhangs must be permanent and with a minimum horizontal projection factor of 0.5. Solar gain and window shading strategies are discussed in more detail in the following chapter.

Table 2-3 Envelope thermal requirements of the Saudi energy conservation code. Adapted from SBC 602 (2018).

Opaque elements	**Zone 1** (Riyadh City)	**Zone 2** (Ha'il City)	**Zone 3** (Asir City)
Roofs	0.202	0.238	0.273
External walls	0.342	0.397	0.453
Ground floor	0.496	0.496	0.496
Opaque doors–all assemblies	2.839	2.839	2.839
Vertical glazing (WWR: 25%)			
All assemblies	2.668	2.668	2.668

2.9 The Building Technology Stimulus Initiative

As previously discussed, Saudi Arabia experiences significant housing demands driven by swift population growth and rapid economic development. The housing market in Saudi Arabia has been known for its short supply. The conventional reinforced concrete frame construction system is both labour intensive and time consuming, making commonly applied construction methods and techniques inefficient to satisfy the significant housing demand (Abdulmajeed et al., 2022; Alabbasi, 2021). Thus, adopting new building methods and techniques is urgently needed to deliver high-quality dwellings at a faster pace.

The Housing Program, launched in 2018 as one of the Vision Realization Programs, was developed to help the country achieve the goals of Vision 2030. The program is committed to providing suitable accommodation for all Saudi citizens and to improving the efficiency and

performance of the real estate sector, thus maximizing the industry's contribution to the local economy and fulfilling the social and economic objectives of Vision 2030.

Recently, the Ministry of Municipal and Rural Affairs and Housing began to roll out a series of initiatives and solutions, in collaboration with the private sector, to relieve housing shortages in the market, broaden financing options, and reform the housing sector and planning policies (Shahrouri et al., 2022). The Building Technology Stimulus Initiative (BTSI), or the Modern Building Initiative, was developed as part of the country's efforts to reform the housing sector and respond to increasing demand (Alangari & Alzamil, 2020).

The initiative stimulates the adoption of modern and innovative building technologies in Saudi Arabia's construction industry to address the gap in demand for affordable residential units at reasonable prices. The primary goal of BTSI is to support and transform the construction industry from the dominant conventional method to modern construction techniques by investing in innovative and modern technologies that facilitate industrial development, thereby emphasizing the country's leadership in this field.

To ensure that the country's aspirations are being achieved, the initiative is managed by three departments: the Housing Program, the Private Sector Stimulus Program, and the National Industrial Development and Logistics Program (Ministry of Municipal Rural Affairs and Housing, 2022). BTSI outlines a set of strategic goals centred around social, economic, and technical concerns:

- Reduce construction time to less than three months.
- Improve construction quality and raise satisfaction levels around building technology products.
- Reduce construction expenses by between 5% and 20%.
- Increase the contribution to gross domestic product to about 80 million Saudi Riyal (21.33 million US dollar) and improve the utilization of local goods by 70%.
- Create up to 7,000 job opportunities in the construction field and reduce the number of low-skilled construction workforces.

On top of these benefits, Alangari and Alzamil (2020) indicated that increasing housing demand in Saudi Arabia has caused the need for the emergence and development of new building technologies. The country aims to increase the share of new houses constructed through modern construction techniques to 40% by 2030 (Ministry of Municipal Rural Affairs and Housing, 2022). BTSI seeks to transform the construction industry in Saudi

Arabia by incorporating feasible, sustainable, and intelligent construction methods. In addition, it aims to cope with the Fourth Industrial Revolution by creating an attractive environment for innovative construction methods, including additive manufacturing and robotic technologies, in the local construction market through a subsidisation scheme.

Alangari and Alzamil (2020) discussed the most prominent forms of modern building technologies adopted by the BTSI, which include insulated concrete forms (ICF), insulted precast systems (IPS), and 3D printing techniques. This study will focus on 3D printing technology since it is considered the most recent technology applied in the construction industry (Alangari & Alzamil, 2020). Advances in the construction industry will be discussed in more detail in Chapter 4.

2.10 Summary

This chapter presented an analysis and background review of the KSA. The KSA is experiencing severe energy and environmental challenges. The building sector is a major contributor to the significant growth rates of energy demand and CO_2 emissions, with residential buildings alone accounting for approximately 50% of total national energy consumption (see sections 2.4 and 2.5).The shift away from vernacular architecture, which incorporated climate-responsive design strategies, to modern energy-intensive houses was discussed in Section 2.6. This transition has contributed to the considerable energy consumption of the building sector and increased CO_2 emissions, as modern housing developments often neglect KSA's unique climate challenges.

Given expected future growing energy demands, especially from residential buildings, this chapter highlighted governmental efforts to enhance energy efficiency in the building sector. Due to its rapidly growing population, and because conventional construction materials and techniques may not be sufficient to cope with growing housing demands, Saudi Arabia has been pushed towards digitizing its construction industry (see Sections 2.7–2.9). Therefore, it is worth noting that modern, innovative constructions should be considered in this research to assess their thermal performance, ascertain their suitability to the severe climate context of KSA, and provide insights for future housing development and the building code.

It is worth noting that the two selected case study buildings—a 3D-printed house and a conventionally constructed house—are located in different urban contexts within Riyadh, which introduces variations in microclimate exposure; further details are provided in Chapter 5. In light of the broader energy, environmental, and construction trends highlighted in this

chapter, this thesis evaluates key building fabric and passive design strategies (summarized in Sectio 5.9) to improve the thermal performance of residential buildings and contribute a more sustainable built environment in Saudi Arabia

CHAPTER 3

ENVELOPE DESIGN AND THERMAL COMFORT

- Building's envelope
- Thermal transmission and heat gain control
- Thermal comfort
- Adaptive design strategies in hot regions
- Envelope design and energy performance

Chapter 3: ENVELOPE DESIGN AND THERMAL COMFORT

3.1 Introduction

As discussed in Chapter 2, contemporary buildings in KSA are designed without considering the local climate, resulting in a heavy reliance on active systems to cope with severe climate conditions and thus contributing significantly to the country's energy consumption and CO_2 emissions. Hence, improving building thermal performance by applying various design measures is considered one of the most effective strategies to reduce this consumption.

This chapter discusses the multifunctional building envelope to understand the environmental and energy performance of this key building element. It reviews passive cooling techniques recommended for areas and regions with hot climates with the aim of establishing an analytical framework for interpreting empirical data in the later chapters of this thesis. Indoor thermal comfort is also outlined in this chapter, including the key factors affecting thermal comfort. Lastly, the chapter discusses previous studies concerned with improving the thermal performance and energy efficiency of residential buildings through the application of passive strategies, including thermal optimization of the building envelope, in hot and arid regions.

3.2 The building envelope

According to the American Society of Heating, Refrigerating and Air-Conditioning Engineers (ASHRAE) (2013a), the envelope is not only the building's external element that separates conditioned and unconditioned spaces but also encloses semi-heated spaces where heat may be transferred to or from the exterior, to or from conditioned spaces, or to or from unconditioned spaces. Thus, it greatly influences the maintenance of the indoor environment, which is significantly impacted by outdoor environmental conditions, at comfortable levels throughout the year. Szokolay (2004) considered the envelope to be a 'selective filter' that excludes undesired environmental influences while allowing desirable ones such as daylight and ventilation. This description gives the envelope the function of controlling indoor thermal conditions (John, Owen, & Theo, 1992), facilitating both passive and active systems for cooling and heating demands (Hyde, 2008), and protecting the building and its indoor environment from extreme climatic conditions (Mirrahimi et al., 2016). Thus, the building envelope can significantly reduce a building's energy consumption by preventing the penetration of unwanted solar radiation, facilitating natural ventilation, and serving as a thermal barrier.

Lechner (2014) stated that the use of efficient thermal envelopes is a key strategy to improve energy efficiency and make buildings 'resilient' against extreme and undesirable events, including weather conditions. The design of a 'tight thermal envelope' is considered the most efficient strategy for heating and cooling a building and forms the base level of the hierarchical three-tier design approach proposed by Lechner (2014, p. 484):

- Using heat avoidance-related strategies and reducing heat flow through the envelope.
- Utilizing passive cooling strategies and systems based on natural energies.
- Using mechanical systems and renewable energy, if needed, within the already passively optimized design.

As indicated by DeKay and Brown (2014), a building's energy consumption is mainly influenced by the three major factors: (1) climate, which includes changes in outdoor conditions (e.g. temperature, wind patterns, relative humidity, etc.), (2) the building's use, which includes operational features concerning a building's program and occupants, and (3) the building's design, which includes the envelope and construction materials. Of these factors, the building's design is the most controllable by designers and architects. Through various design strategies, designers can provide comfortable environments with little to no use of active systems. In this case, Szokolay (2004) described buildings as a 'thermal system' with various heat inputs and outputs, similar to the human body's need to maintain its thermal balance, as discussed later in this chapter. As demonstrated in Figure 3-1, this system can be described by Equation (3-1) (Szokolay, 2004, p. 34).

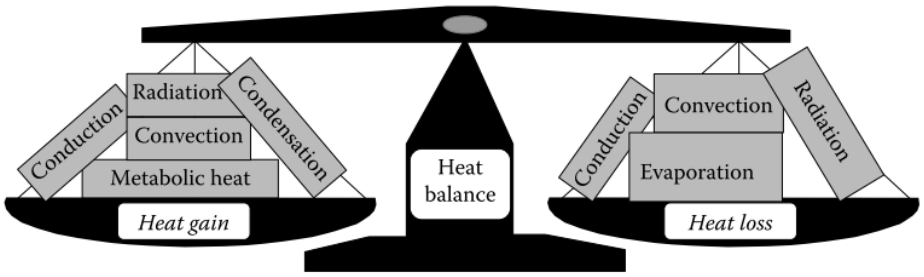


Figure 3-1 Representation of the heat balance equation (Parsons, 2014).

$$\boldsymbol{Qi + Qc + Qs + Qv + Qe = \Delta S} \qquad \textbf{(3-1)}$$

Where:

- Qi is internal heat gain.
- Qc is conduction heat gain or loss.
- Qs is solar heat gain.
- Qv is ventilation heat gain or loss.
- Qe is evaporative heat loss.
- ΔS is a change in heat stored in the building.

According to Szokolay (2004), thermal balance occurs when ΔS equals zero. If ΔS is greater than zero, the indoor temperature is increasing; if it is less than zero, the indoor temperature is decreasing. As indicated by Kiamba (2016), this equation can be manipulated using heat avoidance and modulation strategies to boost cooling in hot regions. A number of scholars have highlighted the crucial role of the envelope's components and characteristics in indoor thermal performance due to its consistent exposure to the outdoor environment. In the following sections, the multi-functions of the envelope are discussed in terms of heat transfer, solar control, and ventilation, in addition to strategies to mitigate unwanted gain through the envelope.

3.3 Thermal transmission and heat gain control

Buildings continuously exchange heat with the outdoor environment. Heat transfers from a higher temperature zone to a lower temperature zone through conduction, convection, and radiation (ASHRAE, 2013b). The heat flow rate through the envelope is influenced by several factors, including volume-to-area ratio (ratio of the skin area to floor area), the properties of wall construction materials and insulation thickness for opaque surfaces, glazing area and type for transparent surfaces, along with the function of the building and its occupancy, which determine the difference between indoor and outdoor temperature (DeKay & Brown, 2014).

From the heat flow point of view, a building envelope can be categorized into two main components: opaque surfaces, which include walls, roof, and floor, and transparent surfaces, which include windows and skylights (Mirrahimi et al., 2016). Each of these categories exhibits distinct thermal transmission characteristics, necessitating different control strategies to manage heat transfer effectively. According to the literature review, implementing heat gain control strategies is crucial for mitigating indoor temperature and preventing excessive heat buildup inside a building. These strategies can significantly reduce energy requirements for cooling while maintaining occupants' thermal comfort.

As discussed in Section 2.8, thermal transmittance (U-value) is a function of materials properties in the envelope and can be reduced by adding insulation layers. According to Szokolay (2004), insulation controls the flow of heat through the envelope. For this purpose, three different insulation mechanisms can be identified: reflective, resistive, and capacitive. Reflective and resistive insulations are used mainly to reduce the magnitude of heat flow (i.e. radiant and conductive heat, respectively), while capacitive insulation has the additional

advantages of affecting the timing of heat flow by relying on the material's thermal capacity and ability to delay heat flow.

Kiamba (2016) suggested that by delaying heat flow, heat gain can be avoided when internal spaces are occupied, thereby reducing active system loads. Szokolay (2004) stated that the mass effect performs better in hot and dry regions with high diurnal temperature differences. Figure 3-2 illustrates the lag time of a thick wall, which can insulate the building to prevent overheating indoor spaces, especially during the summer in a hot and dry climate area. The application of thermal mass as a cooling strategy in hot climates is explored further in Section 3.5.

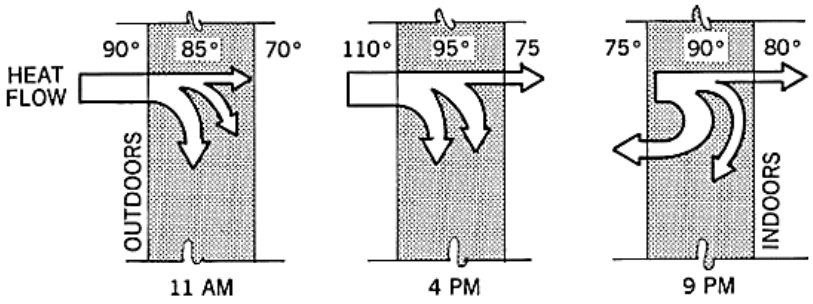


Figure 3-2 The time lag effect of a massive wall at various times of the day during the overheating season in hot and dry climates. Adapted from Lechner (2014).

According to Szokolay (2004), the dynamic properties of a multi-layer envelope element depend not only on the material's properties and thickness but also on the layers' arrangement relative to the heat flow direction. In this case, the placement of the insulation layer must be considered and examined (e.g. outer, inner, and middle layer). For example, placing the insulation material on the external layer of the wall or in the cavity with exposed thermal mass in the indoor environment allows the inside to benefit from the resulting heavyweight material (i.e. thermal storage mass) with significantly less heat gain. Conversely, when insulating the inner layer, the inside will become lightweight (i.e. without thermal storage mass), and the resulting heat gain can risk overheating during the day. According to Baker and Steemers (2000) and Saulles (2019), isolating a heavyweight material with lightweight finishes reduces the thermal mass's effect on the thermal behaviour of the building.

As for the transparent elements of the envelope, Givoni (1998) identified four independent factors influencing the U-value in glazing:

- The existence of air gaps between glazing layers and their number.
- The type of gas used to fill air gaps.

- The properties and/or treatment of the glazing material and surfaces.
- The materials and detailing of the window's frames.

Compared with other building materials, glazing has a lower resistance to heat flow and thus more heat is transmitted through glazing (DeKay & Brown, 2014). Windows can be made with a single pane or multiple panes (e.g. double or triple glazing) with an air gap (or gaps) between the glazing layers. The air gaps tend to improve the window's thermal resistance to heat flow (i.e. reducing its U-value). Across the air gap, heat is transmitted mainly by convection and radiation. The convection part is affected by the width of the space, whereas the radiation effect can be modified by applying special treatments (i.e. coatings) on the glazing layer. A window's U-value is also affected by the type of gas used to fill the air gap, such as argon or krypton, which have lower thermal conductivity than air.

Solar radiation is a major contributor to heat gain in buildings, particularly in hot and arid regions. Controlling solar heat gain is crucial for preventing indoor overheating and reducing cooling energy demands. The following section explores various strategies to mitigate the impact of solar heat gain.

3.3.1 Solar heat gain

According to Szokolay (2004), solar heat gain through the building envelope is considered differently from opaque and glazing elements. DeKay and Brown (2014) indicated that the portion of the available solar heat reaching the indoor environment through opaque surfaces is between 0% and 12%, depending on the insulation quality and the colour of the exterior surfaces of the envelope. Despite the significant solar heat gain through opaque surfaces in some cases (e.g. inadequately insulated roofs), it is often a small percentage compared to the gain through glazing, which can be as high as 85% of the total incident insolation. Solar gain is highly dependent on the area of the glazed surfaces of the building envelope, their orientation, and heat transmittance, in addition to the climate, which determines the availability and intensity of solar radiation.

The glazed elements of the building envelope are highly associated with solar gain due to their nature to admit solar radiation. While different glazing types transmit different amounts of solar radiation, all are opaque to the long-wave radiation emitted from indoor elements (Givoni, 1998). Thus, the trapped heat inside the building will cause the indoor temperature to increase, creating the 'greenhouse effect'.

Solar energy input requirements are opposed due to the different thermal requirements caused by the change of seasons. For the most efficient control of solar radiation input into buildings, it is important to determine the need for shading, such as when solar radiation should be excluded (overheating seasons) or when it would be acceptable energy input (solar heating) (Szokolay, 2004). To avoid overheating risks, which is the case in hot climates, Kiamba (2016) noted that solar heat gain can be controlled by two main methods: orientation and the application of shading.

Building orientation is one of the most important considerations during the early stages of the design process. Solar radiation intensity patterns on vertical surfaces are different from time to time throughout the year and are highly dependent on the latitude of the location of the building and the surface's orientation. In areas near the equator, horizontal surfaces (e.g. roofs) receive the highest solar radiation input owing to the high altitude of the sun in these areas (see Figure 3-3). Due to the daily apparent movement of the sun, solar radiation on the eastern and western walls is much greater year-round than on the southern and northern walls.

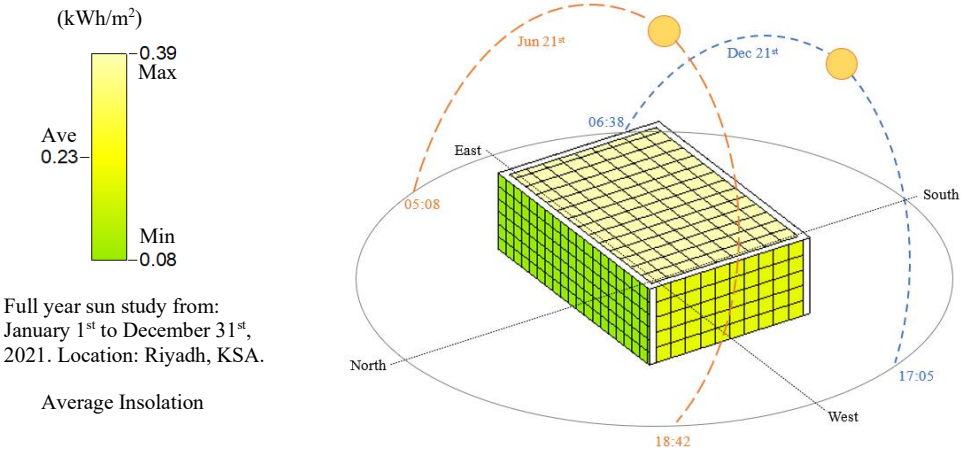


Figure 3-3 Solar radiation received by envelope elements in Riyadh City, Saudi Arabia. Note that the preferred orientation is along the east and west axis to maximize northern and southern exposure. Reproduced from Autodesk Rivet (2022).

Considering the high year-round temperatures in arid regions, avoiding summer overheating takes precedence over winter needs (Givoni, 1998; Olgyay, 2015). Thus, windows should be avoided on the west and southwest orientations whenever possible to avoid afternoon overheating risks. North-facing windows, however, can benefit from indirect daylight with minimal heat gain, creating a comfortable environment, especially during the cooling season. South-oriented windows can provide direct and indirect daylight; however, uncontrolled solar gain increases indoor overheating concerns, especially during the cooling season.

Besides controlling solar heat gain, Olgyay (2015) stated that building orientation is also influenced by other contributing factors, including indoor privacy requirements, the pleasure of the view, and the local topography of the site, in addition to other climatic factors, such as ventilation requirements. In many cases, these requirements may override those of solar control, making the application of shading necessary. Shading strategies allow designers to limit the impact of large glazing ratios or unfavourable orientation.

For window glazing, it is important to know the solar heat gain coefficient (SHGC), which measures the window's ability to admit solar energy (see Section 2.8). In hot and arid regions, windows with lower SHGC values can decrease cooling load by excluding solar energy. A typical single-clear glazing has an SHGC value of 0.81. However, increasing the pane number reduces the SHGC of the window (e.g. 0.73 for double-clear and between 0.6 and 0.7 for triple-clear). While in some cases the colour or coated glazing could reduce SHGC values to as low as 0.2, this may risk increasing artificial lighting operation hours and reducing winter heat gain (Lechner, 2014).

Shading devices are a common strategy to reduce solar heat gain and control both visual and thermal environments. The design of shading devices and their shapes and positions are dependent on the geometrical relationship between the sun and the façade of the building (Al-Qahtani & Elgizawi, 2020; Lechner, 2014). According to John et al. (1992), shading systems can be fixed (structural or non-structural objects) or movable (manually or automatically controlled) and can be placed internally (e.g. blinds or curtains), externally (e.g. fins or overhangs), or within double-glazed panels.

Since internal shading is normally fitted behind the glazing, most of the solar radiation that passes through the glazing is absorbed by the shading element (e.g. blinds). The absorbed energy is then converted and re-radiated as long-wave radiation. As a result, heat builds up between the shading system and the glazing, thereby reducing the system's efficiency (John et al., 1992). This may also increase indoor mean radiant temperature (MRT), causing discomfort.

Applying external shading devices is the most effective strategy to control solar penetration (Szokolay, 2004). Many researchers favour these tools as they intercept direct solar radiation before it reaches the transparent surfaces of a given façade (Prieto, Knaack, Klein, & Auer, 2017; Ralegaonkar & Gupta, 2010). There are three distinct categories of external shading devices: horizontal, vertical, and egg-crate elements (see Figure 3-4). When designing

shading devices, it is critical to identify the time of the year when shading is needed (overheated period) or when solar input would be desirable (underheated period). To promote the efficiency of shading devices, a shading mask is used, which can be conveniently structured using a shadow angle protector and a sun path diagram, as explained by Szokolay (2004).

Since shading devices are designed to intercept solar radiation at a given angle, many small elements can achieve shading performance similar to one large shading device. The ratio between the depth of the shading device and the shaded part of the window is, however, the same (Lechner, 2014).

Horizontal shading devices are distinguished by vertical shadow angles (VSA). The VSA is measured on the vertical plane and normal to the surface. Horizontal shading elements are most effective when the sun is nearly opposite to the window (i.e. southern orientation). Vertical shading elements (e.g. vertical fins) are distinguished by horizontal shadow angles (HAS). The HAS is the difference between the solar azimuth and the azimuth of the surface normal (i.e. orientation). It is measured from the surface normal (positive in clockwise and negative in anticlockwise directions) and cannot be greater than 90° or less than −90°, as it would indicate that the sun is behind the surface. Vertical shading elements are most effective when the sun is towards one side of the orientation that the window is facing (i.e. east and west orientations). The egg-crate shading system is basically a combination of the vertical and horizontal shading systems, considering both VSA and HSA (John et al., 1992; Szokolay, 2004).

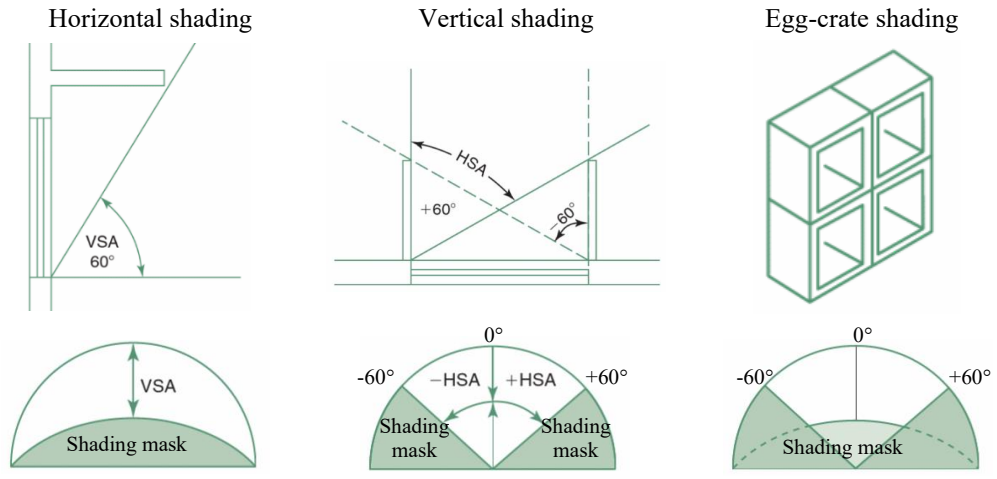


Figure 3-4 External shading devices and their shading masks. Adapted from Szokolay (2004).

3.3.2 Solar reflectivity

Lechner (2014) stated that heat gain through the roof can be reduced not only by applying more thermal insulation but also by reflecting the solar radiation. The solar absorptance of a roofing material is largely influenced by its colour, with lighter colours reflecting more solar radiation. Solar absorptance measures the fraction of incident solar radiation absorbed by a surface and is expressed as a numerical value between 0 and 1. This measurement is crucial for understanding how much heat a roof can retain, which directly impacts building thermal performance and energy efficiency. A lower solar absorptance value (i.e. higher albedo) indicates that a surface absorbs less solar radiation (i.e. reflects more sunlight). The colour white has the highest solar reflectivity, with an albedo of about 0.9 (or 0.1 solar absorptance), which indicates that 90% of the received sunlight is reflected away when it is fresh, clean, and glossy. When applied to an exposed surface, such as a roof, it lowers the external surface temperature, thus reducing heat gain through the roof components.

Many scholars have demonstrated that a cool roof can improve building thermal performance and reduce cooling energy consumption, thus making it an effective solution in hot and arid climates (Givoni, 1998; Hu, Zhang, Nguyen, & Tasdizen, 2023; Lechner, 2014; Mahmoud & Ismaeel, 2019; Saber & Maref, 2019). Despite the proven benefits of cool roofs in reducing heat gain and improving energy efficiency, the SBC neither imposes nor suggests their implementation in modern buildings, neglecting a crucial passive strategy for enhancing the sustainability of the building sector.

Despite the lack of standardised solar absorptance values, especially for roof constructions, in the Saudi building and construction sector, residential buildings are typically constructed using reinforced concrete roof slab (see Section 2.6), which are sometimes finished with terrazzo tiles (Alaboud & Gadi, 2022), concrete tiles (Albatayneh, Alterman, Page, & Moghtaderi, 2016), cement plaster (Alayed, O'Hegarty, & Kinnane, 2021), or gravel (Alkelani, 2025). Table 3-1 presents typical solar absorptance values for selected materials and surface finishes for demonstration purposes.

In this research, the default solar absorptance value of 0.7 assigned to roof construction in IES-VE was adopted for the baseline model. This approach allows for a clear evaluation of the thermal and energy performance improvements resulting from the application of the proposed cool roof option, which has a solar absorptance value of 0.15. The results of these simulations are discussed in more detail in Section 9.3.

Table 3-1 Solar absorptance for commonly applied materials and surface finishes. Adapted from (IES-VE, 2023).

	Material	Absorption
Bricks	White, glazed	0.25
	Light	0.4
	Dark	0.65
Stone	Limestone	0.3–0.5
	White marble	0.45
	Red granite	0.55
Roofs	Concrete tiles	0.65
	Asphalt	0.9
	Red tiles	0.4–0.8
	Mortar screed	0.8
	Whitewashed roof or white tiles	0.3–0.5

3.3.3 Internal heat gain

Heat can also be gained through internal sources (i.e. within a building), which, during overheating seasons and depending on the type of building, can cause a significant increase in indoor temperature unless effective solutions are considered (John et al., 1992; Lechner, 2014). Internal heat sources can be categorized as follows:

- Metabolic heat produced by the occupants.
- Artificial lighting.
- Appliances and equipment.

The magnitude of internal heat gain can vary and is primarily influenced by factors such as occupancy density and the location and type of heat-generating appliances used. According to Szokolay (2004), internal heat gain in buildings can be influenced to some extent by planning and design strategies that involve separating heat-emitting functions from regularly occupied spaces. For example, the kitchen stands out as one of the most significant internal sources of heat gain in domestic buildings. When located away from the living room, this segregation prevents unwanted heat transfer to occupied spaces, thus preventing potential discomfort.

Internal heat gain can be further managed by considering the dissipation of heat generated at or near the source and by utilizing highly efficient domestic appliances, which tend to emit less heat, in addition to placing them in an appropriate location to facilitate heat dissipation (John et al., 1992; Kiamba, 2016). This requires placing the heat-generating source outside, or at least ventilating it separately (e.g. providing cross ventilation). Szokolay (2004) added that a local exhaust may be used close to heat-generating machinery (e.g. kitchen stove).

Internal heat gain associated with artificial lighting can be controlled by maximizing daylight when applicable (without causing solar heat gains) and by using highly efficient artificial

lighting when needed. Additionally, the demand for cooling is impacted by the density of occupants and rate of activities, as heat produced by occupants can be significant depending on their activity rate (John et al., 1992).

3.3.4 Ventilation and infiltration gains

Heat can also be gained through deliberate ventilation and incidental infiltration of the warm outside air into the indoor environment (Lechner, 2014; Szokolay, 2004). Ventilation and infiltration gains are influenced by various factors, such as building openings, closing mechanisms, and the overall airtightness of the building envelope (ASHRAE, 2013b; CIBSE Guide F, 2012; Kiamba, 2016). It is important to note that the heat gained through infiltration depends on both the rate of the outside warm air leaking into the building and the temperature differences between the outdoor and indoor environments.

During the overheating season, unintentional outdoor hot air infiltration replaces the indoor cool air, leading to increased cooling requirements. In naturally ventilated buildings, however, the infiltration of outside air may negatively influence the air flow circulation created by the designed openings (John et al., 1992). Therefore, it is critically important to consider the airtightness of the building envelope to ensure that the infiltration rate remains low, ideally not exceeding approximately 0.5 air changes per hour (ACH) (Szokolay, 2004). The previously discussed heat gain sources are summarized in Figure 3-5.

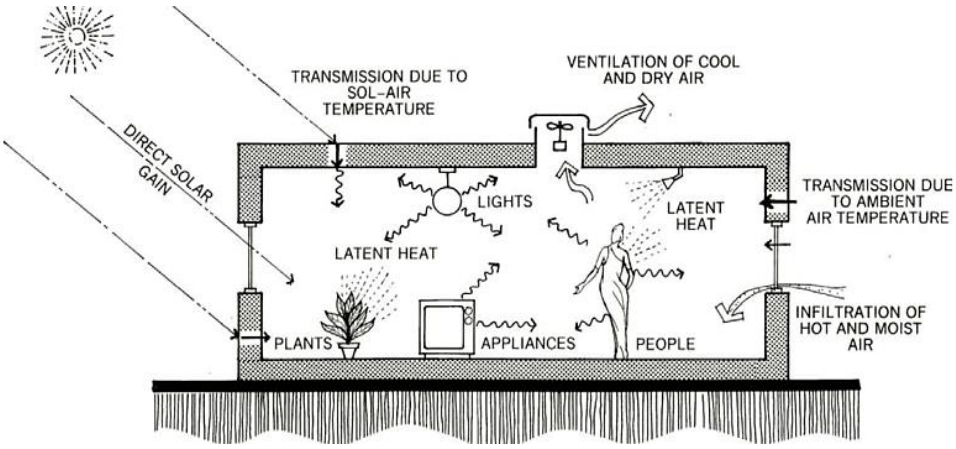


Figure 3-5 Sources of heat gain in indoor environments. Adapted from Lechner (2014).

3.4 Thermal comfort

Thermal comfort is essential for human well-being and productivity and is one of the most critical issues concerning indoor environmental quality (Olgyay, 2015). As people spend most of their times indoors (i.e. in artificial climate) owing to society's growing mechanization and industrialization, there is increased interest in indoor environmental

conditions and quality (Fanger, 1970 as cited in Al-Oraier, 2005). It is generally accepted that thermal comfort is an important factor influencing a building's thermal performance and energy consumption. It is, therefore, important to explore the thermal behaviour of a building to examine various solutions and design strategies to optimize its thermal performance, reduce energy consumption, and increase occupants' comfort.

Defining thermal comfort is not an easy task since there is no 'one-size-fits-all' condition, especially when considering the fact that people can live in different climates around the world that range from tropical to dry to polar (Koch-Nielsen, 2013; Lechner, 2014; Lotfabadi & Hançer, 2019; Olgyay, 2015). Nevertheless, many definitions of thermal comfort can be found. A straightforward definition of thermal comfort is the condition in which an individual is satisfied with their surrounding thermal environment, perceiving a sense of neutrality (i.e. neither too warm nor too cold) while wearing a regular level of clothing (Al-Azri, Zurigat, & Al-Rawahi, 2012; Al-Oraier, 2005; Humphreys, 1978). It can also be defined as 'the absence of thermal discomfort', as indicated by Givoni (1998).

A widely recognized definition of thermal comfort is provided by ASHRAE Standard 55, which defines thermal comfort as 'the condition of mind that expresses satisfaction with the thermal environment and is assessed by subjective evaluation' (ASHRAE, 2017, p. 3). This definition acknowledges that thermal comfort is subjective and individualized; it can be experienced differently from one individual to another based on their preferences and other factors.

Considering the variation in thermal comfort requirements among people, the comfort zone must be considered when designing buildings as it reflects the thermal satisfaction of a large portion (e.g. 80%) of the population (Lechner, 2014). The comfort zone's boundary can be conveniently defined by plotting combinations of comfortable air temperature and relative humidity on a psychrometric chart, as illustrated in Figure 3-6. It is noteworthy that the defined comfort zone (i.e. boundary) is not absolutely fixed, as other variables that can have enormous effects on thermal comfort can shift or raise the comfort zone (Lechner, 2014). The process of generating the comfort zone was effectively explained by Szokolay (2004), who indicated that the comfort zone varies with climate and can be different for each month. A discussion about the factors affecting thermal comfort is provided in the following section.

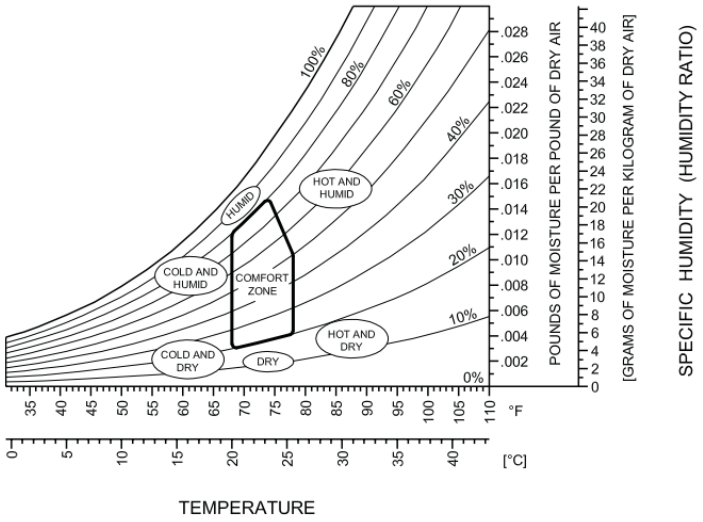


Figure 3-6 The comfort zone plotted on the psychrometric chart with different types of discomfort (Lechner, 2014).

3.4.1 Thermal comfort factors and models (indices)

Thermal comfort is achieved through a certain combination of various factors that affect heat dissipation of the human body (Lechner, 2014; Szokolay, 2004). Based on a laboratory study conducted under steady-state conditions, Fanger (1970) found that thermal comfort is mainly influenced by six factors (cited in Lotfabadi & Hançer, 2019). The first four are environmental factors and the last two are personal.

- **Air temperature** (Ta)

Air temperature can significantly impact human comfort by determining the rate at which heat is lost, mostly by convection and evaporation. The comfort range for most people extends from 20 °C in winter to 25 °C in summer (Lechner, 2014). Koch-Nielsen (2013) stated that, when the temperature drops below 16 °C, high activity rates and excessive clothing are required, whereas above 30 °C, high air velocity and sweat can help maintain thermal comfort at low activity rates. When the ambient temperature is above 37 °C, the temperature of the skin increases by convection (i.e. the body gains heat) and cools by evaporation (Lechner, 2014).

- **Relative humidity** (RH)

Relative humidity can have an impact on thermal comfort through the evaporation mechanism of skin moisture. Dry air with low relative humidity can reduce skin temperature by absorbing moisture, resulting in an evaporation cooling effect. When relative humidity reaches the saturation point, RH 100%, the evaporative cooling effect stops as the air cannot

hold more moisture (Lechner, 2014). In general, the recommended range for humidity is between 30% and 60%.

- **Air movement** (Va)

Air movement (or air velocity) greatly increases the rate of heat loss by convection and evaporation from the skin, thus producing a physiological cooling effect (Lechner, 2014; Szokolay, 2004). Table 3-2 describes the subjective reactions to various air velocities. In the presence of air movement, the skin and clothing surface resistance to heat transfer is reduced (Szokolay, 2004). While air motion is highly desirable in summer, it should be kept low in winter so that thermal comfort can be achieved at low temperatures. At high air temperatures (e.g. above 37 °C), the cooling effect by air flow is reduced and can cause undesirable convective heat gain (Lechner, 2014).

Table 3-2 Subjective reaction to air movement. Adapted from Szokolay (2004).

Reaction	stuffy	unnoticed	pleasant	awareness	draughty	annoying
Velocity (m/s)	<0.1	to 0.2	to 0.5	to 1	to 1.5	>1.5

Givoni (1998) indicated that these reactions are dependent on local temperature, humidity, and clothing level. This can be explained by the fact that higher air velocities may be acceptable in summer while resulting in an undesirable chill effect in winter. According to Szokolay (2004, p. 41), the apparent cooling effect of air movement (dT) can be estimated using Equation (3-2):

$$dT = 6 \times Va_e - 1.6 \times Va_e^2 \quad (3\text{-}2)$$

Where:

- Va_e is the effective air velocity and is equal to Va-0.2, where Va is the air velocity (m/s) at the body surface. The expression is valid up to Va = 2 m/s.

As the effect of natural ventilation on achieving thermal comfort is profound, it is discussed in greater detail in Section 3.3.4.

- **Mean radian temperature** (MRT)

Human thermal comfort can be also affected by the radiant heat exchange between human body and the surrounding environment (Guo et al., 2020). At any point in a given environment, there is a dynamic heat exchange by radiation. Radiant temperature (RT) is defined as “the temperature of a black body source that would give the same value of some measured quantity of the radiation field as exists in reality” (McIntyre, 1980, as cited in

Parsons, 2014, p. 16). Number of scholars have indicated that the radiant heat exchange can be asymmetrical within in the indoor environment, e.g., when radiant source/sink is present.

Heat exchange by radiation is influenced by the temperature of the surrounding surfaces within an enclosed environment, measured by the men radiant temperature (MRT) (Szokolay, 2004). This indicates the overall mean value of the radiant heat exchange between the human body and its surroundings.

The effect of MRT becomes particularly noticeable when there is a substantial difference between MRT and the air temperature (Lechner, 2014). For instance, exposure to direct solar radiation can cause a significant increase in MRT, potentially reaching uncomfortable levels, even if the air temperature remains within an acceptable range. Thus, well-insulated buildings and effective shadings can help maintain MRT closer to the indoor air temperature. Radiant heat gain takes place when MRT surpasses the body's temperature.

Various definitions of MRT can be found in the literature. A frequently cited definition appears in ISO 7726, which defines MRT as "the uniform temperature of an imaginary enclosure in which the radiant heat transfer from the human body is equal to the radiant heat transfer in the actual non-uniform enclosure" (as cited in Parsons, 2014, p. 17). This definition of MRT is directly related to the human body. Therefore, the use of a spherical sensor (described below) is regarded as an approximation of MRT (Parsons, 2014).

It should be noted that the MRT cannot be directly or accurately measured. Besides the computational complexity of characterising the geometric relationship between the human body and the surrounding environment, accounting for different body segments with varying skin emissivity and dynamically changing skin temperatures—affected by factors like vasoconstriction, vasodilation, sweating, and clothing coverage—further complicates the calculation. Therefore, the concept of MRT must be simplified in order to be determined.

The MRT can be measured by a black globe thermometer, which responds to radiant inputs and air temperature. Due to its low cost and simplicity of use, globe thermometer is considered the most used instrument to evaluate MRT. The globe thermometer is an ordinary thermometer located inside a mat black copper sphere about 100-150 mm diameter. Its reading reflects the convective and radiative heat exchange around the globe thermometer (d'Ambrosio Alfano, Ficco, Frattolillo, Palella, & Riccio, 2021; Guo et al., 2020).

Szokolay (2004) considered a simplified formula for measuring the MRT from the temperature of the black globe temperature (Tg). He suggested that in situations where air velocity is zero, MRT tends to equal Tg, yet Equation (3-3) can be used for air movement correction (Szokolay, 2004, p. 18). ISO 7726 provided Equation (3-4) for natural convection (e.g. Va ≤ 0.15 ms) and Equation (3-5) for forced convection (e.g. Va > 0.15 ms) (as cited in Parsons, 2014, p. 105). However, the accuracy of the correction can be influenced by the error from other measurements (e.g. Ta, Tg, and Va). The selected instruments and their specification are discussed in more detail in Section 5.4.

$$\boldsymbol{MRT = T_g \times \left(1 + 2.35\sqrt{V_a}\right) - 2.35 \times T_a\sqrt{V_a}} \quad \textbf{(3-3)}$$

Where:

- MRT (mean radiant temperature), Tg (globe temperature), and Ta (air temperature) are given in °C and Va (air velocity) in m/sec.
- In still air (i.e. Va = 0), MRT is equal to Tg.

$$\boldsymbol{MRT = \left[\left(T_g + 273\right)^4 + \frac{0.25 \times 10^8}{\varepsilon}\left(\frac{|T_g - T_a|}{d}\right)^{1/4} \times \left(T_g - T_a\right)\right]^{0.25} - 273} \quad \textbf{(3-4)}$$

$$\boldsymbol{MRT = \left[\left(T_g + 273\right)^4 + \frac{1.1 \times 10^8 V_a^{0.6}}{\varepsilon d^{0.4}} \times \left(T_g - T_a\right)\right]^{0.25} - 273} \quad \textbf{(3-5)}$$

Note:
For the standard globe, values of ε (emissivity) = 0.95 and d (diameter) = 150 mm can be used.

- **Clothing** (Icl)

Clothing can affect body temperature by preventing convective thermal exchange between the body and the ambient environment, thus acting as an insulation layer of the body (Szokolay, 2004). Owing to its insulation properties, clothing can help maintain thermal comfort in various climatic conditions (i.e. adjustment mechanism of thermal comfort). However, architects generally do not specify the clothing to be worn in the building. Indeed, clothing is often influenced by social, cultural, and traditional factors, such as fashion trends, workplace customs, and so on, which may sometimes conflict with thermal comfort requirements (Lechner, 2014).

According to ASHRAE (2017), the thermal insulation provided by clothing is measured in units of *clo*. In overheated conditions, a low clo value is required. To promote both sensible and latent heat dissipation, loose, billowing clothing can be considered as it allows air to pass across the skin.

- **Metabolic rate** (M)

Metabolic rate refers to the heat generated within the body through its metabolic process. The rate at which this heat is produced is highly dependent on the body's metabolic rate, which is a function of activity level (Szokolay, 2004). In other words, an increase in muscular activities can lead to a significant increase in both internal and skin temperatures, necessitating the dissipation of this heat to prevent overheating (Lechner, 2014; Szokolay, 2004). It is expressed in the units of met (1met = 58.2 W/m^2). Metabolic rates and the corresponding produced heat for typical household tasks are illustrated in Table 3-3. As previously indicated, heat from the human body must be lost at the same rate as it is generated through metabolism to maintain thermal equilibrium (Lechner, 2014).

Table 3-3 Metabolic rates for typical household tasks. Adapted from ASHRAE (2017).

Activity	Metabolic rate	
	Met unit	W/m^2
Sleeping	0.7	40
Reclining	0.8	45
Seated	1.0	60
Standing	1.2	70
Light work (e.g. cooking)	1.6 to 2.0	95 to 115
Medium work (e.g. house cleaning)	2.0 to 3.4	115 to 200

The thermal environment for a given environment can be evaluated by collecting and interpreting measurements of the various environmental parameters at suitable points within the occupied zones in that environment. If the occupancy distribution cannot be estimated (e.g. in an unoccupied space), ASHRAE Standard 55 guidelines suggest taking measurements from nearly the centre of the room or at one meter inward from the largest window in the space. In addition to their location in the room, the specifications of the selected instruments and the duration of the measurements must be considered.

In recent decades, substantial research efforts have been dedicated to comprehending human thermal comfort and developing models that can effectively assess and predict thermal comfort within specific environments. These models take into account the various factors that collectively affect individuals' thermal response and shape their perception of thermal environments, including physiological and psychological factors; they aim to assess the acceptability of thermal sensations experienced in particular settings. According to Auliciems and Szokolay (2007) and Peeters, Dear, Hensen, and D'haeseleer (2009), thermal comfort model research is divided into two methods:

- Based on a controlled environment or climate chamber (heat balance model).
- Based on a field survey (adaptive comfort model).

Fanger's predicted mean vote (PMV) model is based on the principles of the human body's heat balance, relating thermal comfort to the thermal exchange process between the body and the surrounding environment. This index involves a complex mathematical process that takes into account both physiological and physical measurements to quantify thermal comfort (Asimakopoulos, 1996).

The PMV provides a prediction of the mean value of the thermal sensation votes of a large group of individuals on a seven-point sensation scale, ranging from cold (−3) to hot (+3), where zero demonstrates thermal neutrality (see Table 3-4). The predicted percentage of discomfort (PPD) is determined from the PMV, quantifying the percentage of individuals dissatisfied with the thermal environment (i.e. voting −3, −2, +2, or +3 on the sensation scale) (ASHRAE, 2017; Asimakopoulos, 1996; ISO-7730, 2005). Figure 3-7 illustrates the relationship between the PPD and PMV.

Table 3-4 Thermal sensation scale for the PMV. Adapted from Asimakopoulos (1996).

Sensation	Cold	Cool	Slightly cool	Neutral comfort	Slightly warm	Warm	Hot
Scale	−3	−2	−1	0	+1	+2	+3

Fanger's method of evaluating thermal comfort is widely recognized and is accepted by several building regulations and standards, including ASHRAE-55 standards and ISO 7730. Achieving thermal comfort for all people in a given environment is difficult as individuals can have different metabolic rates, dressing preferences, and psychological influences, which, as previously indicated, play a major role in determining thermal comfort. Under ideal thermal conditions, when PMV is equal to zero, at least 5% of any population will remain dissatisfied (see Figure 3-7) (Asimakopoulos, 1996; Auliciems & Szokolay, 2007). Thus, thermal comfort must be provided for the majority of the occupants (e.g. 80%) in a given space. The acceptable range is between $-0.5 < PMV < +0.5$ and $PPD < 10\%$ (ASHRAE, 2017; Asimakopoulos, 1996; de Dear & Brager, 1998; ISO-7730, 2005).

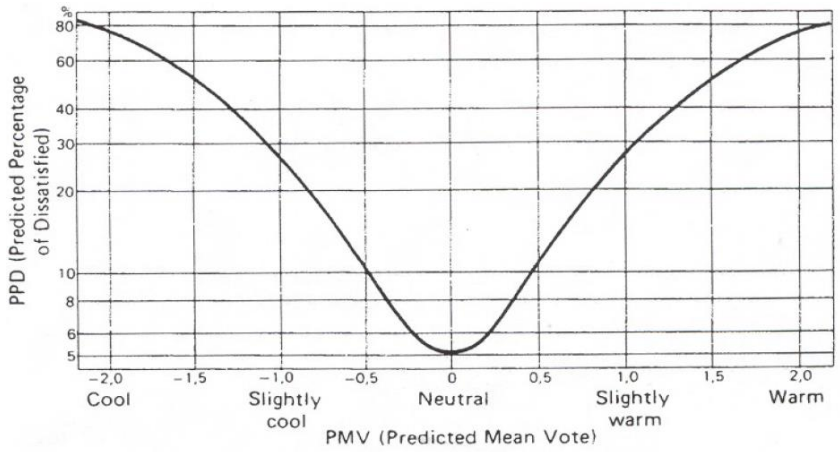


Figure 3-7 PPD as a function of PMV (note that a minimum of 5% dissatisfaction is found under ideal conditions). Adapted from Auliciems and Szokolay (2007).

While climate chambers enabled researchers to study the heat balance of the human body under carefully controlled environments, de Dear, Brager, and Cooper (1997) argued that field surveys are the most suitable and effective means of assessing the potential effects of both psychological and behavioural adaption as they occur in real-world scenarios.

Based on their review of the results of field studies, de Dear and Brager (1998) found that occupants in naturally ventilated buildings were more tolerant of a wider range of thermal conditions compared to those in mechanically controlled environments. Additionally, the PMV model tended to over-predict thermal sensations in naturally ventilated buildings compared to what people actually felt (Yau & Chew, 2012). As Brager and de Dear (1998) noted, the limited capability of the PMV model to accurately predict thermal comfort in passive buildings may be attributable to the adaptive actions that occur in real-life settings but are not considered in laboratory experiments.

Consequently, the PMV model is more suitable for environments relying on mechanical systems, where indoor conditions are relatively stable and occupants have limited adaptive opportunities. In contrast, the adaptive comfort model is applicable to naturally ventilated or free-running buildings, where occupants can actively modify their thermal environment through behavioural adjustments (e.g. opening windows or changing clothing).

The adaptive method refers to the processes by which people gradually become less responsive to repeated environmental stimulation; it highlights the occupants' active roles in achieving thermal comfort and coping with changes in thermal conditions, such as seasonal variation. Several scholars, such as Auliciems and Szokolay (2007), Brager and de Dear (1998), and Zhang and Lin (2020), have mentioned that thermal comfort can be influenced by factors beyond the physical and physiological—factors are not explicitly considered in the

PMV model. Several studies (de Dear & Brager, 1998; Yau & Chew, 2012; Zhang & Lin, 2020) have indicated that these additional factors are associated with people's thermal adaptation methods, which can be categorized into three distinct processes:

- Physiological adaptions (acclimatization and genetic adaption)
- Psychological adaptations (based on experience and expectation of the prevailing conditions)
- Behavioural adaptations (clothing levels, activity rates, and personal environmental control)

ASHRAE Standard 55 (2017) defines the adaptive model as a 'model that relates indoor design temperatures or acceptable temperature ranges to outdoor meteorological or climatological parameters' (p. 2). The adaptive model can be used to predict the acceptable thermal conditions of a particular location by considering the concept of thermal neutrality, which considers the aspects of thermal acceptability. As expressed by Szokolay (2004), the desired indoor temperature (Tc) is a function of the monthly mean outdoor temperature (Tout) and can be determined in free-running buildings by applying the model developed by (de Dear & Brager, 2002, p. 553), as shown in Equation (3-6):

$$\boldsymbol{Tc = 0.31T_{out} + 17.8} \tag{3-6}$$

A similar conclusion was reached in the model proposed by J. F. Nicol and Humphreys (2002, p. 569), demonstrated in Equation (3-7):

$$\boldsymbol{Tc = 0.54T_{out} + 13.5} \tag{3-7}$$

The adaptive approach has been acknowledged by current standards, such as ASHRAE 55 and ISO 7730 (J. F. Nicol & Humphreys, 2002). As explained by de Dear and Brager (2002), the adaptive comfort standard can be used to approximate acceptable indoor conditions during the design phase of new buildings or for the evaluation and operation of existing buildings. The model may also be used to evaluate the acceptability of the predicted indoor conditions (i.e. through an energy simulation tool) and investigate the feasibility of various passive strategies, thus developing more energy-efficient and comfortable indoor environments.

3.5 Passive cooling

Maintaining acceptable indoor thermal conditions is a crucial aspect of building design and operation, especially in regions with severe climates such as Saudi Arabia. After understanding humans' engagement with thermal environments and reviewing heat avoidance strategies (see Sections 3.3 and 3.4), this section aims to discuss suitable passive cooling techniques. As mentioned by Lechner (2014) and Kiamba (2016), passive cooling techniques are mainly used to create thermal balance, thus achieving thermal comfort, especially when relying solely on heat avoidance strategies proves insufficient to keep the indoor temperature within the comfort range.

3.5.1 Thermal mass

Thermal mass refers to a material's ability to absorb, store, and subsequently release heat over time (Baker & Steemers, 2000; DeKay & Brown, 2014), providing 'inertia' against outdoor temperature fluctuations (Saulles, 2019). In buildings with minimal internal heat generation (e.g. residential buildings), the hourly cooling load pattern can be notably influenced by the building's thermal mass (Givoni, 1998). Lightweight structures (i.e. buildings with low thermal mass) typically respond rapidly to outdoor temperature fluctuations and solar gain, resulting in significant variation in their cooling demands and potentially high peak cooling loads compared with buildings with high thermal mass (Baker & Steemers, 2000; Givoni, 1998). As illustrated in Figure 3-8, heavyweight structures (categorized by high thermal mass) act as regulators that smooth indoor temperature swings and delay peak temperatures, thereby influencing a building's thermal behaviour and indoor microclimate.

A heavyweight structure usually acts as a heat sink. During daytime, the gained heat is absorbed by the thermal mass, thus preventing an excessive heat rise and reducing overheating risk during the day. At night, when the outdoor temperature drops, the mass loses its heat (by convection and radiation) to the outdoor environment, thereby restoring its capacity to store heat for the following day (Givoni, 1998; Lechner, 2014).

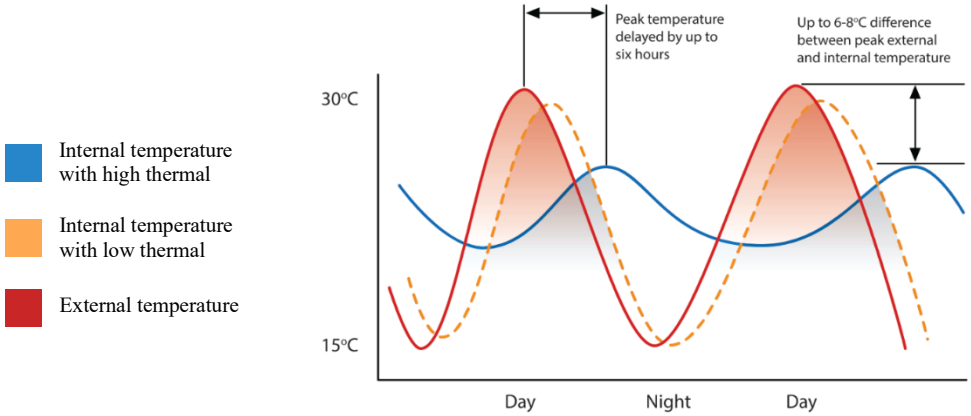


Figure 3-8 Applying thermal mass helps stabilize temperature fluctuations within a building across its diurnal cycle. Adapted from Saulles (2019).

Thermal mass may be created by using dense materials (e.g. concrete, brick, and stone) and is usually part of the building's structure or envelope (Baker & Steemers, 2000). As indicated by Saulles (2019), the concerned materials must have specific thermal properties (i.e. high specific heat capacity and moderate thermal conductivity) to ensure that heat flow across the material is in step with the building's diurnal cooling and heating cycle. Table 3-5 shows the thermal properties of commonly used construction materials. It also shows that some materials, such as wood, have high heat capacity (meaning they can store more heat per kg), yet have low thermal conductivity. Conversely, steel has high thermal conductivity, but it absorbs and releases heat much faster than the other materials. Consequently, unlike concrete, brick, and stone, both wood and steel exhibit ineffective thermal mass.

Table 3-5 Thermal properties of commonly used building materials. Adapted from Saulles (2019).

Construction material	Density (kg/m^3)	Specific heat capacity (J/kg·K)	Thermal conductivity (W/m·K)	Thermal mass
Timber	500	1600	0.13	Low
Steel	7800	450	50.0	Low
Lightweight aggregate block	1400	1000	0.57	Medium-high
Precast and in-situ concrete	2300	1000	1.75	High
Brick	1750	1000	0.77	High
Sandstone	2300	1000	1.80	High

As previously discussed, the location of the thermal mass concerning the insulation or internal finishing is of particular importance. Generally, the thermal mass must be exposed to the indoor environment. Thermal mass can be combined with natural ventilation to promote a comfortable indoor thermal environment. The impact of natural ventilation as a cooling strategy is discussed in the following section.

3.5.2 Natural ventilation

Natural ventilation is widely recognized as one of the primary passive cooling techniques for hot and arid climates (Givoni, 1998; Lechner, 2014). Given the substantial energy consumption associated with active cooling systems, as discussed in Chapter 2, this approach can be effectively employed to conserve cooling energy requirements while maintaining satisfactory indoor thermal comfort.

This cooling strategy is typically utilized when outdoor temperatures are lower than indoor temperatures, but heat gains cause indoor temperatures to rise above comfort limits. Promoting natural ventilation in such situations effectively flushes out the built-up heat, leaving the building cooler and maintaining a comfortable indoor environment. Besides expelling internal built-up heat, the movement of air provides a physiological cooling effect, even when the temperature is slightly above the upper comfort limit, as discussed earlier in this chapter (see Section 3.4.1) (Baker & Steemers, 2000; Givoni, 1998).

Design decisions related to the openings in a building envelope—including factors such as orientation, size, number, location, and details of the windows—in relation to the direction of the wind and the pressure distribution around the building can have a profound effect on natural ventilation and air movement patterns inside the building. Szokolay (2004) indicated that air movement inside a building can be naturally induced by providing cross ventilation, relying on pressure differences primarily caused by either wind or the stack effect. In this case, both inlet and outlet openings must be provided.

As air blows against a building, it creates a positive pressure zone on the windward side and a negative pressure zone (or suction zone) on the leeward side. The difference between the positive and negative pressures provides the driving force. Therefore, positioning the openings (i.e. inlet and outlet openings) and their accessories (e.g. shading elements) in relation to the pressure distribution around the envelope is crucial in determining the potential for natural ventilation and the airflow pattern inside the building (Givoni, 1998; John et al., 1992; Lechner, 2014; Szokolay, 2004).

The stack effect is primarily driven by thermal buoyancy, which results from the density difference between outdoor and indoor air. This phenomenon occurs when the indoor air (within a vertical stack or a room with significant height) is warmer than the outdoor air. To facilitate the stack effect, it is necessary to provide both a high outlet and a low inlet, allowing warm air to escape from the top opening and replaced at the bottom by cooler

outdoor air. It is important to note that the efficiency of the stack effect is proportional to the difference between the indoor and outdoor air. Therefore, it is unlikely to provide efficient comfort ventilation (or sensible air velocity) in warm climates (Szokolay, 2004).

While natural ventilation plays a crucial role in improving a building's thermal performance, energy efficiency, and indoor air quality, it must be carefully controlled, especially in hot climates when outdoor temperatures far exceed the upper comfort limit. Doing so helps prevent undesirable convective heat gain and ensures comfortable indoor environments (Baker & Steemers, 2000). Field measurements in Chapter 6 (see Section 6.4.3) and numerical simulation results in Chapter 8 (see Section 8.2) show that, under Riyadh's hot summer conditions—when outdoor temperatures remain higher than indoor temperatures—applying daytime ventilation can worsen the indoor thermal environment.

As Baker and Steemers (2000) stated, a selective coupling between the indoor and outdoor environments is essential to maintain the mean indoor temperatures below the mean outdoor temperatures and is most effective when outdoor temperatures fall well below the indoor temperatures. This can be achieved by providing nighttime ventilation.

Nighttime ventilation is most effective in hot climates with large diurnal temperature ranges. In such conditions, the building is deliberately kept closed during the daytime to reduce ventilation while still providing the minimum fresh air requirements. At night, ventilation can be used to promote the heat dissipation process and allow the massive structure to store the cooling effect, thus effectively acting as a heat sink for the following day, as explained earlier in this section (Baker & Steemers, 2000; Lechner, 2014).

3.6 Research on thermal performance and energy efficiency measures

Maintaining an acceptable indoor thermal condition is a crucial aspect of building design and operation, especially in regions with harsh climate conditions such as KSA, where air-conditioning systems contribute to over 50% of households' energy consumption. Passive design strategies, which are not efficiently utilized in contemporary Saudi houses, have proven to be effective in enhancing the indoor thermal environment and improving buildings' energy efficiency. After discussing the multifunctionality of the building envelope, understanding human interaction with the thermal environment, and exploring passive cooling strategies, this section provides a review of previous research addressing thermal and energy performance optimization by focusing on passive design and cooling measures.

Applying design measures in hot climates is crucial for improving indoor thermal conditions and reducing demand for active cooling systems. The impact of passive design and cooling strategies on building thermal and energy performance has been investigated extensively by a number of scholars in Saudi Arabia. For example, Alrashed (2015), Krarti et al. (2017), Alosaimi (2023), and Alkhalifah (2024) investigated the energy performance of various retrofit strategies for a typical residential building across major cities in KSA, providing valuable insights into their effectiveness in reducing total annual energy demand. Using energy simulation tools, the studies demonstrated the feasibility of implanting retrofit measures in KSA's climate conditions.

Similarly, Alaidroos and Krarti (2015) investigated the energy-saving potential of various building envelope optimization strategies for a prototypical house model. Using EnergyPlus, design solutions, which included external wall insulation, roof insulation, thermal mass, window area, glazing types, and window shading, were assessed across five climate zones in KSA. The results demonstrated that energy savings of up to 39.5% (subsidized energy cost scenario) and 47.3% (non-subsidized energy cost scenario) can be achieved in Riyadh's climate zone. Building upon this work, Krarti et al. (2017) further demonstrated that applying energy retrofit measures and design strategies, which included building envelope optimization, lighting upgrades, cooling setpoint adjustments, and high-efficiency HVAC systems, could reduce energy consumption by between 52.2% and 62.7%, depending on the climate.

Taleb and Sharples (2011) employed DesignBuilder energy simulation software to investigate the energy performance of an apartment building in Jeddah City and offered distinctive recommendations for enhancing energy efficiency. The results allowed the authors to develop guidelines to enhance the sustainability of future dwellings in KSA. Alaboud and Gadi (2022) evaluated the indoor thermal environment for a residential building in Makkah, KSA. In their study, thermal analysis software (TAS) was employed to conduct a thermal analysis and identify key areas for potential improvement. Their developed baseline energy model was validated against field monitoring of indoor thermal conditions. The study concluded that upgrading building envelope components (i.e. adding thermal insulation to walls, roof, and ground floor) led to a 56.4% savings in total annual cooling load compared to the uninsulated baseline model.

Also, Lasker (2016) evaluated the impact of thermal wall insulation on a residential building in Riyadh using IES-VE simulation software. The study found that applying 50 mm polyurethane insulation resulted in a 42% reduction in the total annual cooling load compared to the uninsulated wall option. Additionally, placing the insulation on the outside achieved the lowest cooling load, with a daily load 0.39% lower than internal insulation during a typical summer day. These findings are consistent with Al-Sanea, Zedan, and Al-Hussain (2012), who investigated the impact of varying the amount and location of thermal mass in insulated building walls while maintaining a constant R-value. In this study, the transmission load during a typical summer day for an outside insulated wall was 0.35% lower than that for an inner insulated wall in the same region. They found that optimizing the thermal mass thickness of the same R-value can achieve savings in annual cooling and heating transmission load by up to 17% and 35%, respectively.

Aldossary, Rezgui, and Kwan (2014) investigated domestic energy consumption patterns in the hot and arid climate of Riyadh using a multiple case study approach. Their IES-VE simulation results indicated that implementing various thermal retrofitting measures, such as efficient glazing, external window shading, and on-site renewable energy, achieved energy consumption reductions in the range of 15%–34%. In 2017, the same authors proposed three low-carbon protype houses that could reduce energy consumption by up to 71.6% compared to standard houses. The energy simulation results allowed the authors to establish domestic low-energy reference levels between 77 kWh/m^2 and 98 kWh/m^2 (Aldossary, Rezgui, & Kwan, 2017). These figures demonstrate a substantial development over those reported in their previous study (Aldossary et al., 2014), in which the annual energy consumption for a typical house in Riyadh was about 163 kWh/m^2.

Al-Qahtani and Elgizawi (2020) used DesignBuilder simulation software to evaluate the thermal and energy performance of various passive design strategies for a residential building prototype in Riyadh. The study emphasized the important role of adding external shading, upgrading window glazing, and applying thermal insulation to the external walls and roofs in improving the indoor thermal environment and energy efficiency. Al-Qahtani and her colleague reported a significant drop in cooling load from 93.49 kWh of their baseline model to 39.54 kWh after implementing these strategies, achieving a 57.7% reduction in total cooling load. The results highlighted the potential benefits of integrating passive-design strategies in KSA's residential sector. While the study provides valuable insights into

envelope improving strategies using simulation-based analysis, its lack of proper validation may limit the reliability of its findings for practical implementation.

Alardhi, S Alaboodi, and Almasri (2020) carried out a simulation study to evaluate the impact of SBC 602 on reducing residential energy consumption. They reported the annual energy end-use distribution of Riyadh was found to be 67% for space cooling. The results showed that the most effective way to improve energy efficiency is to reduce the U-values of the walls.

Another study by Almushaikah and Almasri (2020) assessed various design measures for the building envelope using DesignBuilder simulation software. In Riyadh, the researchers found that these measures contributed to energy consumption reduction of 27.4% for walls, 14% for roof, 6.4% for window glazing, and 4.1% for window shading. It is worth noting that the findings regarding window glazing and shading differ from those in (Alyami & Omer, 2021), who reported energy savings of 2.46% as a result of upgrading window glazing and 2.18% for shading, despite both studies being conducted in Riyadh. Alyami and his colleague also reported potential energy savings of 11.7% by improving the airtightness of the envelope (i.e. reducing infiltration rates by 75%), which is relatively close to the approximately 10% savings reported by (Krarti et al., 2017).

In addition, natural ventilation has been found to be an effective passive cooling strategy in hot and arid regions, including KSA. For example, the study by Alaidroos and Krarti (2016) investigated the potential of natural ventilation to reduce cooling energy requirements in residential buildings across different climate zones in KSA. EnergyPlus software was used to perform an energy simulation analysis for a prototypical house. In Riyadh's climate, the results indicated that applying natural ventilation alone, when applicable, reduced cooling energy by 22% and total building energy consumption by 10%.

Similarly, Alaboud (2021) evaluated the impact of natural ventilation on Saudi houses. In this study, the application of natural ventilation was limited to nighttime when the outdoor temperature is lower than the cooling setpoint temperature of 25 °C. The simulation results indicated that along with improving the building fabric components, the proposed ventilation strategy achieved an additional reduction of 4.5% in annual cooling load in Riyadh.

Table 3-6 summaries the relevant published studies and research on the potential impact of various passive design strategies on the thermal and energy performance of residential buildings and hot and arid regions.

Table 3-6 Summary of previous studies on the potential impact of various design strategies on the thermal and energy performance of residential buildings

Source	Study focus
(Taleb & Sharples, 2011)	Assessed energy and water consumption of a typical residence (apartment complex) in Jeddah, KSA, using DesignBuilder software to establish guidelines and recommendations for delivering sustainable homes
(Al-Sanea et al., 2012)	Evaluated the effect of thermal mass on energy performance
(Aldossary et al., 2014)	A multiple-case study analysis that evaluated energy consumption patterns of residential buildings located in Riyadh, KSA, using IES-VE simulation software
(Taleb, 2014)	Investigated the potential of passive cooling strategies to improve thermal and energy performance of residential buildings located in UAE using IES-VE simulation software
(Alaidroos & Krarti, 2015)	Examined optimizing building envelope design to improve energy performance of KSA's residential buildings using EnergyPlus simulation software
(Lasker, 2016)	Evaluated commonly applied construction materials for external walls in KSA's residential buildings using IES-VE simulation tool
(Aldossary et al., 2017)	Established energy consumption definition for low-energy residential buildings in Saudi Arabia using IES-VE software
(Krarti et al., 2017)	Evaluated the economic and environmental impacts of improving the energy efficiency of residential building stock in KSA
(Algarni, 2018)	Evaluated the impact of cool roof systems on building thermal load of residential buildings in KSA using energy simulation tool, eQuest
(Ahmed, Asif, & Alrashed, 2019)	Investigated the application of a building performance simulation tool in KSA's construction sector to deliver energy-efficient houses
(Al-Qahtani & Elgizawi, 2020)	Evaluated various passive design techniques through simulation tool to improve thermal and energy performance of residential buildings in Riyadh, KSA
(Ahmed & Asif, 2020)	Technological and economic assessment of energy retrofitting of Saudi dwellings
(Alardhi et al., 2020)	Investigated the role of the Saudi Building Energy Conservation Code (SBC 602) in improving the energy efficiency of residential buildings
(Almushaikah & Almasri, 2020)	Case study analysis that assessed various energy efficiency measures for residential buildings in Saudi Arabia
(Alyami & Omer, 2021)	Investigated potential energy savings and CO_2 reduction techniques for a typical dwelling in Riyadh using DesignBuilder simulation software
(Alaboud & Gadi, 2022)	Assessed indoor thermal environment of an existing residential building to identify and test alternative options using TAS simulation tool to improve energy efficiency
(Elnabawi & Saber, 2022)	Assessed the impact of applying hybrid ventilation system on reducing energy demand of an education building in Bahrain using the dynamic simulation software IES-VE
(Elnabawi, Saber, & Bande, 2024)	Evaluated the effectiveness of building envelope retrofitting measures in improving energy efficiency of residential buildings in UAE using a validated DesignBuilder model

3.7 Summary

The significant contribution of cooling demand to building energy requirements in Saudi Arabia has necessitated the improvement of buildings' thermal performance through the application of various design strategies while maintaining indoor thermal comfort requirements. This chapter provided a review of the building envelope as one of the main building components playing a crucial role in determining the indoor thermal environment, enhancing the energy efficiency of the building, and providing shelter against various outdoor climatic conditions. The building envelope should be designed to allow desirable outdoor

influences, such as natural ventilation and winter solar gain, while also acting as a thermal barrier between conditioned and unconditioned environments. To this end, a discussion of the design strategies and factors influencing indoor thermal comfort was provided in Sections 3.3 to 3.5.

In this chapter, two main categories of design strategies were discussed: heat avoidance strategies and passive cooling techniques. The first, which forms the basis of passive design strategies in hot climates, reduces undesired heat flow between indoor and outdoor environments. Most of the reviewed studies demonstrated that applying such strategies has a direct impact on improving building thermal performance, saving cooling energy requirements, and reducing emission levels. Some scholars have suggested that these measures can be further enhanced by incorporating passive cooling techniques, which can lead to a significant impact on indoor thermal conditions and cooling consumption.

Therefore, studying the building envelope in depth and trying to integrate passive and low-energy solutions learned from vernacular architecture and modern sustainable building technology could reduce issues concerning overheating and high energy consumption in modern KSA's dwellings. The following chapter explains the research methodology in detail (Section 5.2), describes the selected case study buildings (Section 5.3), details the employed assessment tools, simulation inputs, and validation method (Sections 5.4–5.8), and reviews the design strategies and measures for building performance improvement (Section 5.9).

Field measurements from the selected case study buildings in Riyadh are presented in Chapter 6, while energy modelling, simulation outputs, and a detailed evaluation of the proposed measures are given in Chapters 7–9.

CHAPTER 4

DIGITAL FABRICATION IN THE CONSTRUCTION INDUSTRY

- Introduction
- Innovative technologies in building design and construction
- Categories of digital fabrication for concrete
- Development of 3D concrete printing
- Feasibility of 3D printing in the construction industry
- Example of large-scale 3D-printed structures
- Thermal performance and properties of 3D-printed envelope

Chapter 4: DIGITAL FABRICATION IN THE CONSTRUCTION INDUSTRY

4.1 Introduction

As discussed in Chapter 2, significantly growing housing demands in KSA have necessitated the adoption of modern and innovative construction methods, transforming the construction industry to accelerate the building process and address the urgent need for new buildings at a fast pace. Digital fabrication using large-scale 3D concrete printing is one of the most recently applied technologies in the construction industry and one that has the potential to revolutionize the building and construction industry due to the numerous benefits it offers compared to conventional construction methods.

This chapter outlines the application of digital fabrication in the construction industry, including robotic and additive manufacturing methods. It presents an overview of the development of additive manufacturing and explores the feasibility of 3D printing in the construction industry in comparison with conventional construction methods. Lastly, the chapter reviews previous studies concerning the thermal and energy performance of 3D concrete printing, with a specific focus on hot and arid climates.

4.2 Innovative technology in building design and construction

The Fourth Industrial Revolution, also known as Industry 4.0, promotes the digitalization of complex industrial tasks. Many industries (e.g. medical and automotive) have benefited from the digital advances and technologies brought about by the Fourth Industrial Revolution, including improvement in the quality and performance of their products. However, such a trend has not been adopted in the construction field at the same pace as it has in the manufacturing industry. According to El-Sayegh, Romdhane, and Manjikian (2020), the application of Industry 4.0 in the construction field is still in its early stages. Additive manufacturing, or 3D printing, is an example of the digital fabrication of concrete and one of the most recent technologies introduced to the construction field, pushing the sector towards digitalisation.

The Information Age, like the Industrial Revolution before it, has significantly changed not only the way buildings are designed but also their manufacturing and construction methods (Alabbasi, 2021). As Kolarevic (2005) indicated, the Guggenheim Museum in Bilbao, Spain, designed by Frank Gehry, is a well-known example that demonstrates the influence of the

Digital Information Age revolution on the building industry. The implementation of digital technologies in the construction industry increases efficiency and the possibility of creating complex geometries. In recent years, building design and the construction industry have been profoundly impacted by developments in computer-aided design (CAD) and computer-aided manufacturing (CAM) technologies.

The introduction of digital modelling tools into architectural design has allowed designers to produce geometries with highly curvilinear surfaces, mathematically described as non-uniform rational basis splines (NURBS) (Kolarevic, 2005). Kolarevic noted the possibility of construing NURBS digitally through the 'file-to-factory' processes of computer numerically controlled (CNC) fabrication methods. New digitally enabled processes of fabrication (e.g. additive, subtractive, and formative) provide the opportunity to produce complex geometries that, until recently, were difficult to design, construct, and assemble using conventional construction methods.

Kolarevic (2005) pointed out that these new digitally driven design and fabrication processes challenge the historical relationship between architecture and its construction means. In his book *Architecture in the Digital Age*, Kolarevic states that the digital age has revolutionized the relationship between conception and production, creating a direct link between what can be imagined and what can be built. One of the earliest digitally developed and realized projects is the large *Peix* sculpture at the entrance of the Vila Olimpica, a retail complex in Barcelona, Spain.

The complex curvilinear surfaces that characterize the new digital architecture pose challenges and constructability concerns, leading some to question the credibility of the spatial complexity introduced by the evolving digital era. The opportunities provided by digital manufacturing have made constructability a direct function of computability. The question now is not whether a given design can be built, but rather what new digital tools are available to construct it (Kolarevic, 2005).

4.3 Digital fabrication of concrete

Despite growing concerns related to its environmental impacts, concrete remains one of the most commonly used materials in the field of construction. The natural conversion of concrete to a solid state is one of its main features as a construction material (Bos, Wolfs, Ahmed, & Salet, 2016). While the additive fabrication of concrete is an evolving technology in the construction field, its implementation in building design and the construction industry

is still in its early stages (El-Sayegh et al., 2020). The technique, however, remains a branch of the digital fabrication industry. It is expected that digital fabrication techniques will promote sustainability in the construction industry by reducing construction waste, especially waste associated with formwork. It is important to note that the enormous potential of the digital fabrication of concrete techniques is not just limited to 3D printing technology (Alabbasi, 2021).

The adoption of innovative construction techniques has become increasingly important for delivering energy-efficient and sustainable dwellings in KSA (see Sections 2.4–2.9). In addition to its constructability and sustainable benefits, the recent advances in 3D concrete printing have highlighted its potential to enhance building thermal performance by enabling complex design solutions that are often difficult or impossible to achieve using conventional methods (see Section 4.6). This technology has the potential to revolutionize the building energy footprint and support ongoing national efforts to improve energy efficiency in the building sector. A review of previous research on the thermal and energy performance of 3D-printed buildings is provided in Section 4.7.

4.4 Categories of digital fabrication for concrete

Alabbasi (2021) grouped the digital fabrication processes for concrete formwork into three categories: subtractive, formative, and additive manufacturing. To demonstrate the impact of the new digital technology on building design and construction practice, this section will provide an overview of each category along with its application in the construction industry.

4.4.1 Subtractive

The subtractive fabrication process involves the removal of a specified volume of material from solids using a multi-axis milling machine. CNC milling technology has been innovatively used in the construction industry to produce geometrically complex formwork (moulds) for both in-situ and off-site casting of concrete elements with complex, irregular surfaces. The concrete formwork of the external walls of Zollhof Tower in Dusseldorf, designed by Frank Gehry, is an example of this fabrication process. The load-bearing external wall panels were produced using lightweight polystyrene blocks, which were CNC milled to manufacture 355 different curved moulds, as illustrated in Figure 4-1 (Kolarevic, 2005). As the elements were produced using CNC-milled moulds, Sitnikov (2020) mentioned in his PhD thesis that the project did not require highly skilled labourers during construction.

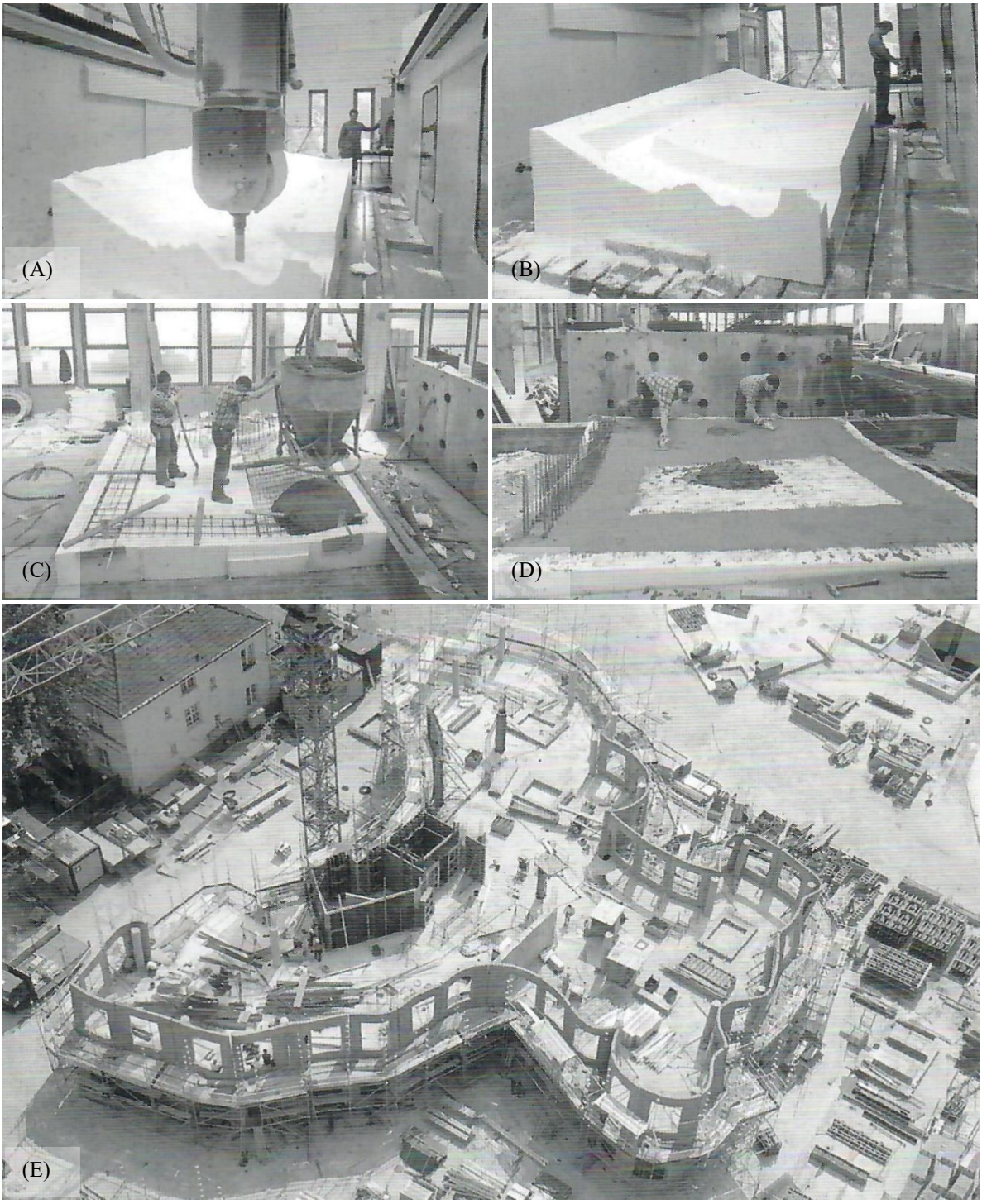


Figure 4-1 The fabrication process of the Zollhof Tower's reinforced concrete panels using CNC-milled moulds: (A–B) CNC milling of the moulds; (C–D) Concrete casting into the moulds; (E) On-site assembly of the precast concrete panels. Adapted from Kolarevic (2005).

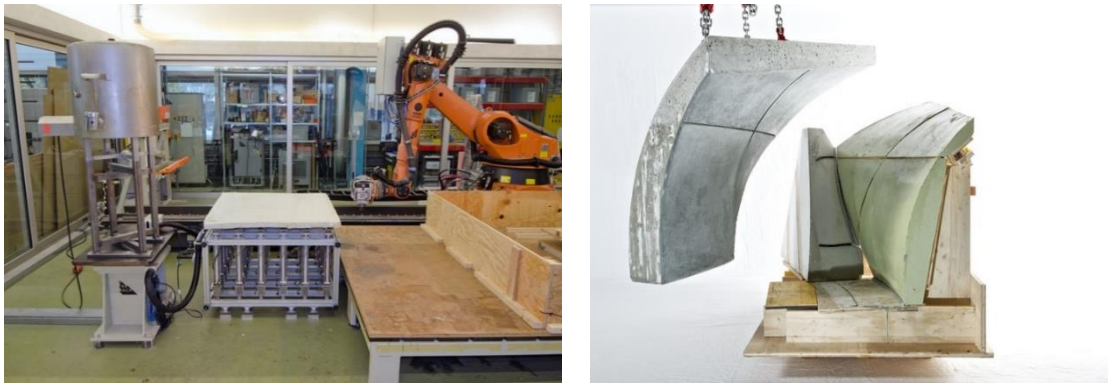
Although the robotic milling of polystyrene moulds produces complex structures with high levels of detail, it is considered a time-consuming process that produces a high volume of material waste (Alabbasi, 2021). As shown in the previous example, hundreds of surfaces required a uniquely fabricated individual single-use mould made of polystyrene blocks for concrete casting. Researchers are experimenting with other materials to produce formworks

for concrete casting using a CNC machine without generating waste. A PhD study carried out by Sitnikov (2020) focused on the use of ice to produce the formwork as it can be re-frozen, thus closing the loop. Here, CNC was used to mill the ice to create the formwork for concrete casting.

4.4.2 Formative manufacturing

Formative manufacturing refers to methods of applying mechanical forces to a material to form it into a desire shape. Unlike subtractive fabrication, this process does not involve removing material from the raw material; rather, it is deformed (Nithesh, 2018). Gramazio Kohler Research at ETH Zurich proposed a new method in which a flexible robotically actuated mould is utilized to produce 'entirely recycled' wax inlays for standard concrete formworks (Figure 4-2a). As indicated by Hawkins et al. (2016), the mould can be reshaped between uses as it can adapt to various geometries depending upon the condition of the support.

The process cycle begins with producing the wax-based formwork elements by a flexible actuated mould, onto which the liquid wax is poured. After solidification, the wax components are removed from the mould, transported to the construction site, and placed onto standard concrete formwork elements. Steel reinforcements are placed before assembling the second side of the wax mould. Finally, the concrete is cast and, after curing, the formwork is disassembled. The wax inlays can then be melted and reused to produce a new element. See Figure 4-2b.

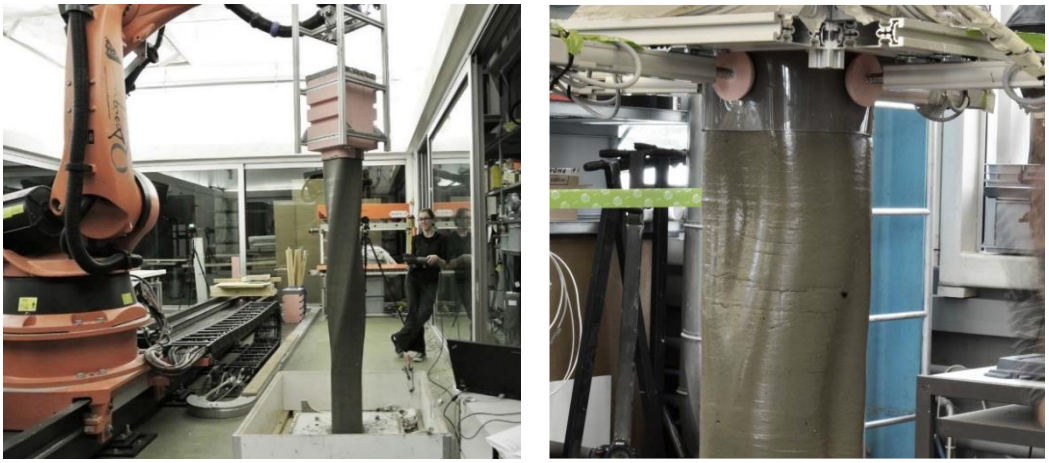


(A) (B)

Figure 4-2 TialorCrete project by Gramazio Kohler Research at ETH Zurich: (A) Flexible mould; (B) Final concrete element with wax inlay. Adapted from Gramazio Kohler Research (2023).

Building on innovative fabrication methods, Smart Dynamic Casting (SDC) was an interdisciplinary research project at ETH Zurich that explored the possibility of combining the well-known slipforming technique with industrial robots. The project intended to

completely eliminate the need for individually customized formworks for the construction of complex concrete structures. SDC exhibits the formability and structural ability of the technology to produce architectural components such as columns and thin folded structures with a significantly smaller, flexible formwork (Lloret-Fritschi, 2016). In this method, the formwork is moved vertically along a pre-programmed slip-forming trajectory that incorporates rotations and dynamic mechanical actuation of the formwork itself, as shown in Figure 4-3.



(A) (B)

Figure 4-3 The fabrication process of a free-form structure using a robotic slip-forming technique: (A) A square formwork that rotates as it moves vertically; (B) Applying a flexible formwork with four actuators. Adapted from Lloret-Fritschi (2016).

4.4.3 Additive manufacturing

The intensive waste involved in the subtractive fabrication of formwork has promoted many studies to focus on using additive manufacturing (AM) techniques to produce nonstandard concrete elements with little to no material waste (Alabbasi, 2021). Additive manufacturing, also known as 3D printing, is defined by the International Organization for Standardization (ISO) and the American Society for Testing and Materials (ASTM), and cited by many scholars, such as El-Sayegh et al. (2020), Lim et al. (2012), and Pessoa et al. (2021), as 'the process of joining materials to make objects from 3D model data, usually layer upon layer', in contrast to the subtractive manufacturing process. As illustrated in Figure 4-4, the process of 3D printing involves slicing up a three-dimensional digital (CAD) file into a series of 2D sections, which are then deposited by the printer layer by layer until the physical product is completely constructed.

Unlike the formative and subtractive manufacturing processes, the AM process can be used to fabricate highly complex forms with no part-specific tooling and does not generate intensive

material waste, thus filling the gap left by the previously discussed fabrication processes. Advancements in AM allowed the transformation from rapid prototyping (RP) productions to include functional end-use products (Camacho et al., 2018). Despite its widespread adoption in the manufacturing industry over the course of decades, 3D printing technology has only recently been introduced in the construction field to produce residential buildings (houses and villas) (Wu, Wang, & Wang, 2016).

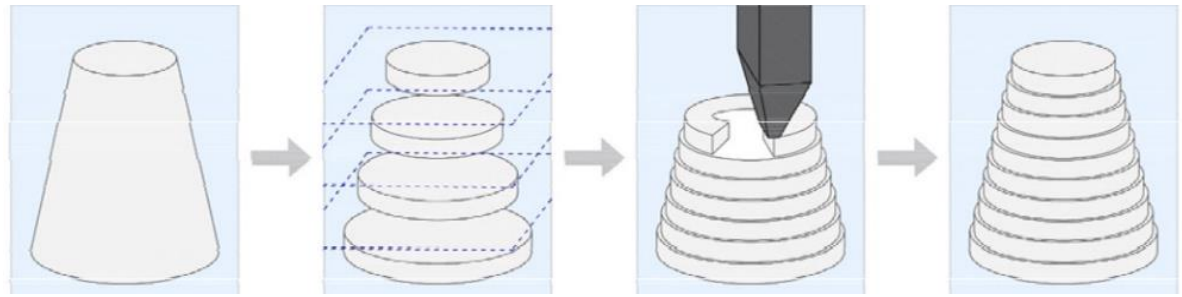


Figure 4-4 Illustration of concrete 3D printing process: (A) Preparing the digital model; (B) Slicing the model into layers; (C) Depositing the concrete layer by layer; (D) Final product. Adapted from Pessoa et al. (2021).

4.5 Development of 3D concrete printing

The earliest attempts to apply AM in the construction industry started to appear in the late 1990s. These initiatives allowed researchers to identify the advantages and challenges associated with the application of AM in construction practice (Camacho et al., 2018). In 2006, Dr. Behrokh Khoshnevis, a researcher from the University of Southern California, successfully developed a 3D printing system called Contour Crafting (CC) to upscale the 3D printing practice to involve large-scale structures, including buildings and bridges (Nithesh, 2018; Vu, 2014). Since then, this innovative technology has made it possible to print an entire house within 24 hours, thereby revolutionizing the construction industry (Ibrahim, Eltarabishi, Abdalla, & Abdallah, 2022). The construction industry's desire for a cost-effective and rapid production process has paved the way for rapid advancements in 3D printing technology, including concrete with contour crafting systems (Nithesh, 2018).

With CC, the computer-controlled extrusion nozzle is mounted on a manipulator such as a gantry system or mobile robot (Alabbasi, 2021; Khoshnevis, 2004). As illustrated in Figure 4-5, the top and side trowels are attached to the extrusion nozzle to smooth the vertical and horizontal surfaces as the material is being extruded. Further, the side trowels can be deflected (by computer control) at different angles to produce various non-orthogonal surfaces (Camacho et al., 2018; El-Sayegh et al., 2020; Khoshnevis, 2004; Lim et al., 2012). According to El-Sayegh et al. (2020), this technology is considered the first AM process for

the on-site production of nonstandard structures. In this method, the external surfaces of the walls and the internal cross-bracing are extruded. The inner core, however, is hollow in most cases.

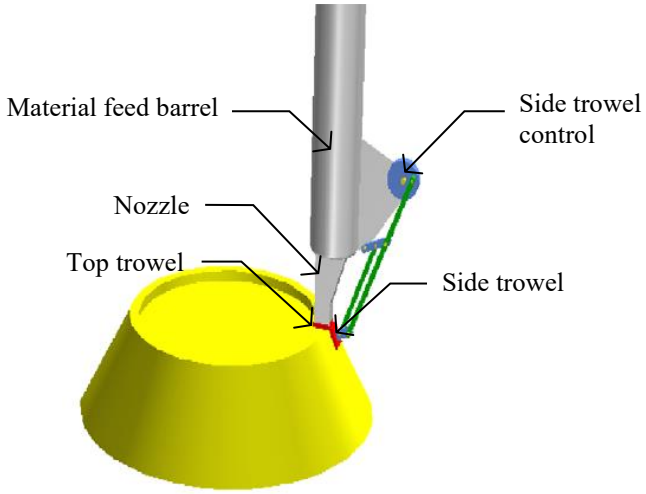
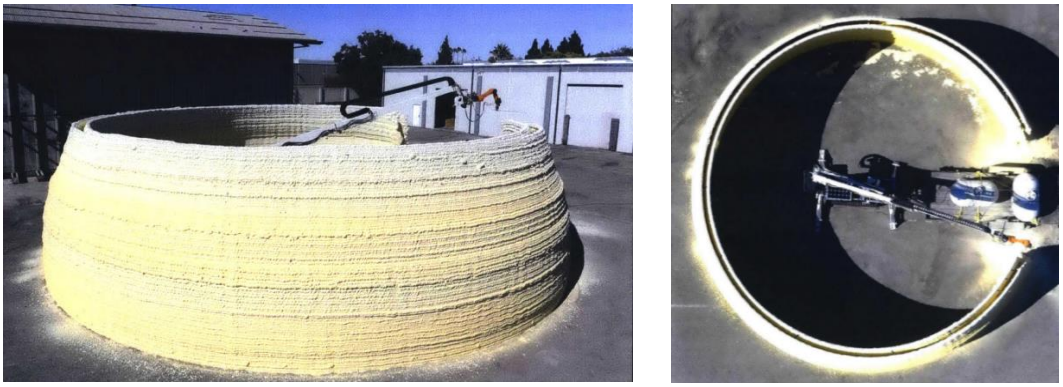


Figure 4-5 3D printing process of Contour Crafting. Adapted from Khoshnevis (2004).

Rather than extruding the concrete, a research team from the Massachusetts Institute of Technology developed an additive robotic fabrication process for on-site 3D printing of concrete formwork using quick-setting insulating foam. In his doctoral research, Keating (2016) pointed out that the fabricated concrete formwork can also act as thermal insulation when left in place after casting the concrete. The research team was able to successfully print a 14.6m diameter and 3.7m high concrete formwork for an open dome within two days, and the actual printing time was less than 13.5 hours (Figure 4-6). Similar to the current insulated concrete formwork (ICF) method, the study concluded that the fabricated moulds could be filled with any castable material (e.g. concrete) to complete the construction of a permanent building.



(A) (B)

Figure 4-6 Onsite 3D printing of insulating foam: (A) View of the successfully printed formwork; (B) Top view showing an open section of the form for the mobile robotic arm to enter and leave the construction site. Adapted from Keating (2016).

Benjamin Dillenburger and his research group at ETH Zurich developed a 3D sand-printing process that not only allows of the efficient fabrication of concrete moulds but also material reuse (Stouhi, 2018). Using this technology, the research team was able to create the formwork for an 80 m^2 lightweight concrete slab at DFAB House in Switzerland, shown in Figure 4-7. According to Watkin (2018), the team was able to fabricate a highly complex geometry without a resulting increase in construction cost. Aouf (2018) stated that the slab was computationally designed to use the least possible amount of structural material, thus reducing its overall weight. Meibodi et al. (2018) provided a more in-depth discussion about the developed slap and the applied fabrication processes.



(A) (B)

Figure 4-7 Images of the produced concrete slab: (A) On-site assembly; (B) Internal view after assembling the concrete slab segments (Meibodi et al., 2018).

4.6 Feasibility of 3D printing in the construction industry

As previously indicated, AM is a novel technology in the construction industry, and many scholars find it a promising and beneficial technology despite its unpredictable application. Camacho et al. (2018) considered the current challenges and limitations in the traditional construction industry, which can include a harsh local climate, material waste, and a lack of skilled labour, to be opportunities for AM application in the construction industry. The various construction stages associated with conventional techniques (see Figure 4-8) involve workforces and various tools at different parts of the structure, which impact construction duration and overall cost. In contrast, the 3D printer is simultaneously considered a tool and a manufacturer. Nithesh (2018) pointed out that automating construction tasks is more efficient, with less user involvement in the printing process.

El-Sayegh et al. (2020) grouped the benefits of applying 3D printing technology in the construction industry into two main categories, constructability and sustainability, which will be discussed in greater depth below.

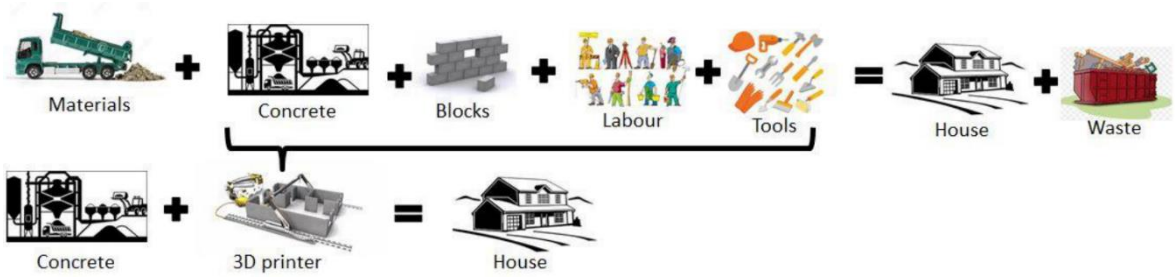


Figure 4-8 Conventional construction process versus 3D concrete printing (Nithesh, 2018)

4.6.1 Constructability benefits

- **Faster construction**:

For any construction project, time is a critical and sensitive factor. 3D printing technology can speed up the construction process with much shorter construction durations than conventional construction methods. As mentioned earlier, the construction of a house can be completed in as few as 24 hours. WinSun, a private Chinese firm, was able to produce a group of full-sized detached, single-story houses (200 m^2 each) in just one day using four 10m by 6.6m 3D printers (Nithesh, 2018; Wu et al., 2016).

- **Reduced construction cost**:

In addition to the significant decrease in construction duration, 3D printing technology can also reduce construction costs. A main feature of AM technology is that it requires a smaller workforce compared to conventional construction techniques. As the machine requires just one operator, the overall coast of the workforce is significantly reduced. For example, the labour cost for a 3D-printed office in Dubai was 60% lower than a conventionally constructed building of the same size. Furthermore, 3D printing technology reduces the costs associated with formwork installation and removal, which will be discussed further in subsequent sections (El-Sayegh et al., 2020).

- **Smaller workforce**:

The shortage of skilled labours is another motivation for AM in the construction industry (Ghaffar, Corker, & Fan, 2018). Camacho et al. (2018) stated that it is difficult for contractors to find labourers with the expected and required skills. While implementing 3D printing technology in the construction industry lowers the demand for skilled craftsmen, it offers opportunities for new jobs with different skills than those required in current conventional practice. Moreover, construction productivity can be greatly improved through 3D printing when compared with conventional construction methods (Pessoa et al., 2021). The significant

difference between traditional construction with bricks and AM techniques is illustrated in Figure 4-9.



(A) (B)

Figure 4-9 A comparison between different construction methods: (A) Conventional construction; (B) 3D printing (Pessoa et al., 2021).

- **Complex geometry and mass customization**:

3D printing also allows for more geometrical freedom than conventional methods. A major draw of 3D printing technology is its ability to construct highly complex structures that would not be possible to build by any other means (El-Sayegh et al., 2020). 3D printing technology offers architects the possibility of producing complex geometries that may not be possible or would be costly to construct through other fabrication processes (e.g. subtractive and formative) (Camacho et al., 2018). While prefabricated components are usually standardized to reduce complexity-related costs, AM technology allows customization without resulting in increased costs (Wu et al., 2016). Thus, the technology offers unlimited potential for complexity, allowing architects to create more complex designs and forms without geometric restrictions during construction.

- **Shorter supply chain**:

As mentioned by El-Sayegh et al. (2020), 3D printing technology not only influences the design process but also improves construction productivity. AM allows for the shrinking of the supply chain, especially for elements that need expedited delivery. Using 3D printing technology, customized building components can be autonomously produced on demand directly from the digital model without significant lead time or human intervention (Camacho et al., 2018; Ghaffar et al., 2018).

4.6.2 Sustainability benefits

Implementing 3D printing technology will promote sustainability in the construction industry by reducing the amount of waste generated during the construction phase. Using AM technology, only the required amount of material is used to fabricate the model, eliminating unnecessary waste of materials and thus minimizing the environmental impacts associated with construction processes (El-Sayegh et al., 2020).

As stated by Camacho et al. (2018), the reduction of formwork (or any temporary supports during construction) is another advantage of 3D printing technology. Contrary to the conventional construction method, this process is eliminated, and consequently the waste generated from those formworks is disregarded. For concrete structures, the formworks and labour account for between 35–60% of the overall cost (Camacho et al., 2018). These formworks are typically made of wood using a subtractive process and produce waste before they are even used. With 3D printing, the model is directly fabricated without the wooden moulds required for regular concrete. Minimizing the use of formwork reduces not only the costs and time associated with placing and removing the moulds but also material waste, which accounts for about 23% of total construction material waste.

Safety is a main concern in the construction industry. El-Sayegh et al. (2020) noted that construction work-related injuries and deaths cause substantial losses to people, organizations, and society as a whole. As technology allows for automation of the construction process, 3D printing promotes worker safety by performing most hazardous tasks. In addition to automating some construction activities, AM can reduce on-site labour exposure to harsh environments when working in extreme conditions (e.g. high temperatures) cannot be avoided (Camacho et al., 2018). Thus, AM in the construction industry provides a safer environment for workers and reduces the number of construction-related injuries.

4.6.3 Examples of large-scale 3D-printed structures

Nowadays, several examples of 3D-printed structures can be found across the world, thus demonstrating the construction industry's eagerness to test the effectiveness of this method (de Rubeis, Ciccozzi, Giusti, & Ambrosini, 2024). What follows are some striking examples of the application of large-scale 3D printing in building construction.

- **Yhnova™ (2017)**:

Yhnova™ is a social housing unit constructed in Nantes, France, in 2017 using the BatiPrint 3D printing technique. This one-story 95 m^2 house features a Y-shape structure, curved lines,

and rounded angles. The house was 3D-printed on-site using a robotic arm and an automatic guided vehicle (AGV) by gradually depositing three layers of materials (see Figure 4-10). In addition to acting as thermal insulation for the house, the two polyurethane foam walls were used during construction as formwork for the inner concrete layer. According to Pessoa et al. (2021), the house was printed in 52 hours and has been occupied since the end of its construction.

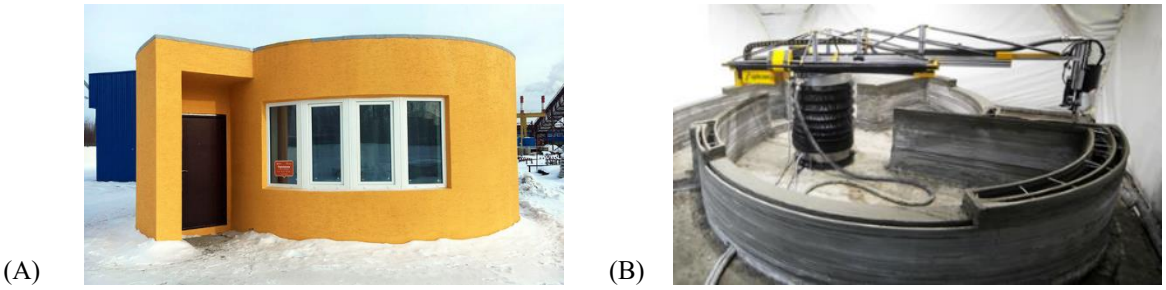


(A) (B) (C)

Figure 4-10 YhanovaTM house: (A) Wall cross-section; (B) External view of the 3D-printed house without coating; (C) The final finished product (Pessoa et al., 2021).

- **Small house by Apis Cor (2016)**:

Apis Cor, an innovative American construction company, has demonstrated the possibility of rapid construction using 3D printing technology. The team successfully 3D-printed the 38 m^2 house on-site (see Figure 4-11), with a total net printing time of 24 hours (Pessoa et al., 2021; Yin, Qu, Zhang, & Lim, 2018). Further to the fast printing process, the 3D printing method allowed for savings up to 70% for construction materials compared with conventional construction methods (Nithesh, 2018). The printing process was carried out in a controlled environment during the severe winter season when the outdoor temperature reached −35 °C, thus demonstrating the capability of the printer to operate in extreme conditions.



(A) (B)

Figure 4-11 Apis Cor produced the first on-site 3D-printed house in Russia within 24 hours: (A) External view of the house; (B) Apis Cor 3D printer in action (Nithesh, 2018).

- **Office building in Dubai by WinSun (2016)**:

The Office of the Future in Dubai, the world's first 3D-printed concrete office building, was unveiled in June 2016. The 250 m^2 office building was fabricated using a gantry-based 3D printer developed by Winsun. The building's components were fabricated in a manufacturing facility in China and shipped in large pieces to the site for assembly (see Figure 4-12). It took 17 days to fully print the building, and it was assembled in two days. The walls were printed with a hollow core for the installation of pipes and insulation material. Compared with traditional construction techniques, the 3D printing process resulted in approximately 80% savings in overall construction costs, 60% savings in labour costs, and 60% savings in material waste (Winsun, 2016; Yin et al., 2018).



(A) (B)

Figure 4-12 The world's first 3D-printed concrete office building by Winsun in Dubai: (A) View after construction (Camacho et al., 2018); (B) During on-site assembly (Ibrahim et al., 2022).

- **Dubai municipality building by Apis Cor (2019)**:

Apis Cor developed a mobile 3D concrete printer that was used to construct what was the largest 3D-printed building in the world at that time (2019). The two-story administrative building in Dubai, shown in Figure 4-13, is 9.5m high and occupies a total area of 640 m^2. It was directly printed on-site in an uncovered environment (i.e. without any climatic control). Due to the limitation of the robotic arm, the team moved the 3D printing machine around the site, using a crane to reposition the printer so that it could print different building components (Block, 2019; Pessoa et al., 2021). Alabbasi (2021) stated that this building demonstrates the feasibility and productivity of on-site 3D concrete printing technology when implemented in an arid climate without the provision of any climatic controls during the printing process. According to Ibrahim et al. (2022), only three workers, in addition to the printer itself, were needed to fully construct the building.



Figure 4-13 Apis Core printed the building using a robotic printer, which was moved around the site using a crane (Block, 2019).

- **6-story apartment building in Shanghai by Winsun**:

Winsun took its 3D printing practice to another level, moving from single-story small houses to constructing the world's tallest 3D-printed building in 2015. The 5-story apartment building, shown in Figure 4-14, was constructed utilizing a gantry-based system and recyclable construction waste.

Using a huge offsite 3D printer array (measuring 6.6 m high by 10 m wide by 40 m long), WinSun was able to print out large pieces of the building at the company's factory, which were then transported to the construction site for assembly with steel reinforcement and insulation compliant with local building standards (Alabbasi, 2021; Urbanist, 2023; Winsun, 2016).



Figure 4-14 3D-printed 6-story building by Winsun (Urbanist, 2023)

- **Residential building in Sharjah by CyBe**:

As part of the Sharjah Research Technology and Innovation (SRTI) Park initiative to construct more residential buildings using 3D printing technology, the first 3D-printed house in Sharjah was fabricated utilizing the CyBe robotic arm. The house was designed with local architectural features with the aim of preserving cultural heritage (see Figure 4-15) (Ibrahim et al., 2022). It consists of two bedrooms, a bathroom, and a kitchen. The house was constructed in less than two weeks.



Figure 4-15 3D-printed house in Sharjah utilising the CyBe robotic arm (Ibrahim et al., 2022)

- **Dar Al Arkan 3-story house by COBOD**:

Dark Al Arkan, a private real estate development company in Saudi Arabia, unveiled its first three-story 3D-printed residential building in the country using COBOD's concrete 3D printer. The house is located in Shams Al Riyadh, a new 12 million m^2 development project, and has a total area of 345 m^2 and a height of 9.9 m, making it the world's tallest on-site 3D-printed building (Figure 4-16).

The printing process was carried out without the use of a tent in outdoor temperatures exceeding 40 °C. This project allowed Dar Al Arkan to push the boundaries for the future of the construction industry by demonstrating how 3D-printed buildings can be cost effective and time saving (COBOD, 2022).

It is worth noting that the author of this thesis requested access to this house as part of the research for this study. However, due to confidentiality reasons, it was not possible to consider this house as a case study. The selected case studies and the methods used to carry out this thesis are discussed in detail in the following chapter. The following section discusses previous research concerning the thermal performance of 3D-printed buildings.



Figure 4-16 A 3-story residential building was fabricated on-site using COBOD's gantry-based 3D concrete printer (COBOD, 2022).

4.7 3D printing of concrete and thermal performance

3D concrete printing is one form of additive manufacturing that has been applied in the construction industry for the fabrication of building elements and for constructing entire structures. Since formworks are not used to support the material after extrusion, the 3D printing of cementitious-based materials demands fast setting and low slump. Lim et al. (2012) identified four key properties essential for successful 3D concrete printing: extrudability, workability, buildability, and open time.

According to Ghaffar et al. (2018), it is often difficult to analyse the materials, feedstocks, and formulations used by companies and researchers as they often avoid publicly sharing any crucial technical data due to trade secrets and competitive considerations. Mahadevan, Francis, and Thomas (2020) further highlighted that the limited literature on 3DCP material properties makes it challenging to conduct more in-depth analyses of 3D concrete printing. The thermal properties of different 3D printable concrete mixes are provided in (Alkhalidi & Hatuqay, 2020; Ayegba, Egbe, Matin Nazar, Huang, & Hariri-Ardebili, 2022; Marais, Christen, Cho, De Villiers, & Van Zijl, 2021; Suntharalingam et al., 2021).

As discussed in Chapter 3, the thermal performance and energy efficiency of a building are highly impacted by heat flow through the envelope components. Thermal performance optimization interventions for the building envelope focus mainly on reducing the U-value, which is the most important thermophysical property impacting the building's overall energy balance. Thermal resistance to heat flow can be significantly improved by applying insulation materials (see Section 3.3). Considering the construction advantages of 3DCP discussed in Section 4.6, this section explores the thermal and energy performance of this emerging technology.

The thermal and energy performance of 3D-printed buildings has received considerable attention, with studies focusing on optimizing wall configuration, material composition, and insulation strategies for improving thermal and energy efficiency (de Rubeis et al., 2024; Pessoa et al., 2021; Sovetova & Kaiser Calautit, 2024).

Sovetova and Kaiser Calautit (2024) stated that the thermal performance of a 3D-printed wall can be enhanced by modifying its cross-section design without altering the material composition. Figure 4-17 shows examples of typical 3D-printed wall shapes and cross-sections that are commonly used in building construction. Extensive research has been

carried out to assess the thermal performance of various wall cross-section (Alkhalidi & Hatuqay, 2020; Suntharalingam et al., 2021).

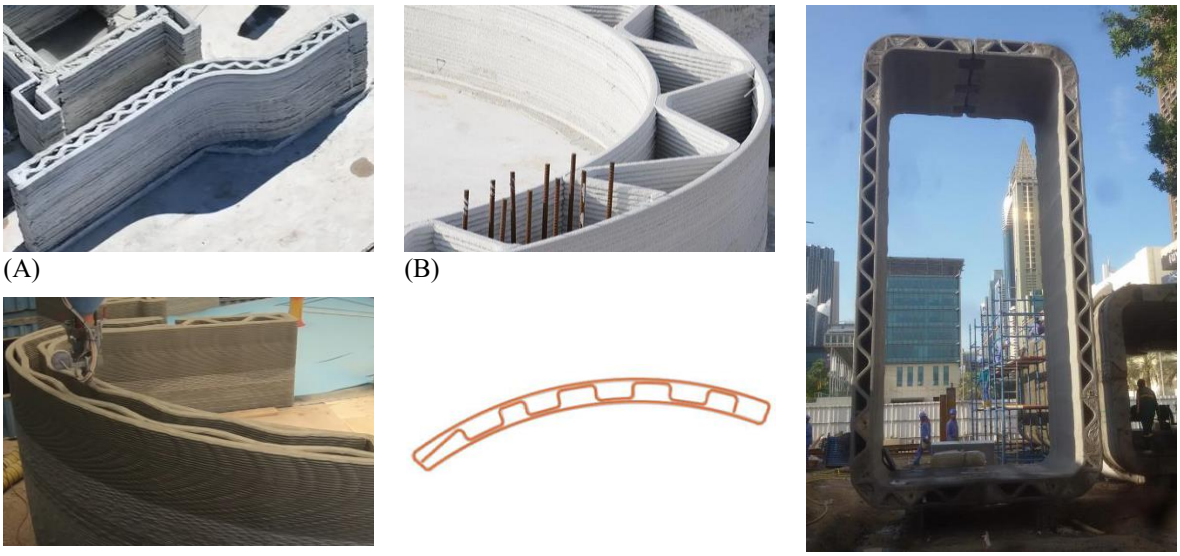


Figure 4-17 Examples of typical 3D-printed wall cross sections: (A) Luyten (Kelly, 2025); (B) Apis Cor (Harrouk, 2019); (C) COBOD (Aerts, 2025); (D) CyBe (CyBe Construction, 2023); (E) WinSun (E.Construct, 2016).

The ability of 3D printing to create components with complex geometries is one of its greatest advantages. A number of scholars have taken this added advantage to investigate the relationship between the geometric design of 3D-printed components and their thermal efficiency. For example, He, Zhang, Zhang, and Zhou (2020) proposed a modular 3D-printed vertical concrete green wall system to improve energy efficiency, demonstrating the potential for 3D printing technology in the construction industry to produce creative design solutions to improve buildings' thermal performance—solutions that might be hard to produce with conventional construction methods.

Kaszynka et al. (2019) built a 3D-printed concrete wall insulated with mineral wool (5 cm) and polyurethane foam (14 cm) between the 3D-printed concrete layers. Based on the stationary method implemented, the thermal conductivity was determined for each of the individual components of the proposed wall. The research showed that the proposed 3D-printed wall had a lower thermal transmittance value than traditional insulated concrete walls despite being of lesser thickness.

Similarly, Alkhalidi and Hatuqay (2020) conducted a numerical study to investigate the thermal performance of 3D-printed concrete walls with different configurations and material mixes for a hypothetical one-story house (95 m^2) across various climate zones, including arid climate, using ANSYS, Revit, and Green Building Studio. Analysing the impact of cavity

configuration design, the study found that multi-row cavity configurations can significantly reduce the U-value of the wall. The lowest obtained U-value of 0.15 $W/m^2 \cdot K$ resulted from a combination of a distinct wall configuration, printing mixture type, and a cavity filled with expanded polylactic acid insulation.

A similar study conducted by Suntharalingam et al. (2021) numerically studied the thermal performance of various 3D-printed concrete wall configurations with and without cavity insulation. Using finite element modelling in Abaqus, the study determined the U-values for various wall thicknesses and cavity configurations. The results indicated that incorporating expanded polylactic acid insulation significantly reduced the U-values of the wall panels, thus improving their thermal performance.

AlZahrani, Alghamdi, and Basalah (2022) investigated the thermal performance of 3D-printed concrete walls with various cavity shapes. Using finite element modelling in Abaqus, the study found that the diamond shape achieved the highest thermal performance, with 0.122W/m·K thermal conductivity. The study indicated that the 3D-printed walls exhibited superior thermal performance compared to conventional brick walls, offering energy-saving potential for the climate conditions of Makkah, KSA.

Despite progress in 3DCP, studies evaluating the thermal performance of full-scale 3D-printed buildings are limited. Sun, Xiao, Li, and Feng (2021) conducted an experimental analysis to investigate the thermal performance of an existing 3D-printed prototype building. The methodology involved infrared thermography and in-situ monitoring of surface temperature and heat flux for U-value calculation. The results demonstrated an unsatisfactory thermal performance of the 3D-printed walls (U-value of 2.27 $W/m^2 \cdot K$), and the authors recommended further investigation to explore and optimize the thermal performance of 3D-printed concrete structures. In contrast, a study by Salandin, Quintana-Gallardo, Gómez-Lozano, and Guillén-Guillamón (2022) demonstrated excellent thermal insulation performance of the 3D-printed façade, with U-value measurements between 0.241 $W/m^2 \cdot K$ and 0.237 $W/m^2 \cdot K$, meeting Spanish building code requirements for external walls.

Few studies have conducted a thermal analysis using energy simulation approaches. For example, Mahadevan et al. (2020) explored the thermal comfort and energy efficiency of a residential building built with 3D printable concrete and compared it with conventional M25 concrete and masonry bricks using Autodesk Revit with the Sefaira plug-in. The study found that the 3D printable concrete demonstrated lower performance than the conventional

materials. However, this poor performance could be improved by enhancing the wall's resistance to heat flow, which was not investigated in the study.

Other scholars have utilized more robust simulation tools. Ayegba et al. (2022) explored the impact of incorporating insulation materials between the 3D printable concrete layers for a single-story house using DesignBuilder simulation software. The results demonstrated that applying insulation material between the 3D-printed concrete layers significantly improved the energy efficiency of the building.

Another study, by Khalili Tari, Reza Faraji, Aslani, and Zahedi (2023), investigated the energy efficiency of a two-story 3D printable building in Boston, US, using DesignBuilder simulation software. The study found that applying 10 cm of spray polyurethane foam insulation reduced energy consumption by about 50%, emphasizing the crucial role of thermal insulation material in improving energy efficiency. Similarly, Ebrahimi, Mohseni, Aslani, and Zahedi (2022) investigated the energy performance of a 3D concrete printed building made with two types of cement along with thermal insulation (spray polyurethane foam) and phase change materials (PCM) using DesignBuilder software. They found that incorporating PCM had minimal impact on reducing energy consumption, whereas insulation led to a 5% reduction in energy consumption.

Kamel and Kazemian (2023) assessed the energy performance of a hypothetical 3D-printed residential building in Dallas, US, using a BIM-to-BED workflow with Revit and OpenStudio-EnergyPlus. The study revealed that an optimized 3D-printed wall system could achieve up to 38.8% energy savings through improved wall design, material selection, and thermal insulation. The study reported an annual energy consumption of 115.22 kWh/m^2 for the optimal wall configuration under Dallas's climate conditions.

Most studies assessing the thermal performance of 3D-printed structures have focused on the thermal properties of 3D-printed components, with only a very limited number of studies assessing full-scale 3D-printed structures. There remains a lack of studies investigating indoor thermal environments and how 3D-printed structures interact with outdoor climates. This limitation is likely due to the limited number of 3D-printed buildings available for study, thus necessitating further investigation, as discussed in (Sovetova & Kaiser Calautit, 2024). While some studies have offered valuable insights into the performance of 3D-printed structures in various climates through the energy simulation approach, there is a need to validate these models.

It is worth noting that the modelling process in energy simulation tools is inherently simplified, typically assuming uniform thermal properties for building elements (e.g. walls). Consequently, applying this method to assess the thermal performance of 3D-printed buildings poses limitations in capturing the effects of mix variability and voids, introducing a degree of modelling uncertainty. This limitation was not considered in previous studies such as the work of Ayegba et al. (2022), Ebrahimi et al. (2022), and Kamel and Kazemian (2023), highlighting an opportunity for future research to integrate two- or three-dimensional heat transfer models with whole-building energy simulation in a multi-scale analytical approach to provide more accurate predictions of thermal and energy performance of 3D-printed buildings.

Evaluating the thermal and energy performance of 3D-printed buildings is important for fostering sustainability in the building industry. The reviewed studies emphasize the need for more research, particularly in hot and arid climates. This becomes more critical in developing countries such as Saudi Arabia, where new initiatives were stablished to transform the local construction industry and cope with the Fourth Industrial Revolution, as discussed in Section 2.9. A summary of the reviewed studies is provided in Table 4-1.

Table 4-1 Summary of previous studies on the thermal and energy performance of 3D concrete printing

Source	Study focus	Method
(Kaszynka et al., 2019)	Determining the thermal properties (U-value) of a printed wall with HPC and insulated with mineral wool	Plate apparatus
(Alkhalidi & Hatuqay, 2020)	Investigating and developing energy efficient and low-cost residential units through distinct 3D printable wall configurations with different mixtures in different climate zones	Ansys and Revit 'Green building studio'
(He et al., 2020)	Developing a modular 3D-printed vertical concrete green wall system to improve building energy efficiency	Energy modelling analysis
(Mahadevan et al., 2020)	Comparing the thermal comfort and building energy efficiency of residential buildings constructed with 3D printable concrete, M25 concrete, and conventional brick masonry	Energy modelling analysis (Revit with Safeira plug-in)
(Marais et al., 2021)	Investigating the thermal performance of 3D printable light-weight foam concrete and HPC elements and strategies toward thermal improvement of 3D concrete printed façade element cavity arrangement	FEM package ABAQUS
(Sun et al., 2021)	Thermal analysis of a 3D-printed prototype building using infrared thermography	IRT and heat transfer monitoring
(Suntharalingam et al., 2021)	Examining the thermal performance of 32 different 3D-printed concrete wall configurations to determine their U-values	ABAQUS
(Ebrahimi et al., 2022)	Investigating the energy performance of a 3D-printed building that used two types of cement along with thermal insulation and phase change material using DesignBuilder software	Energy modelling analysis
(de Rubeis, 2022)	Thermal analysis of a novel 3D-printed thermal insulating block using an infrared thermography technique and a hot box	HFM in Hot-box and IRT
(Ayegba et al., 2022)	Conducting an optimization analysis to determine optimal combination of 3D-printed concrete mix design and insulation type using DesignBuilder simulation software	Energy modelling analysis
(AlZahrani et al., 2022)	Investigating the thermal performance of a 3D-printed wall with various infill structures	ABAQUS
(Salandin et al., 2022)	Assessing the acoustic, thermal, and environmental performance of 3D-printed house in Spain using a case study approach	HFM (existing case study)
(Khalili Tari et al., 2023)	Investigating the energy efficiency and environmental impact of a 3D printable building using DesignBuilder software	Energy modelling analysis
(Kamel & Kazemian, 2023)	Developing multiple scenarios to evaluate BIM-to-BEM workflow for 3D-printed construction using a case study to quantify energy savings	Energy modelling analysis (OpenStudio-EnergyPlus)
(Dey & Panda, 2023)	Investigating the thermal performance of 3D-printed concrete slabs in different cavity patterns with and without insulation as potential wall component	Hot box and IR

For the purpose of the current research, two different buildings in Riyadh, KSA—one constructed using 3D printing and the other using conventional construction methods—will be considered for analysis. More information about the selected case study buildings and the selected methodology is provided in Chapter 5.

4.8 Summary

The Fourth Industrial Revolution has profoundly transformed building design and construction through innovative tools and technologies. This chapter started with an overview of the application of innovative technologies in the construction industry. It outlined the application of digital fabrication of concrete in the construction industry, including 3D concrete printing (or additive manufacturing). The chapter then discussed the development of 3D printing in the construction industry (see Sections 4.2 to 4.5).

Section 4.6 explored the construction and sustainability benefits of applying 3D printing technology in the construction sector over conventional construction methods, such as enabling the construction of complex geometries, accelerating the construction process, and reducing construction waste. The chapter also presented real-world examples of existing buildings, including applications in hot climates, demonstrating the feasibility of 3D concrete printing in the construction industry.

Lastly, the chapter included a review of previous studies in 3D concrete printing from a thermal and energy performance point of view (see Section 4.7). Most of these studies tended to focus on the thermal properties of 3D-printed components; therefore, analyses of thermal and energy performance (through field monitoring and dynamic simulations) of real and existing 3D-printed building, particularly in hot and arid regions, are lacking. Moreover, the number of real, occupied 3D-printed buildings constructed in hot-arid climates remains very limited, which further constrains the availability of empirical data for validating simulation results and understanding their thermal behaviour.

It has been demonstrated that the significant demand for new dwellings in KSA has encouraged the application of innovative construction techniques, with 3D concrete printing offering a promising solution to address the housing supply-demand gap (see Chapter 2). This chapter has shown that the adoption of 3D concrete printing aligns directly with the objectives of the BTSI (discussed in Section 2.9) by promoting faster, more sustainable, and locally manufactured construction solutions that reduce costs and respond to national housing demand. Therefore, it is essential to investigate the thermal behaviour and energy performance of 3D-printed buildings in the climate context of KSA and to test various improvement measures.

For the purpose of this thesis, two houses constructed using different methods—3D concrete printing and conventional construction—were selected as case studies for analysis using energy simulation software. A detailed review of the selected case study buildings is presented in the following chapter (see Section 5.3), while the modelling process of the two houses and the associated limitations are discussed in greater depth in Chapter 7.

CHAPTER 5

RESEARCH METHODOLOGY

- Introduction
- Applied research methods
- Selected case studies
- Thermal assessment tools
- Proposed enhancement measures

Chapter 5: RESEARCH METHODOLOGY

5.1 Introduction

This chapter details the methodology employed to achieve the research objectives and satisfy the aim of this study. It contains a justification and explanation for the selected city in Saudi Arabia, the case study buildings, and data collection and thermal analysis techniques (Sections 5.2 to 5.5). This is followed by a description of the utilized weather data and all details, inputs, and settings for the building energy simulation software (Sections 5.6 to 5.8).

Lastly, the chapter offers a description of proposed design strategies and materials, including the use of EPS insulation, cool roof, window shading options, and external wall alternatives, all of which are used in the simulation process to improve the thermal performance of the selected case study buildings in the climate context of Riyadh, KSA. More details are provided in Section 5.9.

5.2 The selected methodology and tools

This research adopts a case study approach to focus on the thermal performance of residential buildings constructed using different construction methods, namely 3D concrete printing and conventional construction techniques. To this end, two existing houses in Riyadh, KSA, were selected to serve as case studies.

The research methodology was developed based on several interrelated steps and strategies, which included in-situ measurements, dynamic simulations, and sensitivity analysis. This facilitated a comprehensive exploration and detailed assessment of the buildings' current thermal performance and behaviour, enabling the evaluation of how various design strategies learned from vernacular architecture and modern building technology can affect thermal and energy performance.

Field data collection and measurements provided insights into the thermal behaviour of the selected case study buildings under the extreme outdoor conditions of Riyadh (i.e. during peak cooling demand), in addition to providing the fundamental data required for simulations and energy model validation. Insights derived from baseline simulation results were used to evaluate the current performance of the buildings and propose enhancements to the building fabric for each case study.

A summary of the research methodology is provided in Figure 5-1, which illustrates the steps followed to achieve the study's main aim and objectives. Subsequent sections provide a

detailed description and justification of the study location, the selected case study buildings, and the tools utilized for thermal analysis.

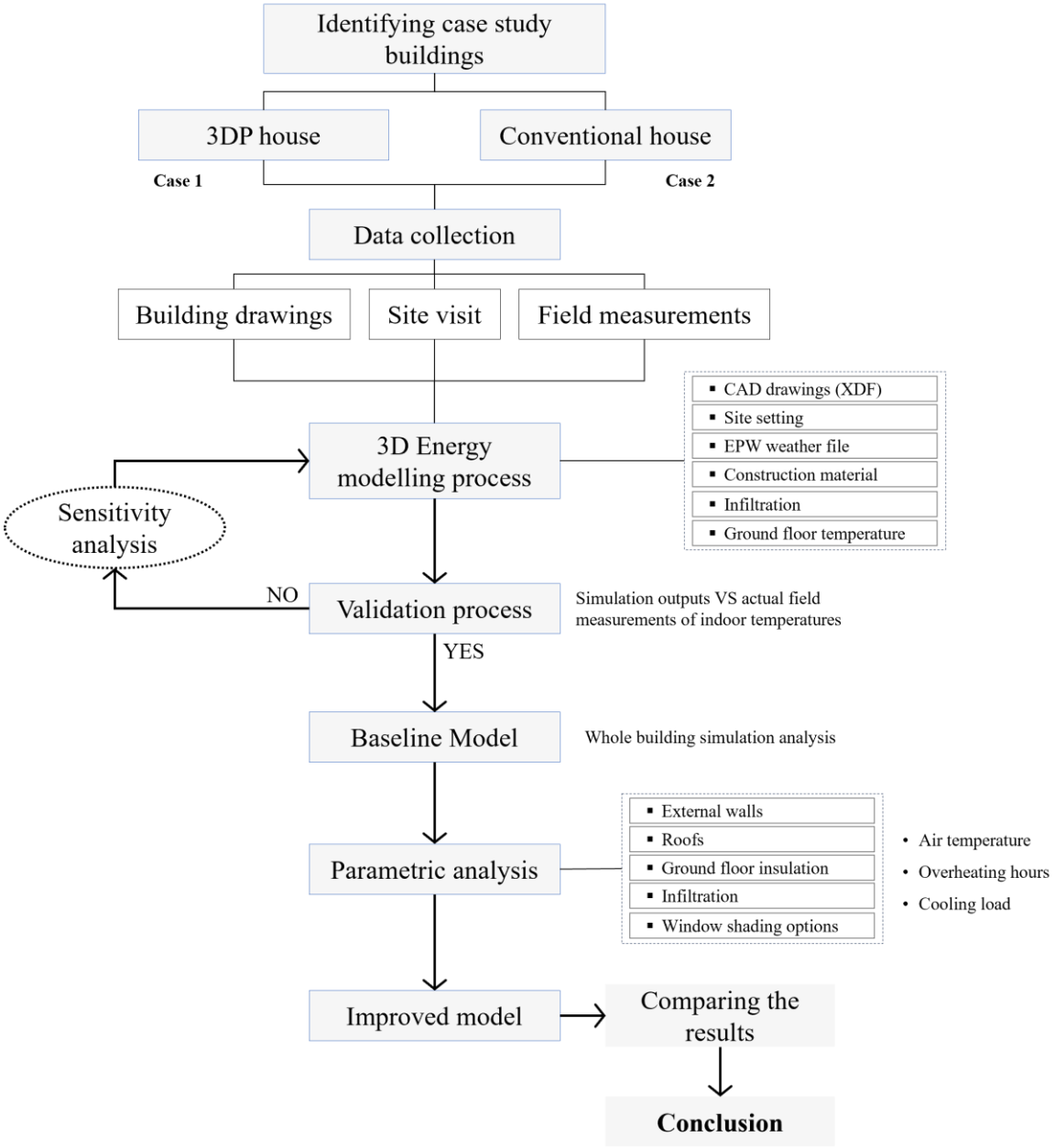


Figure 5-1 The overall methodological approach of this study

5.3 Case study

5.3.1 The selection of Riyadh City

As mentioned in Chapter 2, the SBC 602 classifies the country into three major climatic zones. Riyadh City, the capital and largest city of Saudi Arabia, is located in the central region of the kingdom, which, according to Koppen's climate classification, features a hot desert climate. The severe climate conditions of Riyadh—which is located in Zone1, the

hottest in the country—will serve as a kind of 'worst-case scenario' for the study of building thermal and energy performance in Saudi Arabia.

Moreover, Riyadh has experienced rapid urban development, making it one of the fastest expanding cities in the world. Also, due to its political, administrative, and economic values, Riyadh is one of the most important cities in the Kingdom (Riyadh Urban Observatory, 2022). During the past five decades, Riyadh has grown from a small town with fewer than 500,000 inhabitants (Al-Hathloul, 2017) into a major city occupying a territory of 3,115 km^2, which is more than three times its total urban area in 2000 (Riyadh Urban Observatory, 2022).

According to the *Population Study of Riyadh City* report by the Royal Commission for Riyadh City (2016), the city is occupied by 6.5 million inhabitants, or one-sixth of the total population of Saudi Arabia, and has an average annual growth rate of 4%. This makes Riyadh the most populated city in the country, followed by Jeddah and Makkah at 3.45 million and 1.57 million inhabitants, respectively. Additionally, Riyadh's population is anticipated to increase, reaching 9.5 million by 2050, or 30% greater than its current population (Royal Commission for Riyadh City, 2018).

5.3.2 Local climate consideration in Riyadh

Climate is a major factor influencing building design and energy consumption. This section aims to provide a climate analysis of Riyadh City to identify the key climatic factors that influence indoor thermal comfort in residential buildings.

According to monthly averages calculated for a 30-year period, from 1982 to 2011 (see Figure 5-2), the dry-bulb temperature in Riyadh during the summer season from June to August reaches as high as 43.7 °C during the daytime and above 25 °C at night. July and August are the warmest months of the year in Riyadh, with a monthly average temperature of 35 °C. During overheating periods, the extremely high air temperature, abundant solar insulation, and low levels of humidity are the main causes of discomfort.

In the winter, the average daily maximum temperature is almost halved, to 22 °C, and the nocturnal temperature can fall below 10 °C. January is the coldest month of the year in Riyadh, with a monthly average temperature of about 14 °C. It can be concluded that, in hot and dry climates, as mentioned earlier, there can be large variations in diurnal temperature (between 10 °C to nearly 15 °C).

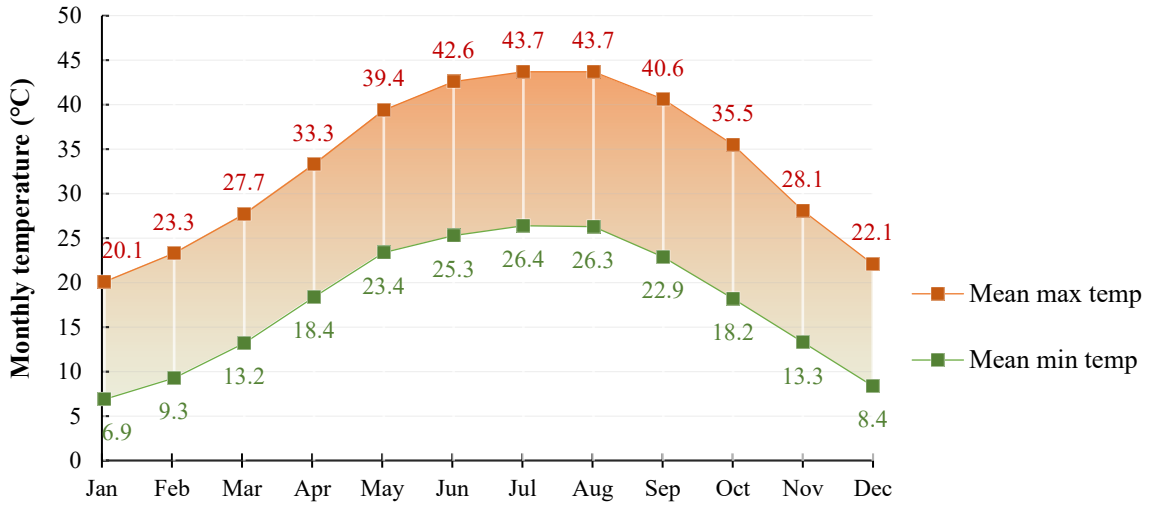


Figure 5-2 Monthly average temperatures for Riyadh based on 30-year historical data. Based on data from World Meteorological Organization (2022).

As the central region is distant from the coastal areas, humidity levels are relatively low, with some months experiencing extreme dryness (see Figure 5-3). The daily average relative humidity in Riyadh falls below 20% from May to September, reaching its lowest levels in July and August, with averages ranging from 8% to 18%. However, the average daily relative humidity rises above 30% from November to March. The most humid months in Riyadh are December and January, with an average relative humidity ranging from approximately 30% to 60%.

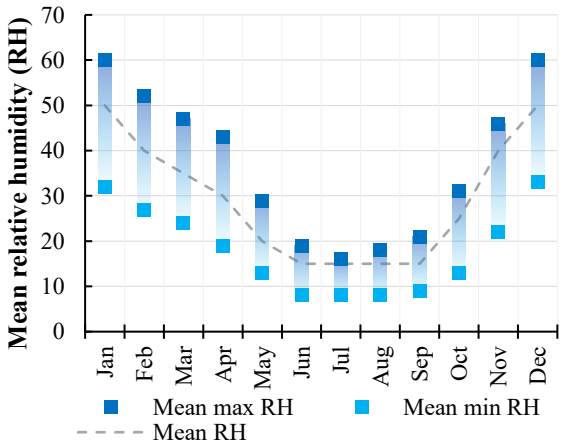


Figure 5-3 Relative humidity averages in Riyadh. Based on data from Weatherbase (2022).

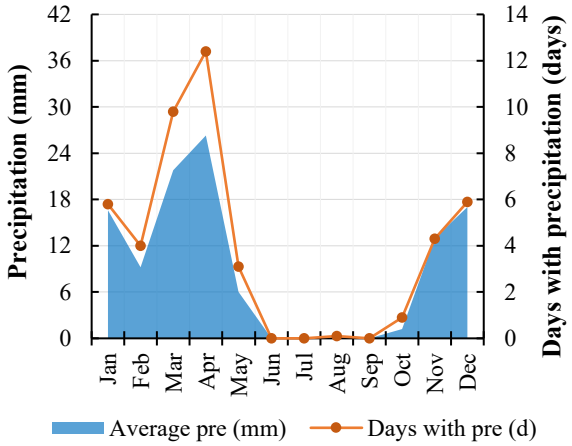


Figure 5-4 Average precipitation in Riyadh. Based on data from World Meteorological Organization (2022).

The overheating season in Riyadh is quite windy, with an average wind speed of above 14.1kph, reaching 15.7kph in July, the windiest month of the year. Winter is the calmest period of the year. The minimum wind speed is recorded in October, which has an average hourly wind speed of 12.3kph. The prevailing wind direction in Riyadh during the summer,

from May to September, is north, while winds come from the east, southeast, and northeast during the cold season (October to March) (Weather Spark, 2022).

The climate in Riyadh is generally dry and hot, with a low and irregular precipitation rate throughout the year. As illustrated in Figure 5-4, the precipitation rate in Riyadh is limited to the winter and spring months. Most precipitation occurs in April, when it can reach 26.3 mm, while summer is the driest season. Annually, Riyadh experiences an average rainfall of less than 10 mm.

As shown in the sun path diagram of Riyadh in Figure 5-6, on 21 June, the summer solstice, the noon solar altitude in Riyadh is 88.48º, when the sun azimuth is 180º. On this day, the sun rises at 05:05 (azimuth angle is 64º) and sets at 18:44 (azimuth angle is 296º), making it the longest day of the year (about 14 hours). The shortest day is 21 December, the winter solstice, when the noon solar altitude is 42º, and daytime extends for about 11 hours, starting from 06:32 (azimuth angle is 116º) to 17:09 (azimuth angle is 244º) (Time and Data AS, 2022).

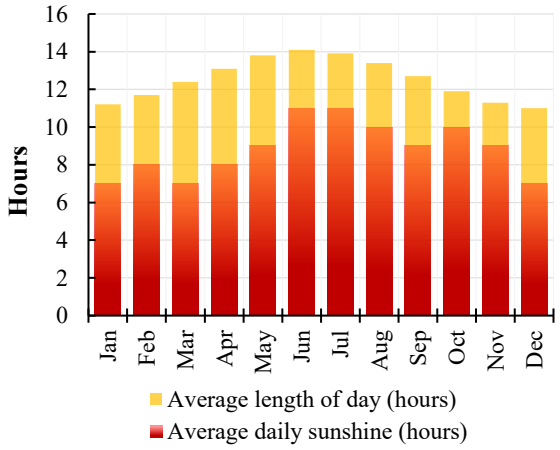


Figure 5-5 Average daylengths in Riyadh. Based on data from Weather Atlas (2022).

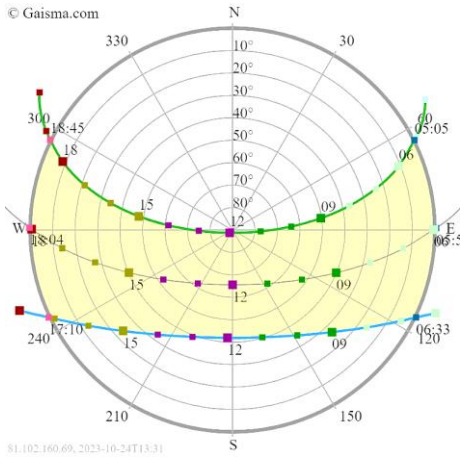


Figure 5-6 Sun path diagram for Riyadh with summer and winter solstices (GAISMA, 2023).

Following this analysis, the thermal comfort limits for Riyadh were predicted using the adaptive model discussed in Section 3.4. By applying Equation (3-6), the comfort temperature (Tc) for each month was calculated, as shown in Table 5-1.

Table 5-1 Adaptive comfort temperatures for Riyadh

	Jan	Feb	Mar	Apr	May	Jun	Jul	Aug	Sep	Oct	Nov	Dec	AV
Tc	21.9	22.8	24.1	25.8	27.5	28.3	28.6	28.6	27.6	26.1	24.2	22.5	25.2

According to the presented results, the predicted comfort temperatures for Riyadh can range from 22 °C to 28.6 °C, with an annual average of 25.2 °C. Notably, this range was found to

be in agreement with that derived for Pakistan (J. Fergus Nicol, Raja, Allaudin, & Jamy, 1999), Mombasa (Kiamba, 2016), and Jeddah, KSA (Bagasi & Calautit, 2020; Ghabra, 2018). It is suggested that the predicted comfort range could be used to define the comfort zone for the entire year. A psychrometric chart analysis was conducted for Riyadh using Climate Consultant 6.0 climate analysis software. See Figure 5-7.

Analysis of the climate data revealed that only 12% of the entire year (1,048 hours) in Riyadh falls within the comfort zone, as shown in Figure 5-7. The analysis also indicated that the application of passive design techniques could satisfy indoor thermal comfort for up to 62% of the year (5,426 hours) by maintaining indoor temperatures within the predicted comfort range (i.e. 22 °C to 28.6 °C) based on the Tc equation results shown in Table 5-1.

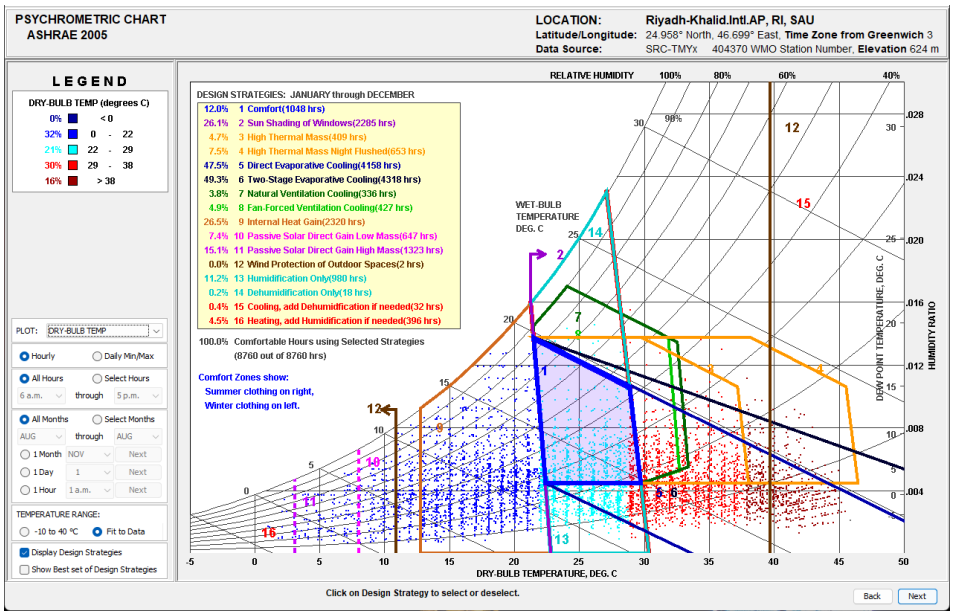


Figure 5-7 Psychrometric chart for Riyadh showing that only 12% of the year falls within the predicted comfort zone (Plotted using Climate Consultant 6.0).

Moreover, it was predicted that even with the application of passive strategies, the temperature would be above 28.6 °C for about 33% of the year (or 2,902 hours), indicating the potential for discomfort during this period. This analysis was deemed significant as it showed the duration that a building in Riyadh could operate using solely passive strategies, without the use of active measures. Even when these strategies prove inadequate to ensure indoor thermal comfort in extreme outdoor conditions, they still play a major role in reducing the energy requirements associated with the indoor thermal environment.

5.3.3 The selection of the case study buildings in Riyadh

For the purpose of this study, two different residential buildings located in Riyadh City, each constructed using different construction methods, were selected as case studies. Notably, the

3D-printed house (Case Study 1) was the only 3D-printed house available for study in KSA during the study period. As for the conventional house (Case Study 2), the study originally intended to assess a housing unit provided by the Ministry of Housing. However, due to the rapid pace of housing construction, especially in Riyadh—intended to achieve the government's ambitious 70% homeownership target, as discussed in Chapter 2—the author opted for a conventionally constructed house in Riyadh developed by a private real estate developer.

In this study, the conventional house (Case Study 2) was selected based on criteria that included building location, uniqueness (not previously tested), recent construction, accessibility during the identified study period, and the availability of drawings and construction details. It is worth noting that the selected housing type (detached house) represents 45.8% of the total housing units in the region, making it the preferred dwelling type in Riyadh (see Section 2.6).

As shown in Figure 5-8, both houses are situated in different urban environments within the city of Riyadh. The 3D-printed house is located in a new development on the northern side of Riyadh known as Al-Narges. This area was in the development phase, with ongoing construction activities in line with the government's plan to increase the housing supply. The area falls under the supervision of the National Housing Company (NHC), which is responsible for real estate investments on behalf of the Saudi Ministry of Municipal and Rural Affairs and Housing. Further, it is part of the extensive real estate developments in the city.

In contrast, the conventional house (Case Study 2) is situated in a fully developed environment and is surrounded on three sides by adjacent buildings. The selected house was in the marketing phase and was not occupied during the study period. Thus, its indoor thermal condition was similar to that of Case Study 1. For these reasons, alongside the discussed criteria, it was found that the selected conventional house could serve as a suitable case study for a comparison of its thermal behaviour with that of the 3D-printed house. It must be noted, however, that the selected conventional house differs from the 3D-printed house in several respects, such as orientation, design, and number of floors. A detailed description of the selected case study buildings is provided in the following subsections.

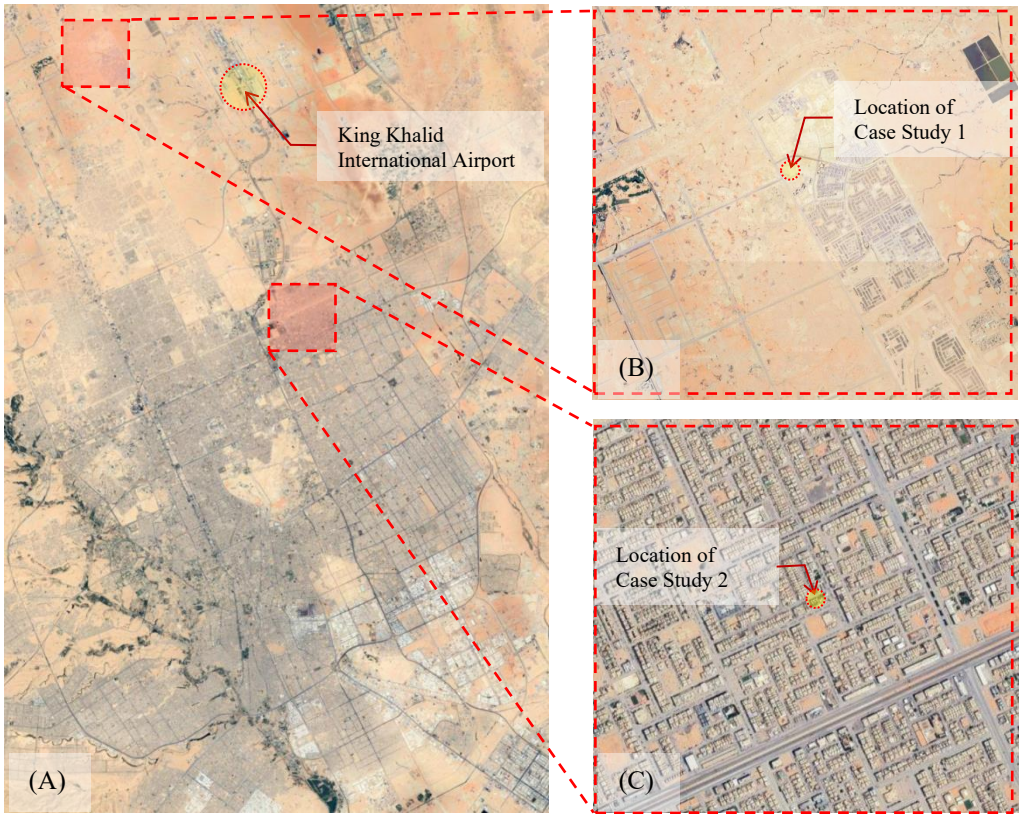


Figure 5-8 Aerial view of the case studies' location: (A) Map of Riyadh City; (B) Location of Case Study 1; (C) Location of Case Study 2. Adapted from Google (2023).

5.3.4 Description of case studies

5.3.4.1 Case Study 1 (3D-printed house)

The 3D Studio 2030 is a prototype of an on-site 3D-printed house constructed using mobile robotic arms provided by CyBe Construction, a building and construction industry technology company founded in 2013 in the Netherlands. The one-story house comprises one bedroom, a living room, a dining room, a kitchen, and a bathroom, with a total area of 78 m^2. The layout of the house consists of two simple rectangular shapes, with its long axis laying along the south-north axis.

The house was designed by Consolidated Contractors Company (CCC), and the construction work was carried out in cooperation with the CyBe team in KSA. The purpose of constructing such a small house was to explore the potential of constructing new and efficient buildings in Saudi Arabia using additive manufacturing technology. The house is considered the first of its kind in the country and has become a showcase for the building of up to 1.5 million houses using new innovative construction technologies, including 3D concrete printing, by 2030. External views of the house are shown in Figure 5-9.



(A) (B)

Figure 5-9 Photos of the 3D-printed house (Case Study 1) taken by the author: (A) South-west view; (B) North-east view

The house consists of 48 3D-printed components, all fabricated on-site within one week (5–13 September 2018), while the entire house, including the finishing works, was completed within five weeks. The fabrication process was carried out in a controlled environment to protect the printing mixture from the extreme outdoor conditions.

The mixture used, CyBe mortar, was developed specifically for 3D concrete printing and comprised a cementitious material mixed with a chemical admixture and water at a specific ratio. The mortar has a setting time ranging from 3 to 5 minutes with high early compressive strength within 24 hours. The roof was constructed using 15 cm thick precast hollow core slabs, and the floor is a 15 cm grade slab (flat concrete structure). Due to the lack of studies certifying the printed walls as bearing loads, and for safety reasons, as this is the first 3D-printed house in the region, the loads from the roof slabs were designed to be carried by bearing-reinforced concrete beams and columns, both of which are embedded in the printed elements. Illustrations of the construction process are presented in Figure 5-10.

All walls were extruded layer by layer, a common practice in the 3D printing method. Due to limitations of the robotic arm, all printed walls had a maximum length of 2.75 m, and an average height of 2.75 m. Insulation material was applied to improve the wall's thermal performance. The walls comprised three layers: an outside layer, an inside layer, and a zigzagged infill layer in between, as shown in Figure 5-10b. Each layer was 40 mm thick and 20 mm high. After printing, all electrical utilities and reinforcement bars were placed manually, and insulation material was applied to improve the wall's thermal performance.



(A) (B)

Figure 5-10 Construction process of the 3D-printed case study building: (A) Preparation of the foundation prior to concrete casting; (B) Layer-by-layer 3D-printed wall system with integrated structural steel and service conduits. Adapted from Consolidated Contractors Group (2018).

It should be noted that the 3D-printed wall construction was simplified during the modelling process in the simulation software. The as-built 3D-printed wall structure, described above, was modelled as two outer concrete layers of 120 mm each, separated by a 60 mm continuous insulation layer, maintaining the current total wall thickness of 300 mm and the material properties (see Table 7-3). This configuration was selected as it produced a strong correlation between field measurements and simulation predictions.

As discussed in Section 4.7, such simplifications—which is one of the limitations of this study—can introduce uncertainty into the model outputs. The selected energy simulation software is described in Section 5.5, while further details on the modelling process, data inputs, and construction-material specifications are presented in Section 7.2. Validation results are discussed in Section 7.3.

During the site visit, some changes were noticed between the drawings provided by CCC and the actual existing layout of the house. According to the contractor, this change was made due to the collapse of the kitchen's internal wall during the construction phase, which eventually was conventionally constructed using 20 cm concrete blocks. It was not possible to use the robotic arm since all surrounding walls had already been elevated. In addition, window details were different from those indicated in the original documents. Therefore, it was necessary to verify the dimensions of each space and create as-built drawings for further analysis. See Figure 5-11.

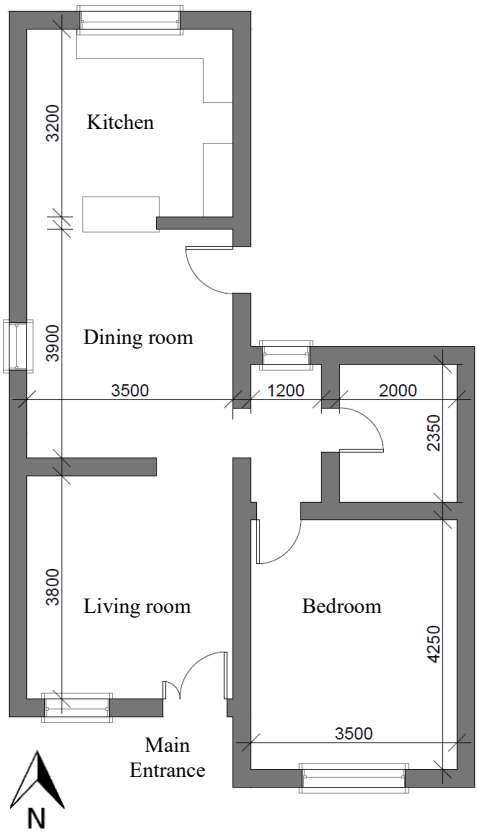


Figure 5-11 Floor plan of the house: As-built drawing produced using Autodesk Revit 2022

As windows' physical and thermal properties contribute significantly to indoor thermal performance and user comfort, their details were observed during the site visit. All rooms have 7 mm tinted double-glazed windows with air gaps and aluminium frames. Further, regardless of their orientation, all windows have about 10 cm egg-crate shading devices, as shown in Figure 5-9. While all windows have similar thermal properties, they are different in size and opening type, thus affecting the openable ratio of a window in each space, as shown in Table 5-2.

Table 5-2 Window types and properties used in the 3D-printed house

Room	W (cm)	H (cm)	Sill (cm)	Opening category	Specifications	Local shading
Living room	110	145	60	Top hung	Max angle open: 20°	10 cm egg-crate
Dining room and corridor	80	145	60	Top hung	Max angle open: 20°	10 cm egg-crate
Kitchen	175	105	100	Sliding	Openable area: 40%	10 cm egg-crate
Bedroom	175	145	60	Sliding	Openable area: 40%	10 cm egg-crate
Bathroom	70	75	130	Top hung	Max angle open: 20°	10 cm egg-crate

5.3.4.2 Case Study 2 (Conventional house)

The selected conventional house in this study is a modern two-story residential building with an upstairs annexe and a total area of 443 m^2. The house has a rectangular layout; its long axis is aligned along the northwest-southeast axis, and its front façade has a northwest

orientation. The ground floor comprises social and guest welcoming areas along with the main kitchen, with a total area of 194 m^2. The first floor consists of four bedrooms, a family living space, and bathrooms, occupying a total area of about 165 m^2. The annexe has a total built-up area of nearly 83 m^2, comprising a large multipurpose area, an additional room, and an external terrace.

As shown in Figure 5-12, the selected house was part of a multiple housing project started in 2021 by a private real estate developer who oversaw the construction process. The original CAD drawings of the house were obtained along with the specifications of the building elements and materials. As indicated in Section 2.6, this housing type represents 45.8% of the total housing units in the region. It must be noted that the house was unoccupied during the study period, which made it a suitable case study as it matched Case 1's conditions.

Two different rooms were selected for field monitoring. Room 1 (R1), located on the first floor, has a total area of 16.3 m^2 and a height of 3.3m. This room has one exposed wall with a window facing southwest. Room 2 (R2) is located on the annexe floor (top floor) and has a total area of nearly 22 m^2 and a height of 3m. This room has four exposed surfaces (three vertical walls and the roof), and its window faces southwest. The floor plans of the house and the selected rooms are shown in Figure 5-13.

The house was constructed using a reinforced concrete frame structure, a conventional structural system in Saudi Arabia, as discussed in Section 2.6. The external walls were constructed using 20 cm sandwich concrete blocks with 3 cm of expanded polystyrene (EPS), whereas the internal walls were constructed using 15 cm concrete blocks. The internal floors and the roof are made of ribbed (Hourdi) slabs, and the ground floor is made of grade slab.

As for fenestration, all rooms have 24 mm double-glazed windows, aluminium frames, 12 mm air gaps, and Low-E coatings. Window details for selected rooms are shown in Table 5-3.



Figure 5-12 External view of Case Study 2 (photo taken by the author)



Figure 5-13 Floor plans of Case Study 2, produced using Autodesk Revit 2022 (highlighted selected rooms): (A) Ground floor layout; (B) First floor layout; (C) Upstairs annexe layout

Table 5-3 Details of window types and physical properties for selected rooms in Case Study 2

Room	W (cm)	H (cm)	Sill (cm)	Opening category	Specifications	Local shading
Room 1	74	250	20	Side hung	Max angle open: 20°	NA
Room 2	76	250	20	Side hung	Max angle open: 20°	NA

5.4 Field monitoring of building thermal performance

The field measurement methodology used specific instruments to monitor the thermal performance of the selected buildings in Riyadh. Various scholars have adopted this method for evaluating building thermal performance and validating computer energy models, such as in the work of Abuhussain (2020), Alaboud (2021), Bagasi (2022), El-Bakkush (2016), Ghabra (2018), Kiamba (2016), and Salandin et al. (2022).

The present research considered two recent houses constructed using different construction methods, as described in the previous section. The thermal performance of each house was monitored during the overheating season, considering air temperature as the most influential factor affecting thermal comfort. Indoor air temperature measurements were taken at specific locations in each house from 11–24 August 2022. Measurements were taken without ventilation and after applying natural ventilation.

In addition to air temperature (Ta) readings, globe temperature (Tg), the surface temperature of external walls (inner surface temperature and external surface temperature), and air velocity (Tv) were measured for selected periods and locations in the 3D-printed house. The process, objectives, and limitations of the field data collection are discussed in more detail in Chapter 6. The utilized instruments and their specifications are described in the following subsection.

5.4.1 Selection of instruments

To monitor the aforementioned parameters, a group of data loggers was carefully selected for the purpose of the field study. It is worth noting that the selection of these tools was largely influenced by several criteria, including the author's budget and the loggers' ability to provide highly accurate continuous readings of environmental parameters. Additionally, technical factors such as battery life and storage capacity were considered to avoid any potential disturbance of the readings. The instruments used in this study, as well as their specifications, are shown in Table 5-4 and Figure 5-14.

Table 5-4 Instruments used in this study and their specifications

Instrument	No.	Parameter and range	Accuracy and resolution
Dual channel data logger with built-in sensor Tinytag Plus 2 #TGP-4500	1	▪ Air temperature: −25 to +85 °C ▪ Relative humidity: 0% to 100% ▪ Suitable for outdoor application	Ta: 0.01 °C or better RH: ±0.3% at 25 °C
Dual channel data logger with built-in sensor Tinytag View 2 #TV-4500	2	▪ Air temperature: −25 to +50 °C ▪ Relative humidity: 0% to 100% ▪ Suitable for indoor application	Ta: 0.02 °C or better RH: better than ±0.3%
Dual channel data logger with built-in sensor Tinytag Ultra 2 #TGU-4500	3	▪ Air temperature: −25 to +85 °C ▪ Relative humidity: 0% to 95% ▪ Suitable for indoor application	Ta: 0.01 °C or better RH: ±0.3% at 25 °C
Multifunction data logger thermometer PCE-WB 20SD	1	▪ Black-globe temperature: 0 to 59 °C ▪ Suitable for indoor and outdoor applications.	± 0.6 °C
Hot wire anemometer data logger with a telescoping probe EXTECH #SDL350	1	▪ Air velocity: 0.2 to 25 m/s	±5% 0.01 m/s
Dual laser infrared thermometer FLUKE #62 MAX plus	1	▪ Surface temperature: −30 to 650 °C ▪ Emissivity 0.10 to 1.00	±1.0% of reading ±1.0 °C

For more information, see the product datasheets provided in Appendix A-B.



Tinytag Plus-2 (TGP-4500)



Tinytag Ultra-2 (TGU-4500)



Tinytag View-2 (TV-4500)



EXTECH: SDL350



Fluke 62 max+



PCE-WB 20SD

Figure 5-14 Instruments employed during fieldwork

- **Tinytag data loggers**

In this study, a total of six dual channel Gemini Tinytag data loggers with built-in sensors were placed in strategic locations to record air temperature inside and outside the building. Tinytag data loggers include compact devices for indoor applications, such as Tinytag View-2 and Ultra-2, and rugged loggers such as Tinytag Plus-2, which are suitable for the outdoor environment. The loggers can measure temperature from −25 °C to above +50 °C, and relative humidity from 0% to 100% with high levels of accuracy and reading resolution, making the results highly reliable. Additionally, Tinytag data loggers have for decades been recognized for their high accuracy and reliability and were commonly utilized in previous research of a nature similar to that of the current thesis.

- **PEC-WB 20SD**

This multifunction wet bulb temperature data logger by PCE Instruments was used to measure indoor black-globe temperature, with a measuring range from 0 °C to +80 °C and high accuracy (±0.6 °C). The device is suitable for indoor and outdoor applications for real-time measurements or data recording of a wide range of environmental variables.

- **EXTECH SDL350**

The hot wire anemometer and data logger allow air velocity between 0.2 m/s and 25 m/s to be recorded at a high resolution (0.01 m/s) and with ±5% accuracy. This portable anemometer is offered as a separate telescoping probe. It allows users to adjust the data sampling rate (record interval) from as low as one second to as high as one hour. The recorded data are stored on an SD card in Excel format, which can be transferred to a PC for analysis. This tool has a large LCD with dual function meter display, allowing air flow or air velocity and temperature to be read simultaneously.

- **FLUKE 62 MAX+**

This handheld dual laser infrared thermometer offers highly reliable and quick ‘non-contact’ measurements of surface temperature. It can measure across a wide range of temperatures, from −30 °C to 650 °C, with ±1.0 °C instrument error. Additional features include the ability to provide minimum, maximum, or average temperature or the difference between two measurements.

5.4.2 Limitations

The field measurements focused on environmental parameters to assess the indoor thermal environment of the two case study buildings: a 3D-printed house and a conventional house. As both houses were unoccupied during the measurement period, personal factors and internal heat gains were not covered in this study. Owing to time constraints and the availability of equipment, monitoring was limited to selected rooms and conducted only for a short period during the summer, capturing peak-season conditions in Riyadh but excluding seasonal variations. Some environmental parameters—such as globe temperature, air velocity, and surface temperature—were recorded only in the 3D-printed house. In addition, the placement of instruments was influenced by safety and accessibility considerations, which limited the number and type of variables measured inside the rooms. Future studies should extend monitoring to other seasons and include a consistent set of measurements, including additional parameters such as indoor relative humidity and heat flux, to provide a more comprehensive evaluation of the thermal performance of both construction types.

5.5 Building energy simulation software

Growing concerns about building performance and indoor environments have heightened awareness of the crucial role played by building energy simulation tools and the need for rapid feedback on various design decisions during the early design process. Clarke (2001) described energy simulation as a robust method for evaluating and optimizing a building's thermal performance and energy efficiency. Researchers have benefited greatly from employing energy simulation to conduct thorough analyses, as it offers flexibility in simulating various room boundary conditions and design alternatives while accounting for variables such as occupancy, lighting, and weather profiles.

Energy simulation tools are frequently employed during the early stages of the design process; they offer insights into a building's energy requirements in specific conditions and predict its performance under various hypothetical scenarios and design strategies, ensuring user comfort and well-being, reducing energy requirements, complying with standards and regulations, mitigating environmental impact, and contributing to climate change abatement (Alosaimi, 2023; Alrashed, 2015; Carratt, Kokogiannakis, & Daly, 2020; Clarke, 2001). Moreover, simulations can be used to address any relevant questions for different scenarios, such as: What are the peak cooling, heating, and lighting demand periods and when do they occur? and What is the contribution of implementing a particular technology, system, or material? (Clarke, 2001).

This method enables a more comprehensive investigation and analysis within a shorter timeframe compared to other approaches, such as experimental or field observations and monitoring methods. According to Carratt et al. (2020), studies that rely solely on monitored data are limited by the specific occupant behaviours and weather conditions absorbed during the study period. All of the studies that conducted a solely theoretical assessment of retrofits utilized building energy simulation tools.

For the scope of this study, the considered simulation tool had to be able to predict indoor thermal conditions, calculate solar gain through the envelope, and estimate cooling loads and thermal comfort. Additionally, material thermal properties had to be available and editable to assess various construction materials and their impacts on energy consumption.

Most of the widely recognized simulation tools today are based on dynamic numerical methods. Dynamic simulation tools, such as the Apache engine within IES-VE (discussed in Section 5.5.1), are integrated with computational techniques for building loads and energy calculations. They usually perform computations on an hourly basis and for each zone individually to account for the dynamic interactions between all thermal-based elements (e.g. building envelope, lighting, HVAC systems, and control systems) associated with comfort and energy consumption (Hong, Chou, & Bong, 2000; Solmaz, 2019).

Several building energy simulation tools have been used in the literature, with DesignBuilder, EnergyPlus, and IES-VE being among the most frequently used tools. A comparison of selected building energy simulation software types is shown in Table 5-5.

IES-VE was selected to carry out this thesis. It has been validated and employed in numerous studies, including doctoral research, of a nature and aim similar to that of this thesis (Aldossary et al., 2014; Alkhalifah, 2024; Alrashed, 2015; Alrashed & Asif, 2015a; Elnabawi & Saber, 2022; IES-VE, 2023; Lasker, 2016). Furthermore, the author of the current research made use of a fully licensed available energy simulation tool at the University of Nottingham. In addition to its accuracy and user-friendly interface, IES-VE provides a variety of conveniently accessible resources, including required training courses for beginners and advanced users, thus conserving the time and effort needed to find suitable and reliable training. A detailed description of IES and the integrated tools used to carry out this study is discussed in the following section.

Table 5-5 Comparison of selected building energy simulation tools. Adapted from Solmaz (2019)

Simulation tool	Major capabilities	Expertise required	Users	License	Company/ Country
DesignBuilder	▪ Whole-building energy simulations ▪ Code compliance checking ▪ Parametric and optimization	No steep learning process	Architects Engineers Researchers	Required	Design Builder software Ltd./UK
EnergyPlus	▪ Whole-building energy simulations ▪ Load calculations ▪ Lighting simulation	Background in building physics and mechanical engineering	Architects Engineers Building auditors and operators Researchers	Free/open source license	Department of Energy & National Renewable Energy Laboratory/US
IES-VE	▪ Whole-building energy simulations ▪ Load calculations ▪ Lighting simulation ▪ Code compliance checking	Training is required Includes documentation for learning	Architects Engineers Energy Consultants	Required	Integrated Environmental Solutions (IES)/UK
EDSL-TAS	▪ Whole-building energy simulation ▪ HVAC system selection and sizing ▪ Parametric and optimization ▪ Detailed cost analysis	Training course is not required Includes comprehensive tutorials	Architects Building services engineers Consulting engineers	Free for academic use	Environmental Design Solutions Limited (EDSL)/UK
Green Building Studio	▪ Whole-building energy simulation ▪ Parametric and optimization ▪ Energy conservation measures	Only 3D-CAD/BIM experience is required for geometry	Architects Engineers Construction managers	Free for academic use	Autodesk In./US
TRNSYS	▪ Whole-building energy simulation ▪ Parametric and optimization ▪ Detailed component simulation	No, only a Fortan background to generate new components	Architects, Engineers, and Researchers	Reduced for academic use	Thermal Energy System Specialists, LLC/US

5.5.1 Integrated Environmental Solution-Virtual Environment (IES-VE)

IES-VE is an example of a whole-building energy simulation tool. It consists of a suite of integrated analysis tools that allow users to analyse and evaluate a wide range of building performance metrics. The analysis capabilities of the software tools cover a wide range of assessment types, including comfort, ventilation, energy efficiency, and optimization. Further, the performance of a building can be investigated across the building's life cycle, from the early design stage to post occupancy (El-Bakkush, 2016; IES-VE, 2023).

IES-VE comprises several linked modules. Each module has its own features and specialization. However, this thesis focused on the following modules for more in-depth analysis:

- **ModelIT**: Allows users to construct a detailed 3D model with proper shading and surrounding context.
- **SunCast**: Used to conduct solar and shading analysis, which includes solar gain calculations based on the location settings and orientation of the model.
- **ApacheSim**: Used to conduct an advanced dynamic thermal simulation and data analysis of indoor thermal conditions and energy consumption. Dynamic thermal simulation is a mathematical representation of the heat transfer processes taking place inside and around the model, which is commonly used for thermal analysis.
- **MacroFlo**: Used to assign openings to the model to investigate the effect of natural ventilation on indoor thermal conditions.
- **VistaPro**: Used to view the simulation results and export data to Microsoft Excel for further analysis.

Performing energy simulations requires intensive data input, including site setting, building geometry, orientation, profiles, infiltration rate, construction materials, and weather data.

With accurate input data, IES-VE can help designers identify peak energy loads for a building in any selected location, providing users with a clear understanding of the behaviour of a building not only under peak conditions but also throughout the year. It offers hourly data analysis of the indoor thermal environment and provides the required output in sufficient levels of detail to fulfil the objectives of this thesis.

Indoor thermal conditions can be monitored with user-controlled intervals down to 60 seconds (IES-VE, 2023). The produced outcomes through simulation include:

- Comprehensive indoor performance such as room loads, surface temperature, humidity, and hourly temperatures.
- Load breakdown (conduction, convection, radiation, and casual gains).
- Energy consumption (hourly, monthly, and annually).
- Energy consumption and CO_2 emissions.

Figure 5-15 summarizes the simulation process adopted in this thesis. The modelling process of the baseline models is discussed in more detail in the next chapter, while a detailed description of the input data is provided later in this chapter (see Sections 5.6 to 5.8).

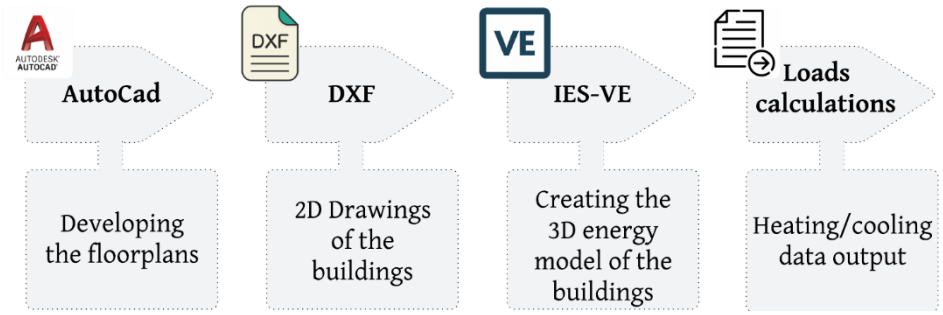


Figure 5-15 Summary of IES simulation process

As per the software manual, all required input data, summarized in Figure 5-16, were identified in IES-VE, including project location, weather data, building geometry, construction material properties, occupancy profile, and internal loads. These data are discussed in more detail in the following sections.

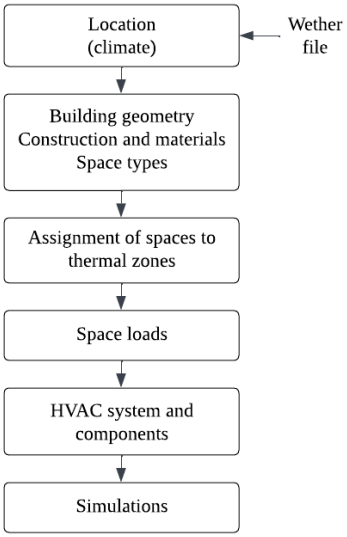


Figure 5-16 Workflow for building energy modelling software. Adapted from Mahgoub and Saber (2022).

5.6 Obtaining the weather data file for simulation

As the local climate plays a significant role in buildings' thermal performance, it is critical to input the appropriate location settings. The accuracy of weather data is crucial for realistic energy simulations. In ApacheSim, IES requires a weather file to run the simulation and perform thermal analysis. The software accepts EnergyPlus Weather Format (EPW) files,

which contain hourly climatic data for a certain region, including dry-bulb temperature, relative humidity, sky cover, wind speed, and more. These data are collected from actual meteorological stations around the world.

Notably, EnergyPlus recommends that users avoid using files of the type Test Reference Year (TRY), which refer to single-year data, as these formats do not accurately reflect local long-term weather patterns. Instead, Typical Meteorological Year (TMY) formats are considered more appropriate for energy simulation tools as they provide results that better represent the local long-term average. This approach offers more realistic weather conditions that reflect typical long-term patterns, thus enhancing modelling accuracy.

Since the local weather files for the selected case study city were not included in the IES-VE database, it was important to find a suitable and reliable alternative source. Various private sources that supply appropriate weather files for energy simulation are referred to by IES-VE (2023) and have been utilized by previous researchers, such as Meteonorm (Alaboud & Gadi, 2020; Alrashed & Asif, 2015a), EnergyPlus database (Ahmed & Asif, 2020; Ayegba et al., 2022), and Climate.OneBuilding.org (Al Rasbi & Gadi, 2021; Alayed et al., 2021).

In this thesis, the EPW weather file was extracted from Climate.OneBuilding.org database (Lawrie & Crawley, 2022). Climate.OneBuilding.org provides free, reliable weather data (TMY) files in EPW format for Riyadh City. The weather data were collected from King Khalid International Airport. It is noteworthy that the obtained data were derived for the most recent 15 years (2007 to 2021).

5.7 Energy model validation

In this thesis, both case study buildings were modelled using the dynamic energy simulation software tool IES-VE. As mentioned earlier, IES-VE has been validated and proven to be a reliable tool for the industry (see Section 5.5). However, it is users' responsibility to implement the simulation process correctly (Asfour, 2018). To increase confidence in the developed energy models and the simulation outputs, the performance of each model was validated against in-situ measurements. The aim of this step was to obtain a strong positive correlation between the predicted thermal behaviour of the IES-VE models and the actual thermal performance of the two houses.

For this purpose, hourly temperature calibrations were conducted between the IES-VE models and the actual monitored data. For hourly data, the acceptable boundary limits are 10% for the normalised mean bias error (NMBE) and 30% for the coefficient of variation of

the root mean square error (CV RMSE) based on AHSRAE guidelines 14-2014 (ASHRAE, 2014). CIBSE TM63 standard, Operational Performance: Building performance modelling and calibration for evaluation of energy in-use, accepts a boundary limit of 2 °C for the mean absolute error (MAE) based on previous studies like (Royapoor and Roskilly, 2015, as cited in CIBSE TM63, 2020).

Next, the energy consumption of the baseline models was predicted and compared with those reported in the relevant literature. The 3D modelling steps and validation process will be discussed in more detail in Chapter 7. The following section describes the main input data and software settings used for the baseline energy simulation.

5.8 Determining the baseline model

After calibrating the constructed IES models, the next step was to predict the energy consumption and thermal loads for both houses. To achieve the objectives of this study, the developed baseline energy models were used to gain insights into the annual energy performance and thermal loads associated with different construction methods for Saudi Arabis's dwellings. In this phase, it was critically important to define energy-related input data for the IES models, particularly for the cooling system, equipment, lighting, and occupancy schedules and profiles, as discussed in the following subsections.

5.8.1 Operational schedules

Project profiles play a crucial role in the energy simulation process, allowing users to regulate the schedules of diverse variables that affect the dynamic thermal properties of the building, such as window operation, cooling and heating systems, lighting, equipment, and occupancy schedules.

A number of scholars have indicated that precisely modelling occupancy behaviour can be difficult due to the unpredictable behaviour of users, leading to considerable uncertainty in the energy model (Abuhussain, 2020; Alshahrani, 2018). Several researchers have conducted interviews with the occupants of a building to more precisely determine their behaviour.

As both houses investigated in this thesis were unoccupied during the study period, which is one of the limitations of this study, it was not possible to obtain occupancy profiles and schedules through interviews; rather, the data were collected from previous studies. It must be noted that this technique offers limitations, as it may not precisely reflect actual occupancy patterns. Typical profiles for occupancy, cooling, lighting, and equipment for different zones are illustrated in Figure 5-17.

This thesis utilized the daily profile for occupancy, artificial lighting, cooling, and equipment proposed by Monawar (2001). Each profile comprises four sub-profiles based on zones (living, kitchen, guests, and sleeping zones). The mentioned study conducted a comprehensive survey targeting 600 householders to determine the typical occupancy daily profile in KSA's dwellings.

It should be noted that the adoption of older occupancy and plug-load schedules may understate the current energy consumption patterns in Saudi dwellings. Future research should therefore aim to establish updated and locally validated occupancy profiles to improve the accuracy of building-energy predictions in KSA.

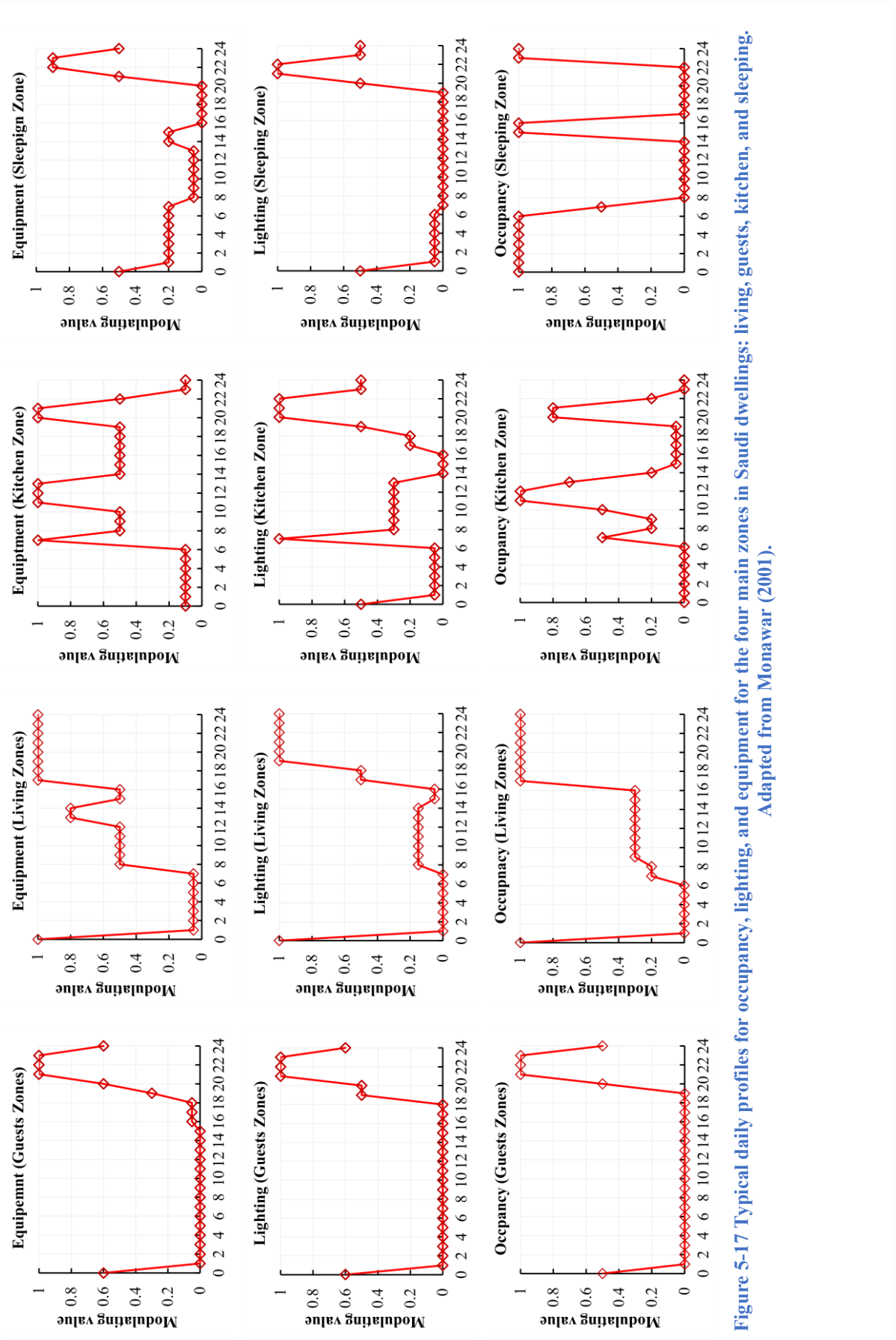


Figure 5-17 Typical daily profiles for occupancy, lighting, and equipment for the four main zones in Saudi dwellings: living, guests, kitchen, and sleeping. Adapted from Monawar (2001).

5.8.2 HVAC system and cooling set point temperature

The heating and cooling requirements for a building at any time can vary significantly depending on external and internal factors (ASHRAE, 2013). Based on the climate analysis presented earlier in this chapter (see Section 5.3.2), AC is required throughout most of the year owing to the extreme weather conditions of Riyadh. A questionnaire survey conducted by Alrashed (2015) aiming to determine the types of household systems used in Saudi Arabia's dwellings revealed that both window-type and mini-split systems were the main air conditioning types used, with the mini-spilt system being more preferred in modern dwellings. Thus, for the purpose of this thesis, a mini-spilt system was selected and defined in the IES models for every conditioned room. Moreover, the system was assumed to be used all year-round, primarily to quantify the effect of the tested energy efficiency measures on the thermal loads and thus energy consumption of the selected dwellings. The main characteristics of the HVAC system are summarized in Table 5-6.

Table 5-6 Description of HVAC systems in a typical house in Saudi Arabia.

Parameter	Description
Types of cooling and heating systems	Mini-split system provided for all conditioned spaces
Energy efficiency	Cooling Energy Efficiency Rating (EER) = 3.21 kW/kW Heating Coefficient of Performance (COP) = 3.62 kW/kW
Flow rate	8 l/s per person
Heating set point	20 °C (SBC 602)
Cooling set point	26 °C (see Chapter 8)
Auxiliary ventilation	50 l/s for kitchens and 25 l/s for bathrooms
Energy of auxiliary ventilation	1 W/(l/s) for kitchens, and 0.5 W/(l/s) for toilets

5.8.3 Power density and internal heat gain

Typically, Saudi residential buildings have four different main zones: living, guests, kitchen, and sleeping. Due to differences in functions and activities, power density and occupant heat gain vary among these zones. The main settings of 'Building Template Manager' in IES-VE require detailed inputs for lighting, equipment, and activity levels. The primary setting for lighting requires the type of lighting fixture and the total lighting power density (W/m^2) for each space. Similarly, detailed inputs for all equipment and electrical appliances, such as computers, cooking, and refrigeration, are required for each space in the building. The occupancy data dialogue in IES-VE requires details concerning occupancy density per room (m^2/person) and the generated heat based on the activity level performed in a specific space.

These data must be provided for each space in the building and linked to a previously identified schedule.

In this study, equipment power density, lighting power density, and occupancy density for each zone were collected from Monawar (2001) based on a comprehensive survey analysis of Saudi dwellings (see Table 5-7). The metabolic rate was calculated from ASHRAE based on the activities performed in each individual space (see Table 5-8).

Table 5-7 Energy model thermal parameters

	Living zone	Guest zone	Kitchen zone	Sleeping zone
EPD (W/m^2)	7	5	30	7
LPD (W/m^2)	8	10	7	7.5

Table 5-8 Heat gain from occupants

W/person	Living zone	Guest zone	Kitchen zone	Sleeping zone
Sensible heat	65	65	80	40
Latent heat	30	30	80	30

5.9 Proposed enhancement measures

The initial simulation results of the baseline models, conducted in Chapter 8, provided insights into the thermal performance of the selected case study buildings in Riyadh under existing construction and identified key areas of the building envelope for potential improvement. By reviewing the construction drawings and data obtained for the selected case study buildings in Riyadh, it was found that both houses failed to meet the minimum requirements of the SBC, particularly for thermal insulation, despite being recently constructed (i.e. after the code's enforcement). This may be due to the gradual application of the code. In general, while the building code specifies minimum requirements of the U-value for building envelope components, as discussed in Section 2.8, it does not provide any suggestions or methods to improve the thermal performance of the buildings.

Based on the simulation results of the baseline models and the reviewed literature, this research attempted to propose and test various improvement measures—learned from vernacular architecture and modern sustainable building technology—to enhance overall thermal performance and, consequently, reduce energy consumption and carbon emissions. It is worth noting that among various types of thermal insulation materials, EPS was selected due to its low thermal conductivity, local availability, and widespread application,

particularly in residential buildings (Abuhussain, 2020; Alaboud, 2021; Alrashed, 2015). The applied improvement measures are briefly discussed below:

- **External walls**:

The application of EPS insulation at various thicknesses and locations was proposed and tested for both houses. The aim was to identify the best scenario for external walls, which can improve the indoor thermal environment and achieve the lowest cooling load, which can in turn improve energy efficiency and reduce CO_2 emissions. The aim of these simulations was to determine whether good performance could be achieved by exposing the indoor environment to externally insulated thermal mass for both construction methods.

- **Roofs**:

As discussed in Chapter 3, the roof component of the building envelope receives the highest solar radiation, making it a major source of heat gain. The SBC requires a minimum U-value of 0.20 $W/m^2 \cdot K$ for roof components on residential buildings in Riyadh. To improve the thermal performance of the existing roof constructions, EPS insulation material of different thicknesses was used. The performance of various EPS thicknesses was simulated in IES-VE.

This study also assessed the impact of applying a cool roof, a roof fitted with a highly reflective surface to reflect solar radiation away from the roof, thus reducing heat gain through the roof components. For each house, this roof type was applied along with the selected EPS insulation thickness, which complies with the SBC.

- **Ground floor**:

This study tested the impact of applying EPS insulation of different thicknesses to the ground floors on indoor thermal conditions and cooling load. The aim was to determine whether good performance could be achieved by preventing thermal transmission between the indoor environment and the ground, particularly during extreme outdoor conditions, and to evaluate the ground floor insulation requirement of the SBC for residential buildings in Riyadh.

- **Infiltration**:

Infiltration rate describes the uncontrolled air that leaks into the building, as discussed in Section 3.3, and is measured in air changes per hour (ACH). In this study, different infiltration rates were tested, from 0.1 ACH to 2.0 ACH. It is noteworthy that a sensitivity

analysis was performed to determine infiltration rates for each baseline model. This is discussed in more detail in Section 7.2.

- **Window shading**:

In an effort to improve building thermal performance in Riyadh, the SBC advises a permanent horizontal overhang projection for vertical openings. The depth of the overhang is determined by the projection factor, which is the ratio of the overhang projection to the distance between the windowsill and the bottom of the overhang. According to the Code, the minimum horizontal projection factor is 0.5 for the proposed shading type regardless of orientation. The projection factor is calculated by dividing the depth of the overhang by the vertical distance between the windowsill and the bottom of the overhang. See Figure 5-18.

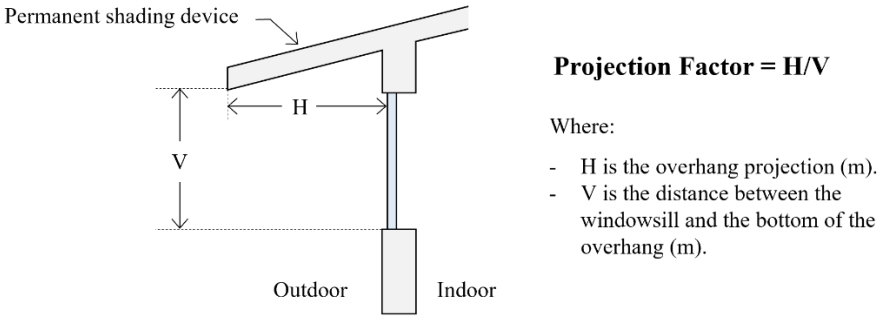


Figure 5-18 Illustration of overhang projection factor ratio. Created based on SBC-602.

In this thesis, three different external shading devices were proposed and modelled for each house:

- Horizontal overhang projection, as advised by the SBC.
- SBC overhang projection with side fins (egg-crate).
- Louvers.

Each shading option was analysed and tested individually for a selected room in each house, with standard double-clear window types for various orientation scenarios. The aim of this analysis was to identify the best shading option for improving indoor thermal performance and maximizing cooling savings. Following this step, the selected shading type was applied to all windows and tested with various window glazing types with different solar heat gain coefficient (SHGC) values. The characteristics of the proposed window glazing are summarized in Table 5-9.

Table 5-9 Characteristics of proposed window glazing cases for both dwellings in Riyadh

Window glazing description	U-value	SHGC value	Window type
Standard double-clear glazing	3.05	0.69	W2
Body-tinted glazing (bronze)	3.05	0.46	W3

- **Mixed mode natural ventilation**:

The current thesis investigated the potential savings achieved for the cooling load, and thus energy consumption and CO_2 emissions, by applying natural ventilation when the outdoor temperature falls to acceptable levels and by implementing the best-case proposed building fabric combination for both houses. The operation scheme must be carefully designed to prevent excessive cooling energy use and to avoid the risk of any conflict that may occur when switching between mechanical cooling and natural ventilation modes. Based on the adaptive comfort analysis results presented in Section 5.3, a temperature of up to 28.6 °C can be found to be acceptable for the indoor environment in naturally ventilated buildings in Riyadh. This temperature is referred to as Tc in Figure 5-19.

The proposed operational control scheme, shown in Figure 5-19, demonstrates that if the indoor temperature (Ta) rises above 24 °C, with a proportional band of 1 °C, and the outdoor temperature (Tout) drops to acceptable levels, the house relies mainly on natural ventilation to satisfy indoor thermal requirements.
When the indoor temperature exceeds the adaptive comfort temperature limit (Tc), and the proposed passive cooling strategies prove to be insufficient to restore indoor comfort conditions, active cooling systems will be appropriate.

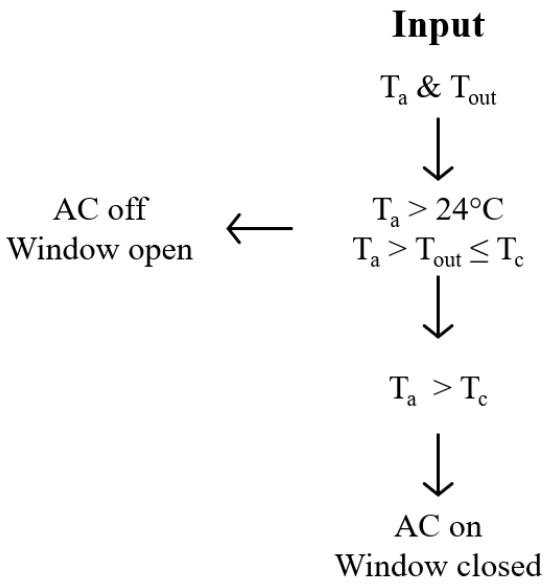


Figure 5-19 Proposed AC and window control scheme

5.10 Summary

This chapter described the methodology applied to carry out this thesis, including a justification of approach selection. It described in detail the research approach and how the computer energy simulation works, setting the stage for a deeper exploration in the following

chapters. A detailed description of the employed methodology, the selected case studies, and thermal assessment tools is provided in Sections 5.2 to 5.5.

After identifying the study location and the selected buildings, the chapter discussed the data collection and thermal analysis tools that allow for building thermal performance analysis. The ApacheSim within IES-VE was considered capable of carrying out the intended simulations with sufficient levels of accuracy based on a complex calculation method of the heat transfer process between indoor and outdoor environments, providing more in-depth data analysis.

After selecting the suitable simulation software, IES-VE, the chapter explored the utilized weather file and provided all details, data inputs, and necessary settings required by the software, as well as validation of the models. These were covered in Sections 5.6 to 5.8.

Lastly, this chapter ended with a brief description of proposed enhancement measures to improve the thermal performance of the selected case study buildings in Riyadh (see Section 5.9). The results of these simulations will be reviewed and discussed in Chapter 9. An analysis of the field monitoring data is provided in the next chapter.

CHAPTER 6

INDOOR THERMAL ENVIRONMENT (Monitored)

- Fieldwork description and objectives
- Utilized tools
- Field monitoring data analysis

Chapter 6: INDOOR THERMAL ENVIRONMENT (MONITORED)

6.1 Introduction

Field monitoring was a vital part of this research as it helped to understand the thermal performance of existing 3D-printed house (Case Study 1) and conventional house (Case Study 2) constructions under the extreme climate conditions of Riyadh, KSA. This chapter focuses on field monitoring data, which were gathered from both indoor and outdoor environments using specific equipment.

The chapter describes field data collection in both houses, taking into account air temperature as the factor most affecting thermal comfort and thus leading to the use of active systems for indoor climate control. It presents detailed field monitoring data from both houses in Riyadh and provides an analysis and discussion of internal environmental conditions. The analysis discussed here will form the basis for the next chapters, where analyses were conducted for both houses using computer simulation software.

In this study, the continuous field monitoring of environmental variables was conducted from multiple zones inside the selected case study buildings during the overheating season. The nature of the current research and the conditions of the studied dwellings led to shorter field monitoring period. As indicated in the climate analysis in Section 5.3, August was selected because it is the warmest month of the year, aligning with peak electricity consumption, as discussed in Chapter 2.

The field monitoring was conducted in August 2022. Multiple data loggers were placed in different zones, allowing for the simultaneous recording of air temperatures in the two selected houses. During the field monitoring period, precautions were taken to ensure that the instruments were positioned in safe locations and to prevent potential risks of data loss.

The fieldwork was divided into two phases. The first phase aimed to collect environmental parameters inside different rooms in both houses, with different orientations, under steady-state conditions. The primary objectives of this phase were:

- To assess the thermal performance of the 3D-printed house and the conventionally constructed house under steady-state conditions.
- To initiate thermal comfort assessment and evaluate the overall thermal performance of both case study buildings relative to outdoor conditions.

- To gather data for use in validating a standard 3D energy simulation model in a later stage of this thesis.
- To verify the provided drawings and construction materials with existing conditions.

After monitoring the indoor thermal conditions under steady-state conditions, the second phase involved investigating the impact of applying natural ventilation on indoor thermal performance. Due to limitations in the number of employed measuring tools, globe temperature, surface temperatures, and air velocity data were collected only from Case 1.

It should be noted that field measurements were taken at particular times and in specific locations, as will be explained in more detail later in this chapter. The selected data loggers and their specifications were discussed in Section 5.4.

6.2 Logger calibration

All instruments used in this study were used for the first time, retained their factory calibration settings, and were within the warranty window. However, a validation process was conducted to ensure the accuracy of the data loggers and thus the reliability of their outputs. Accordingly, the data loggers were positioned together in one environment to record air temperature. In general, the results (shown in Figure 6-1) demonstrated considerable agreement among all data loggers, despite variations in their accuracy levels, thus eliminating the possibility of inconsistent readings caused by a limitation in the data logger. The loggers were then placed in their assigned locations in both houses, as discussed in the section below.

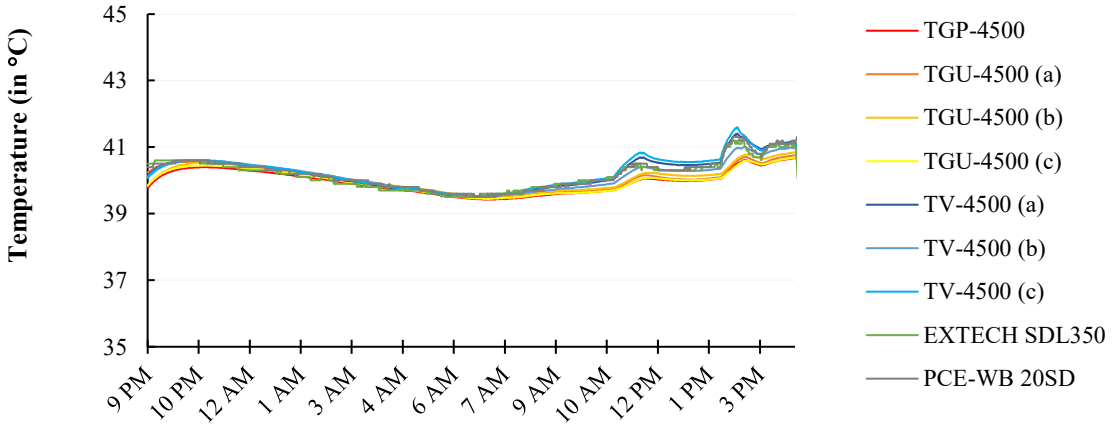


Figure 6-1 Temperature data logger calibration

6.3 Placing the data loggers (setting up)

After obtaining permission for the field study and verifying the accuracy of the data loggers, the instruments were placed in their specific locations. To monitor outdoor air temperature (Tout) and relative humidity (RH), one Tinytag Plus 2 data logger (TGP-4500) was placed on

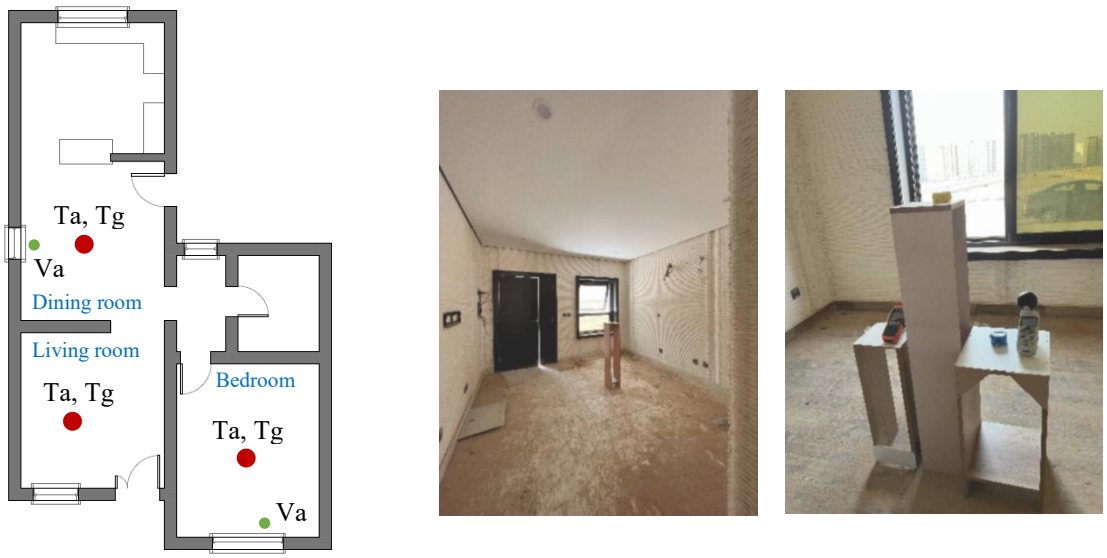
the roof of the 3D-printed house at an approximate height of 1.5 m above the roof surface. The data logger was set to record the selected parameters at 5-minute intervals. During the installation process, the accuracy of the measurements and the safety of the data logger were considered. The data logger was placed in a Stevenson-type Screen to shelter it from direct solar radiation and precipitation while allowing air circulation (see specification sheet in Appendix A-B). The protective screen used in this study can conveniently be assembled on-site. A well-supported wooden stand was used to secure the protective screen, allowing it to stand freely while ensuring the safety of the data logger throughout the study period. Figure 6-2 shows the on-site installation process of the outdoor data logger.



Figure 6-2 Installation process of the outdoor data logger with the protective screen

Indoor air temperature (Ta) was recorded from various locations in both houses using Tinytag data loggers. Measurements were taken from the centre of the selected rooms, approximately 1.5 m away from windows and away from direct solar radiation. Following ASHRAE Standard 55 recommendations for physical measurements, Ta was recorded at 5-min intervals and at a height of 1.1 m above the floor level. To prevent any potential damage to the ceiling or walls, the data loggers were placed on stands explicitly designed for the purpose of this study. The selected rooms in Case 1 and Case 2 are illustrated in Figures 6-3 and 6-4, respectively.

In Case 1, measurements were taken in the three different zones with different orientations: living room, dining room, and bedroom. In Case 2, two rooms at different floor levels were selected for the purpose of this study. Room 1 was located on the first floor, with a total area of 16.31 m^2 and one window facing southwest. Room 2 was located on the top floor (annexe) and had a total area of nearly 22.14 m^2. The room had three walls exposed to the outdoor environment and contained one window facing southwest.



(A) (B)

Figure 6-3 Locations of data loggers in selected zones in Case 1 (3D-printed house): (A) Selected rooms for analysis and measured parameters; (B) Images of the rooms after placing data loggers.



(A) (B) (C)

Figure 6-4 Locations of data loggers in Case 2: (A) Selected room in first floor (R1); (B) Selected room in upper floor (R2); (C) Images of the rooms after being equipped with data loggers.

Black-globe temperature (Tg) was monitored at 1-min intervals from the centre of the selected rooms, at a height of 0.6 m above the floor level, following the measurement guidelines of ASHRAE Standard 55. Due to the need to frequently change the data logger's batteries, measurements of Tg started on 18 August. This decision was made to minimize the author's need to access the building during the first phase of the field study.

Each data logger was carefully labelled during the installation process to avoid any risk of data being mixed during equipment removal. An analysis of the recorded data is provided in the following sections. It must be noted that, due to the limited number of data loggers used in this study, globe temperature (Tg), air velocity (Av), and the surface temperatures of external walls were only measured in Case Study 1 (as previously mentioned).

While indoor relative humidity (RH) can significantly influence occupants' thermal comfort—particularly in hot and arid regions such as Riyadh—this important parameter was not considered in the analysis presented in Section 6.4. Future studies should consider the role of humidity and explore the potential of evaporation as a passive cooling strategy to provide a more comprehensive assessment of the indoor thermal environment.

6.4 Data analysis

As explained earlier in this chapter, the field monitoring was conducted during the warmest month, from 11 August to 24 August 2022. After monitoring the selected environmental variables from each house, the data loggers were removed from the two buildings. The collected data from each data logger was downloaded onto the author's personal computer and carefully organized to avoid any potential risk of data loss or mixing. The collected data from this fieldwork are presented and analysed in the following subsections with the aim of providing a clear representation of the thermal conditions in each house.

6.4.1 Outdoor measurements

The outdoor environmental variables were measured from the roof of Case Study 1 from 11–24 August 2022. The outdoor temperature (Tout) ranged between 46 °C and 29 °C, usually peaking during afternoon hours between 13:00 and 15:00. On average, the difference between the daily minimum and maximum temperature exceeded 10 °C and could reach 17 °C. This significant variation in daily Tout values was expected in this climate.

The monitored outdoor relative humidity (RH) was extremely low during the measurement period, ranging between 0.7% and 26%, with an average of 9.5%. A statistical summary of the averages and ranges of Tout and RH are provided in Table 6-1. The range (RNG) values

shown in this table describe the difference between the daily minimum and maximum readings.

A detailed analysis of the collected data from inside both houses under steady-state conditions from the period 11–19 August 2022 is discussed in the following subsections with respect to the indoor thermal conditions in relation to the outdoor conditions. Readings of environmental variables with natural ventilation strategies are then discussed.

Table 6-1 Summary of monitored outdoor air temperature and relative humidity

Day	Air temperature (°C)				Relative humidity (%)			
	Max	Min	Ave	RNG	Max	Min	Ave	RNG
11 Aug	45.4	33.5	39.5	11.8	20.6	6.7	12.4	13.8
12 Aug	43.6	31.4	38.6	12.1	25.9	5.2	12.5	20.6
13 Aug	43.9	32.1	38.4	11.8	21.3	5	11.1	16.3
14 Aug	44.5	31.7	37.8	12.8	16	2	9.1	13.9
15 Aug	43.5	28.8	36.5	14.7	18	6.3	10.5	11.6
16 Aug	43.2	28.6	36.3	14.5	16.4	4.5	9.4	11.9
17 Aug	43.3	30.2	36.2	13.1	18.8	2	8.8	16.7
18 Aug	45	29.9	36.9	15.1	9.9	3.1	6.1	6.7
19 Aug	45.2	31.1	38	14.1	9.9	0.7	5.3	9.1
20 Aug	45.6	29	37.4	16.5	10.5	1.3	5.8	9.2
21 Aug	46.1	29	37.8	17.1	15.9	2.4	8.0	13.5
22 Aug	45.6	30.4	37.8	15.1	15	2.7	8.1	12.3
23 Aug	44.6	28.8	36.9	15.8	24.6	4.1	11.7	20.5
24 Aug	43.6	30	36.8	13.6	23.1	4.6	11.8	18.5

To evaluate indoor thermal comfort, the adaptive comfort temperature (Tc) was calculated based on the outdoor temperature measurements presented in this section. The mean monitored Tout (37.5 °C) did not significantly differ from the earlier figure of 35.0 °C (derived from historical data and used to calculate the comfort limits for Riyadh in Section 5.3); consequently, there was no expectation of significant variation. Accordingly, the Tc value was calculated to be 29.4 °C using Equation (3-6). For the purposes of this analysis, the comfort limits were determined by extending Tc within the range of ±3.5 °C.

The comfort limits adopted in this chapter thus ranged between 25.9 °C and 32.9 °C. Since the calculated comfort limits were derived from actual site monitoring, it was considered that a higher comfort value of 32.9 °C would represent a worst-case scenario for thermal conditions during the overheating period.

After determining the comfort limits, it was found that the monitored Tout fell within the specified comfort range up to 23.5% of the time, mostly during the early morning hours (i.e. between 03:00 and 06:00). For demonstration purposes, hourly Tout readings in relation to

the discussed comfort limits are provided in Appendix A-C. Hourly measurements of indoor and outdoor air temperatures for a typical summer day are provided in Appendix A-D.

6.4.2 Indoor field monitoring (steady state)

6.4.2.1 Case Study 1 (3D-printed house)

Comparing the thermal behaviour of each room in relation to the outdoor conditions, Figure 6-5 illustrates hourly air temperature measurements recorded from indoor and outdoor environments. In general, the indoor thermal environment was found to be highly influenced by the outdoor climatic conditions. Over the study period, the indoor temperature (Ta) ranged from 41 °C to 37 °C. Notably, a high level of agreement in Ta measurements can be seen, with a maximum difference of 0.6 °C between the readings, despite variations in room orientation.

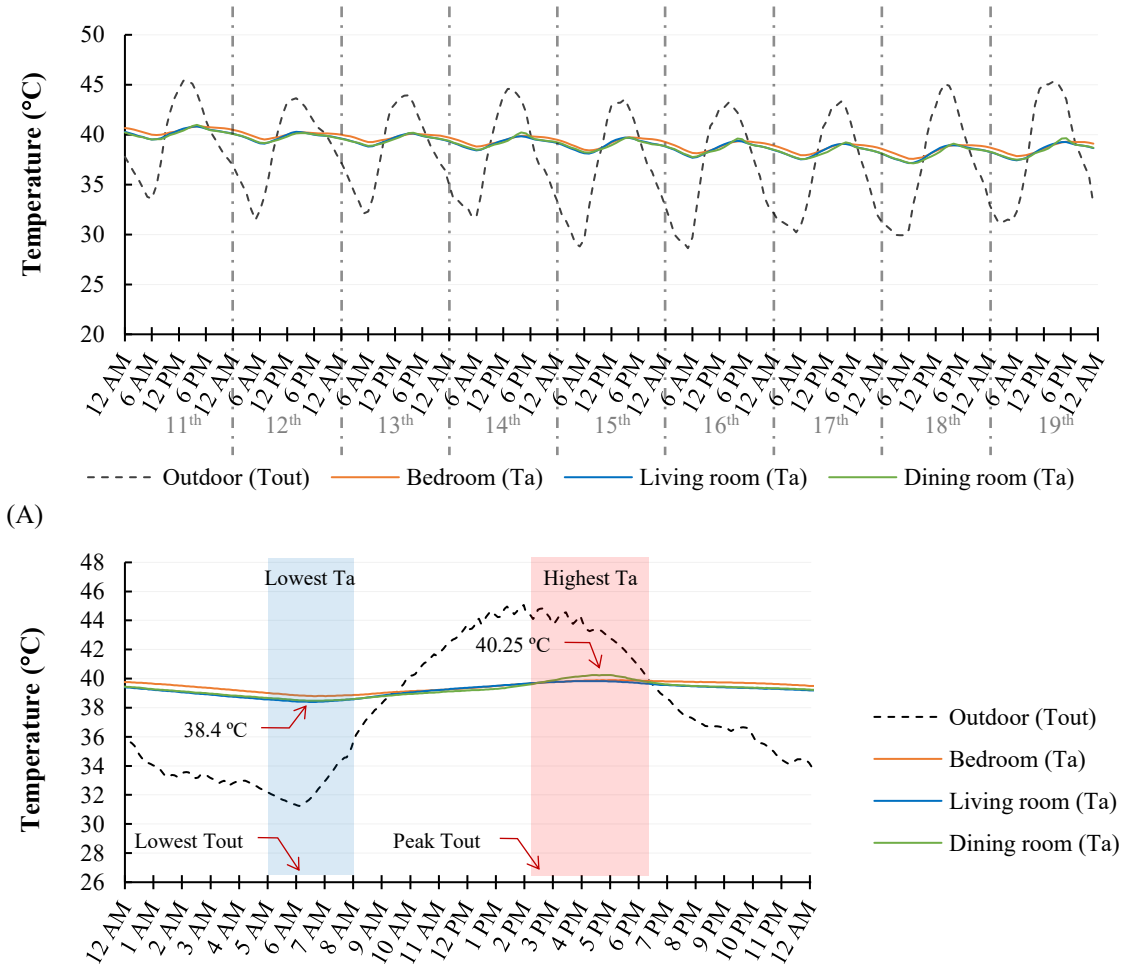


Figure 6-5 (A) Readings of outdoor and indoor air temperatures for the selected rooms in Case 1 (3D-printed house) from 11–19 August 2022; (B) A truncated graph provides a clearer indication of the daily temperature profile.

The lowest Ta measurements were recorded during the early morning hours, between 06:00 and 07:00, while the highest Ta values were recorded between 15:00 and 17:00. A maximum time lag of three hours between peak Ta and peak Tout was observed. Unlike the significant fluctuations in Tout readings, all rooms exhibited steady thermal conditions, with diurnal temperature fluctuations of up to 2 °C.

Overall, the indoor thermal conditions remained consistently higher than the upper thermal comfort level, with relatively limited variation. This can be attributed to the harsh climate conditions in Riyadh in the summer season. The results indicate that Ta values needed to be reduced by up to 7 °C to achieve thermal comfort.

As previously mentioned, all windows and doors during this stage were kept closed, which restricted the building's ability to dissipate internal built-up heat. Additionally, it is worth noting that all three rooms were exposed to the outdoor environment from the roof, which, in the context of this investigation, can be considered a major source of conductive heat gain.

Moreover, measurements of Tg were taken from all rooms at specific times, with closed windows (i.e. without natural ventilation). A strong correlation was observed between Tg and Ta readings in all rooms (see Figure 6-6). In general, the variation between Tg and Ta was minimal (below 0.5 °C).

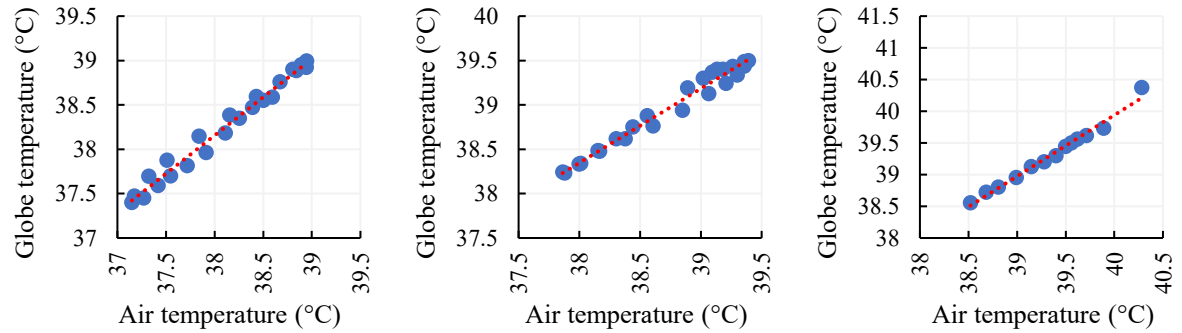


Figure 6-6 Correlation between measurements of indoor air temperature (Ta) and globe temperature (Tg) for the three selected zones in Case 1: (A) Living room; (B) Bedroom; (C) Dining room

6.4.2.2 3D-printed wall surface temperature

The temperatures of the inner and outer surfaces of external walls were measured at specific points and times during this stage of the study. The measurements were taken on 19 August at 06:00, 09:00, 12:00, 15:00, and 18:00. Several measuring points were marked on both sides of the walls at heights of 60 cm, 120 cm, and 220 cm, with a horizontal distance of approximately 150 cm between each point. The average for each surface was then calculated.

The average temperature of the outer surfaces of the external wall are summarized in Table 6-2. The measured surfaces and their orientations are illustrated in Figure 6-7.

Table 6-2 Outer surface temperature measurements recorded on a typical summer day (19 August)

		06:00	09:00	12:00	15:00	18:00
Wester wall	W_1	33.94	34.24	41.29	48.06	44.35
	W_2	36.00	36.33	43.00	48.33	44.00
Northern wall	N_1	34.13	35.88	43.38	43.13	41.50
	N_2	35.13	36.50	43.13	43.00	41.25
Southern wall	S_1	33.63	36.63	45.13	46.75	42.88
	S_2	34.67	36.44	44.67	46.44	43.00
Eastern wall	E_1	34.89	41.00	44.00	43.89	42.33
	E_2	34.58	41.08	44.17	43.75	42.25



Compared with other orientations, the eastern wall surface temperature began to rise in the morning at 09:00 due to its direct exposure to solar radiation, reaching its highest value of about 44 °C at 12:00. There is a direct relationship between wall azimuth and external surface temperature. The results show that the temperatures of the southern and western walls increased significantly at noon, usually peaking at 15:00. In contrast, the northern wall recorded the lowest values, with surface temperatures ranging from 34.1 °C to 43.4 °C.

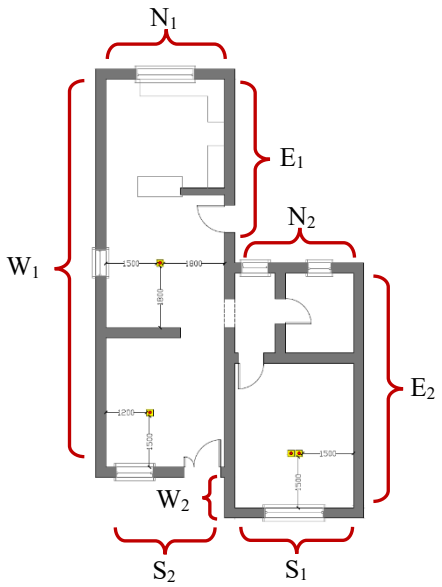


Figure 6-7 Highlighted measured surfaces orientation of the 3D-printed house

The temperatures of the inner surfaces of the external walls (IST) for all rooms remained steady compared to the outer surfaces. In general, all walls showed similar thermal performance as they had similar trend at an average of about 40 °C. The minimum ISTs of 38.5 °C and 39 °C were recorded on the western and northern walls, respectively, at 12:00. The ISTs began to rise during the afternoon hours, reaching the highest value of 40.8 °C on the southern walls. The mean ISTs of the southern and eastern walls were 40.2 °C, which are at least 0.5 °C higher than the means of the northern and westerns walls. It is clear that the use of thermal insulation prevented a significant fluctuation on the inside walls' surface temperature even though the outside wall surface temperature showed a temperature variation of up to 14 °C, as illustrated in the graphs in Figure 6-8.

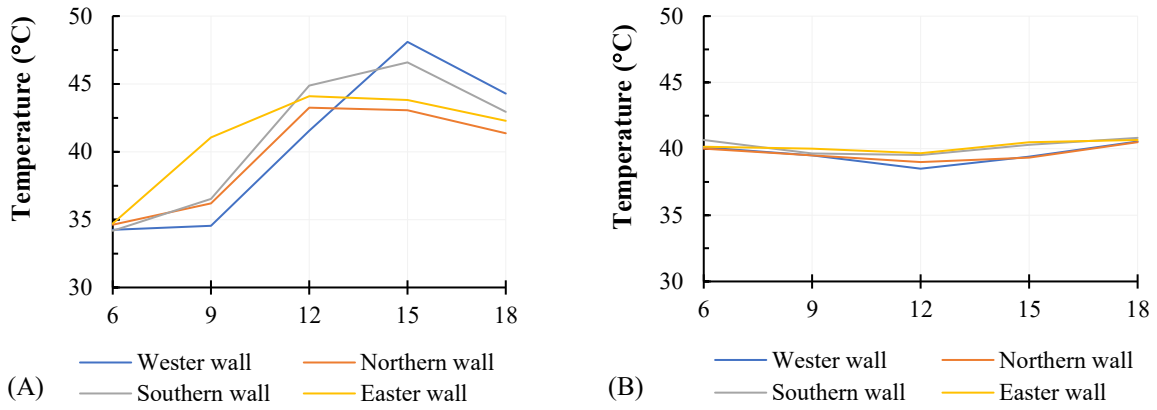


Figure 6-8 Surface temperatures of external walls on a typical summer day (19 August 2022): (A) External surface temperatures; (B) Internal surface temperatures

6.4.2.3 Case Study 2 (conventional house)

As previously mentioned, Ta was monitored from two rooms located on different floor levels. Room 1 (R1) was located on the first floor, while Room 2 (R2) was located on the top floor (annexe). Comparing the indoor thermal behaviour of selected rooms, Figure 6-9 presents Ta measurements for R1 and R2 plotted on the same graph in relation to Tout (recorded from Case Study 1 over the same period). The results show that Ta readings ranged between 39.3 °C and 43.3 °C, with a difference of up to 2.2 °C between both rooms. The lowest Ta values were recorded in R1 during the morning hours, usually at 09:00, whereas the highest Ta was recorded in R2 during the evening, usually at 20:00.

Unlike the significant fluctuations in Tout readings, constant and steady conditions were observed in both rooms. R1 exhibited diurnal temperature swings of around 0.6 °C, whereas R2 had diurnal temperature swings of no greater than 2 °C. Overall, the monitored Ta from both rooms were higher than the mean Tout, with relatively limited variation.

This thermal behaviour could be due to the existing thermal insulation as required by the recently developed building code (discussed in Chapter 2), which prevented significant temperature swings inside the house. In addition, the lack of a heat dissipation process prevented a drop in Tas, particularly at night when Tout dropped far below Ta measurements. Despite the non-significant differences in Ta readings, R2 performed worse during the field monitoring period. Considering the number of surfaces exposed to the outdoor environment in R2 (i.e. three exposed walls and a roof) compared to R1, which had only one exposed wall, this was not unexpected. Finally, Ta measurements in both rooms were far above thermal comfort level. A review of monitored temperatures revealed that Ta needed to be reduced by

up to 8 °C in R1 and up to 10 °C in R2 to satisfy indoor thermal comfort (i.e. if people could cope with 32.9 °C).

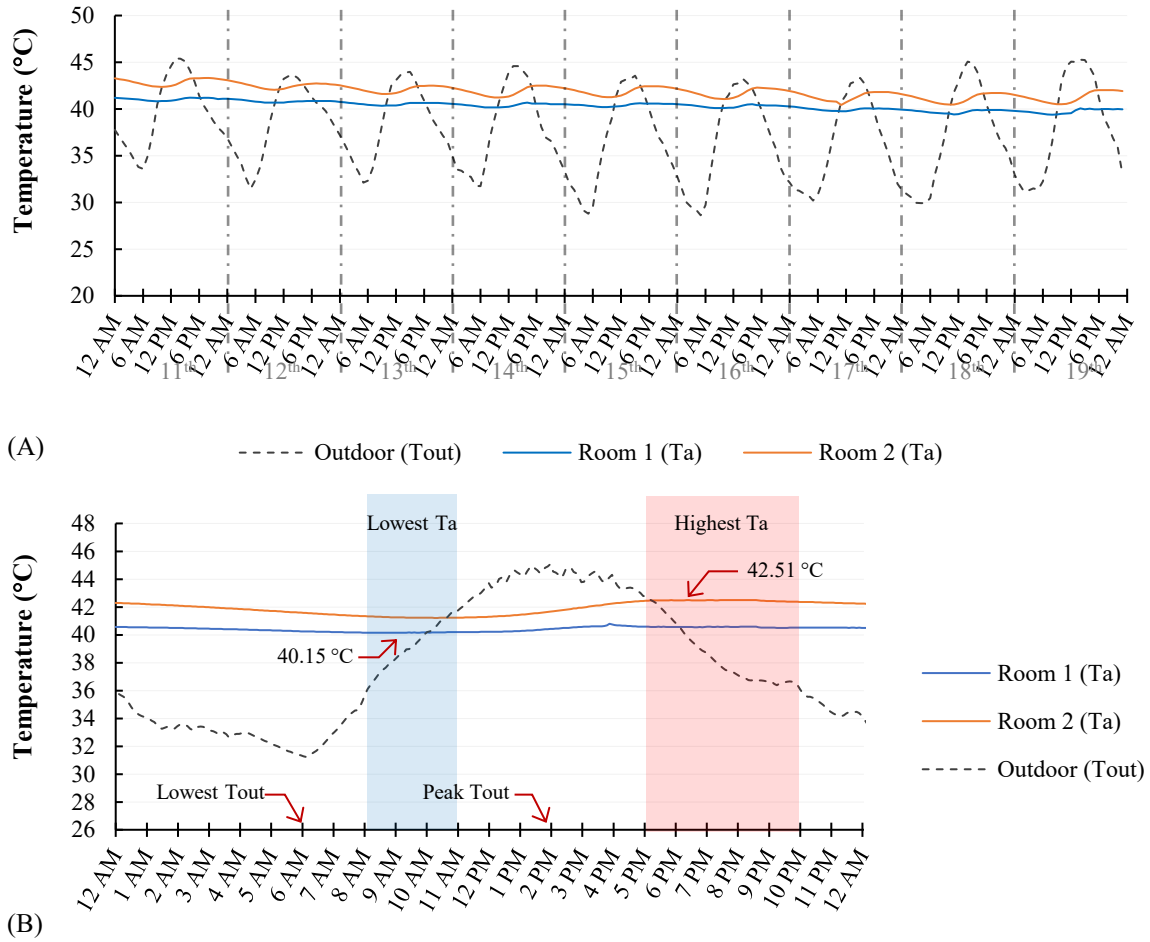


Figure 6-9 (A) Readings of indoor air temperatures for the selected rooms in Case 2 from 11–19 August 2022 in relation to the outdoor temperatures; (B) A truncated graph provides a clearer indication of the daily temperature profile.

It is evident from the above analysis that solar energy input on the building envelope has a significant influence on indoor thermal environment, especially in such a climate and due to the high altitude of the sun. Further analysis conducted for this thesis using computer simulation software will be discussed in detail in subsequent chapters.

6.4.3 Investigating the potential of natural ventilation

After monitoring the indoor thermal conditions under steady conditions, the impacts of applying natural ventilation on the indoor thermal environments were explored for both houses. In Case 1, Ta, Tg, and Av data were gathered from the specified zones and times after applying natural ventilation strategies: daytime ventilation (DTV) and daytime and night-time ventilation (DTV&NTV). In Case 2, however, only Ta was monitored from the

selected rooms with natural ventilation. The gathered data are discussed in the following subsections.

6.4.3.1 Case Study 1 (3D-printed house)

In this house, natural ventilation was allowed for all zones. For demonstration purposes, field measurements from the bedroom and dining room were reviewed. While Tas were continuously monitored in all rooms simultaneously, both Tg and Av were monitored from each individual room on separate days due to limitations in the number of available measurement tools, as previously indicated.

As discussed in Section 5.3.4, the bedroom had a large sliding window (1.75 m wide by 1.45 m high) with two panels that could be slid horizontally to open, offering an effective open area of about 40%. The dining room had a top-hung window (0.8 m wide by 1.45 m high) with one openable panel (0.8 m wide by 0.9 m high) that could be opened outward at an opening angle of approximately 20°. Descriptions of the window types and their properties are summarized in Table 5-2.

Starting with daytime ventilation (DTV), measurements of Ta, Tg, and Av were taken from the bedroom in Case 1 on 21 August. On this day, all windows and the internal door to the bedroom were kept open from 06:00 to 18:00. The bedroom's large window, which faced the main road, posed a potential risk of unauthorised access and vandalism during night hours, particularly following previous incidents of theft from the study site, thereby restricting the assessment of night-time ventilation (NTV).

The dining room, in contrast, offered a safer opportunity to expand natural ventilation analysis as it had a top-hung window type located on the western side of the building (which was not visible from the main road when kept open). This allowed the author to assess the influence of NTV on the indoor thermal environment without risking the safety of the equipment. Measurements of Tg and Av were taken from 23 August at 06:00 to 24 August at 06:00 with natural ventilation. During this period, all windows in the house, except for the bedroom window, were kept open. The internal door to the bedroom was also kept closed at this stage to minimize the impact of radiant heat from the bedroom.

- **Daytime natural ventilation (DTV)**

Figure 6-10 presents the air temperature measurements in the tested rooms and outdoor environment with the DTV strategy on 21 August. A sudden drop in Ta measurements by up

to nearly 2 °C was observed in both rooms when the windows were opened in the morning at 06:00. This behaviour was likely influenced by the considerable temperature difference between indoor and outdoor environments at this time, which promoted indoor heat dissipation and convective heat loss. Later in the afternoon, Tas increased in both rooms, reaching up to 41.25 °C and 41.69 °C in the bedroom and dining room, respectively. The collected data suggest that, during the peak Tout period, NV could worsen indoor thermal conditions due to convective heat gain in both rooms.

On this day, as mentioned earlier, both Av and Tg were also recorded in the bedroom. The hot wire sensor recorded a minimum Av of 0 m/s, accounting for over 97% of total readings (see Figure 6-11). This was likely due to the orientation of the sensor's coloured dot—the spot at which the reading is taken—which was facing the window (i.e. in this setup, the sensor was positioned to measure airflow entering the room from the leeward window). The recorded Tg values closely followed Ta measurements. The correlation between Ta and Tg is illustrated in Figure 6-12.

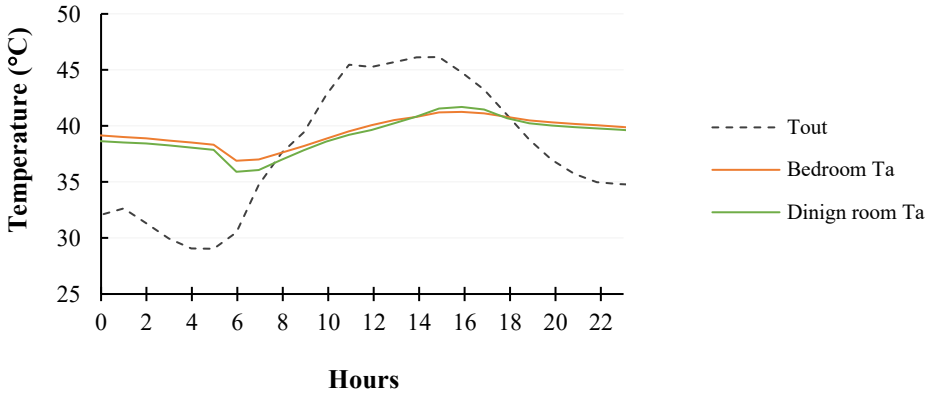


Figure 6-10 Readings of outdoor and indoor air temperatures for bedroom and dining room on 21 August with daytime ventilation strategy (06:00 to 18:00).

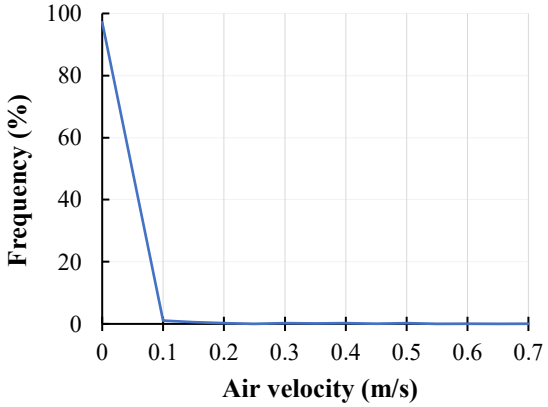


Figure 6-11 Frequency of air velocity measurements for the bedroom on 21 August.

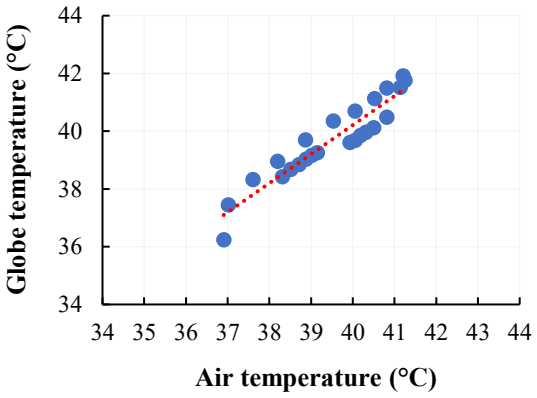


Figure 6-12 Correlation between Tg and Ta readings for the bedroom (with DTV strategy).

- **Open window VS closed window (DTV & NTV)**:

Figure 6-13 illustrates the average hourly Ta measurements for the selected rooms in relation to Tout on 23 August. As previously indicated, the windows were open in all rooms but kept closed in the bedroom. This facilitated a comparison between the two rooms to better understand the impact of natural ventilation in 3D-printed dwellings in the climate context of Riyadh.

Ta readings in the dining room dropped by up to 2.5 °C as a result of opening the windows during the early morning hours. A minimum temperature of 36 °C was recorded at 07:00, compared to 37.8 °C in the bedroom. However, it was observed that convection gain worsened the indoor thermal environment of the dining room, causing an increase of nearly 1° C in Ta measurements during the peak Tout period compared to those recorded in the bedroom.

Notably, a drop in Ta readings was recorded in the dining room during evening hours (after 17:00), responding to a reduction in Tout at night, compared to the constantly steady condition in the bedroom. This was attributed to the NTV effect employed in the dining room. However, the reductions in Ta achieved with the employed natural ventilation (NV) strategy were not satisfactory from a thermal comfort point of view. According to the monitored data, Ta would need to be further reduced by at least 3.1 °C to achieve thermal comfort.

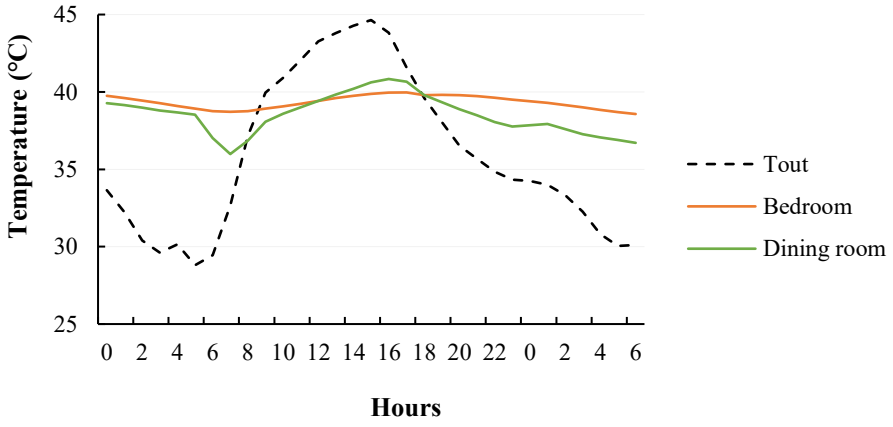


Figure 6-13 Readings of outdoor and indoor air temperatures for bedroom and dining room after employing NV (from 23 Aug at 06:00 to 24 Aug at 06:00).

On this day, both Av and Tg were also recorded in the dining room. As shown in Figure 6-14, Av ranged from 0 m/s to 1.2 m/s, with an average of 0.12 m/s. The frequency of Av between 0.1 m/s and 0.5 m/s was 42.7%, while above 0.5 m/s it was 6%. The monitored Tg values

showed a similar trend to that of Tas during this period. Figure 6-15 shows the correlation between the Ta and Tg measurements.

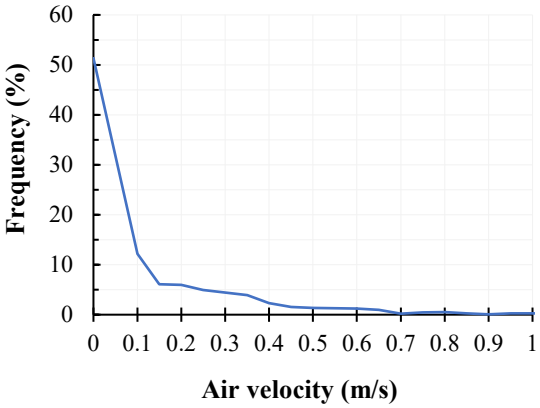


Figure 6-14 Frequency of air velocity measurements for the dining room on 23 August.

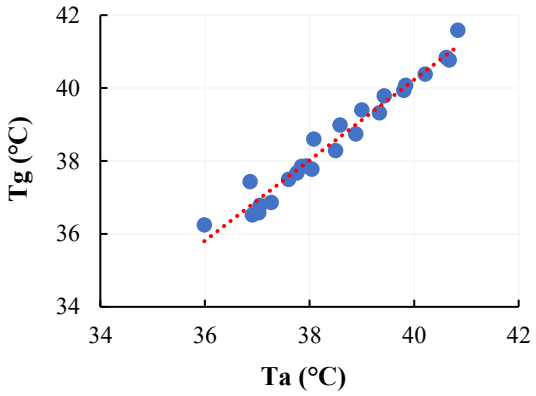


Figure 6-15 Correlation between Tg and Ta readings for the dining room with NV.

6.4.3.2 Case Study 2 (conventional house)

In this house, natural ventilation was assessed in the selected rooms (Room 1 and Room 2). As indicated in Section 5.3.4, both rooms had side-hung windows measuring 0.7 m in width and 2.5 m in overall height. Each window included one openable panel that could be opened inward at an angle of approximately 20°, with a panel height of 1.7 m in Room 1 and 1.5 m in Room 2. Descriptions of the window types and their properties are summarized in Table 5-3.

Evaluating the impact of natural ventilation, the graph in Figure 6-16 illustrates the hourly averages of Ta readings for both rooms on 22 August. It should be noted that internal doors were kept closed during the study period. As previously indicated, Tout was monitored from the rooftop of Case Study 1.

Slight reductions in Ta measurements were observed during the morning hours in both rooms. This can be attributed to NV facilitating internal heat dissipation, thus reducing indoor temperatures. However, Ta readings during peak Tout periods in both rooms increased, following the Tout pattern, reaching 41.1 °C in R1 and 42.8 °C in R2. These figures were at least 1 °C higher than those recorded on 18 August (i.e. before applying NV).

The collected data suggest that employing NV during peak Tout periods can worsen indoor thermal conditions due to convection heat gain. Finally, the internal temperatures in both rooms remained higher than the upper comfort limit even though the NV strategy was employed.

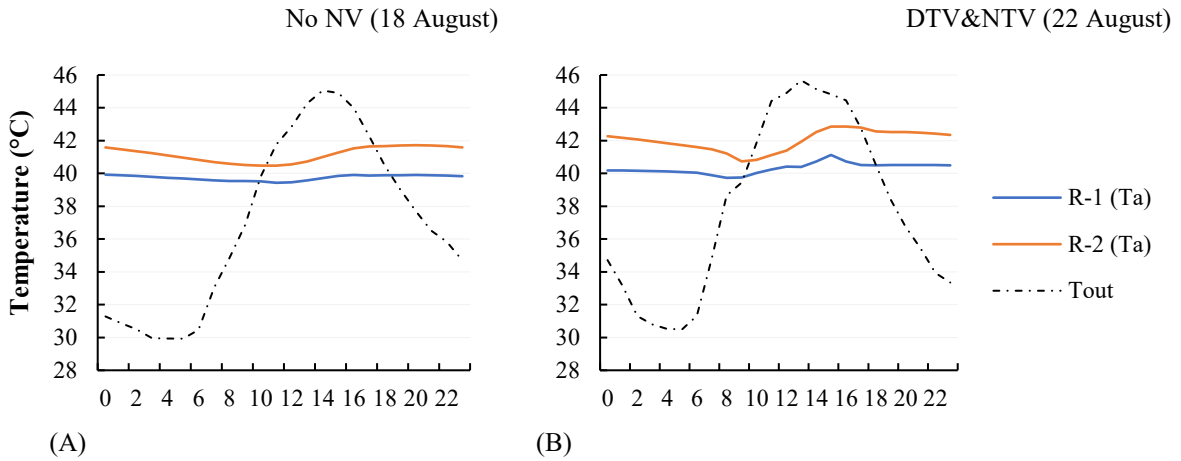


Figure 6-16 Indoor air temperature readings from selected rooms in Case 2: (A) Data gathered on 18 August (with closed windows); (B) Data gathered on 22 August (with open windows).

6.5 Summary

This chapter presented a detailed analysis of the data gathered from a field study conducted during the cooling season. The fieldwork was carried out in two different houses located in Riyadh, KSA, constructed using different construction methods: the 3D printing technique and a conventional construction method. Multiple data loggers were strategically positioned in different zones of each house to enable concurrent indoor air temperature recording. First, measurements were taken under steady-state conditions from 11 August to 19 August. The impact of natural ventilation on indoor thermal conditions was then explored.

The external temperatures ranged between 28.6 °C and 46.1 °C, with daily temperature swings ranging between 11 °C and 17 °C. In general, Ta measurements in both houses were found to be constant and steady during the first stage of the fieldwork. It was found that the current envelope played a major role in preventing high fluctuations in Ta measurements. In Case 1, variations in Ta readings were found to be constant for all zones and matched each other, with diurnal temperature fluctuations of up to 2 °C. In Case 2, due to the variation in room levels, the fluctuation of Ta was as high as 0.6 °C in R1 (located on the first floor) and around 2 °C in R2 (located on the top floor).

The second phase of the fieldwork demonstrated that allowing NV into the rooms during the period when Tout was significantly lower than Ta contributed positively to improving indoor conditions. This improvement effect was distinguished by a reduction in indoor temperatures, particularly during the early morning hours. However, during overheating periods, when Tout exceeded Ta, employing NV could not be relied upon to improve indoor thermal conditions as it caused an increase in Ta due to convective heat gain. Overall, a strong correlation

between Ta and Tg was noticed during the measurement period. Finally, all recorded values inside both houses remained above the upper limit of the comfort zone during the monitoring period despite reductions in Ta readings achieved with NV strategies.

The data presented in this chapter, which were gathered from existing residential buildings in Riyadh, formed the basis for understanding the thermal performance of the tested houses. As part of this study, computer energy simulation software was used to conduct further analysis. The results of these simulations will be covered in Chapters 8 and 9. Chapter 7 will discuss the modelling process and the validation results of the baseline models.

CHAPTER 7

BUILDING MODEL DEVELOPMENT

- Building 3-dimensional energy models
- Sensitivity analysis
- Energy model validation
- Solar analysis

Chapter 7: BUILDING MODEL DEVELOPMENT

7.1 Introduction

The field study results contribute significantly to advancing knowledge about the thermal behaviour of residential buildings, especially those constructed using modern construction methods (i.e. 3D printing techniques) in the extreme climate conditions of Saudi Arabia. However, due to the limitations discussed in previous chapters, dynamic simulation software was employed for this thesis as part of the evaluation of the thermal and energy performance of the selected houses in Riyadh.

This chapter provides a detailed description of the modelling process and validation of the selected case study buildings. The chapter is classified into two main parts. The first part covers the modelling process of the two case study buildings in the simulation software and specifications of the applied construction materials. Moreover, it presents a sensitivity analysis of key parameters—namely infiltration rate and ground temperature—to assess the model's sensitivity to these inputs and their influence on simulation outputs related to indoor thermal environment predictions.

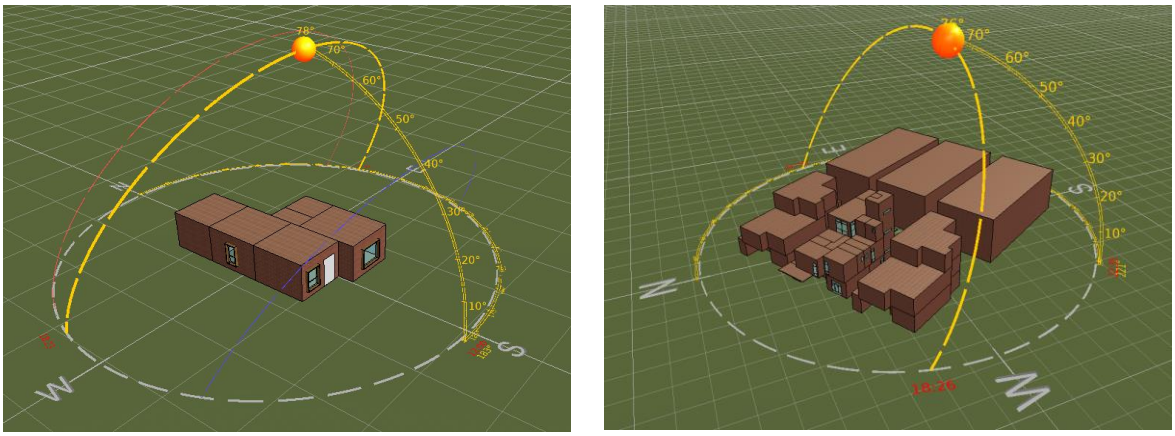
The second part of this chapter discusses the validation stage of the two energy models. A comparison between the field monitoring data (physical measurements) and the energy simulation results (predictions) was conducted and discussed. In this study, the correlation between measured and predicted data was statistically analysed to ensure the validity of the models, which will be utilized in the following chapters to carry out further investigations to assess and improve the overall thermal performance of the selected houses in Riyadh.

7.2 Constructing the energy model

7.2.1 Defining the buildings' geometry

A 3D energy model was developed in IES-VE for the two houses based on the obtained and gathered details presented in Chapter 5. While the geometrical parameters of the building can be conveniently modelled in IES, the 2D CAD drawings were imported in IES using the DXF file format to ensure modelling accuracy. A summary of the IES simulation process is presented in Figure 5-15 in Section 5.5. Thus, each building's layout was traced using the ModelIT tool and then separated into zones according to the architectural drawings of the houses presented in Section 5.3 (see Figures 5-11 and 5-13).

The defined parameters during this stage of the modelling process included location, building geometry, layout, orientation, room size and height, and opening details (e.g. size, height, location in the room, and existing shading). Figure 7-1 demonstrates the developed 3D models for the 3D-printed house and the conventional house. The orientations of both houses were defined based on the data gathered during the site visit. It is noteworthy that in the IES-VE software, north is used as the reference direction, with all deviation angles measured relative to it. The front elevation of the 3D-printed house (Case Study 1) faced an azimuth angle of 180°, while the conventional house (Case Study 2) had an azimuth angle of 330°—a deviation of 30° from the north-south axis towards the west.



(A) (B)

Figure 7-1 The constructed IES models: (A) A 3D view of Case Study 1; (B) A 3D view of Case Study 2

As mentioned in Chapter 5, the two houses had different orientations, window characteristics, and window-to-wall ratios (WWR). The WWR of Case 1 and Case 2 were 40% and 35%, respectively. The key characteristics of the building façades for Case 1 and Case 2 are summarized in Table 7-1 and Table 7-2, respectively.

Table 7-1 Mean features of external façade for Case 1

Case 1	North (0°)	East (90°)	South (180°)	West (270°)	Total
Gross wall area (m^2)	20.90	35.45	20.90	32.18	109.45
Window area (m^2)	3.54	0	4.13	1.16	8.83
WWR (%)	16.95	0	19.77	3.61	40.33

Table 7-2 Mean features of external façade for Case 2

Case 2	Northwest (330°)	Northeast (60°)	Southeast (150°)	Southwest (240°)	Total
Gross wall area (m^2)	104.28	178.40	104.25	185.33	572.25
Window area (m^2)	16.58	2.8	0	32.94	52.33
WWR (%)	15.90	1.57	0	17.78	35.25

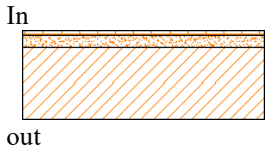
7.2.2 Building envelopes and construction materials (thermal and physical properties)

Following the development of the 3D models for the two houses, the construction material properties and the configuration of the construction elements were specified in the Apache Constructions Database in IES-VE, for which comprehensive inputs are required, including construction layer details (in the order of outside to inside) and the thermal properties of each layer (such as name, thickness, thermal conductivity, density, and specific heat capacity).

Summaries of the construction details and material properties for Case 1 and Case 2 are presented in Tables 7-3 and 7-4, respectively. The thermal properties of the 3D-printed mixture were provided by CyBe Construction (2023), whereas specifications of other building materials and their thermal properties were obtained from relevant literature. The U-values of the construction elements were calculated using the ASHRAE method (calculated by IES). Window details and specifications were discussed in Section 5.3.

Table 7-3 Description of Case 1's construction elements and their thermal properties

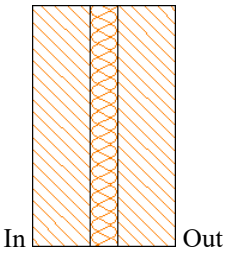
A) Ground floor (slab on grade):



U-value = 3.263 W/m^2·K Thickness (mm) = 185

Construction layers (outside to inside)	Thickness (mm)	Conductivity (W/m·K)	Density (kh/m^3)	Specific heat capacity (J/kg·K)
Cast concrete	150	1.95	2240	900
Mortar	25	0.88	2800	896
Porcelain	10	1.10	2100	837

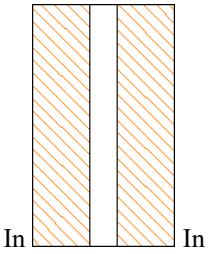
B) External walls:



U-value = 0.511 W/m^2·K Thickness (mm) = 300

Construction layers (outside to inside)	Thickness (mm)	Conductivity (W/m·K)	Density (kh/m^3)	Specific heat capacity (J/kg·K)
CyBe mixture	120	0.781	2100	1100
Foam insulation	60	0.040	25	1400
CyBe mixture	120	0.781	2100	1100

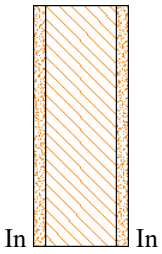
C) Internal walls:



U-value = 1.601 W/m^2·K Thickness (mm) = 300

Construction layers (outside to inside)	Thickness (mm)	Conductivity (W/m·K)	Density (kh/m^3)	Specific heat capacity (J/kg·K)
CyBe mixture	120	0.781	2100	1100
Cavity	60	-	-	-
CyBe mixture	120	0.781	2100	1100

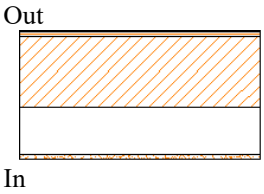
D) Internal wall (kitchen wall):



U-value = 2.251 W/m^2·K Thickness (mm) = 200

Construction layers (outside to inside)	Thickness (mm)	Conductivity (W/m·K)	Density (kh/m^3)	Specific heat capacity (J/kg·K)
Stucco	25	0.72	1856	840
Concrete block	150	1.11	800	920
Stucco	25	0.72	1856	840

E) Roof (precast hollow core slab):

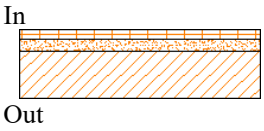


U-value = 1.399 W/m^2·K Thickness (mm) = 274

Construction layers (outside to inside)	Thickness (mm)	Conductivity (W/m·K)	Density (kh/m^3)	Specific heat capacity (J/kg·K)
Bitumen layer	4	0.50	1700	1000
Foam insulation	10	0.04	10	1400
Concrete slab	150	1.95	2240	900
Cavity	100	-	-	-
Gypsum board	10	0.16	640	1150

Table 7-4 Description of Case 2's construction elements and their thermal properties

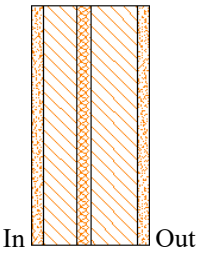
A) Ground floor:



U-value = 3.590 W/m^2·K Thickness (mm) = 145

Construction layers (outside to inside)	Thickness (mm)	Conductivity (W/m·K)	Density (kh/m^3)	Specific heat capacity (J/kg·K)
Cast concrete	100	1.95	2240	900
Mortar	25	0.88	2800	896
Granite	20	2.90	2650	900

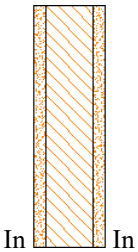
B) External walls (outside to inside):



U-value = 0.751 W/m^2·K Thickness (mm) = 250

Construction layers (outside to inside)	Thickness (mm)	Conductivity (W/m·K)	Density (kh/m^3)	Specific heat capacity (J/kg·K)
Stucco	25	0.72	1856	840
Concrete block	100	0.47	800	1000
Polystyrene	30	0.04	15	1400
Concrete block	70	0.47	800	1000
Stucco	25	0.72	1856	840

C) Internal walls:

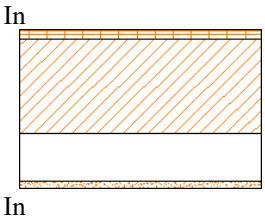


U-value = 2.506 W/m^2·K Thickness (mm) = 150

Construction layers (outside to inside)	Thickness (mm)	Conductivity (W/m·K)	Density (kh/m^3)	Specific heat capacity (J/kg·K)
Stucco	25	0.72	1856	840
Concrete block	100	1.11	800	920
Stucco	25	0.72	1856	840

D) Internal floors/ceiling:

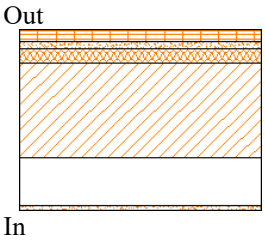
U-value = 1.716 W/m^2·K Thickness (mm) = 335



Construction layers (outside to inside)	Thickness (mm)	Conductivity (W/m·K)	Density (kh/m^3)	Specific heat capacity (J/kg·K)
Granite	20	2.90	2650	900
Reinforced concrete	200	2.30	2300	1000
Cavity	100	-	-	-
Gypsum board	15	0.16	640	1150

E) Roof:

U-value = 0.836 W/m^2·K Thickness (mm) = 385



Construction layers (outside to inside)	Thickness (mm)	Conductivity (W/m·K)	Density (kh/m^3)	Specific heat capacity (J/kg·K)
Terrazzo tiles	25	1.80	2560	790
Mortar	15	0.88	2800	896
Foam insulation	30	0.04	10	1400
Reinforced concrete	200	2.30	2300	1000
Cavity	100	-	-	-
Gypsum board	15	0.16	640	1150

7.2.3 Infiltration

As discussed in Chapter 3, infiltration rate is a significant factor affecting indoor thermal environments and building energy performance. Infiltration sources are usually outside doors, gaps around windows, and even small cracks in the building envelope. In addition to climate conditions, infiltration rate is influenced by factors such as building age, type, and method of construction. In air-conditioned buildings with poor airtightness, infiltration can significantly increase cooling loads.

The infiltration rate of a dwelling can be measured through a blower door test, which uses a large computer-controlled fan, installed in a doorway, to pressurize (blow air into the building) or depressurize (blow air out of the building) the indoor environment. Test results are typically used to estimate the airtightness of the building envelope and to determine its infiltration rate (ASHRAE, 2002).

According to the literature, infiltration rate has not been measured in Saudi Arabia's dwellings and has been mostly assumed among researchers. This has resulted in a conflict in air infiltration values among scholars. It has been assumed to be 1.0 ACH (Albogami & Boukhanouf, 2019; Alyami & Omer, 2021), 0.8 ACH (Krarti, Aldubyan, & Williams, 2020), 0.7 ACH (Abuhussain, 2020), and 0.5 ACH (AlFaraidy & Azzam, 2019), whereas the SBC requires an airtightness value of 4 ACH at 50 Pa for all modern houses.

Due to the limited availability of field measurements, it was not possible to measure the infiltration rate for the selected case studies. For the purpose of this thesis, a broad range of infiltration rates (from 0.1 ACH to 1.0 ACH in 0.1 increments) was input into the baseline model to test the sensitivity of the indoor temperature predictions to different infiltration rates.

Simulations were conducted for a selected room in both case studies on a typical summer day and a winter day (12 August and 31 January) under steady-state conditions. Since the field study was conducted in the summer, winter results were provided for information purposes. For demonstration purposes, the results are shown for selected rooms (south-facing bedroom in Case Study 1 and top-floor room, room 2, in Case Study 2).

In general, a negative relationship between indoor air temperature and infiltration rate was observed for both models (see Figure 7-2). While increasing the uncontrolled infiltration of outdoor air resulted in a reduction in mean indoor temperatures, varying infiltration rates caused significant fluctuations in indoor air temperature, directly affecting cooling and heating loads.

It can be concluded that in a thermally controlled environment where the temperature between the indoor and outdoor environments far exceeds 10 °C, a reduction in cooling load is unlikely to be achieved by increasing the uncontrolled outdoor air infiltration rate (Al-Saadi & Al-Jabri, 2017; Albatayneh, 2021; Alyami & Omer, 2021). As discussed in Section 3.2, uncontrolled airflow into the building, particularly during the overheating season, could significantly increase heat buildup. Therefore, as part of this study, the impact of controlled ventilation combined with different passive cooling techniques on the indoor thermal environment was explored to improve the overall thermal performance of the selected buildings in Riyadh. These simulations are covered in more detail in the Chapter 9.

For the purpose of this thesis, air infiltration values of 0.5 ACH and 0.1 ACH were applied to the Case Study 1 and Case Study 2 baseline models, respectively. The selection of these values was influenced by a comparison of simulated indoor temperatures (with various air infiltration rates) with actual field measurements. As field measurements were only taken during the overheating season, winter results were provided for information purposes.

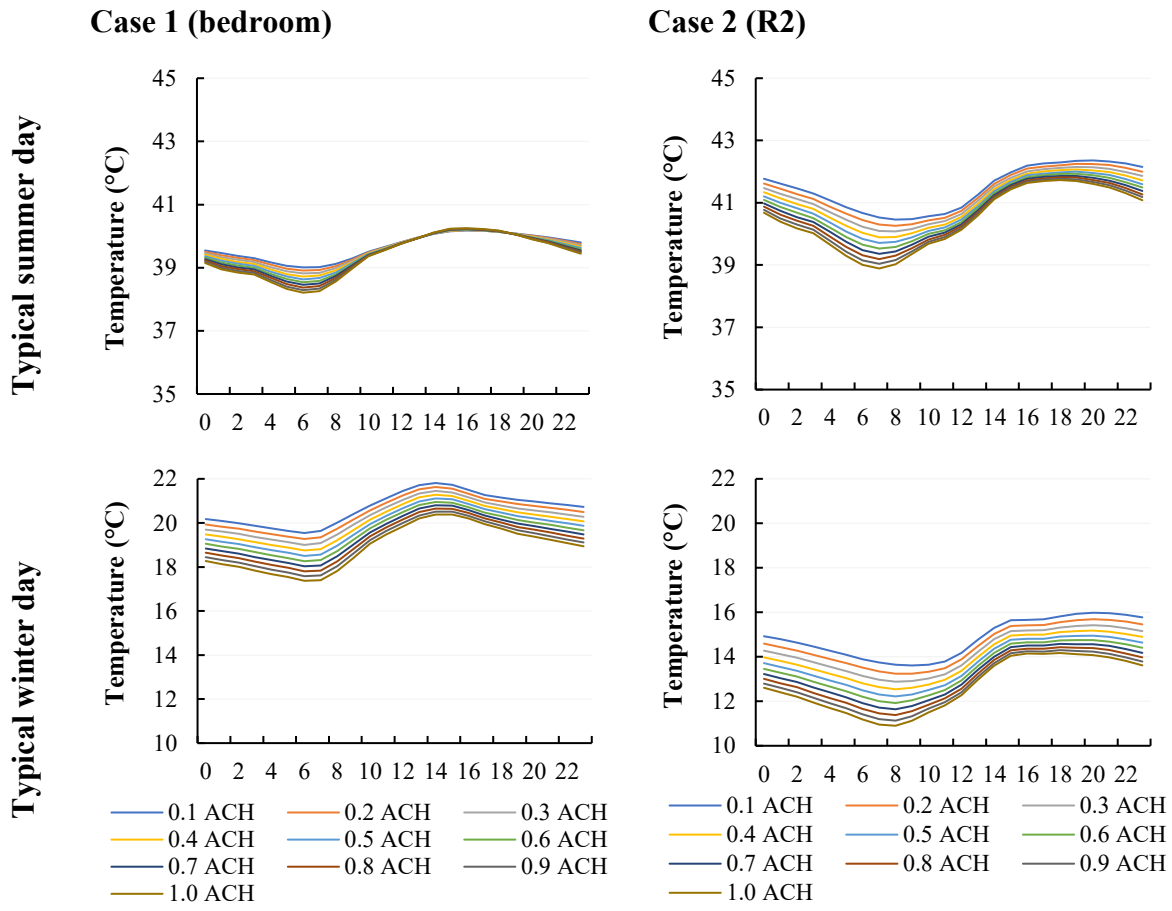


Figure 7-2 Sensitivity analysis of air infiltration impacts on indoor air temperature

7.2.4 Ground temperature

Several simulations were conducted for the two models using the previously discussed weather data to predict the hourly indoor air temperature under free-running conditions, with mechanical systems and internal gains (i.e. occupancy schedule, lighting, and equipment) switched off. The initial simulation results showed a considerable difference between predicted and measured indoor temperatures, especially for Case Study 1. Further investigations through a significant number of simulations revealed that the *adjacency data* setting for the ground floor was the reason for this difference.

The adjacency data for a building element describe what lies on the other side of the selected element and the assumed thermal boundary conditions applied there (IES-VE, 2023). These data are set automatically according to the geometry of the building and the category of the element (e.g. external walls, ground floors, or roofs). A review of this data revealed that the default input for the adjacent conditions of the ground floor was ‘outside air with offset temp. 0’, meaning that the software treated the ground floor as if it were in direct contact with the outside air. However, this may not accurately reflect the actual thermal behaviour of the

ground, especially in areas with extreme diurnal temperature fluctuations such as Saudi Arabia.

There is insufficient data in the literature about ground temperature profiles in Saudi Arabia. IES-VE suggests that users set 'constant' or 'time-varying' temperature boundary conditions for the ground floor (e.g. 13 °C in the UK). However, the seasonal ground temperature amplitude can vary from one region to another and from month to month, impacted by factors such as precipitation, incident solar radiation, soil type and properties, and vegetation cover (Hijazi, 2018). Moreover, it cannot be assumed that the ground temperature is constant due to the influence of seasonal air temperature fluctuations.

For this thesis, a sensitivity analysis was performed by applying different ground temperature values (13 °C, 18 °C, 23 °C, 28 °C, 33 °C, and 38 °C) to explore the sensitivity of the models' predictions to these inputs. This initial modelling phase aimed to explore the variability of the ground temperatures and their impact on indoor thermal environments (see Figure 7-3). For the purpose of this analysis, simulation results are shown for a typical summer day and a winter day for a selected zone in each house.

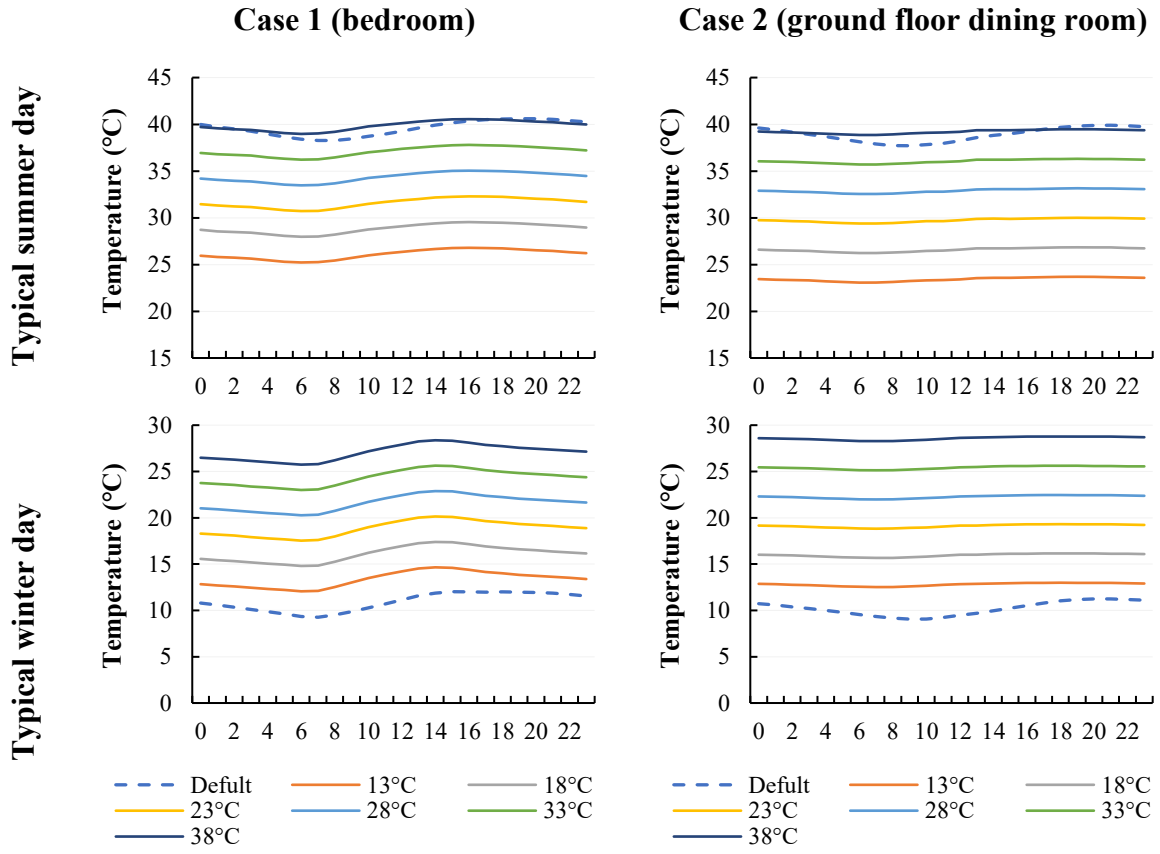


Figure 7-3 Sensitivity analysis of ground temperature impacts on indoor air temperatures for a typical summer day and a winter day in both case studies

The sensitivity analysis of ground temperature in this study demonstrated a considerable impact on the indoor thermal environment, consequently affecting cooling loads. It is evident that the default settings for ground floor adjacent condition in IES-VE led to inconsistencies in simulation outputs, directly affecting the energy model's results. This became more apparent when comparing these simulation results with the field measurements discussed in Section 6.4. Moreover, the fixed value of 13 °C suggested in the software's manual may be suitable for studies in the UK, where IES-VE was originally developed, but is clearly unsuitable for studies conducted in arid regions.

Despite the critical impact of ground temperature on the indoor thermal environment, previous studies in building thermal performance, especially those carried out using IES-VE in a climate condition similar to that investigated in this thesis, neither reported nor involved ground temperature values in the energy modelling process (Aldossary et al., 2014, 2017; Alkhalifah, 2024; Alrashed, 2015; El-Bakkush, 2016; Lasker, 2016). It is evident that an increase in ground temperature corresponds to an increase in mean indoor temperature.

Abdel-Ghany, Al-Helal, Alsadon, Ibrahim, and Shady (2022) conducted an experimental study to measure in-ground temperatures in Riyadh at multiple depths over a one-year period. The study reported that the annual variation of ground temperature decreases with increasing depth. Since IES-VE does not explicitly model soil depths and layers, monthly mean values of shallow-ground temperatures were considered. This modelling approach has been applied in previous studies utilizing building energy simulation conducted in Saudi Arabia, such as the work of Abuhussain (2020).

For the purposes of this thesis, the ground temperature boundary condition was specified using the monthly mean in-ground temperatures measured at 1.7 m depth by Abdel-Ghany et al. (2022) (Table 7-5), as this depth exhibits significantly reduced diurnal temperature variations while remaining representative of shallow ground conditions beneath building slabs. The adopted ground temperature profile indicates that the peak ground temperatures occur between July and September, while the lowest ground temperatures occur in January and February.

Table 7-5 Average monthly ground temperatures in Riyadh (Abdel-Ghany et al., 2022).

Month	Jan	Feb	Mar	Apr	May	Jun	Jul	Aug	Sep	Oct	Nov	Dec
(°C)	24.7	24.2	25.3	28.4	31.9	34.4	35.8	37.3	37.3	36.3	27.9	26.9

7.3 Model validation

In this phase, following the previous process associated with constructing the energy models and the selected ground temperature, simulations for both case studies were run under a steady-state condition. The objective was to validate predicted indoor temperature against actual measurements. This method provides more confidence in the developed energy models and the results for further investigations covered in this and following chapters.

The simulation was run for both houses under the specified conditions and for the same period corresponding to the actual measurements' conditions and period. The graphs in Figures 7-4 and 7-5 illustrate hourly comparisons between the actual measurements and the predicted indoor air temperature values while all rooms were in a steady-state condition for selected rooms in Case 1 and Case 2, respectively. The purpose of putting the simulation results alongside the monitored data was to validate the analytical work.

The comparisons demonstrated that the predictions of indoor air temperatures generated from the IES models closely followed the same trends of the monitored temperatures for all rooms in Case 1 and Case 2. Despite high levels of agreement between the simulation predictions and the field measurements, slight deviations can be noticed in some cases. Generally, the difference between the simulation results and the field measurements did not significantly exceed 2 °C, with a maximum error percentage of less than 6%.

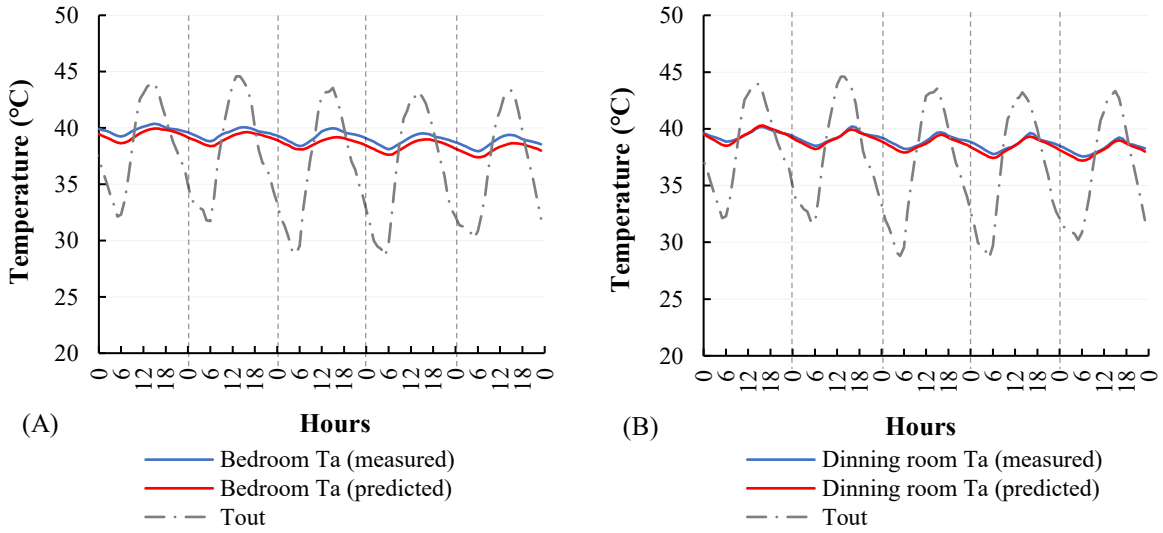


Figure 7-4 Measured and predicted air temperature for selected rooms in the 3D-printed house (Case Study 1) from 13 August to17 August: (A) Bedroom; (B) Dining room.

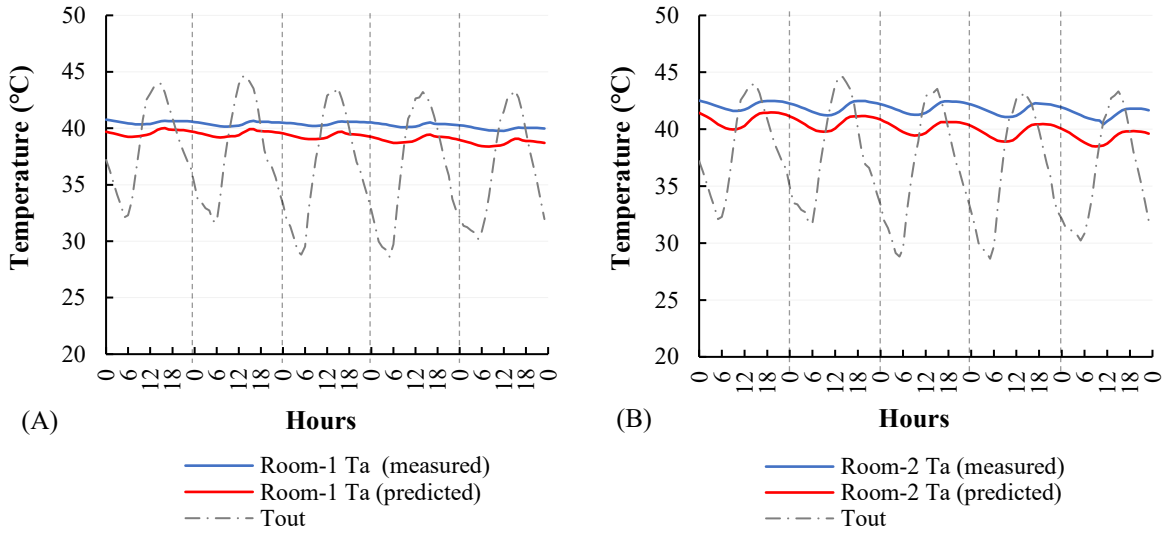


Figure 7-5 Measured and predicted air temperatures for selected rooms in the conventional house (Case Study 2): (A) Room 1 (first floor); (B) Room 2 (top floor).

Further to the graphical comparison between the simulation predictions and field measurements, a statistical analysis was conducted to ensure that the simulation results were statistically validated. Several statistical indices that are widely recognized and accepted by various international standards, such as ASHRAE and CIBSE, were adopted by previous scholars to evaluate the produced error between simulated results and real measurements (Abuhussain, 2020; Alaboud & Gadi, 2019, 2020; Kiamba, 2016; Pachano & Bandera, 2021).

The square of the Pearson correlation coefficient (R^2) measures the correlation (linear relationship) between two sets of data (e.g. simulation predictions and field measurements), indicating how alike the simulated model result curve appears to the measured one. See Equation (7-1). However, due to a substantial bias in terms of error distance, it is recommended that this index be used with other indices, such as the normalized mean bias error (NMBE) and the coefficient of variation of the root mean square error (CVRMSE).

$$R^2 = \left(\frac{\sum_{i=1}^{n} (m_i - \overline{m}) \cdot (s_i - \overline{s})}{\sqrt{\sum_{n=1}^{n} (m_i - \overline{m})^2 \cdot \sum_{n=1}^{n} (s_i - \overline{s})^2}} \right)^2 \quad (7\text{-}1)$$

Where:

- $\overline{m}$ is the mean of measured values.
- $\overline{s}$ is the mean of simulated values.
- m_i is the measured value.
- s_i is the simulated value.
- n is the number of data points.

The NMBE is used to calculate the average error between real measurements and simulated values, which is normalized by the mean of the real measurements. The NMBE can be calculated using Equation (7-2). The CVRMSE is calculated by normalizing the root mean

square error between measured and simulated values with the mean of the real measurements and can be calculated using Equation (7-3). The mean absolute error (MAE) is the average of the absolute error between the predicted and monitored values. In this study, the MAE was calculated using Equation (7-4) (Pachano & Bandera, 2021, p. 6).

$$\boldsymbol{NMBE} = \frac{\mathbf{1}}{\overline{\boldsymbol{m}}} \cdot \frac{\sum_{i=1}^{n}(\boldsymbol{m_i} - \boldsymbol{s_i})}{\boldsymbol{n} - \boldsymbol{p}} \times \mathbf{100}(\%) \tag{7-2}$$

$$\boldsymbol{CVRMSE} = \frac{\mathbf{1}}{\overline{\boldsymbol{m}}} \cdot \sqrt{\frac{\sum_{i=1}^{n}(\boldsymbol{m_i} - \boldsymbol{s_i})^2}{\boldsymbol{n} - \boldsymbol{p}}} \times \mathbf{100}(\%) \tag{7-3}$$

$$\boldsymbol{MAE} = \frac{\sum_{i=1}^{n}|\boldsymbol{m_i} - \boldsymbol{s_i}|}{\boldsymbol{n}} \tag{7-4}$$

It must be noted that in this study, the hourly temperatures for the predicted and monitored data were averaged from sub-hourly values. Thus, the analysis in this section was conducted based on the calculated hourly values of air temperatures for the selected rooms during the specified period.

The analysis results of the MAE, R^2, NMBE, and CVRMSE for the selected rooms in Case 1 (3D-printed house) and Case 2 (conventional house) are given in Table 7-6. The comparison between the simulation predictions and the field measurements revealed a highly positive correlation between the two sets of data, with R^2 ranging between 0.81 and 0.95 (within the range of $R^2 \geq 0.75$). This resulted in NMBE values ranging between 0.54% and 4.01%, while the CV of the RSME ranged between 0.63% and 4.08%. The calculated MAE did not exceed 1.0 °C in Case 1 and 1.6 °C in Case 2. See Table 7-6.

The results complied with the requirements of ASHRAE guidelines at hourly interval ($R^2 \geq 0.75$, NMBE $\leq \pm$ 10%, and CV RMSE $\leq$ 30%) and also met CIBSE TM63 standard, Operational performance: Building performance modelling and calibration for evaluation of energy in-use, with MAE < 2 °C. Accordingly, the validation results demonstrate that the simulation predictions satisfactorily reflected the actual thermal behaviour of the houses in Riyadh, thus proving the validity and reliability of the developed IES models for use in further simulations.

Table 7-6 Validation results of the statistical analysis for the selected rooms in Case 1 and Case 2

	Analysed room	MAE (< 2 °C)	NMBE (≤ 10%)	CV RMSE (≤ 30%)	R^2 (≥ 0.75)
Case 1	▪ Bedroom	0.52	1.34	1.38	0.95
	▪ Dining room	0.21	0.54	0.63	0.97
Case 2	▪ Room 1	1.09	2.73	2.77	0.81
	▪ Room 2	1.66	4.01	4.08	0.85

7.4 Incident solar radiation rate

As discussed in Chapter 3, a high solar radiation rate contributes significantly to indoor thermal behaviour, and, by extension, cooling energy consumption. For this analysis, the SunCast module within IES-VE was used. The graphs in Figure 7-6 illustrate the external surface solar radiation per area unit (i.e. W/m^2) for Case 1 and Case 2 in both summer and winter. This quantifies the variation in external surface solar radiation rates due to differences in surfaces orientation.

As demonstrated in the figures below, the rates of solar radiation received by the building envelope are generally higher in summer than in winter. This pattern is due to the seasonal movement of the sun in relation to the building envelope and corresponds directly with the heat-gain analysis discussed in Sections 8.3–8.4. The analysis presented in Chapter 8 suggested that cooling loads are predominantly driven by external heat gain sources, which accounted for approximately 76% of the total cooling load in Case 1 and 71% in Case 2 (see Figure 8-16). Therefore, analysing incident solar radiation on the external surfaces of the building fabric is essential for understanding the mechanisms of heat gain through the envelope—both opaque and transparent surfaces—and for proposing and evaluating strategies to improve the building's thermal and energy performance.

In general, Case 1 experienced greater total and mean incident solar radiation per area unit compared to Case 2, particularly in winter. This could be attributed to a number of factors, including variation in the orientation of each house and surrounding environments. In winter, the effect of the adjacent buildings surrounding Case 2 can be more profound as they obstruct direct solar radiation from reaching some parts of the walls, especially when the sun is at lower solar altitudes (see Table 7-7).

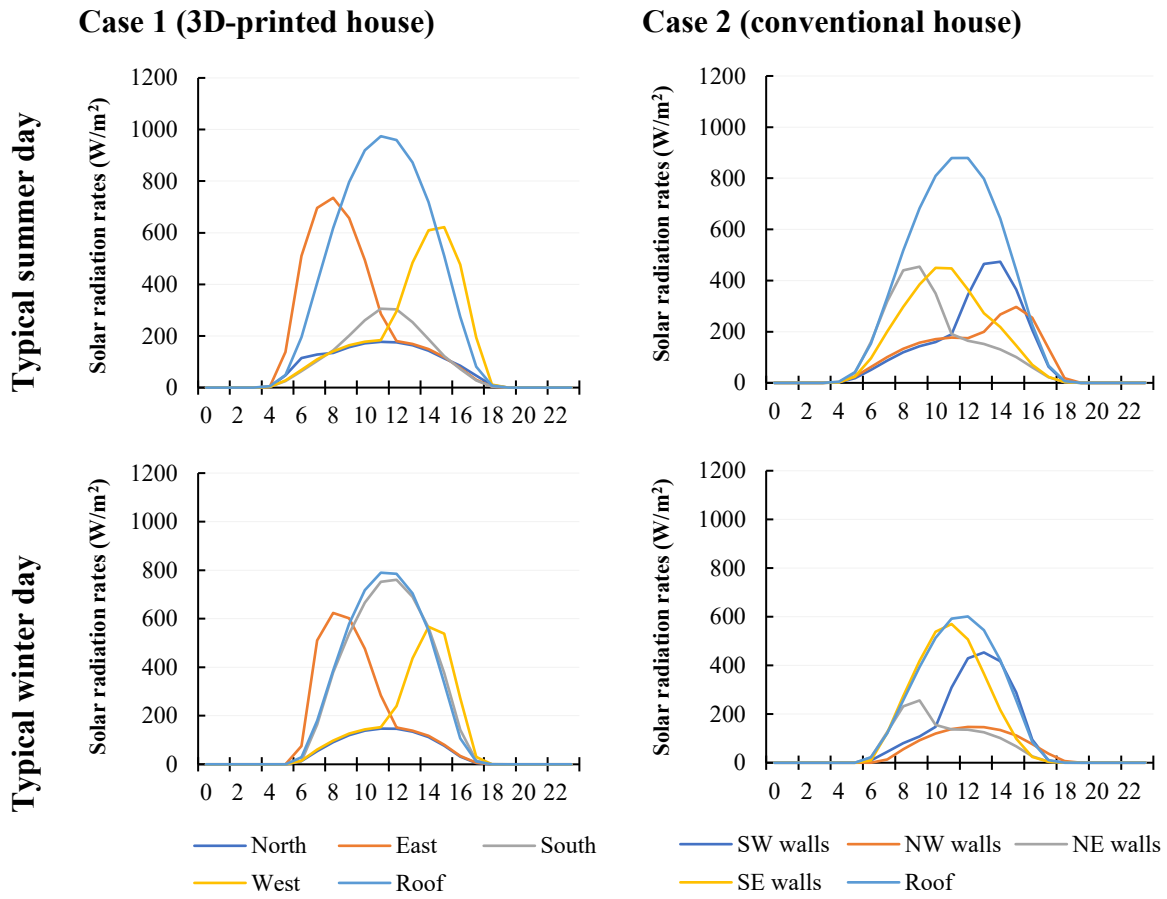


Figure 7-6 Incident solar radiation on external surfaces (in W/m^2) for both houses during a typical summer day and a winter day

Note the reduction in solar radiation of the roof in winter, while it significantly increases on the south-facing wall in Case Study 1.

On a summer day, Case 1 had a mean solar radiation rate of 157.9 W/m^2, while Case 2 had a slightly lower mean of 141.1 W/m^2. The roof received the highest solar radiation rates compared to other surfaces, with daily averages of 307.7 W/m^2 in Case 1 and 270.1 W/m^2 in Case 2. This is primarily due to the high solar altitude in Riyadh during the summer.

For vertical surface (i.e. external walls), the east and west walls in Case 1 had the highest solar radiation per unit area at approximately 177 W/m^2 and 148.7 W/m^2, respectively, while the north wall received the least, at 69.5 W/m^2. In Case 2, both the southeast and southwest walls received the highest solar radiation compared to other wall orientations, at about 125 W/m^2 and 112 W/m^2, respectively.

On a winter day, the south wall in Case 1 received 210.7 W/m^2, which is 143.7% higher than in summer. This increase is due to the lower solar altitude in the winter, which enables the radiation to reach vertical surfaces at almost an orthogonal angle. In Case 2, the southeast

wall received the greatest solar radiation rates compared to the other wall orientations, at 131.2 W/m^2 (about 5% higher than in summer).

Table 7-7 Daily average incident solar radiation rate (W/m^2) of external surfaces (external walls and roofs) for typical summer and winter days

A. Case 1 (3D-printed house)

	North	East	South	West	Roof	Total	Mean
Summer	69.5	176.9	86.5	148.7	307.7	789.3	157.9
Winter	44.6	129.2	210.7	111.8	215.7	712	142.4

B. Case 2 (conventional house)

	Southwest	Northwest	Northeast	Southeast	Roof	Total	Mean
Summer	112.1	90.6	107.8	125.1	270.1	705.6	141.1
Winter	99.5	44.9	57.8	131.2	159.2	492.6	98.5

7.5 Summary

This chapter focused on detailing the process of constructing and validating the 3D energy models of the selected case study buildings in the hot climate of Riyadh. Since validation of the energy models is necessary to ensure the reliability of the simulation outputs, which will be covered in the next chapters, the simulation results of the indoor air temperatures for the selected rooms in each house were compared against field-monitored data over the specified period during the summer season. The correlation between measured and simulated data was assessed using various statistical indices. The computer predictions of indoor temperatures showed similar behaviour to the monitored data, with the difference between the two data sets not significantly exceeding 2 °C. Based on the presented analysis of the error between predicted and monitored data, it was safe to assume that simulation predictions were within the acceptable range.

In general, it can be concluded that with the right, detailed input data and appropriate adjustments to the settings, IES-VE's indoor thermal environment predictions can be significantly improved. It was observed that the default settings for ground-adjacent conditions in IES-VE were not suitable for the climate features investigated in this thesis. This was due to the high diurnal temperature fluctuations in Riyadh, which resulted in inconsistent results when compared to the monitored data. Based on the adopted monthly ground temperature data, the energy models were validated for further analysis, as described in subsequent chapters.

CHAPTER 8

ANALYSIS OF INDOOR THERMAL ENVIRONMENT USING COMPUTER SIMULATION SOFTWARE

- Introduction
- Predictions of indoor thermal conditions
- External heat gain analysis
- Cooling load and load breakdown
- Energy consumption and CO_2 emissions of baseline models

Chapter 8: ANALYSIS OF INDOOR THERMAL ENVIRONMENT USING COMPUTER SIMULATION SOFTWARE

8.1 Introduction

Following the validation of both energy models conducted in the previous chapter, simulations were conducted over the course of the year as part of fulfilling the research objectives of this thesis. The simulations discussed in the following sections aimed to explore the thermal performance of both houses under steady-state conditions. This approach allowed for an evaluation of the buildings' inherent thermal performance in the specified climate, without the influence of external interventions. These results form the basis of the next chapter, which will investigate various passive cooling techniques learned from vernacular architecture and modern sustainable building technology to improve the thermal performance and energy efficiency of both houses. It should be noted that the selected rooms for the field work were considered here for demonstration purposes.

Finally, this chapter attempted to predict cooling load, energy consumption, and carbon emissions for the selected case study buildings in Riyadh, based on the baseline assumptions and boundary conditions established in Chapter 5 (see Sections 5.5–5.8) and the modelling parameters defined in Section 7.2. This will facilitate an investigation of the energy efficiency of each house before and after applying the proposed enhancement measures in the following chapter.

8.2 Indoor air temperature results

The field work results (discussed in Chapter 6) revealed that summertime indoor air temperatures in the investigated region are generally far above comfort limits. This is due to high outdoor temperatures accessing the building in the summer, thus raising indoor temperatures and consequently the cooling load. In general, indoor temperatures and outdoor temperatures have a direct linear relationship.

Figure 8-1a shows the indoor air temperature results for selected rooms in Case 1 and Case 2. The predicted results indicate that more than 60% of the total hours of the year in both houses fall above 26 °C, with 38 °C being the most frequent indoor temperature. This aligns with the reviewed literature, thus indicating the high cooling demands in the investigated climate, particularly during the overheating season due to the high outdoor temperatures. Besides, simulation results (discussed in Sections 8.4–8.5) revealed that the peak cooling loads in both

houses occurred on 12 August (the peak month) at 15:30, coinciding with an outdoor temperature of 44 °C. Overall, it was observed that both houses had relatively low underheating hours (i.e. the number of hours when indoor temperatures were predicted to fall below the SBC heating setpoint temperatures), particularly in Case 1.

The hourly temperature predictions for the entire year are shown in Figure 8-1b. The results show that both houses in Riyadh had high mean temperatures. The temperatures in Case 1 ranged between 18.5 °C and 40.2 °C in the south-facing bedroom and between 17.6 °C and 40.6 °C in the west-facing dining room. In Case 2, temperatures ranged between 15.9 °C and 40.5 °C in the first-floor bedroom (R1) and between 13.6 °C and 42.3 °C in the second-floor bedroom (R2). This means that both the bedroom in Case 1 and the upper room (R2) in Case 2 had the highest mean temperatures: 31.1 °C and 30.6 °C, respectively.

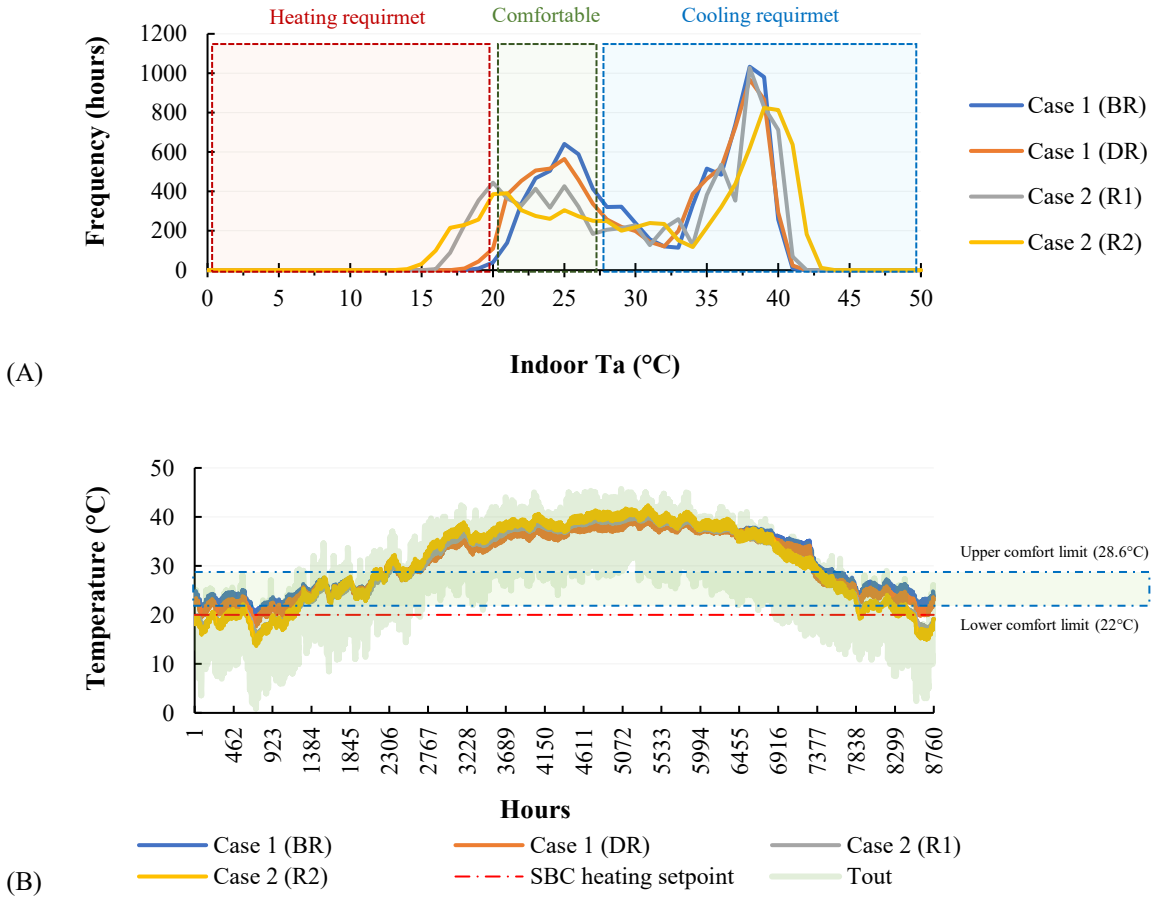


Figure 8-1 Hourly simulation results for selected rooms in each house: (A) Predicted indoor air temperature frequencies for Case 1 and Case 2; (B) Predicted hourly indoor temperatures for both houses in Riyadh

Based on the presented results, 12 August and 31 January were identified as the hottest and coldest days of the year, respectively, for both houses. Accordingly, these days were selected

for reporting simulation results in this and the following chapter, as they represent the most extreme weather conditions in the investigated climate.

Figures 8-2 and 8-3 demonstrate hourly simulation results of the indoor thermal conditions, including indoor air temperature (Ta), mean radiant temperature (MRT), and operative temperature (To)—which is the average of the last two—for a typical summer day and a winter day (i.e. 12 August and 31 January, respectively). It should be noted that the simulation results are shown for the selected rooms for demonstration purposes. In general, a strong positive relationship between Ta and To was observed in both houses. See Appendix B-A for year-round correlations between Ta and To for selected rooms in each house.

Despite the significant daily outdoor temperature swings in Riyadh, the indoor temperatures in both houses were relatively stable in both seasons. This could be attributed to thermal insulation applied to the baseline model, which limited thermal exchange between indoor and outdoor environments, as indicated in Chapter 6 (see Appendix B-B and Appendix B-C for more information). Various simulations were conducted to explore the impact of improving the building envelope on indoor temperatures. The results of these simulations are discussed in Chapter 9.

In Case 1, during a typical summer day, both rooms showed similarities in thermal behaviour, with minor differences despite variation in orientation. This could be attributed to the high solar altitude in Riyadh (near the zenith), with the roof having the highest absorptance of solar energy, as indicated in previous chapter. However, the west-facing dining room exhibited a greater maximum Ta compared to the south-facing bedroom, which can be explained by the penetration of solar radiation into the indoor environment given the daily movement of the sun, as discussed in Section 7.4. This resulted in a greater daily Ta fluctuation of 2.1 °C compared to 1.6 °C in the bedroom.

In winter, the south-facing bedroom exhibited a larger temperature fluctuation of 2.6 °C compared to 2.1 °C in the dining room. This variation in thermal behaviour, when compared to the summer results, can be explained by the low solar altitude during this time of the year, resulting in the mean Ta in the south-facing bedroom being about 1 °C higher than in the dining room.

In Case 2, however, the summer Ta ranged between 39.6 °C and 40.5 °C in R1 and between 40.4 °C and 42.3 °C in R2, with mean temperatures of 40 °C and 41.5 °C, respectively. In the winter, Ta was consistent in R1 with a daily difference of up to 0.5 °C compared to R2,

where the daily temperature swing reached up to 2.4 °C. The mean Tas were 16.3 °C and 14.8 °C, respectively. The difference in thermal performance between R1 and R2 can be explained by the location of the rooms, as R1 was located on the first floor with only one wall exposed to the outdoor environment while was R2 on the top floor.

By comparing the predicted results for each room, it appears that the tested rooms in Case 1 performed better than the tested rooms in Case 2 during both seasons. This superior performance was distinguished by consistently stable and lower temperatures in the summer and higher temperatures in winter. See Figure 8-4.

It is likely that Case 1 benefited from the effect of the ground, which allowed thermal exchange between the indoor environments and the ground (i.e. heat dissipation in the summer and heating effect in the winter). The ground temperatures adopted in this study were discussed in Section 7.2.

Nevertheless, this thesis investigated the impact of applying ground floor insulation—as per SBC requirements, to improve the energy efficiency of residential buildings in KSA—on the overall thermal performance of both houses throughout the course of the year. The results of these simulations are discussed in the following chapter.

Further to the above analysis, the percentage of hours when indoor temperatures were predicted to be within/outside the identified comfort range was evaluated for the selected rooms in each house (see Figure 8-5). According to the results, Case 1 demonstrated higher percentages of comfort hours, with 35.8% in the south-facing bedroom and 31.6% in the west-facing dining room, compared to Case 2, where comfort hours were 23% in R1 and 19.8% in R2.

The lower percentages of comfort hours in Case 2 were primarily due to the high number of underheating hours, which could be attributed to surrounding buildings obstructing solar radiation, especially in winter when solar altitude is lower. Notably, the lowest percentage of overheating hours, 56.2%, was observed in R1 (first-floor bedroom), likely due to the low number of exposed surfaces to the outdoor environment, leading to less heat gain compared to the other tested zones.

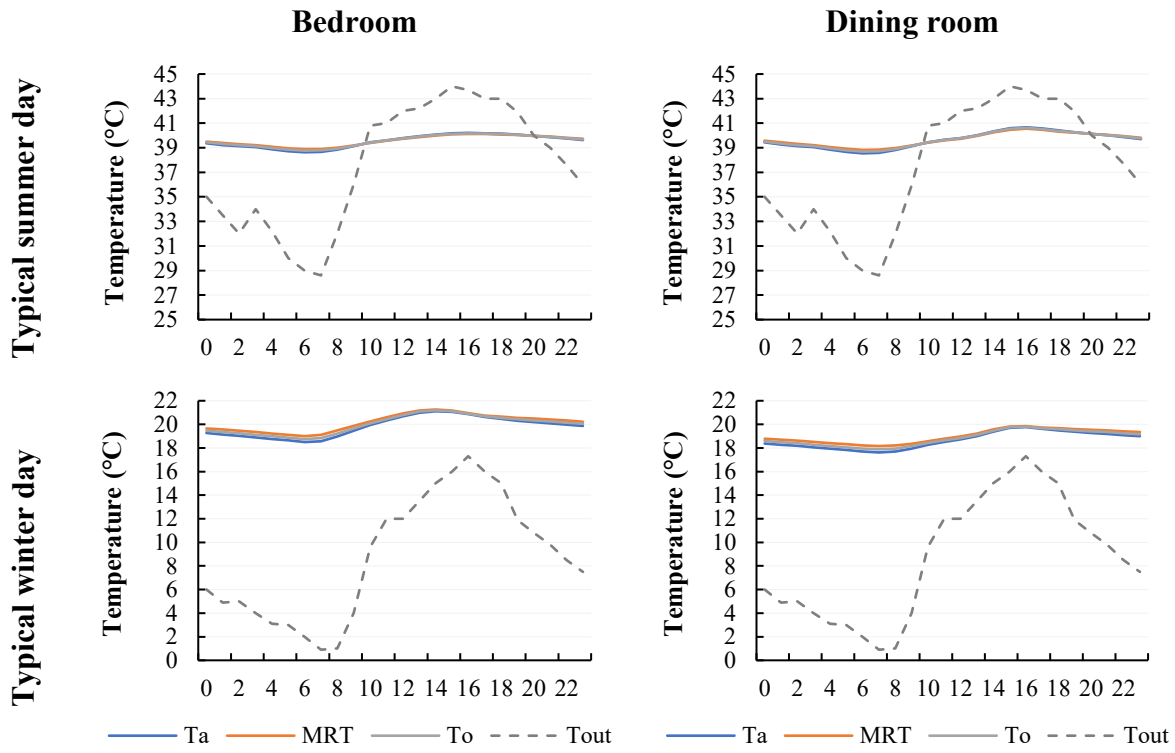


Figure 8-2 Hourly Ta predictions for the selected rooms in Case 1 during a typical summer day and a typical winter day

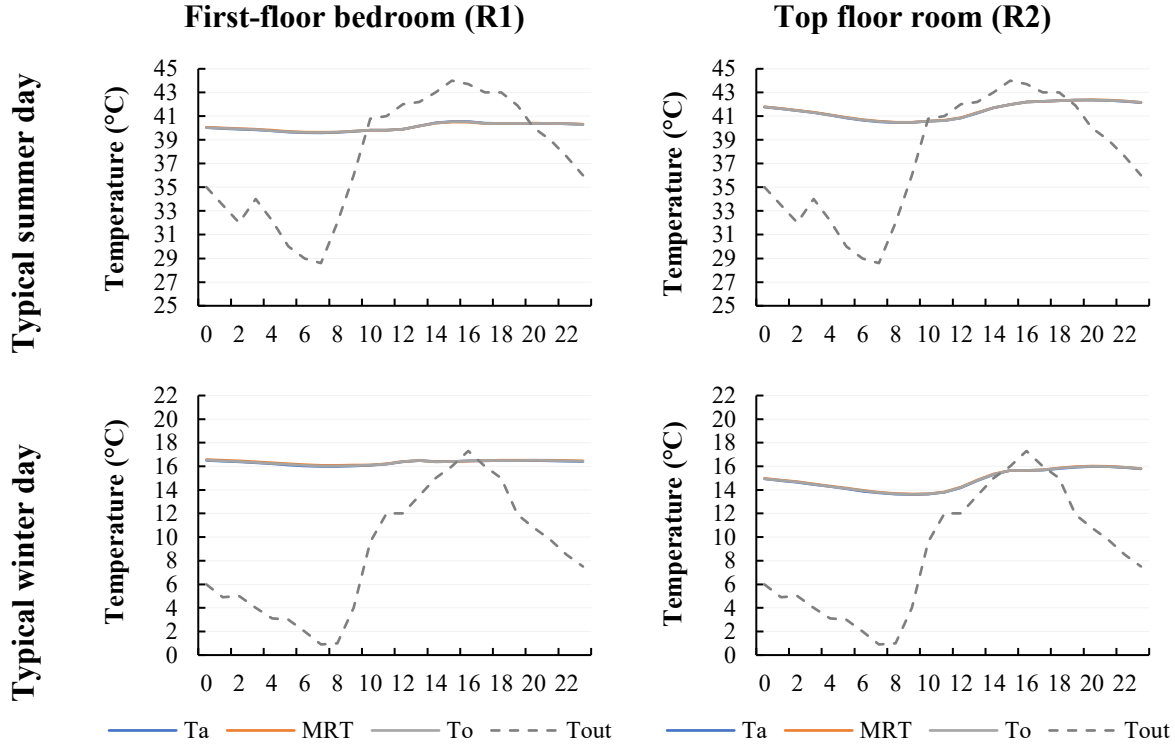


Figure 8-3 Hourly Ta predictions for the selected rooms in Case 2 during a typical summer day and a typical winter day

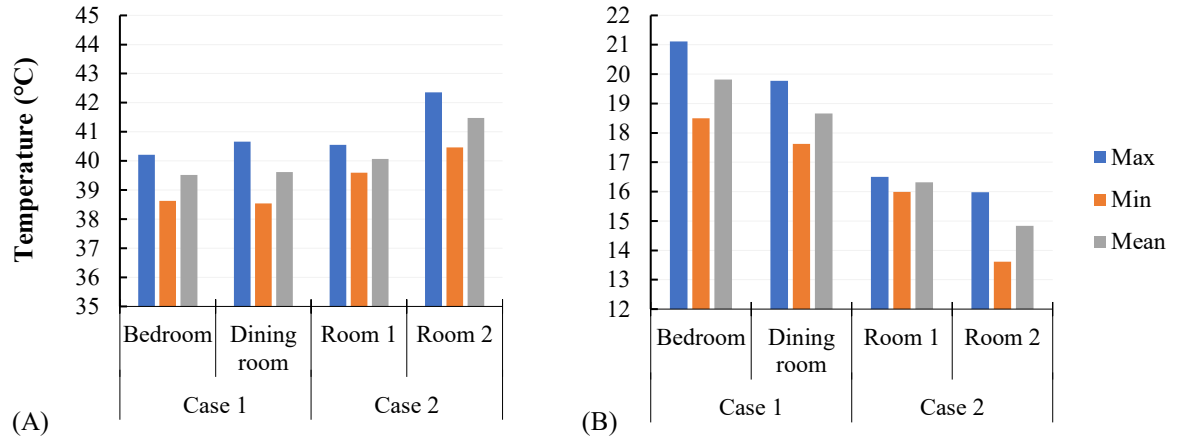


Figure 8-4 Comparison of maximum, minimum, and mean indoor temperatures for selected rooms in both houses: (A) Simulation results for a typical summer day; (B) Simulation results for a typical winter day

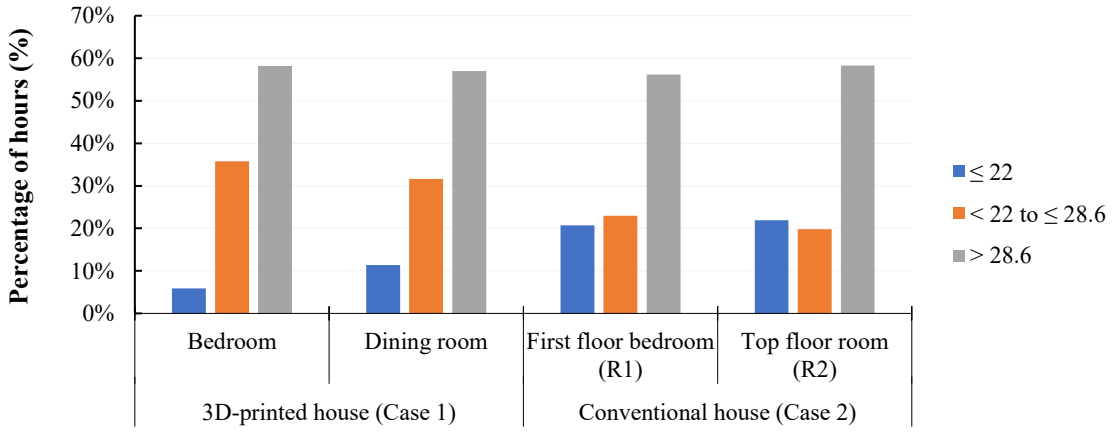


Figure 8-5 Thermal comfort analysis for selected zones in Case 1 and Case 2

As part of this study, the effect of natural ventilation on the indoor thermal environment was investigated. Existing window properties for each house (in terms of size, location, and opening characteristics) were considered in this analysis (see Figures 8-6 and 8-7). The same rooms investigated during the fieldwork were considered for this analysis. To illustrate the effect of applying natural ventilation strategies, indoor air temperature profiles were plotted for a typical summer day (12 Augus). It should be noted that although the cooling season spans from May to September, August was selected for illustration purposes as it is considered the warmest month of the year and the one with the greatest cooling demand.

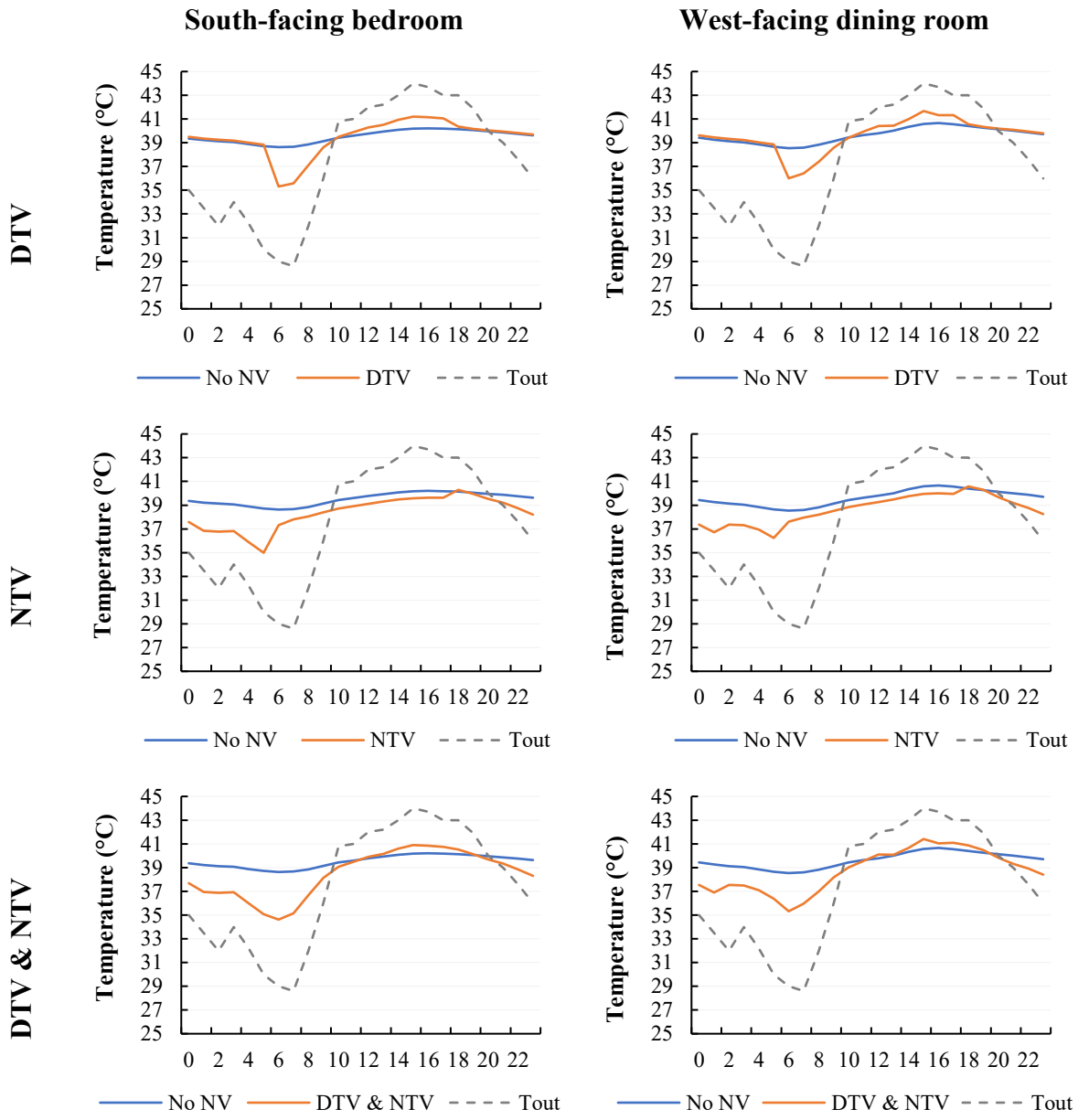


Figure 8-6 Assessing the impact of proposed natural ventilation strategies on improving the indoor thermal environments of selected rooms in Case 1 (3D-printed house) during a typical summer day. Note that results shown are before and after applying NV.

When daytime ventilation (DTV) was applied (from 06:00 to 18:00), Ta was greatly reduced during the morning hours by up to 3 °C in Case 1 and by nearly 2 °C in Case 2. However, in Case 1, it was noticed that Ta increased by up to 1 °C during peak Tout period. This was likely due to convective heat gain through ventilation, which is consistent with the field measurements reported in Chapter 6. In Case 2, the impact of DTV during peak Tout periods on the indoor thermal environments was insignificant. This variation in indoor thermal response between Case 1 and Case 2 could be attributed to several factors, including variation in window configuration and orientation and different surrounding built environments.

Generally, the mean indoor temperature was not significantly reduced in either house with the application of DTV alone, likely due to the significant Tout during this time of the year, which limited the cooling effect of the applied natural ventilation strategy. Moreover, it was observed that Ta did not tend to respond to a reduction in outdoor temperature at night. Thus, following this step, further analysis was conducted to assess the impact of the introduction of nighttime ventilation (NTV) on the indoor thermal environments. This was mainly to allow indoor environments to take advantage of the cooler nighttime outdoor temperatures, thereby improving indoor thermal conditions.

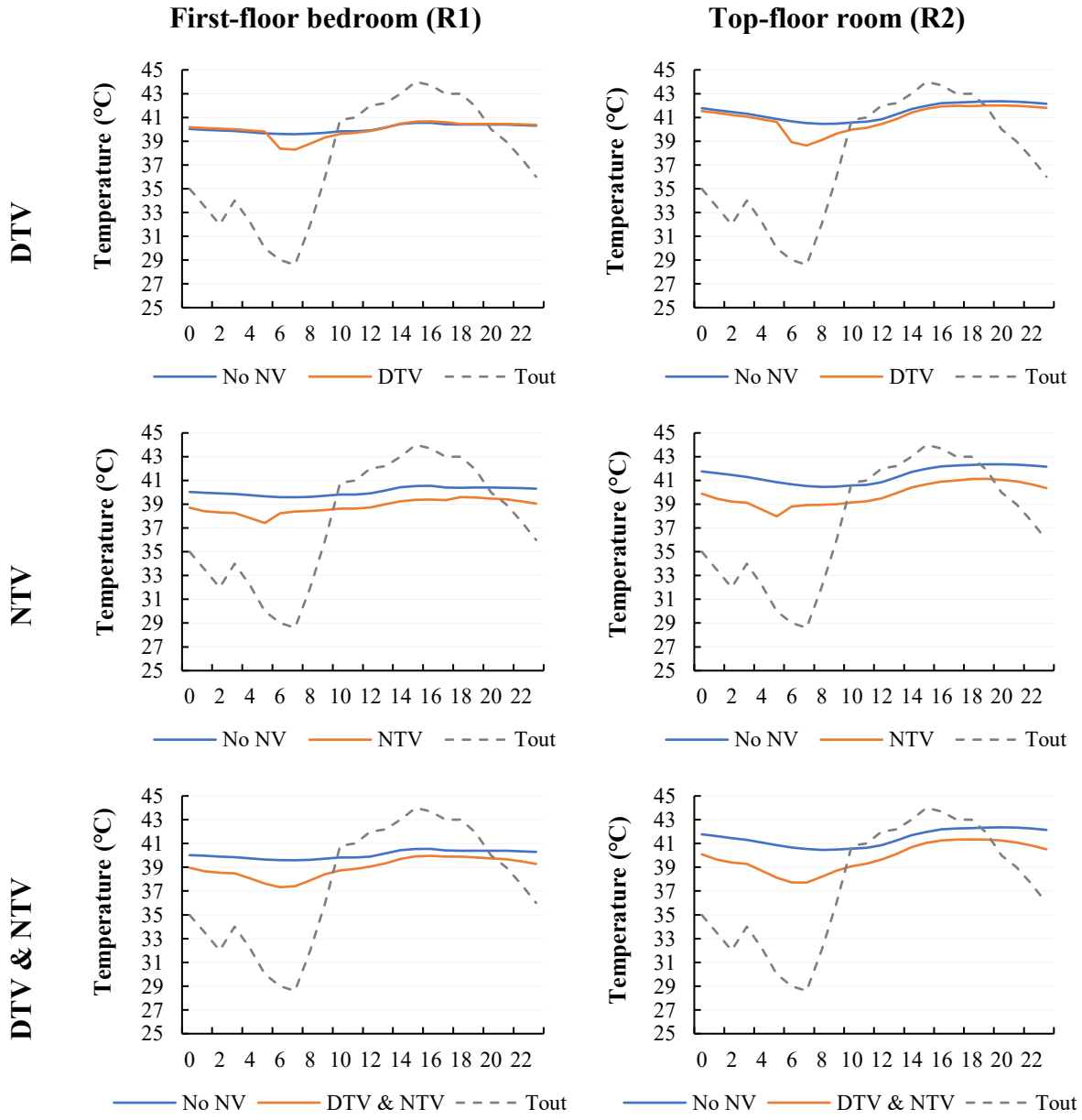


Figure 8-7 Assessing the impact of proposed natural ventilation strategies for selected rooms in Case 2 (conventional house) during a typical summer day. Note that the results shown are before and after applying NV.

For both houses, the introduction of NTV resulted in a reduction in the mean indoor temperature by up to 1.2 °C in Case 1 and up to 1.6 °C in Case 2 during the typical summer day. Moreover, allowing nighttime ventilation meant that the indoor temperatures for all rooms tended to fluctuate in a similar way to the outdoor temperatures at night, thus assisting the dissipation of internal built-up heat. This contributed to a reduction in Ta during peak Tout periods, with reductions of up to 0.6 °C in Case 1 and up to 1.3 °C in Case 2. Indeed, the introduction of outside air facilitated the flushing out of the accumulated heat inside the rooms, thus reducing the rooms' temperatures. It is evident from this analysis that NTV is an effective ventilation strategy for assisting the heat dissipation process, particularly in climates with significant temperature swings, such as Riyadh.

Further, the percentage of overheating hours (i.e. when the Tas were predicted to exceed the identified upper comfort limit in Riyadh, which is 28.6 °C) for the tested rooms with various ventilation strategies was evaluated for the entire year. The objective of this analysis was to assess the potential reduction in total overheating hours by applying natural ventilation strategies, thereby reducing the buildings' reliance on active cooling systems to achieve indoor thermal comfort. It should be noted that all other parameters were kept the same during this analysis. Figure 8-8 illustrates the potential reduction in the percentages of overheating hours for the selected rooms with various ventilation strategies.

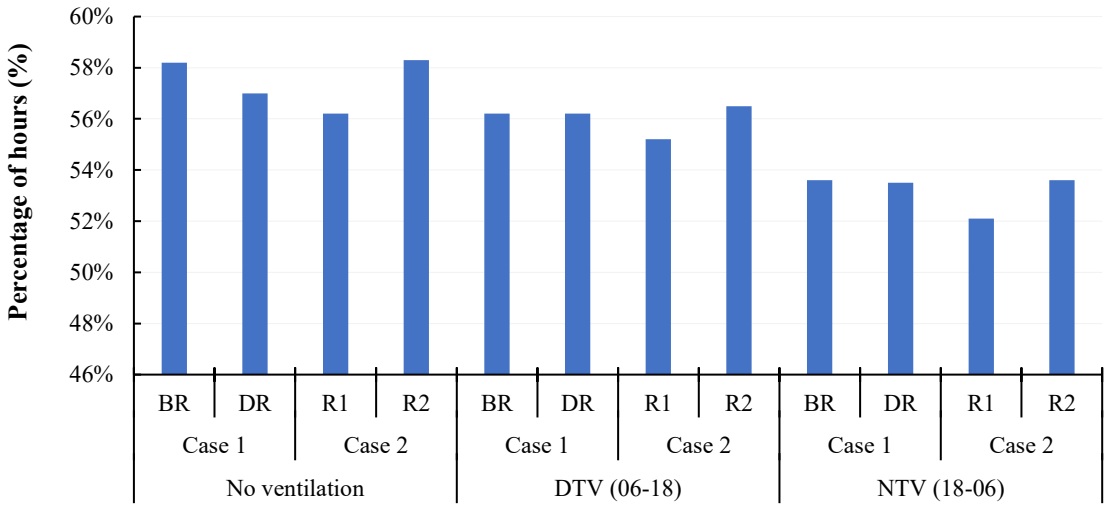


Figure 8-8 Evaluation of the percentage of overheating hours (above 28.6 °C) for the tested rooms in both buildings over the course of the year under various ventilation strategies

A review of the results in Figure 8-8 indicates that the percentage of overheating hours in Case 1 was reduced with the DTV strategy to 56.2% from 58.2% in the south-facing bedroom and from 57% in the west-facing dining room. However, this figure dropped further to about 53.5% in both rooms when the NTV strategy was applied. Similarly, in Case 2, the NTV strategy led to a greater reduction in the percentage of overheating hours, which was reduced from 56.2% to 52.1% in the first-floor bedroom (R1) and from 58.3% to 53.6% in the top-floor room (R2), compared to 55.2% and 56.5%, respectively, a reduction achieved with the DTV strategy.

The findings of these simulations demonstrate the effectiveness of NV as a passive cooling strategy that reduces overheating hours, thus improving the indoor thermal environment and energy efficiency. As previously indicated, the purpose of this analysis was to demonstrate the potential of NV to reduce overheating hours over the course of the year in the climate of Riyadh. However, NV must be controlled to avoid undesired convective heat gain/loss.

As part of this research, further simulations were conducted after applying a window operation scheme with various design strategies (previously discussed in Section 5.9). These simulations are covered in the following chapter. The following section provides an analysis of the heat gain sources through the building fabric components of both case studies.

8.3 Heat gain through the building fabric

As part of this study, heat gain/loss through various components of the building fabric (i.e. external walls, roof, ground, infiltration, and windows) was analysed for each house for both summer and winter days (see Figure 8-9). For the purpose of this analysis, the graphs below present the sum of the total heat gain/loss for all rooms during the selected days. To facilitate a comparison of the thermal performance of the two houses, the results were expressed per unit volume (cubic meter), suggesting that the conventional house (Case 2) is more thermally efficient than the 3D-printed house (Case 1). This superior performance in Case 2 can be attributed to its more effective regulation of heat flow through the building envelope components, whereas Case 1 exhibited significantly higher heat gain and loss per m^3 during both seasons.

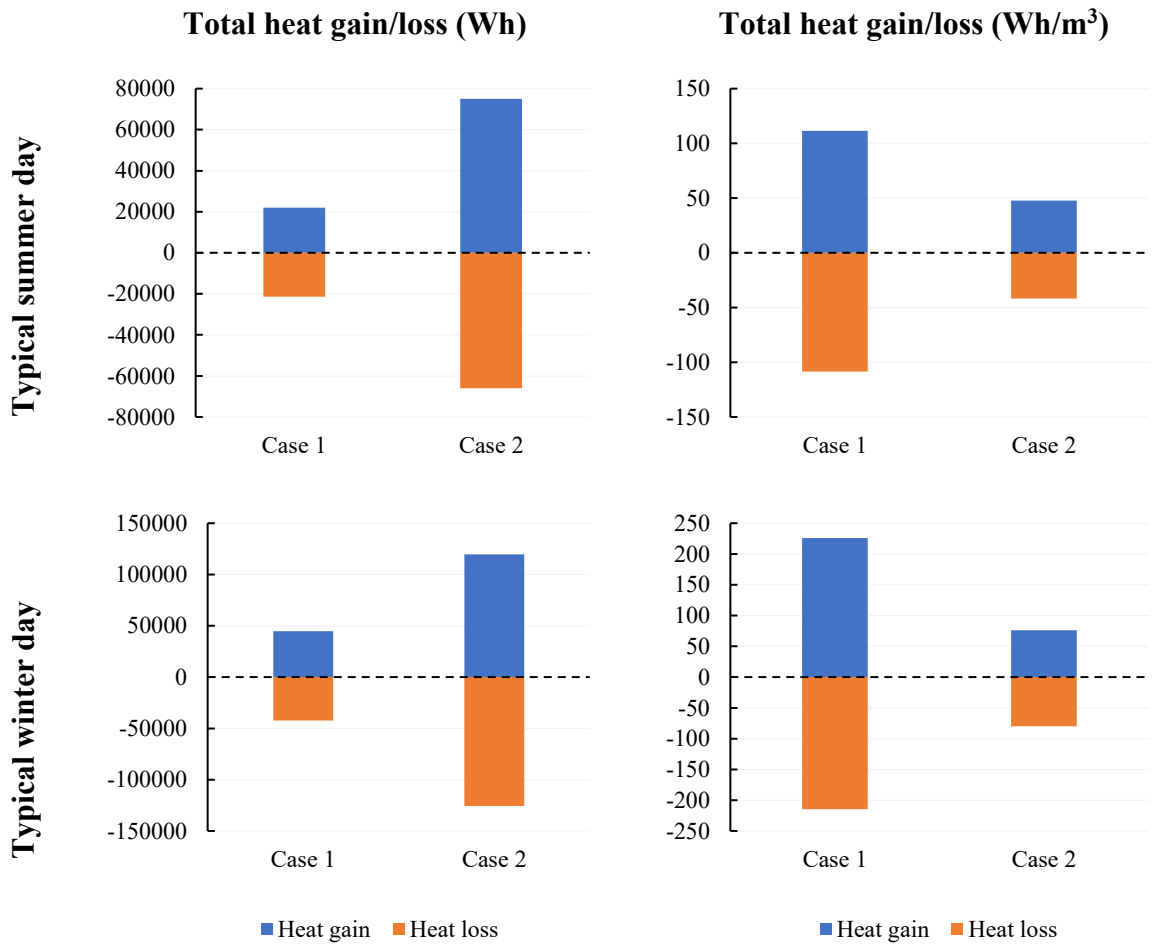


Figure 8-9 Heat gain/loss analysis for both case study buildings in summer and winter. Note the significant heat flow per m^3 in Case 1 compared to Case 2

Further to the above analysis, a breakdown of the heat gain/loss by source for both houses on a summer day and a winter day is presented in Figure 8-10. The purpose of this analysis was to provide insight into the thermal interaction between various components of the building fabric and the outdoor environment. By identifying the sensitive parts of the building envelope that contribute to the building's thermal performance, suitable improvements can be implemented in areas where they would lead to a significant impact. This will not only enhance indoor thermal comfort but also improve the building's thermal efficiency and reduce its operational carbon emissions. For both buildings, it was revealed that the major sources of external heat gain/loss were the external walls, roofs, windows, and infiltration.

Roof:

An analysis of the heat gain/loss breakdown by source for Case 1 revealed that the roof contributed the most to total heat gain in the summer and to heat loss in the winter, accounting for 46% and 43%, respectively, compared to only 10% and 17% for Case 2.

A comparison of the total heat gain/loss through the roof components of both houses revealed that the total amount of heat gain through the roof in Case 1 was 10 kWh (50.9 Wh/m^3) on a typical summer day, while total heat loss was −18.2 kWh (−92.4 Wh/m^3) on a typical winter day. These figures (i.e. per m^3) were far lower in Case 2, with 7.5 kWh (4.7 Wh/m^3) of heat gain on a typical summer day and −21.1 kWh (−13.4 Wh/m^3) of heat loss on a typical winter day. This variation between Case 1 and Case 2 can be attributed to the improved roof insulation applied in Case 2, which enhanced the roof's resistance to heat flow.

External walls:

The external walls played a crucial role in heat transfer for both buildings, particularly in Case 2, where they contributed significantly to heat gain in the summer and heat loss in the winter, accounting for 41% and 50%, respectively, compared to 17% and 27% in Case 1.

A comparison of the total heat gain/loss through the external walls for Case 1 revealed that the total amount of heat gain and loss on a typical summer day were 3.8 kWh (19.2 Wh/m^3) and −2.4 kWh (−12.4 Wh/m^3), respectively. In Case 2, the total heat gain and loss were 31 kWh (19.6 Wh/m^3) and −12.6 kWh (−8 Wh/m^3), respectively. This means that Case 2 exhibited a higher net heat gain of 18.3 kWh (11.6 Wh/m^3) compared to 1.3 kWh (6.7 Wh/m^3) in Case 1.

On a typical winter day, constant heat loss took place through the external walls during most of the day, with a total heat loss of −11.5 kWh (−58.4 Wh/m^3) in Case 1 and −62.6 kWh (−39.7 Wh/m^3) in Case 2. This was due to the outdoor temperature being constantly lower than indoor temperatures at this time of the year. These figures suggest that the conventional walls in Case 2 outperformed the 3D-printed walls in Case 1 during the short winter season of Riyadh under the existing conditions of each house.

Ground floor:

According to the results, the floor components showed a limited amount of heat gain during a typical summer day and heat loss during a typical winter day in both houses. This can be attributed to stable ground temperatures compared to outdoor temperature fluctuations.

On a typical summer day, thermal analysis indicated a constant heat loss through the floor at all times, with a total amount of −74.2 Wh/m^3 in Case 1 and −22.7 Wh/m^3 in Case 2. This means that the internal surface temperature of the floors would be higher than the floors' external surface temperature (i.e. the surface exposed to the soil) during this time of the year.

This could be attributed to the fact that, in summer, the ground temperature is lower than the indoor temperature.

The results revealed that heat flow through the floor components differed between summer and winter, as heat gain through floors took place mostly in winter, with total amounts of 168.9 Wh/m^3 and 58.2 Wh/m^3, respectively. This could be explained by the winter temperature of the ground being higher than the indoor temperature. Ground temperature inputs were discussed in Chapter 7 (see Section 7.2.4).

Infiltration:

Infiltration heat gain/loss in Case 1 was greater than in Case 2, accounting for 4% and 2% of the total heat gain on a typical summer day and for 20% and 9% of the total heat loss on a typical winter day, respectively. This variation was due to the lower rates applied to Case 2's baseline model, as discussed in Section 7.2.

On a typical summer day, the total amount of heat loss through infiltration significantly exceeded the heat gain, resulting in a net cooling effect, which is desirable in the investigated climate. However, in winter, uncontrolled airflow led to significant heat loss, particularly for Case 1, where total heat loss through uncontrolled airflow was −8.3 kWh (−42 Wh/m^3) compared to −11 kWh (−7 Wh/m^3) for Case 2.

Glazing:

The results revealed that windows contributed 33% of the total heat gain on a typical summer day in Case 1 and 47% in Case 2. On a typical winter day, they accounted for 10% and 19% of the total heat loss in Case 1 and Case 2, respectively. The significant heat gain through windows is due to the high solar radiation penetrating the indoor environments.

The total amount of heat gain through glazing surfaces on the summer day and the winter day for Case 1 were 7.3 kWh (36.9 Wh/m^3) and 11 kWh (55.7 Wh/m^3), respectively, while for Case 2 they were 34.9 kWh (22.1 Wh/m^3) and 23.4 kWh (14.8 Wh/m^3), respectively.

The variation between summer and winter heat gain in Case 1 was expected due to the low solar altitude in the winter, allowing greater solar gain. The lower gain in Case 2 in the winter can be explained by the presence of adjacent buildings, which sheltered the building envelope from direct solar radiation, as the sun has a lower altitude in winter.

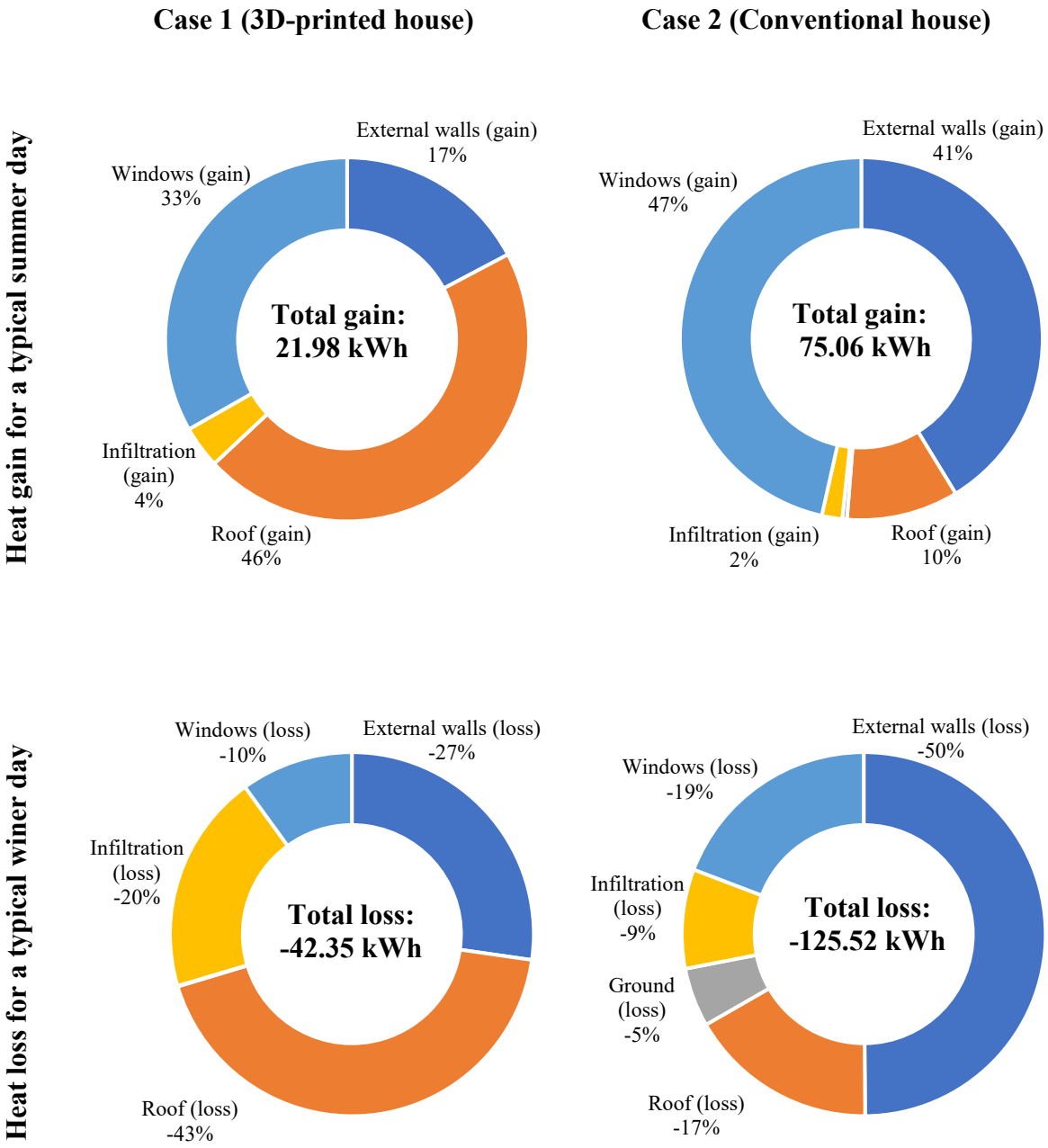


Figure 8-10 Breakdown of total external heat gain/loss by source for both case study buildings during a typical summer day and a typical winter day

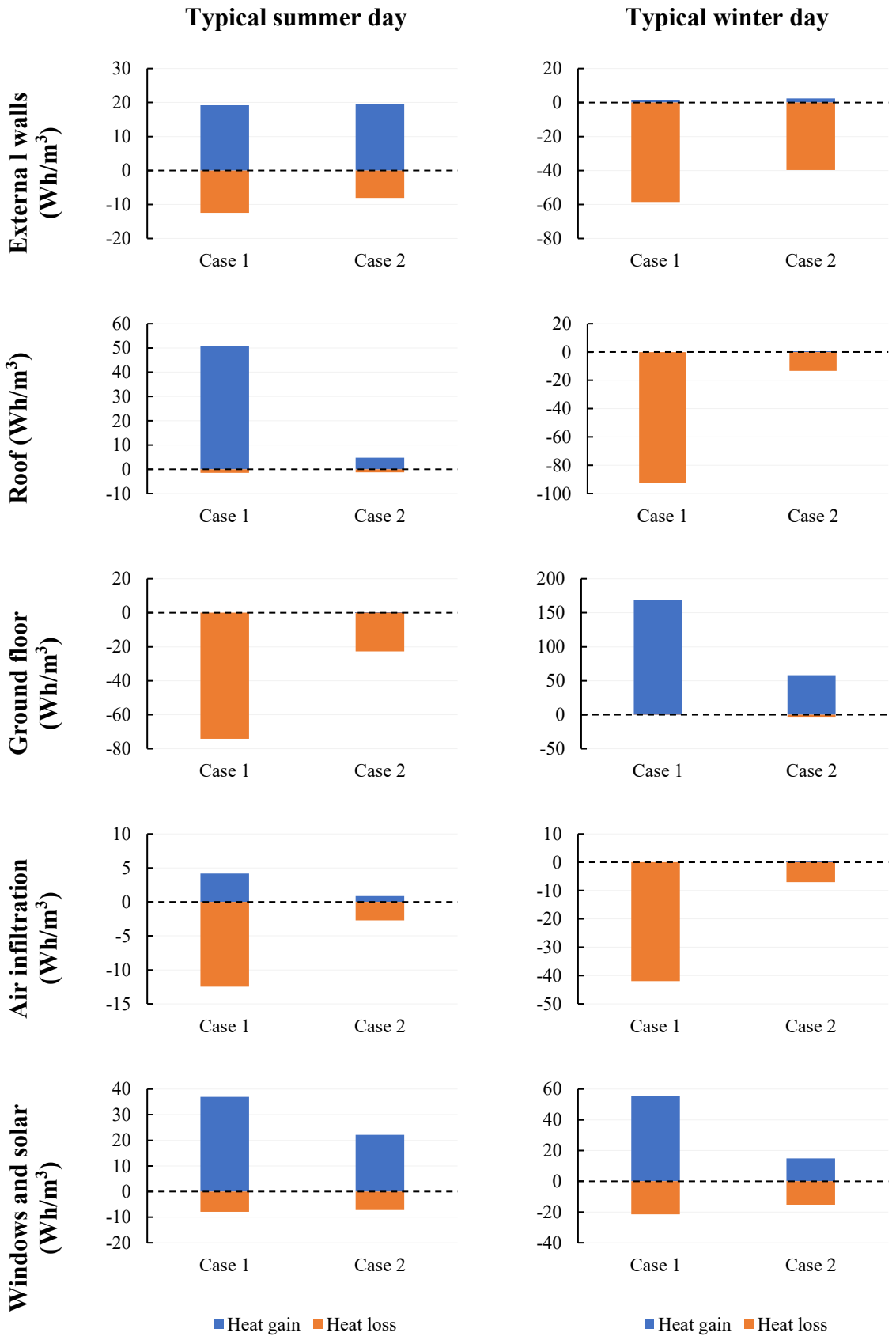


Figure 8-11 Heat gain/loss through the building envelope for selected case study buildings in Riyadh. Note that the results shown are in kWh per unit volume of each house.

Following the heat gain analysis, the inner surface temperatures of the external walls were analysed for both houses to provide deeper insight into the thermal performance of the two distinct case study buildings investigated in this thesis. For the purpose of this analysis, the results are presented for the selected rooms in summer and winter. The simulation results for Case 1 and Case 2 are presented in Figures 8-12 and 8-13, respectively.

The results indicate that the existing thermal insulation significantly reduced heat transfer through the external walls on both summer and winter days. This led to more stable inner surface temperatures, particularly in the summer, thereby contributing to consistent indoor temperatures and a potentially lower cooling load. These findings align with the field observations discussed in Chapter 6. Moreover, a high correlation between Tas and the inner surface temperatures of the external walls (IST) was observed in all rooms during both seasons (see Appendix B-C).

In Case 1, IST increased by approximately 0.7 °C on both east and south walls and by up to 1 °C on the west wall on a typical summer day. In winter, the IST increase was about 1.5 °C on the south wall, 1.2 °C on the east wall, and 0.9 °C on the west wall. Overall, IST fluctuations in Case 1 were minimal, despite variations in room orientation, indicating effective thermal performance and stable indoor conditions.

By removing the existing insulation, IST would increase by at least 1.8 °C on the south wall and by up to 2.2 °C on the east wall in the summer. In winter, these figures would be higher, reaching 3.4 °C on the south wall due to the low solar altitude.

In Case 2, higher IST fluctuations were observed compared to Case 1. On a typical summer day, IST increased by up to 2 °C in R1 (southwest wall), while in R2 it increased by approximately 2.4 °C on the northeast wall and approximately 2.6 °C on both southeast and southwest walls. In winter, R1 experienced a 1.6 °C increase in IST on the southwest wall, while R2 showed increases of 2.6 °C on the northeast wall and 3.6 °C on both southeast and southwest walls.

By removing the existing insulation, IST in R1 would increase by up to 3.9 °C and 3.2 °C in summer and winter, respectively, while in R2 the increase in IST would range between 4.6 °C and 5.4 °C in the summer and between 5.5 °C and 7.5 °C in the winter.

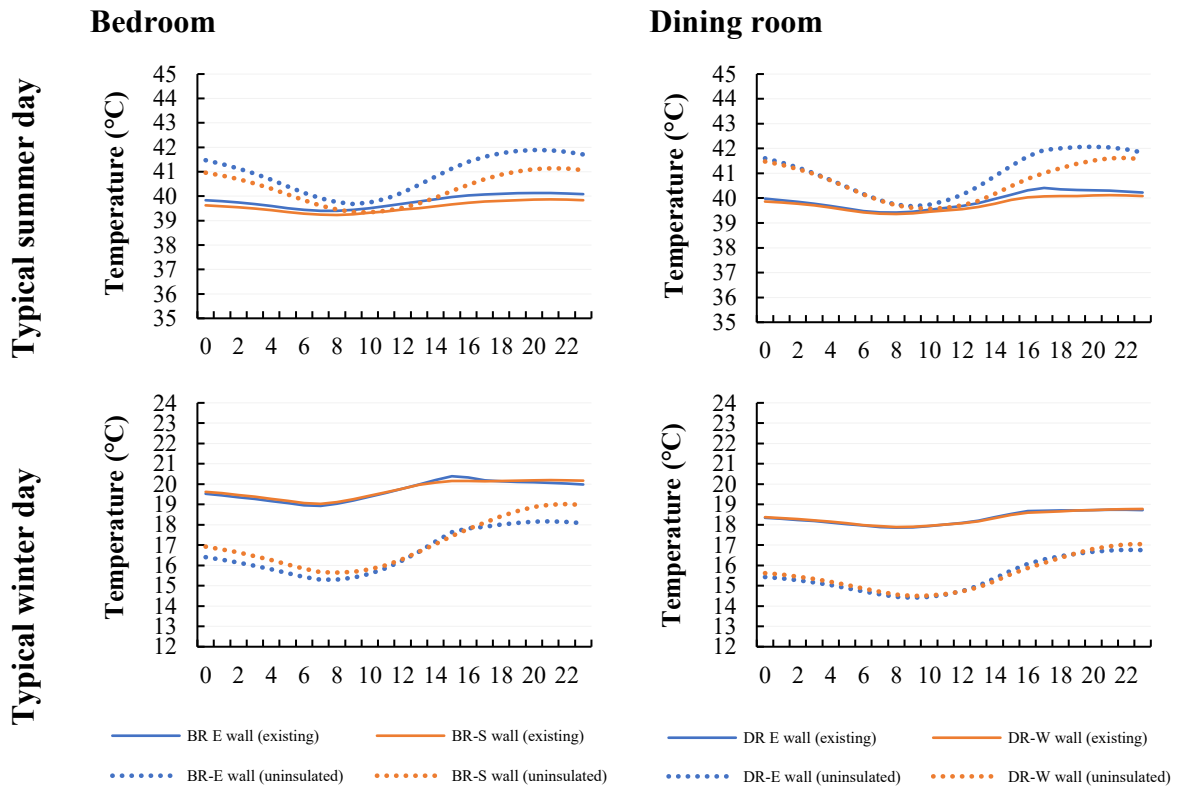


Figure 8-12 Predicted inner surface temperatures of external walls for the selected rooms in Case 1

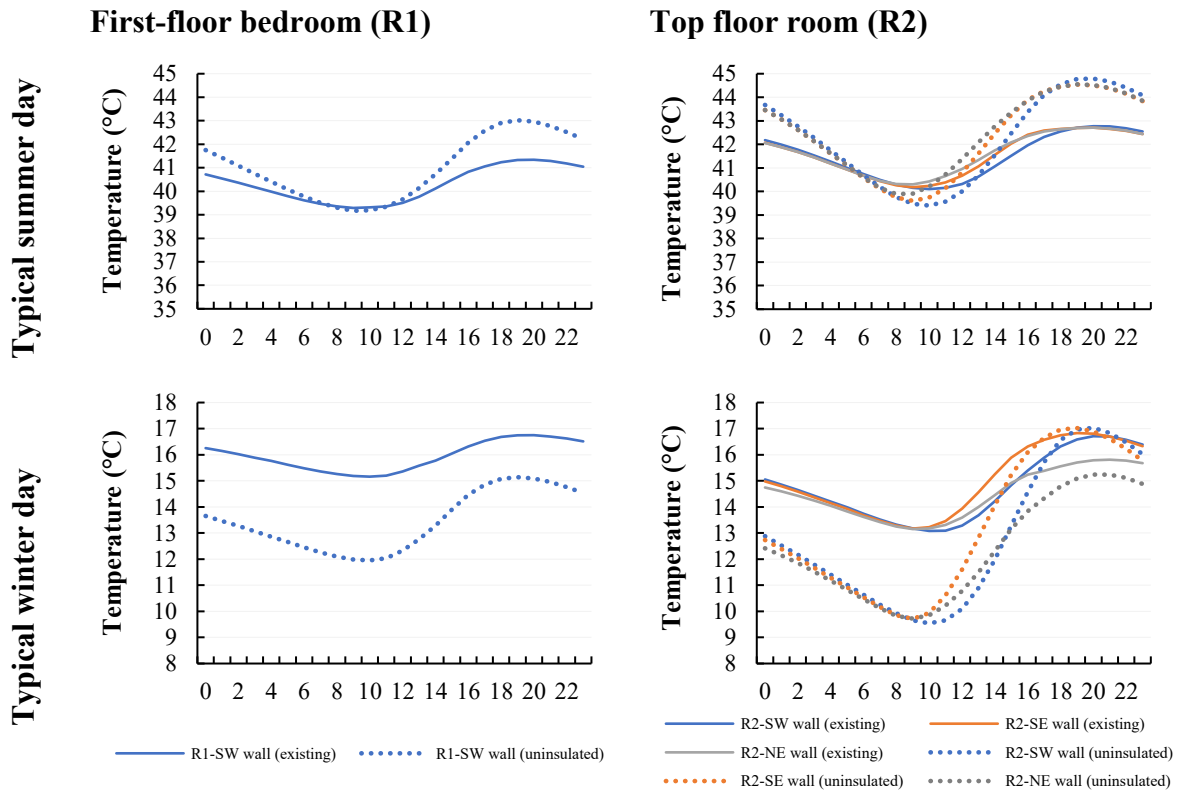


Figure 8-13 Predicted inner surface temperatures of the external walls for selected rooms in Case 2

Note the large fluctuation in IST for the uninsulated models.

These findings demonstrate the effectiveness of the existing insulation in moderating inner surface temperature fluctuations and consequently reducing cooling demand. Following this analysis, cooling load was estimated for both houses under their existing conditions.

8.4 Cooling load

In this study, sensible cooling load calculations were carried out to provide a database for investigating and optimizing the intended measures to promote the energy efficiency of residential buildings constructed with 3D printing technology and conventional methods. To do so, IES-VE requires a setpoint temperature to predict the total cooling demand for each house.

The SBC states that all heated zones in residential buildings must maintain a fixed setpoint temperature of no less than 20 °C. The Code does not provide any recommendations for cooling setpoint temperature, resulting in a clear conflict in the literature. For example, Alosaimi (2023) interpreted the SBC's heating setpoint requirement as a fixed thermostat setpoint temperature across the year. Other scholars, such as Ahmad (2004), Al-Qahtani and Elgizawi (2020), Al-Saadi and Al-Jabri (2017), Al-Saadi and Budaiwi (2007), Alaidroos and Krarti (2015), Almushaikah and Almasri (2020), and Alrashed and Asif (2015a), applied higher cooling setpoint temperatures in Saudi Arabia or in regions with climate conditions similar to those investigated in this thesis, which aligns with SEEC recommendations (i.e. no less than 24 °C).

In this research, various cooling setpoint temperatures (20 °C, 22 °C, 24 °C, 26 °C, and 28 °C) were assigned to the baseline model primarily to quantify the savings achieved in cooling load (see Figure 8-14). The results indicated that raising the cooling setpoint from 20 °C to 24 °C reduced the total annual cooling loads from 33.4 MWh (428.5 kWh/m^2) to 22.2 MWh (285.7 kWh/m^2) in Case 1, and from 115 MWh (259.6 kWh/m^2) to 77 MWh (174 kWh/m^2) in Case 2, achieving about 33% savings for both houses. This adjustment also contributed to a reduction in peak monthly loads (in August) by about 21%—from 4.9 MWh (62.8 kWh/m^2) to 3.8 MWh (49.3 kWh/m^2) in Case 1, and from 17.4 MWh (39.4 kWh/m^2) to 13.7 MWh (30.9 kWh/m^2) in Case 2.

Further increases in the cooling setpoint to 26 °C and 28 °C resulted in total annual savings of 46% and 58%, respectively, compared with a 20 °C setpoint. Accordingly, the annual cooling loads dropped to 17.7 MWh and 13.9 MWh (227.9 kWh/m^2 and 178.2 kWh/m^2) in Case 1, and to 61.9 MWh and 48.6 MWh (139.7 kWh/m^2 and 109.7 kWh/m^2) in Case 2. Peak-month

(August) loads at these setpoints (26 °C and 28 °C) were reduced by approximately 32% and 43%, respectively, dropping to 3.3 MWh and 2.7 MWh (42.6 kWh/m^2 and 35.8 kWh/m^2) for Case 1, and 11.8 MWh and 9.9 MWh (26.7 kWh/m^2 and 22.5 kWh/m^2) for Case 2.

From the above analysis, it can be concluded that, given the consistently high indoor temperatures in residential buildings in Saudi Arabia for most of the year (see Figure 8-1), raising the cooling setpoint reduces overall energy demand. For the purpose of this thesis, the cooling was set at a constant temperature of 26 °C for further analysis. The predicted current annual cooling loads of 17.7 MWh (227.9 kWh/m^2) for Case 1 and 61.9 MWh (139.7 kWh/m^2) for Case 2 will be compared in the following chapter after applying the proposed combination of building fabric alternatives (see Section 9.7).

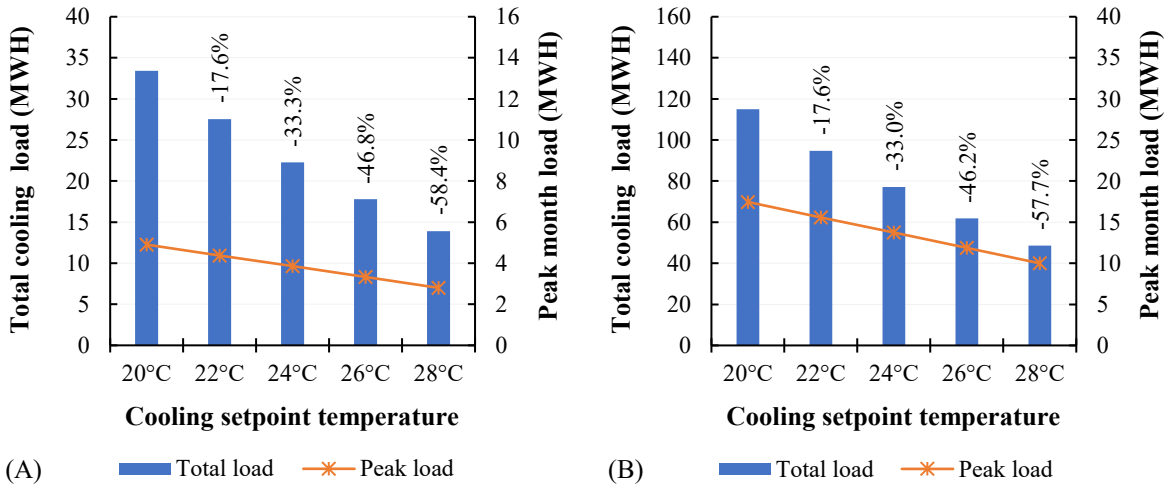


Figure 8-14 Predictions of total cooling load with various setpoint temperatures: (A) Simulation results for Case Study 1; (B) Simulation results for Case Study 2

By assigning the models' cooling setpoint temperature, it was possible to predict cooling and heating demand for both buildings during the year (see Figure 8-15). The blue and red areas represent cooling and heat hours, respectively, while the green area indicates hours of comfortable conditions (i.e. no cooling or heating requirements). The 3D-printed house achieved higher percentages of acceptable indoor thermal conditions without cooling or heating systems (nearly 30% of the time) compared to only 11.5% of the time in the conventional house. This can be attributed to the exposure of the building fabric to direct sunlight, thus reducing heating system requirements and increasing comfort hours in the winter.

As expected, cooling hours were dominant due to high temperatures throughout most of the year, accounting for slightly more than 67% of the time in both houses. Cooling requirements may be influenced by various factors affecting indoor temperatures, which will be

investigated in the next chapter to improve the thermal performance of the selected case studies.

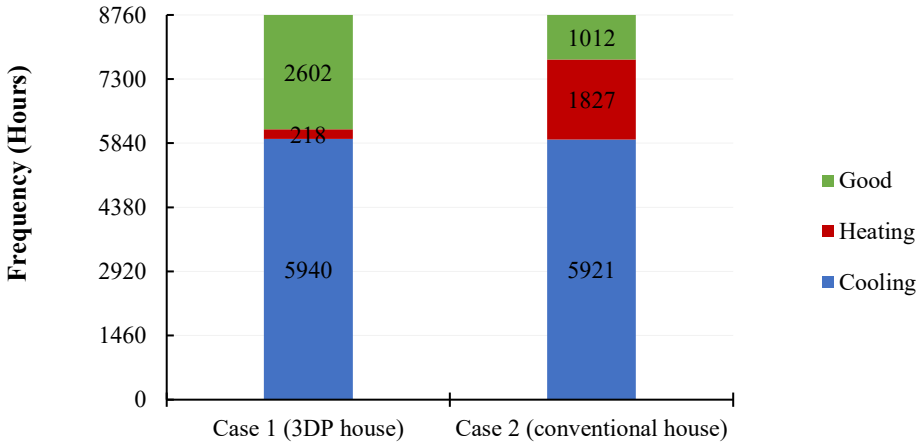


Figure 8-15 Predicted cooling and heating load hours for both case study buildings in Riyadh

The graphs in Figure 8-16 illustrate the monthly cooling load breakdown for both case study buildings. Sensible cooling load refers to the heat energy that needs to be removed to maintain the desired indoor temperature. It is noteworthy that the following analysis was conducted based on internal gain and the daily operational profiles discussed in Chapter 5. As can be seen, external heat gain sources dominated the cooling load, accounting for 76% and 71% of the total loads predicted for Case 1 and Case 2, respectively.

In Case 1, the ground floor contributed most to cooling load, accounting for 8,827 kWh/year (41%), whereas the external walls, windows, and roofs were respectively responsible for 6%, 13%, and 14% of the total cooling load. Similarly, in Case 2, the ground floor contributed significantly to the cooling load, accounting for 28,503 kWh/year (38%), whereas the external walls, windows, and roofs were responsible for 14%, 13%, and 6% of the total cooling load, respectively.

It was noted that the existing thermal insulation in the external walls and roof minimized heat transfer through these components of the building envelope. In contrast, the ground floor exhibited significantly higher heat gains due to the absence of insulation, allowing thermal exchange between the conditioned indoor environment and the ground. The ground floors in both case studies had significantly high U-values—3.2 W/m^2·K in Case 1 and 3.5 W/m^2·K in Case 2—compared to other components of the building envelope, as shown in the baseline construction materials (see Tables 7-3 and 7-4).

Internal heat sources (i.e. occupants, lighting fixtures, and household equipment) formed only 24% and 29% of the total cooling load in Case 1 and Case 2, respectively.

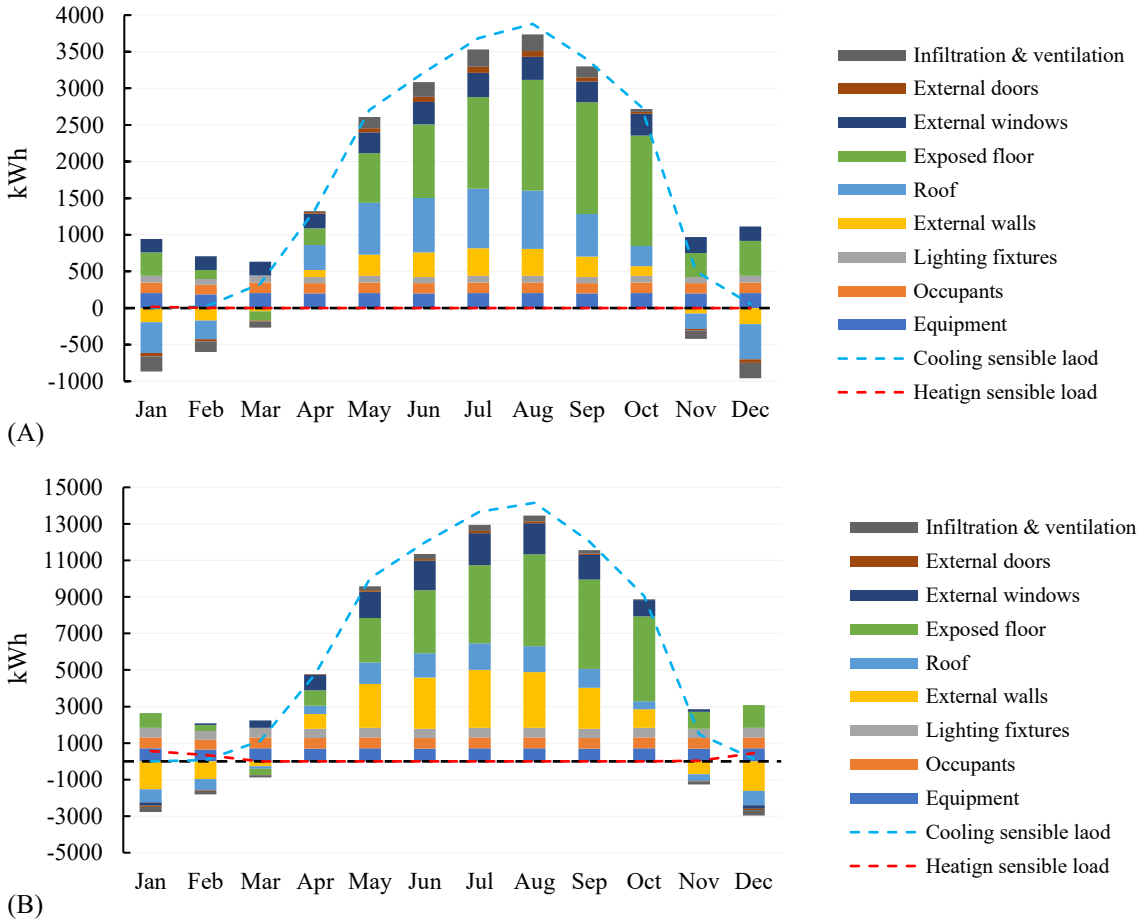


Figure 8-16 Monthly cooling load analysis by element (in kWh): (A) Simulation results for Case 1; (B) Simulation results for Case 2

8.5 Baseline energy consumption and CO_2 emissions

The results of the IES-VE simulation of the baseline models predicted annual energy demands of 14.96 MWh for Case 1 and 54.77 MWh for Case 2. This resulted in a respective energy usage intensity (EUI) of 191.82 kWh/m^2 for Case 1 and 123.63 kWh/m^2 for Case 2. Consumption per square meter for Case 1 was approximately 35% higher than for Case 2. This could be attributed to many factors, including lower external heat gain through the building fabric in Case 2 (as discussed earlier in Section 8.3), which resulted in better energy efficiency compared to Case 1. Moreover, despite the large floor area of Case 2, Case 1 had a higher form-to-floor area ratio and thus the higher energy consumption rate per square meter. This aligns with the findings of a study conducted in similar climate conditions by Shehata and Waheeb (2018), who indicated that compact buildings with smaller form-to-floor area ratios are more efficient in arid climates.

The graphs in Figures 8-18a and 8-19a detail electricity consumption for Case 1 and Case 2, respectively, and correlate the monthly energy demand of each house with the mean temperature of Riyadh. It is evident from the graphs that energy consumption in Riyadh is highly influenced by its seasonal temperature profile. Consumption rates rise according to the cooling requirements inside the houses, particularly during the summer season. According to the results, electricity consumption peaks in August at about 2,157 kWh for Case 1 and 7,868 kWh for Case 2, with respective cooling energy requirements of 1,702 kWh and 6,235 kWh.

This behaviour aligns with the monthly consumption (simulated and actual) of residential buildings reported in previous studies, particularly in the Riyadh Region (Albogami & Boukhanouf, 2019; Aldossary et al., 2014; Almushaikah & Almasri, 2020; Alosaimi, 2023; Alyami & Omer, 2021; Krarti et al., 2020). A high correlation was found between the predicted energy consumptions of both houses in this thesis and that reported in the relevant literature, with R^2 values generally above 0.95 (see Appendix B-D). Figure 8-17 shows a comparison between the predicted EUI results with the relevant literature and indicates that the baseline consumptions in the current research are reasonably close to the average consumptions per unit area of residential buildings (villas) in Riyadh, which ranged between 110 kWh/m^2 and about 240 kWh/m^2.

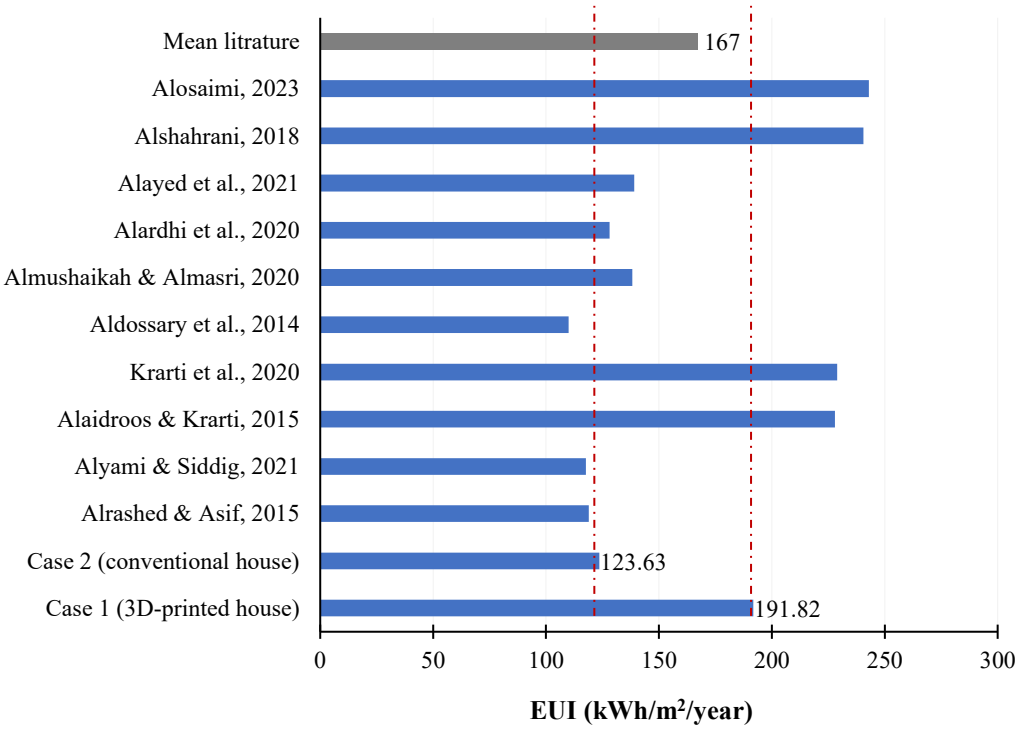
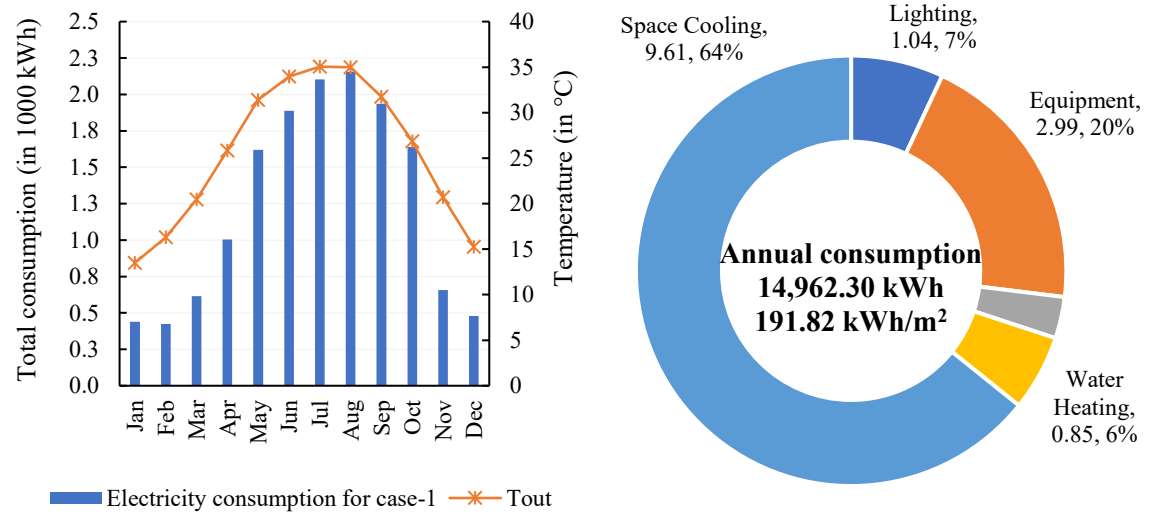


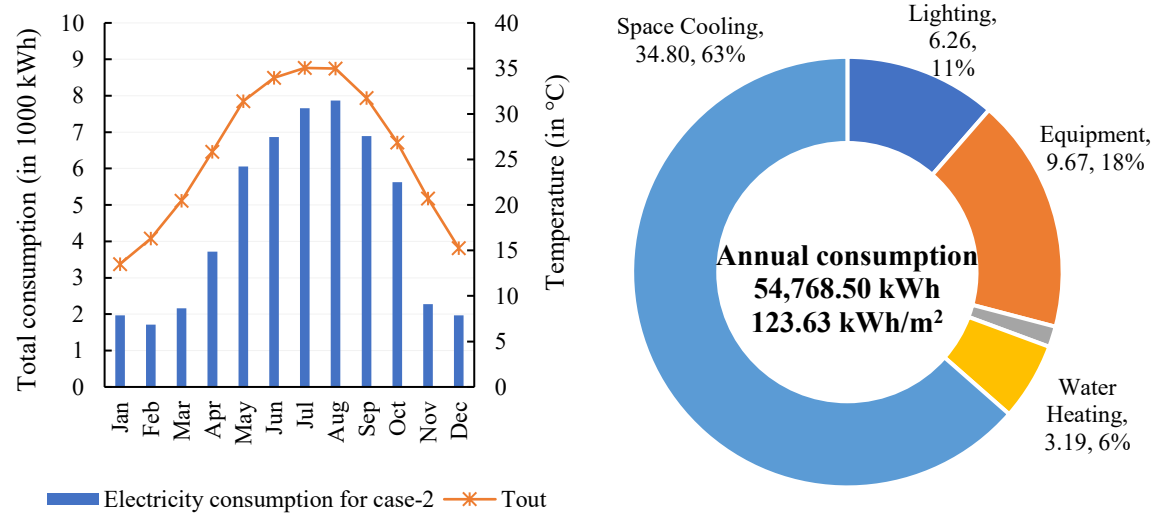
Figure 8-17 Energy consumption per unit area for residential buildings in Riyadh, KSA.

As shown in the graphs in Figures 8-18b and 8-19b, a significant share of the total energy consumption in both houses was due to cooling requirements. The total annual energy requirement for space cooling was 9,611 kWh (equivalent to 123 kWh/m^2) in Case 1 and 34,796 kWh (equivalent to 78 kWh/m^2) in Case 2, constituting more than 60% of the total energy consumption in both houses. This was followed by domestic appliances at 20% in Case 1 and 18% in Case 2, while lighting consumption was around 7% and 11%, respectively. Energy requirements for space heating, however, made up only a small portion of the annual consumption, which was expected owing to the local climate conditions of Riyadh.



(A) (B)

Figure 8-18 Baseline energy consumption predictions for Case 1: (A) Monthly energy consumption in relation to outdoor temperature; (B) Distribution of annual energy consumption (in MWh).



(A) (B)

Figure 8-19 Baseline energy consumption predictions for Case 2: (A) Monthly energy consumption in relation to outdoor temperature; (B) Distribution of annual energy consumption (in MWh).

IES-VE was also used to predict CO_2 emissions for each building based on the type and amount of fuel used for power generation at the building level. Calculating the CO_2 emissions requires the CO_2 emission factor, which is the factor of CO_2 emissions for each kWh of electricity. A default value of 0.519 $kgCO_2$/kWh was estimated by IES-VE based on the specified location in APlocate (i.e. Riyadh, Saudi Arabia). However, based on recent data analysis, the emission factor of 0.614 $kgCO_2$/kWh (Climate Transparency, 2022) was adopted in this study and applied to both IES models.

The simulation results of the CO_2 emissions for the baseline models are illustrated in Figure 8-20. Monthly CO_2 emissions for both houses varied across the year according to the cooling requirement. The graphs demonstrate a clear correlation between CO_2 emissions and AC use.

The total annual CO_2 emissions for Case 1 were approximately 9,187 $kgCO_2$/year, with monthly emissions ranging from 261 $kgCO_2$ to 1,324 $kgCO_2$. This translates into annual emissions of 117.78 $kgCO_2/m^2$ and 4,593 $kgCO_2$/capita. In Case 2, the total annual CO_2 emissions were about 33,628 $kgCO_2$/year, with monthly carbon emissions ranging between 1,052 $kgCO_2$ and 4,831 $kgCO_2$. This translates into annual emissions of about 75.91 $kgCO_2/m^2$ and, 4,203 $kgCO_2$/capita. While CO_2 emissions per square meter for Case 1 were found to be significantly higher than those calculated for Case 2, the per capita emissions were nearly similar.

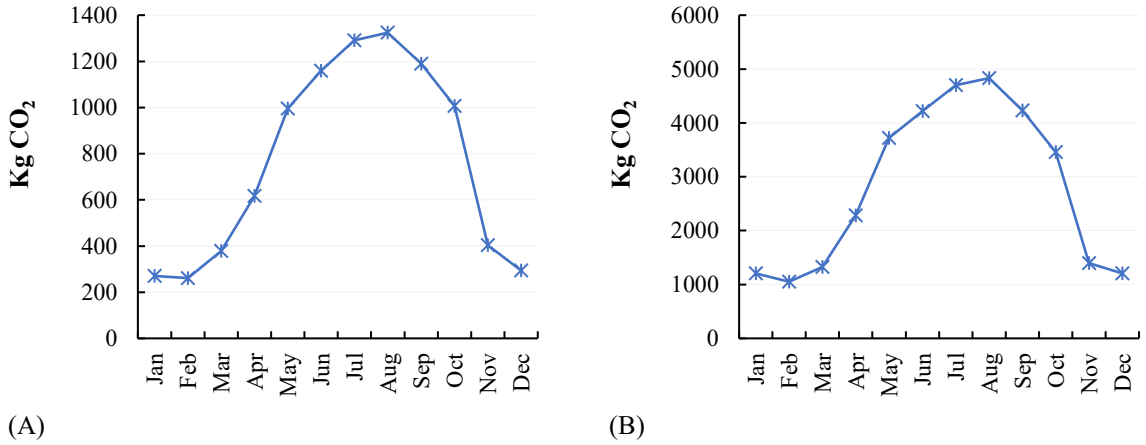


Figure 8-20 Monthly predictions of CO_2 emissions for selected case study buildings in Riyadh: (A) Simulation results for Case 1; (B) Simulation results for Case 2.

It must be noted, however, that these figures were found to be significantly lower than the country's emissions per capita, as discussed in Chapter 2. This is due to the involvement of the different applications and industries, such as transportation, industrial, commercial, governmental, and so on, that contribute to the country's total CO_2 emissions.

As active cooling system requirements contributed the most to total energy consumption, and thus operational carbon emissions, in both houses in Riyadh, this thesis was oriented to improve the thermal performance of both buildings. The impact of various cooling strategies learned from vernacular architecture and modern sustainable building technology will be assessed. Given the significant contribution of external heat gain to total and peak cooling demand, as discussed earlier in this chapter, this thesis focuses on evaluating the effect of building fabric improvements on enhancing indoor thermal environments and consequently improving the overall efficiency of the building.

8.6 Summary

This chapter analysed the indoor thermal environments and energy performance of the two distinct case study buildings in Riyadh using IES-VE energy modelling software. It also investigated the role of building envelope components on the thermal performance of both buildings.

It was found that the existing thermal insulation resulted in a consistent indoor temperature for both seasons by mitigating heat flow through the building fabric components. The simulation results for a summer day indicate that the tested rooms in both houses showed an improved indoor thermal environment when nighttime ventilation was implemented, contributing to a reduction in peak temperatures by up to 0.6 °C in Case 1 and 1.3 °C in Case 2. This reduction in peak temperatures was due to the cooling effect of NTV, which facilitated heat dissipation from the inner mass and thus reduced indoor temperatures. This process allowed the inner mass to absorb more heat the following day without raising indoor temperatures.

Heat gain/loss analysis indicated the significant effects of various components of the building fabric on the thermal performance of the building. A comparison between both buildings revealed that Case 2 had lower heat gain/loss rates per unit volume compared to Case 1, making it more efficient. Simulation results revealed that space cooling was the greatest contributor to total energy demand and CO_2 emissions. The load breakdown for both houses showed that the roof, ground floors, and external walls were among the greatest contributors to heat gain through the building fabric elements, and thus the cooling load. These elements can be potential areas for improvement, which is further explored in the following chapter.

It should be noted that the analysis presented in this chapter is subject to several limitations and sources of uncertainty. These include the use of a historical weather file that may not

fully represent recent climatic warming, uncertainties in infiltration rates and ground temperature inputs, and the adoption of older occupancy and plug-load schedules from previous studies. Although these inputs reflect the best available and validated data in the literature, they inevitably introduce a level of uncertainty into the simulation results.

CHAPTER 9

PARAMETRIC STUDY AND OPTIMIZATION USING ENERGY SIMULATION SOFTWARE

- Introduction
- Simulation results of various improvement strategies
- Proposed combination of the building fabric alternatives
- Final results
- Comparison between improved models and baseline models

Chapter 9: PARAMETRIC STUDY AND OPTIMIZATION USING ENERGY SIMULATION SOFTWARE

9.1 Introduction

The baseline results presented in Section 8.5 indicated that cooling energy consumption accounted for a significant portion of the total energy demand in both houses and consequently their CO_2 emissions. Thus, there is a great potential to maximize energy savings and reduce CO_2 emissions by improving the thermal performance (i.e. minimizing cooling demand) of the selected buildings in Riyadh. This chapter presents the simulation results for both case study buildings after applying the proposed enhancement measures, which are briefly discussed in Section 5.9.

In this study, the energy simulation software IES-VE was utilized to achieve the aim of this research. The simulations were conducted for a whole year for the two houses in Riyadh, Saudi Arabia. As discussed in Section 5.6, the simulations were performed using a Typical Meteorological Year (TMY) weather file for Riyadh, constructed from long-term climate data (2007–2021) recorded at King Khalid International Airport, in EPW format obtained from Climate.OneBuilding.org.

To ensure the reliability of the simulation outputs and provide accurate predictions that can reflect the actual impact on the model in the optimization phase, the study was carried out using the validated energy models, as discussed in Chapter 7. It is worth noting that all input data, assumptions, and simulation settings were kept the same for this analysis.

The proposed design variables of the building fabrics were applied for each house separately, and the potential improvements to indoor thermal performance throughout the year were investigated by altering one variable at a time. The impact of natural ventilation was also investigated in this study.

In the previous chapter, the simulation results of DTV and NTV demonstrated improved indoor thermal performance as a result of allowing nighttime ventilation. Building upon the findings presented in Chapter 8, further simulations were conducted (described in this chapter) to explore potential improvement in indoor thermal performance by allowing natural ventilation when desired (i.e. as a desired passive cooling technique) to ensure indoor thermal comfort while avoiding undesired heat gain or heat loss.

In this regard, an operational window control schedule was developed in IES-VE allowing 'openable windows' to open when the outdoor conditions were favourable and below indoor temperatures (see Figure 5-19 in Section 5.9).

The results were presented and discussed for selected rooms for a typical summer day and a winter day for demonstration purposes. As part of this study, cooling load was estimated after applying the suggested improvements, separately, to evaluate their effectiveness in improving the overall thermal performance of the buildings and to determine the best-performing cases of the building envelope components.

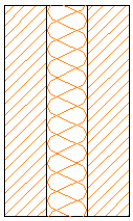
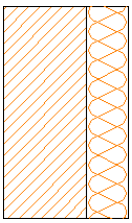
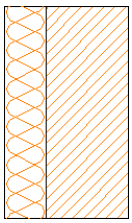
Following this step, the best cases were simulated, and their combined influences were presented. Later in this chapter, the total annual energy consumption and CO_2 emissions were estimated for the improved model of each house and subsequently compared with the baseline models. The simulation results are discussed in subsequent sections.

9.2 External walls

This section aims to investigate the impact of varying the thermal characteristics of the external walls on the indoor thermal environment. The SBC requires the application of thermal insulation to meet the maximum acceptable U-value for external walls (0.34 $W/m^2 \cdot K$) without specifying or providing recommendations for its location. The impact on the indoor thermal environment of varying the amount of thermal insulation and changing its location was investigated in this study. The properties of the wall construction types for the 3D-printed house and the conventional house are illustrated in Table 9-1.

Air temperature results for the selected rooms are discussed to demonstrate the impact of the proposed external wall options on the thermal performance of the tested rooms. Following this step, the potential reductions in cooling load achieved with the selected wall options were calculated.

Table 9-1 Characteristics of the proposed external wall options for Case Study 1 and Case Study 2

Wall configuration	Insulation thickness	3D-printed house		Conventional house	
		Thickness	U-value	Thickness	U-value
	20 mm 40 mm 60 mm 80 mm 100 mm 120 mm	220 mm 240 mm	1.023 0.645	220 mm 240 mm	0.872 0.582
	20 mm 40 mm 60 mm 80 mm 100 mm 120 mm	260 mm 280 mm 300 mm	0.471 0.371 0.306	260 mm 280 mm 300 mm	0.436 0.349 0.291
	20 mm 40 mm 60 mm 80 mm 100 mm 120 mm	320 mm	0.260	320 mm	0.249

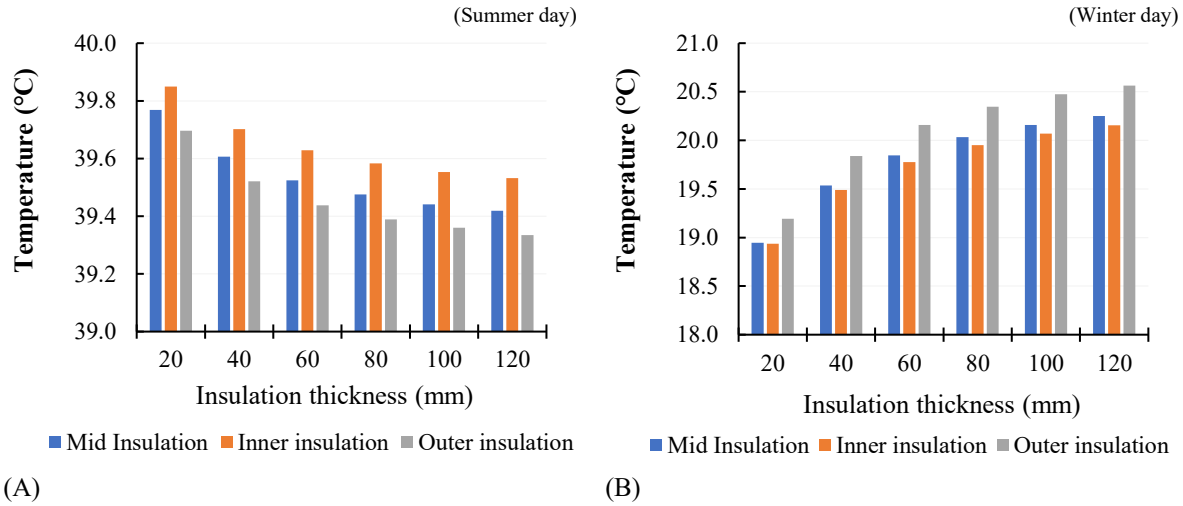
9.2.1 Air temperature

Figures 9-1 and 9-2 illustrate the indoor air temperature results for Case 1 and Case 2 after applying proposed wall cases for a typical summer day (12 August) and a typical winter day (31 January). The results indicate that increasing the insulation thickness directly impacted the indoor thermal environment. In general, it was observed that the effect of insulation on improving the indoor thermal environment was reduced as the thickness of the insulation increased. This is because increasing the thermal insulation beyond a certain point minimizes its impacts.

The simulation results revealed that the thermal performance of the houses worsened as a result of increasing the walls' U-value (i.e. reducing insulation thickness). It was observed that increasing insulation thickness led to a reduction in indoor temperatures in the summer, likely due to reducing heat gain through the external walls. In winter, this resulted in higher indoor temperatures by reducing heat loss.

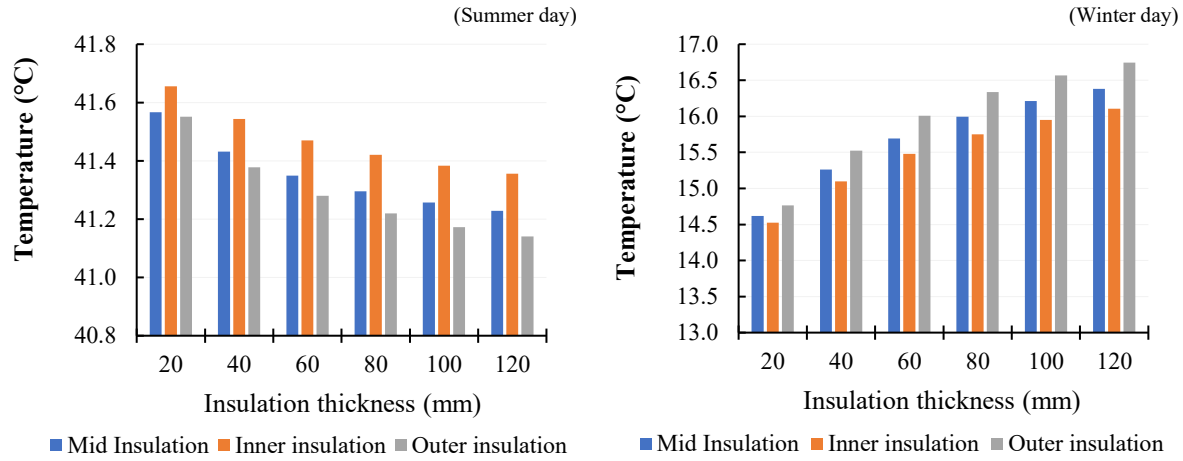
Nevertheless, the conducted thermal analysis revealed that reducing the U-value of the wall does not necessarily achieve better performance. For instance, by applying insulation to the external surface of the wall, a reduction in indoor temperatures of up to 0.45 °C for Case 1

and approximately 0.8 °C for Case 2 was observed during peak outdoor temperature periods compared with positioning the insulation on the inner surface of the wall—while maintaining the same U-value. This can be explained by the exposure of the indoor environment to the thermal mass, which helped regulate indoor temperatures (see Figures 9-3 and 9-4).



(A) (B)

Figure 9-1 Indoor temperature predictions for Case 1 with varying insulation thicknesses and locations: (A) Results for a typical summer day; (B) Results for a typical winter day



(A) (B)

Figure 9-2 Indoor temperature predictions for Case 2 with varying insulation thicknesses and locations: (A) Results for a typical summer day; (B) Simulation results for a typical winter day

To better understand the impact of the insulated thermal mass on indoor thermal behaviour, Figures 9-3 and 9-4 show hourly indoor temperature profiles for the selected rooms in each house with varying thermal insulation locations for a typical summer and a typical winter day. The results indicate that placing insulation material on the external surface of the walls resulted in a reduction in mean indoor temperature in the summer while increasing the temperature in the winter.

This behaviour is primarily caused by the thermal mass effect, which helped maintain stable indoor thermal conditions in both seasons. This finding agrees with Alayed, Bensaid,

O'Hegarty, and Kinnane (2022), Baker and Steemers (2000), Lechner (2014), and Saulles (2019), who indicated that one of the main benefits of thermal mass is that it reduces indoor temperature swings, thus maintaining a stable indoor temperature.

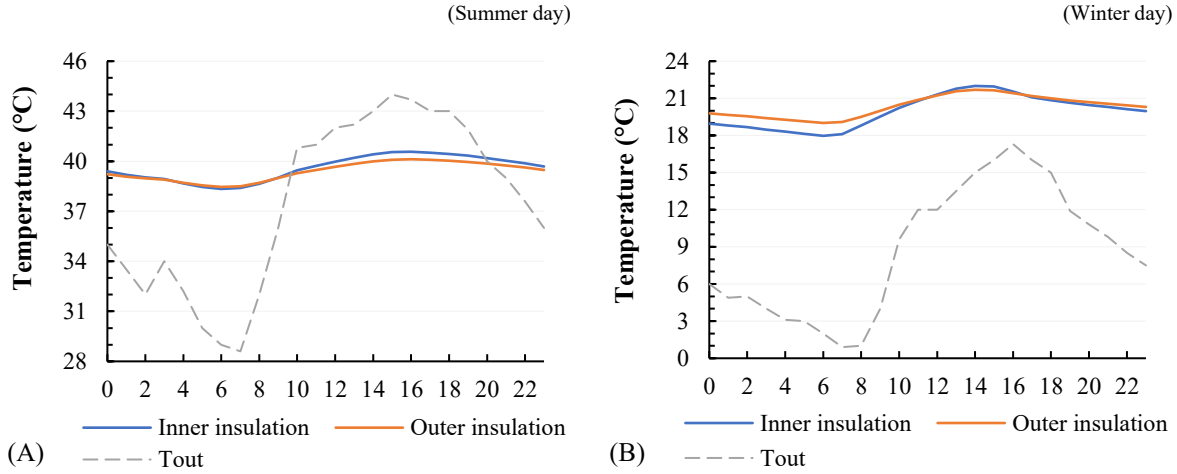


Figure 9-3 Hourly air temperature profile for Case 1 with different insulation locations: (A) Simulation results for a typical summer day; (B) Simulation results for a typical winter day

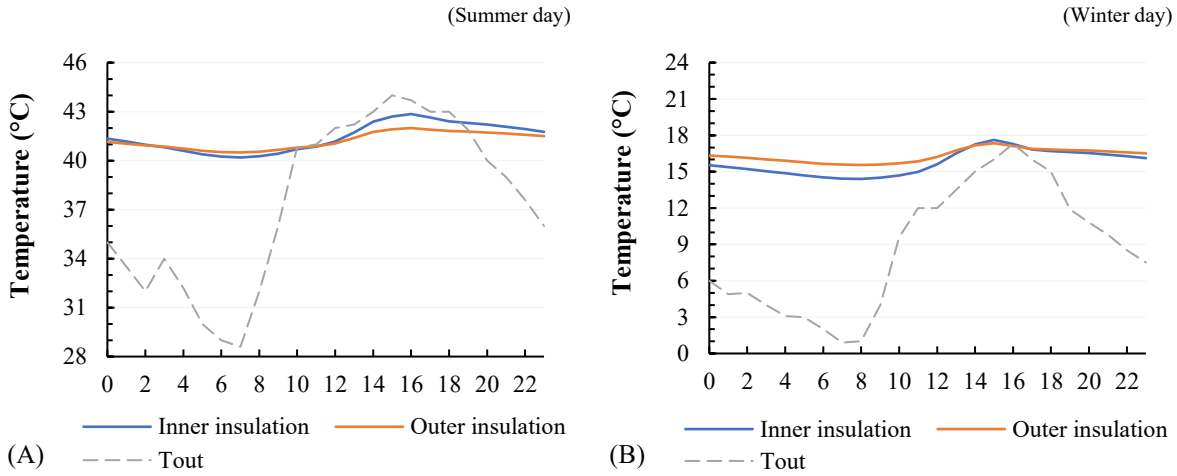


Figure 9-4 Hourly air temperature profile for Case 2 with different insulation locations: (A) Simulation results for a typical summer day; (B) Simulation results for a typical winter day

As discussed in Chapter 3, thermal mass can benefit from nighttime ventilation. Therefore, as part of this study, the impact of natural ventilation was tested and simulated with two wall options (i.e. inner and outer insulation) for both houses (see Figure 9-5). It should be noted that the U-value was the same for both wall options. For the purpose of this analysis, the results were reviewed for a typical summer day only.

When the proposed ventilation strategy was simulated, Ta remained lower in the heavyweight construction than in the lightweight option during the peak outdoor temperature period. Moreover, a reduction in indoor temperature at night was observed for all cases as a result of

nighttime ventilation, causing indoor temperatures to fluctuate in a manner similar to the outdoor temperatures during this period.

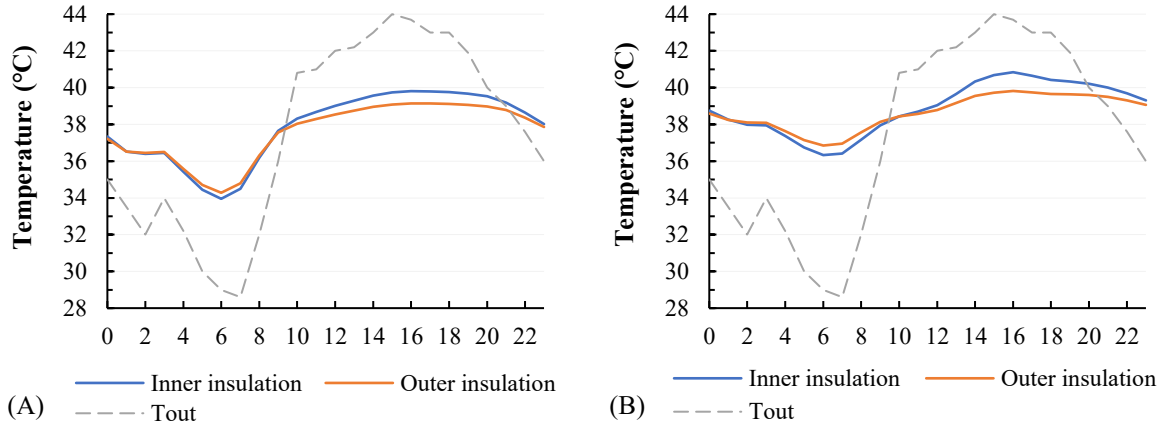


Figure 9-5 Hourly indoor air temperature predictions for selected rooms after applying proposed natural ventilation on a typical summer day: (A) Simulation results for Case 1; (B) Simulation results for Case 2. Note the reduction in indoor temperatures during peak outdoor temperature periods for the external insulation option.

The analysis indicates that the proposed ventilation technique facilitates heat dissipation from the building's thermal mass at night (when the outdoor temperature drops below indoor temperatures), thus acting as a heat sink for the following day. Consequently, this process helps maintain lower indoor temperatures during peak outdoor temperature periods, thus reducing cooling requirements.

Further to the above analysis, an evaluation of the frequency of Ta results relative to Tc throughout the year (see Figures 9-6 and 9-7) revealed that placing insulation on the internal layer of the walls (i.e. exposing the indoor environment to a lightweight mass) performed worse in both houses. This was particularly evident when the proposed natural ventilation strategy was applied, as the percentage of overheating hours was about 51.8 % in Case 1 and 51.5% in Case 2, with external insulation, compared to 52.4% and 52.0%, respectively, with inner insulation.

As a result, the percentage of time when the indoor air temperature fell within the comfort range (22 °C and 28.6 °C) was nearly 43% in Case 1 and 28.6% in Case 2. These figures were 1.4% and 0.4% higher than the internal insulation option for Case 1 and Case 2, respectively. In no ventilation mode, the effect of changing the location of the thermal insulation was minimal.

The analysis demonstrated that applying insulation to the external layer allowed the indoor environment to benefit from the thermal mass more profoundly when coupled with the

natural ventilation strategy. The following analysis involved investigating the effect of changing the location of the thermal insulation on cooling load.

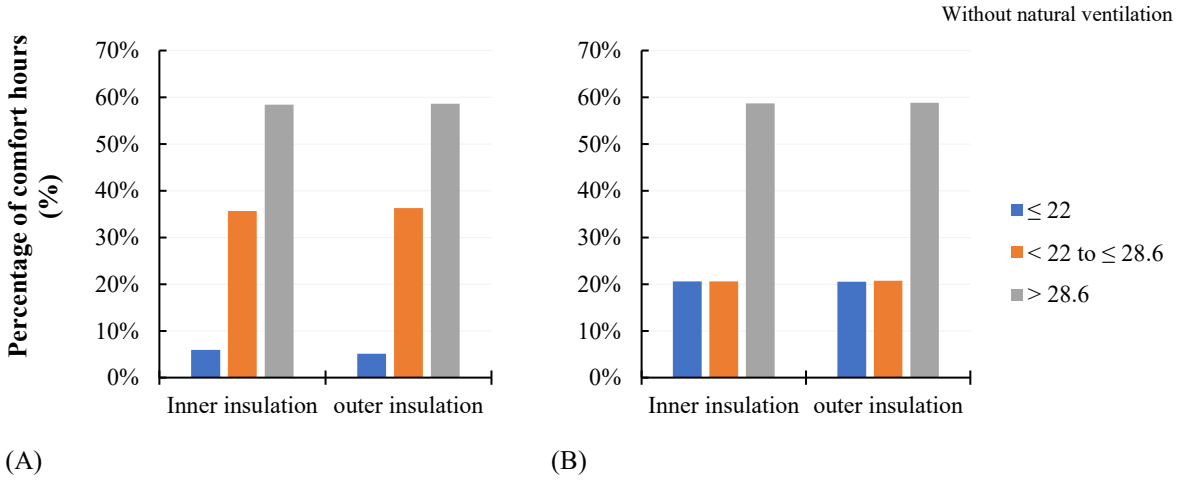


Figure 9-6 Indoor thermal comfort analysis with various thermal insulation locations while maintaining same U-value: (A) Case 1 (bedroom); (B) Case 2 (upper room)

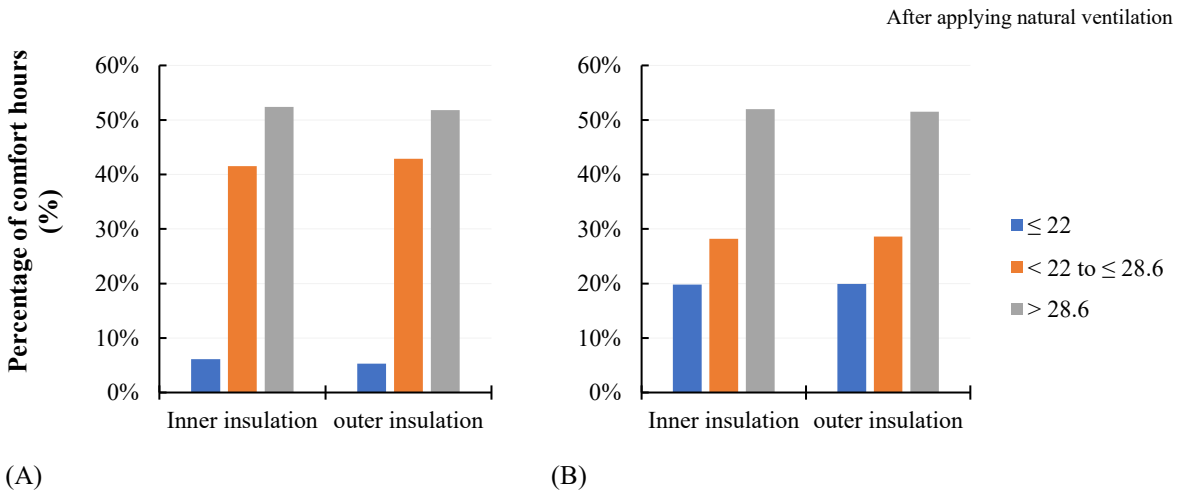


Figure 9-7 Indoor thermal comfort analysis with various thermal insulation locations while maintaining same U-value after applying NV: (A) Case 1 (bedroom); (B) Case 2 (upper room)

9.2.2 Cooling load

As part of this study, cooling load was estimated for the selected rooms with the insulation material in different locations of (i.e. inner versus outer insulation). See Figure 9-8. The purpose of this analysis was to identify the best external wall option with the lowest cooling load, which can in turn improve the energy efficiency of the selected case study buildings.

The results suggest that placing insulation material within the wall layers can impact total and peak cooling loads, thus affecting the thermal and energy performance of the houses. Applying 80 mm EPS insulation on the outside performed better for both the 3D-printed house and the conventional house compared to the inner insulation option. The difference in

cooling load between the outer and inner insulation options reached up to 0.43% for Case 1 (bedroom) and 0.32% for Case 2 (Room 2).

According to the results, the proposed outside insulation reduced the rooms' total cooling load to 5,225 kWh in Case 1 and 2,309 kWh in Case 2, thus achieving 2.3% and 23.7% savings, respectively, compared to the baseline model of each house. See Appendix C-A for more information.

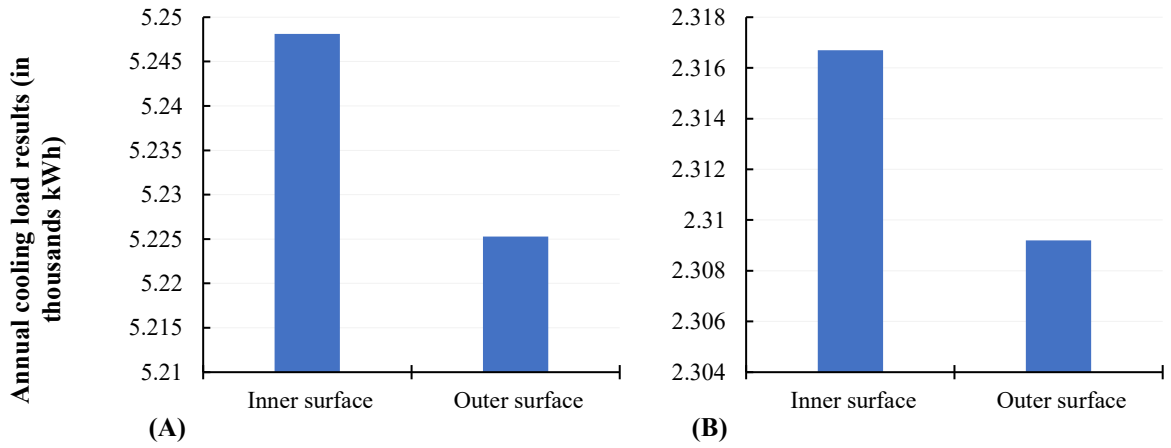


Figure 9-8 Total annual cooling load predictions for selected rooms with various insulation locations: (A) Case 1 (bedroom); (B) Case 2 (upper room)

These results are in agreement with what is commonly reported in the literature, such as Al-Sanea et al. (2012), who indicated a reduction in daily summer thermal transmission by up to 0.35% for an externally insulated concrete masonry wall in Riyadh compared with an inside insulation wall while maintaining the same U-value under stable conditions. The potential for internal thermal mass to reduce cooling load has also been demonstrated in the work of Lasker (2016), Albayyaa, Hagare, and Saha (2019), and Ghoreishi (2019).

However, the findings clearly contradict Alayed et al. (2022), who concluded that internal mass can increase energy demand, particularly during both summer and winter months in Riyadh. This conflict can be attributed to the operational profile of the cooling system as the discussed analysis in this thesis was conducted under steady-state conditions (i.e. continuous operation of AC system). However, the aforementioned study concluded that the effect of internal thermal mass on stabilizing indoor temperatures around the setpoint temperatures offset cooling and heating requirements in moderate months.

9.2.3 Conclusion

From the discussed results in this section, it was revealed that the proposed wall options with external insulation performed better for both case study buildings. This was distinguished by

reducing the rooms' summer mean indoor temperature and cooling load, thus improving both the indoor thermal environment and energy efficiency. The results did not conflict with winter thermal requirements as an increase in indoor temperatures was observed in both rooms. Therefore, these wall types were selected to construct the improved model of each house for the further analysis later in this chapter.

9.3 Roof

In this section, various roof options, including thermal insulation and high solar reflectance, were explored for the selected case study buildings. As discussed in Chapter 2, the SBC requires a U-value of no greater than 0.20 W/m^2·K for residential buildings located in Climate Zone 1 (such as Riyadh). The performance of the proposed roof options was investigated using the IES-VE simulation tool. The simulation results for the bedroom in Case 1 and the upper room in Case 2 (R2) are presented and discussed here for demonstration purposes. The characteristics of the proposed roof options for Case 1 and Case 2 are shown in Table 9-2.

The analysis began with an evaluation of the impact of applying various thicknesses of roof insulation on the indoor thermal environment. Ten different thicknesses of EPS thermal insulation were applied to the baseline models to allow for indoor air temperature evaluation. For each run, the insulation material was increased by 20 mm. Following this step, the possibility of achieving further improvement was investigated, and potential reductions in indoor temperature and cooling load are provided and discussed for both buildings with selected roof options.

9.3.1 Air temperature

Figures 9-9 and 9-10 show the indoor air temperature results for Case 1 and Case 2 after applying various thicknesses of roof insulation for a typical summer day and a typical winter day. The results suggest that increasing roof insulation thickness has a direct positive impact on the thermal performance of the houses and, consequently, their energy efficiency. The improvement in indoor thermal performance was distinguished by a reduction in mean indoor temperature in summer.

In winter, the mean indoor temperatures tended to increase in both houses as insulation thickness increased. This was due to improving the roofs' resistance to heat flow, thereby reducing heat gain and loss through the roof components.

However, increasing insulation thickness beyond that specified by the SBC did not significantly improve the thermal performance of the houses. This is due to the law of diminishing returns, which suggests that the benefit of insulation decreases as its thickness increases. This can also be observed in the work of Abuhussain (2020), Alaboud (2021), Alosaimi (2023), and Glew et al. (2021).

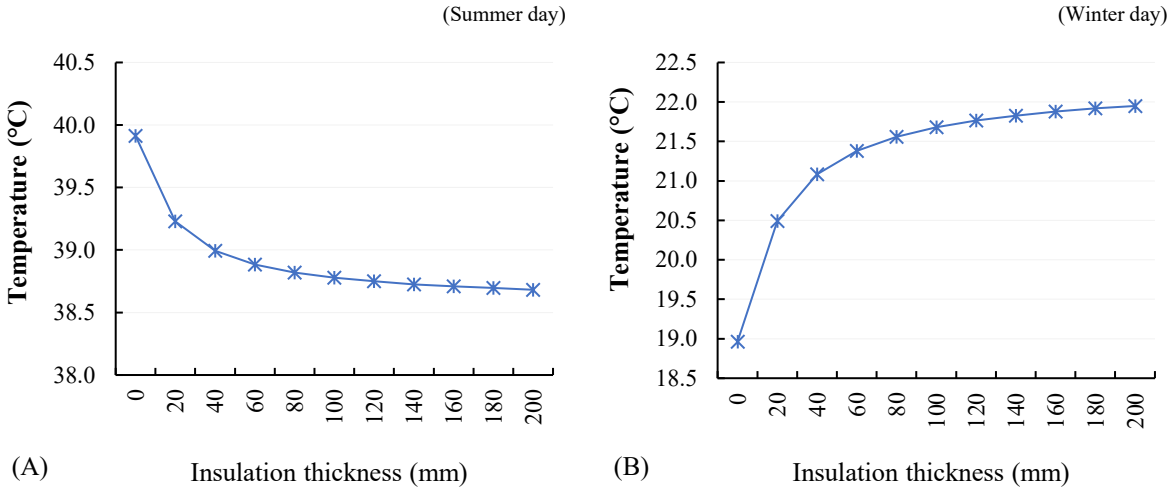


Figure 9-9 Indoor temperature predictions for Case 1 with varying roof insulation thicknesses: (A) Simulation results for a typical summer day; (B) Simulation results for a typical winter day

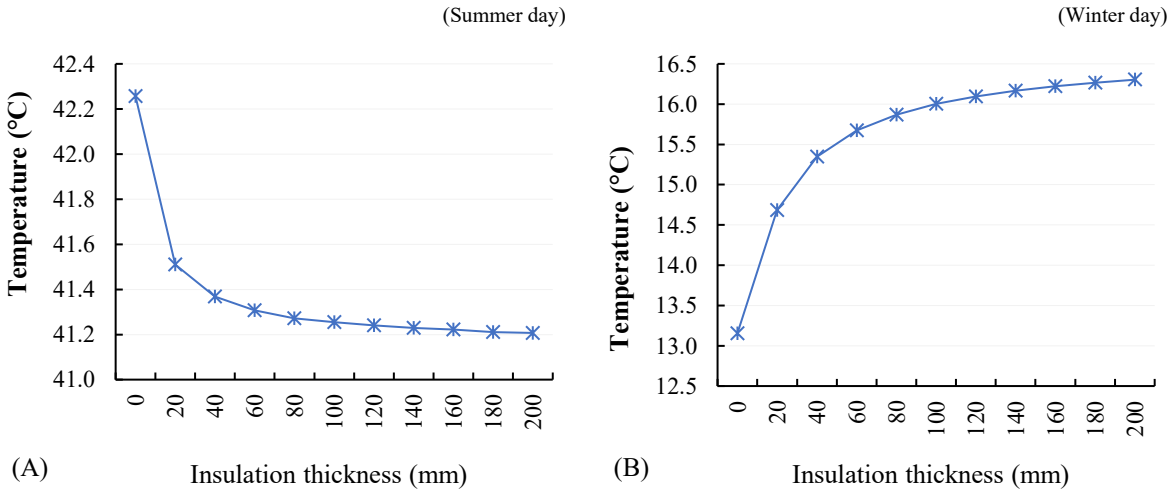


Figure 9-10 Indoor temperature predictions for Case 2 with varying roof insulation thicknesses: (A) Simulation results for a typical summer day; (B) Simulation results for a typical winter day

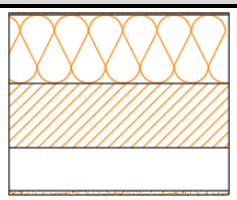
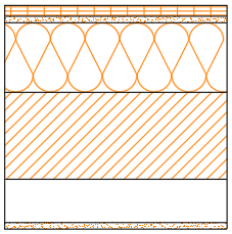
Compared with the current roof type of each house, applying 160 mm EPS insulation material to the roof construction (R1-2 in Case 1 and R2-2 in Case 2) reduced mean indoor temperatures by 0.81 °C and nearly 0.25 °C for Case 1 (bedroom) and Case 2 (upper room), respectively, during the summer. In the winter, increases in mean indoor temperatures of up to 2 °C and 1.4 °C were observed for Case 1 and Case 2, respectively. See Figures 9-11 and 9-12.

These results demonstrate the impact of enhancing roof thermal insulation on the indoor thermal performance of the selected buildings in Riyadh. According to the reviewed literature, the roof is an essential component of the building envelope due to its exposure to direct solar radiation, which contributes to increasing the temperature of the indoor thermal environment and the building's energy requirements, especially during the cooling season. Thus, an additional analysis was conducted to determine whether further improvements could be made by applying reflective roofing to the standard SBC roof construction option for each house.

In this study, a low solar absorptance value of 0.15, corresponding to a solar reflectance value of 0.85, was input in IES-VE and applied to the proposed SBC roof constructions for each house (R1-3 in Case 1 and R2-3 in Case 2). This method allowed for the investigation of the impact of applying highly reflective roof coating without changing the U-value of the roof.

Figures 9-11 and 9-12 demonstrate the hourly air temperature predictions for Case 1 and Case 2, respectively, after applying the proposed roof improvements. The results are shown for a typical summer day and a winter day. The thermal analysis results revealed that while applying the SBC roof insulation requirements (R1-2 and R2-2) improved indoor thermal performance compared with the existing roof constructions, reducing the U-value of the roof solely did not necessarily achieve better performance. Moreover, a conflict in the results was noticed as a result of the impact of seasonal variation.

Table 9-2 Proposed and simulated roof alternatives for the selected case study buildings in Riyadh

	Roof configuration	Roof case	Layer description (outside to inside)	Thickness mm	U-value W/m^2·K
3D-printed house (Case 1)		Standard SBC roof type (R1-2)	▪ Bitumen layer (4 mm) ▪ EPS insulation 160 mm ▪ Cast concrete 150 mm ▪ Air cavity 100 mm ▪ Gypsum board 10 mm	424	0.19
Conventional house (Case 2)		Standard SBC roof type (R2-2)	▪ Terrazzo tiles 25 mm ▪ Mortar 15 mm ▪ EPS insulation 160 mm ▪ Structural concrete 200 mm ▪ Air cavity 100 mm ▪ Gypsum board 15 mm	515	0.19

The results revealed that applying the proposed R1-3 in Case 1 and R2-3 in Case 2 (reflective roof integrated with SBC insulation requirements) could further reduce indoor temperatures in both houses, particularly during the cooling season, making it an effective cooling strategy in Riyadh.

Notably, the improvement in indoor thermal environment is proportional to the roof's solar reflectance value (see Appendix C-B). By applying R1-3 in Case 1 and R2-3 in Case 2, the mean summer indoor temperature was reduced by 0.3 °C in Case 1 and by nearly 0.5 °C in Case 2 compared to the proposed standard SBC roof construction types (i.e. R1-2 and R2-2, respectively).

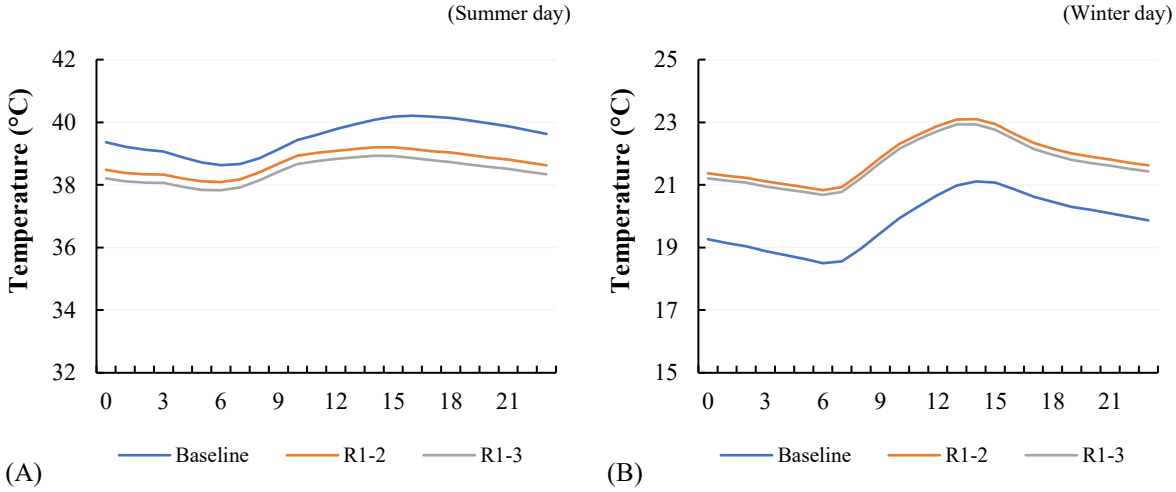


Figure 9-11 Hourly air temperature profile for Case 1 after applying various roof types: (A) Simulation results for a typical summer day; (B) Simulation results for a typical winter day

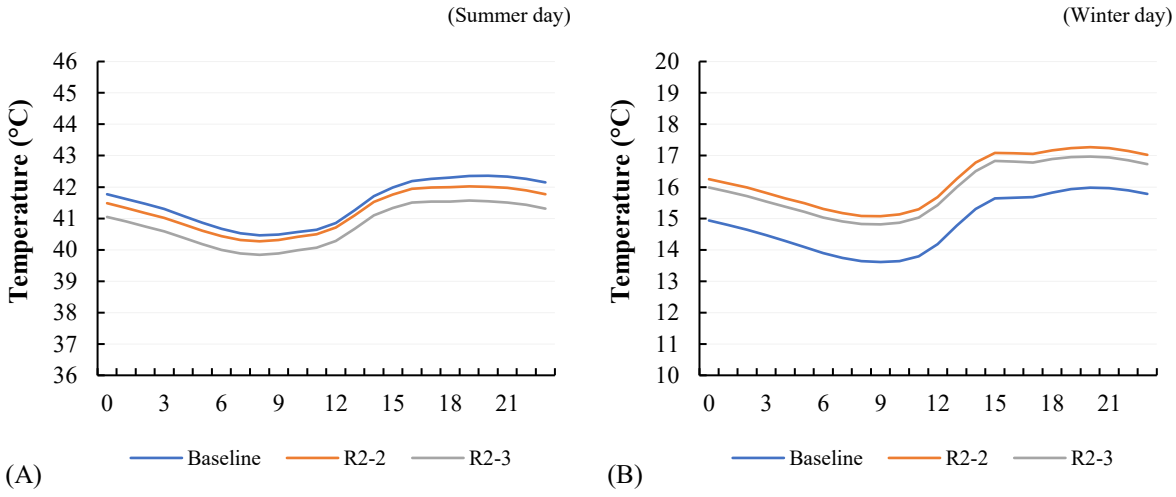


Figure 9-12 Hourly air temperature profile for Case 2 after applying various roof types: (A) Simulation results for a typical summer day; (B) Simulation results for a typical winter day

The results demonstrate that the proposed white reflective SBC roof constructions (R1-3 and R2-3) resulted in a minor reduction in indoor temperatures in winter compared to R1-2 and

R2-2, which may cause a negligible increase in heating demand compared to the standard SBC roofs. However, when comparing the results with the baseline models, we see that the proposed roof options outperformed the existing roof constructions. This could likely be attributed to the enhanced insulation properties of the proposed roofs, which reduced heat flow into and out of the buildings.

The effect of the proposed roof options was evident when investigating the frequency of indoor air temperature predictions in relation to the adaptive comfort limits. The results, demonstrated in Figures 9-13 and 9-14, indicate that the proposed standard SBC roof constructions and the reflective options achieved better performance in both buildings compared to the existing roof constructions. This improvement was distinguished by a reduction in the percentage of times (annual) when Tas were predicted to be outside the adaptive comfort limits.

Applying the proposed reflective options contributed to a reduction in the percentages of overheating hours from 58.2% to 57.5% in Case 1, and from 58.3% to 57.4% in Case 2 under no ventilation mode. When natural ventilation was applied, greater reductions were achieved (from 52% to 50.5% in Case 1 and from 58.3% to 51% in Case 2). This can be attributed to the roof surface's ability to reflect most of the solar radiation, in addition to its thermal insulation properties, which reduced undesired thermal transmission between indoor and outdoor environments compared to the baseline roof constructions.

It should be noted that the potential reductions in cooling load were estimated for both houses as a result of applying the proposed roof options. These results are discussed in the following subsection.

In winter, the proposed reflective roof options (R1-3 for Case 1 and R2-3 for Case 2) contributed to decreasing the percentages of underheating hours in both houses. However, it can be seen that they exhibited slightly higher underheating hours compared to the proposed standard SBC roof options (R1-2 for Case 1 and R2-2 for Case 2). This can be explained by the lower solar absorptance value of the reflective roof options, thus reducing solar heat gain into the building.

Notably, applying the R1-3 and R2-3 led to an increase in the percentage of comfort hours throughout the year, from, respectively, 41.8% in Case 1's baseline model to 48.1% and from only 26.7% in Case 2's baseline model to 28.7% when natural ventilation was applied.

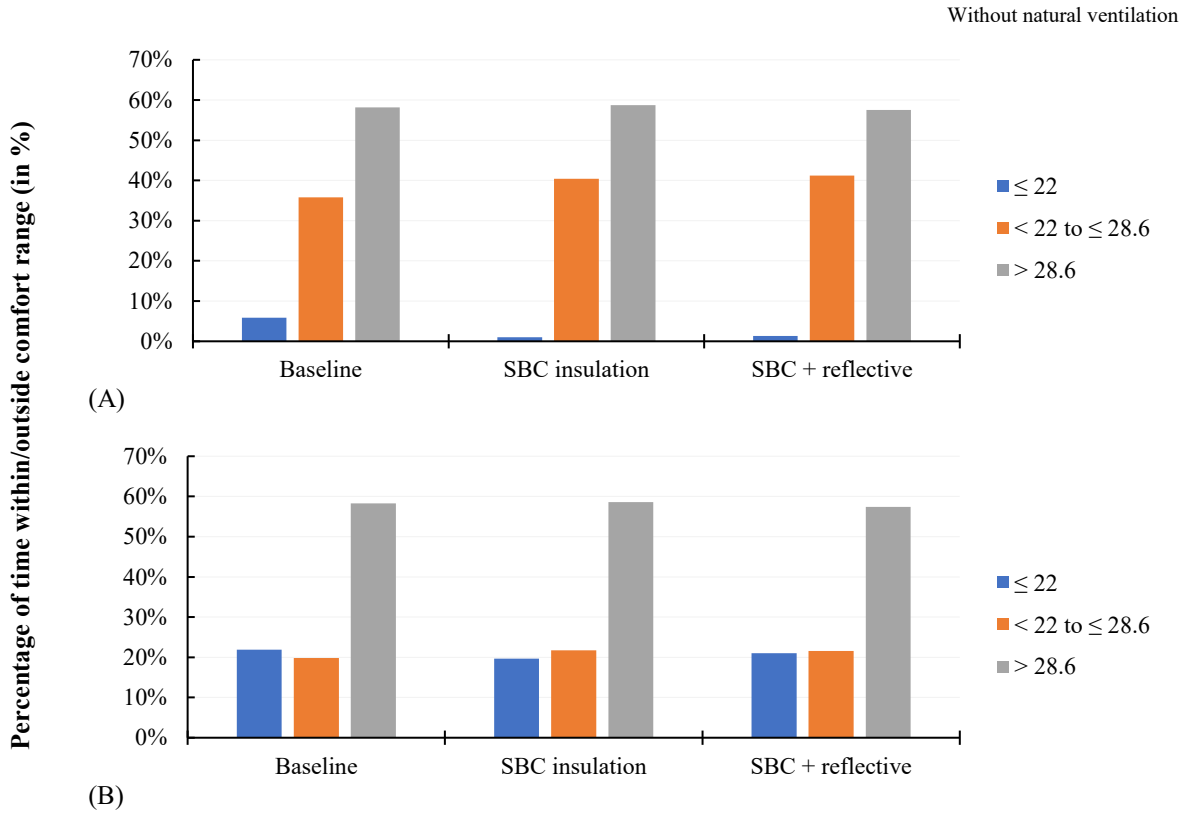


Figure 9-13 Indoor thermal comfort analysis with various proposed roof options: (A) Simulation results for Case 1 (bedroom); (B) Simulation results for Case 2 (upper room)

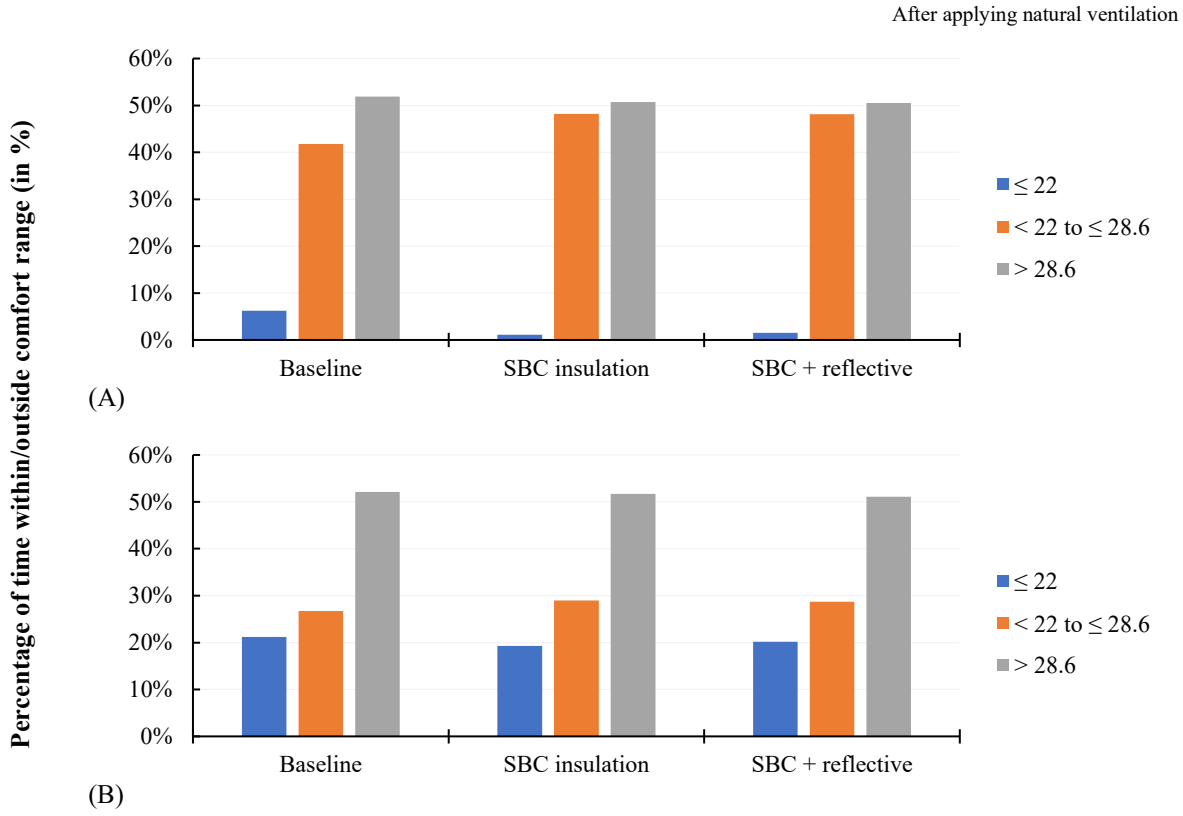


Figure 9-14 Indoor thermal comfort analysis with various proposed roof options after applying natural ventilation: (A) Simulation results for Case 1 (bedroom); (B) Simulation results for Case 2 (R2)

9.3.2 Cooling load

As part of this study, the cooling load for selected rooms in both houses was estimated with the implementation of the proposed roof improvement strategies. The purpose of this analysis was to identify the roof option that can best achieve the lowest cooling loads and, consequently, improve the energy efficiency of the selected case study buildings. See Figure 9-15.

The results suggested that applying the proposed standard SBC roof constructions (R1-2 in Case 1 and R2-2 in Case 2) would reduce the total predicted cooling load for the bedroom in Case 1 and the upper room in Case 2 to 4,534 kWh and 2,380 kWh, respectively. This would achieve respective savings of 15.2% and 21.3% compared with the baseline models. According to the graphs in Figure 9-15, improving the roof's resistance to heat flow alone (i.e. by reducing the U-value of the roof) may not be the most effective strategy for maximizing cooling load savings and the overall energy efficiency of the house.

Further reductions in cooling load can be achieved by applying white reflective coating to the proposed SBC roofs (i.e. reducing their solar absorptance). It was observed that the savings achieved were proportional to the solar reflectance value of the roof (see Appendix C-B). Applying a white high-reflective roof with SBC insulation requirements (i.e. R1-3 in Case 1 and R2-3 in Case 2) resulted in a total cooling load of 4,393 kWh for Case 1 and 2,234 kWh for Case 2. This translated into annual cooling savings of 17.8% and 26.1%, respectively, compared with the current roof constructions. The additional cooling savings of 2.6% (or 8.0 kWh/m^2) for Case 1 and 4.8% (or 6.6 kWh/m^2) for Case 2 were due mainly to the benefit of reflecting direct solar radiation.

These savings correspond fairly closely to those reported in Algarni (2018), who assessed the impact of improving roof construction for residential buildings located in 13 major cities in Saudi Arabia, including Riyadh, using the eQUEST simulation tool. According to the aforementioned study, applying a well-insulated roof construction (e.g. with an R-value of 1.75 $m^2 \cdot K/W$) combined with a white high-reflective coating with a solar reflectance value of 0.85 could reduce the total annual cooling load of the house by up to approximately 21% in Riyadh's climate compared to the base case.

Furthermore, Algarni (2018) reported a negligible increase in heating demand relative to the savings achieved in cooling load by applying highly reflective coating to a well-insulated roof, which is consistent with the findings observed in this study. This was particularly

evident in Case 2, in which the heating load increased slightly from 4.7 kWh/m^2 with R2-2 to 5.5 kWh/m^2 with R2-3. Nevertheless, both values were still considerably lower than the baseline figure of 7.7 kWh/m^2 (see Appendix C-B).

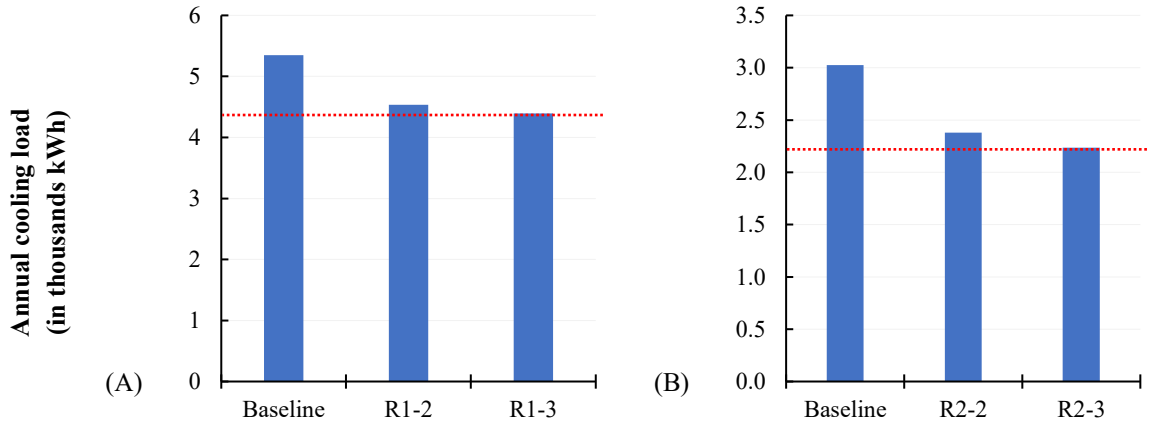


Figure 9-15 Total annual cooling load predictions for selected rooms with various roof improvement strategies: (A) Case 1 (bedroom); (B) Case 2 (upper room)

9.3.3 Conclusion

Based on the results discussed in this section, it was revealed that the proposed SBC roof constructions integrated with high solar reflectance outperformed both the current roof construction and the proposed standard SBC roof options for the selected houses, particularly during the cooling season. Consequently, R1-3 and R2-3 were selected for Case 1 and Case 2, respectively, for further analysis to improve the indoor thermal environment of the selected case study buildings in Riyadh.

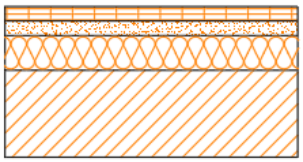
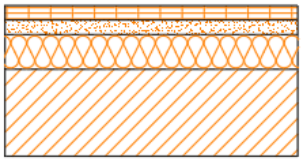
9.4 Ground floor insulation

The sensitivity analysis of ground temperature presented in Section 7.2 demonstrated its significant impact on indoor temperatures and thus cooling load. In this section, the impact of applying ground floor thermal insulation, as per SBC requirements, was investigated for the selected houses using the IES-VE simulation tool primarily to identify the ground floor option that can best improve the indoor thermal environment and achieve the lowest cooling load. For the purpose of this analysis, the bedroom in Case 1 and the dining room in Case 2 were selected.

As previously mentioned, both houses' baseline models lacked ground floor thermal insulation. The SBC (as discussed in Chapter 2) requires a maximum ground floor U-value of 0.496 W/m^2·K, which is significantly lower than the current U-values of 3.26 W/m^2·K and 3.59 W/m^2·K for Case 1 and Case 2, respectively (see Chapter 7). The load breakdown

analysis shown in Section 8.4 revealed that the ground floor contributed significantly to cooling load in both houses, particularly during summer months. Thus, the simulation results discussed in this section were based on a systematic incremental increase of EPS insulation thicknesses, adding 10 mm per run from 0 mm (baseline) to 100 mm. Table 9-3 illustrates the proposed ground floor characteristics for Case 1 and Case 2.

Table 9-3 Description of proposed insulated ground floor types for both case study buildings

	Ground floor configuration	Layer description (inside to outside)	Thickness (mm)	U-value ($W/m^2 \cdot K$)
Case 1	In  Out	In ▪ Terrazzo tiles (10 mm) ▪ Mortar (25 mm) ▪ EPS insulation (60 mm) ▪ Cast concrete (150 mm) Out	245	0.49
Case 2	In  Out	In ▪ Granite tiles (20 mm) ▪ Mortar (25 mm) ▪ EPS insulation (60 mm) ▪ Cast concrete (100 mm) Out	205	0.50

9.4.1 Air temperature

The graphs in Figures 9-16 and 9-17 show the indoor air temperature results for Case 1 and Case 2, respectively, after applying the proposed ground floor insulation with various thicknesses for a typical summer and a typical winter day. The results suggest that applying ground floor insulation negatively impacted the indoor thermal environment in both seasons. A positive relationship was observed between insulation thickness and indoor temperature for summer, while a negative relationship was noticed for winter.

This could be attributed to the insulation material restricting thermal exchange between the indoor environment and the ground. For example, it may have restricted the dissipation of internal built-up heat to the cooler ground during the summer peak period when the indoor air temperatures were higher than the ground temperatures.

The analysis of heat gain/loss conducted in Section 8.3 revealed that heat loss through the ground floor on a summer day was significantly higher than heat gain, while winter heat gain was higher than heat loss. Thus, it can be observed that applying 60 mm EPS ground floor

insulation increased summer mean indoor temperatures by approximately 1.7 °C in the tested rooms. In winter, it decreased mean indoor temperatures by 3.2 °C and 4.3 °C in the tested rooms in Case 1 and Case 2, respectively. See the hourly Ta results for a typical summer and a winter day before and after applying the proposed SBC ground floor construction options in Figure 9-18 for Case 1 and in Figure 9-19 for Case 2.

Notably, the results agree with Staszczuk, Wojciech, and Kuczyński (2017), who indicated that removing ground floor thermal insulation led to a reduction in the mean indoor temperature of up to 3.8 °C. However, it should be noted that the aforementioned study was carried out in two laboratory rooms during the hottest two weeks in Poland (moderate climate), where the average outdoor temperature was 22.1 °C.

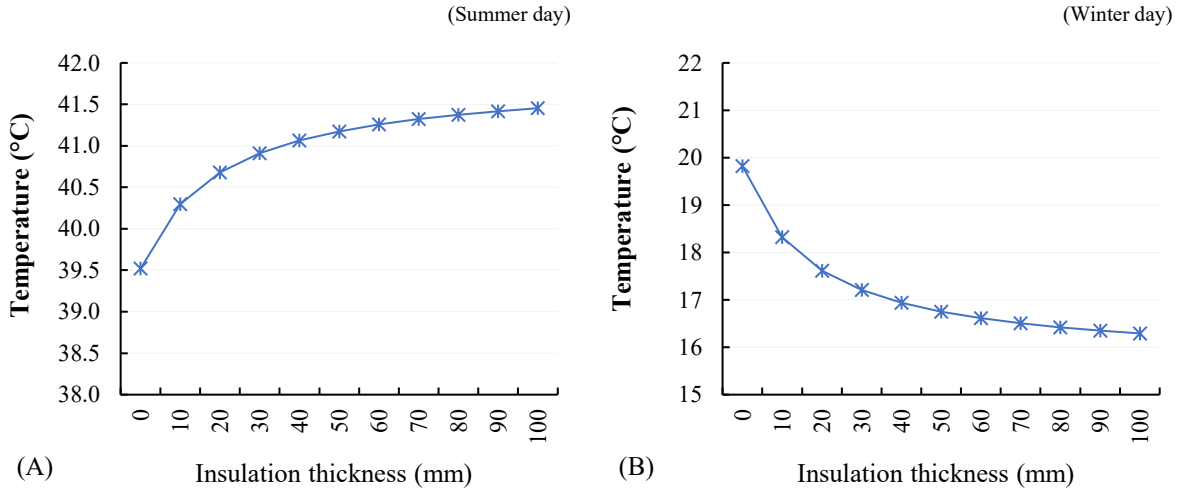


Figure 9-16 Indoor temperature predictions for Case 1 with varying ground floor insulation thicknesses: (A) Simulation results for a typical summer day; (B) Simulation results for a typical winter day

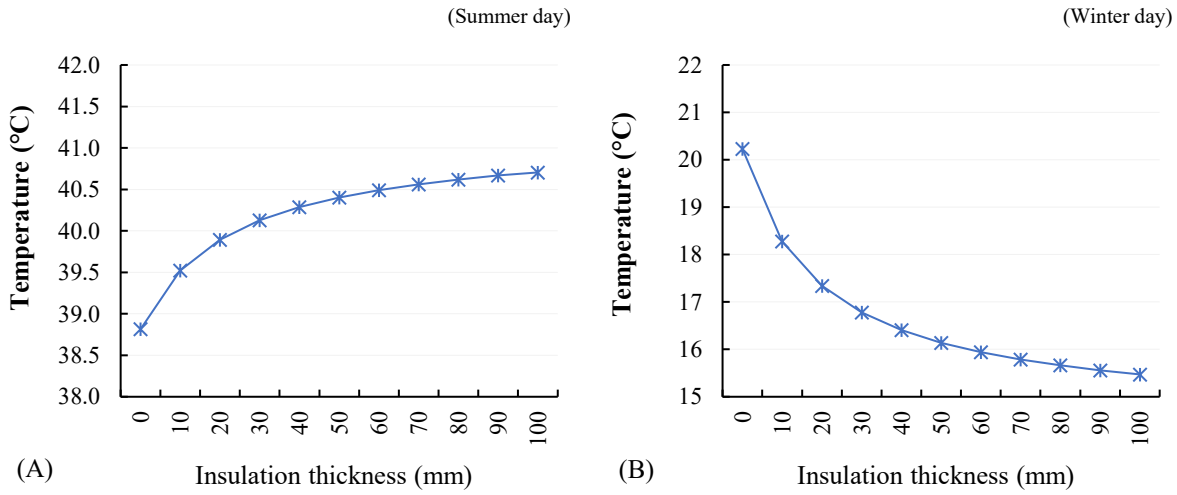


Figure 9-17 Indoor temperature predictions for Case 2 (ground floor dining room) with varying ground floor insulation thicknesses: (A) Simulation results for a typical summer day; (B) Simulation results for a typical winter day

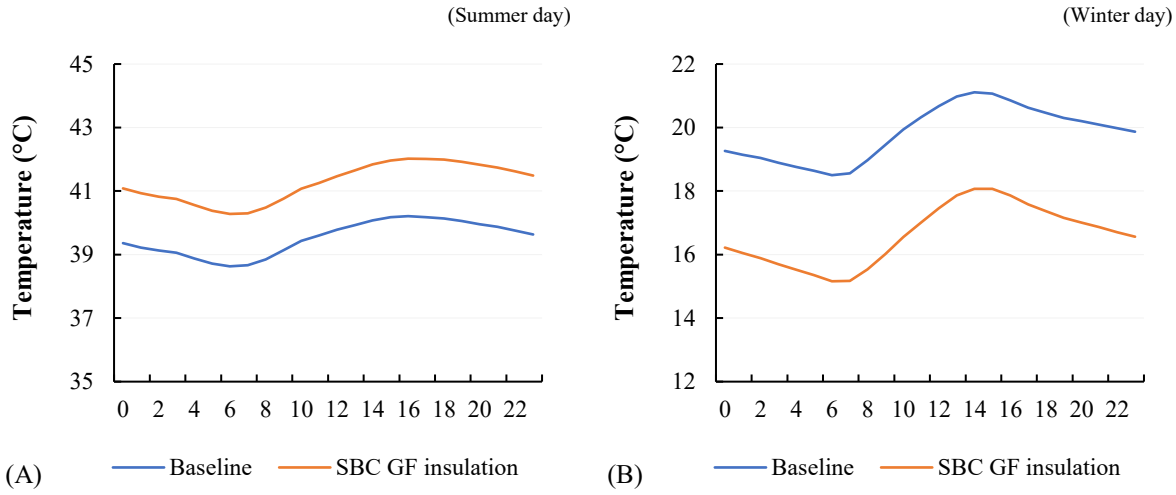


Figure 9-18 Hourly air temperature profile for Case 1 with and without SBC ground floor insulation: (A) Simulation results for a typical summer day; (B) Simulation results for a typical winter day

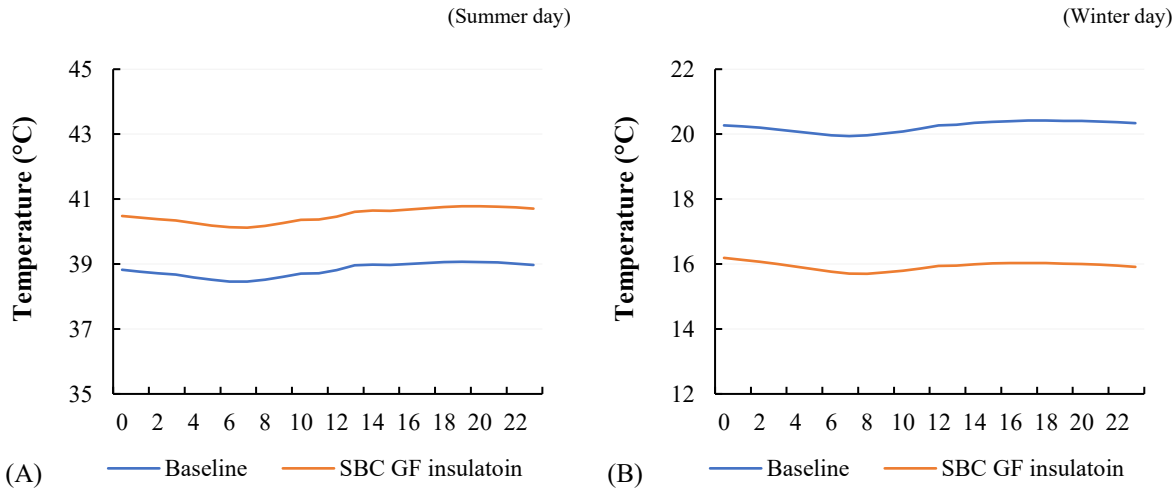


Figure 9-19 Hourly air temperature profile for Case 2 (ground floor dining room) with and without SBC ground floor insulation requirements: (A) Simulation results for a typical summer day; (B) Simulation results for a typical winter day

An evaluation of the frequency of indoor air temperature predictions in relation to the adaptive comfort limits before and after applying SBC ground floor insulation is illustrated in the graphs in Figures 9-20 and 9-21. The results indicate that applying ground floor insulation worsened indoor thermal conditions in both houses throughout the year. This poor performance was distinguished by a reduction in the percentage of comfort hours (i.e. when indoor temperature is predicted to fall within the adaptive comfort limits). This percentage decreased to 25% in Case 1 and to 19.7% in Case 2 under no ventilation mode and to 33.7% and nearly 29%, respectively, when natural ventilation was applied.

The results show that the increase in the percentage of time outside comfort was due mainly to the restrictive role of the ground floor insulation, which minimized desirable heat gain through the ground during the underheating period (from December to February), thereby

increasing the percentages of underheating hours. Consequently, an increase in heating load may occur to restore indoor thermal comfort in winter. As heating load was found to be insignificant in this climate (see Section 8.5), this study was oriented to focus on reducing cooling demands.

Moreover, the graphs below show that applying the SBC ground floor insulation requirements made it possible to reduce the overheating hours in the selected rooms by up to 1.1% and 3% for Case 1 and Case 2, respectively. It is worth noting that this improvement was achieved after applying natural ventilation as a negative effect was noticed under no ventilation mode.

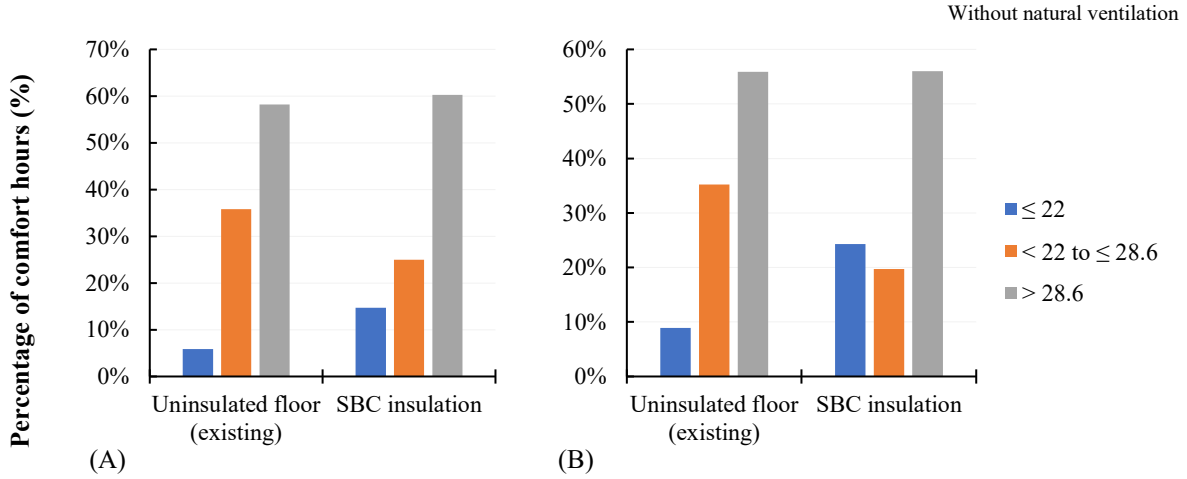


Figure 9-20 Indoor thermal comfort analysis before and after applying SBC ground floor insulation requirements without natural ventilation: (A) Case 1 (bedroom); (B) Case 2 (ground floor dining room)

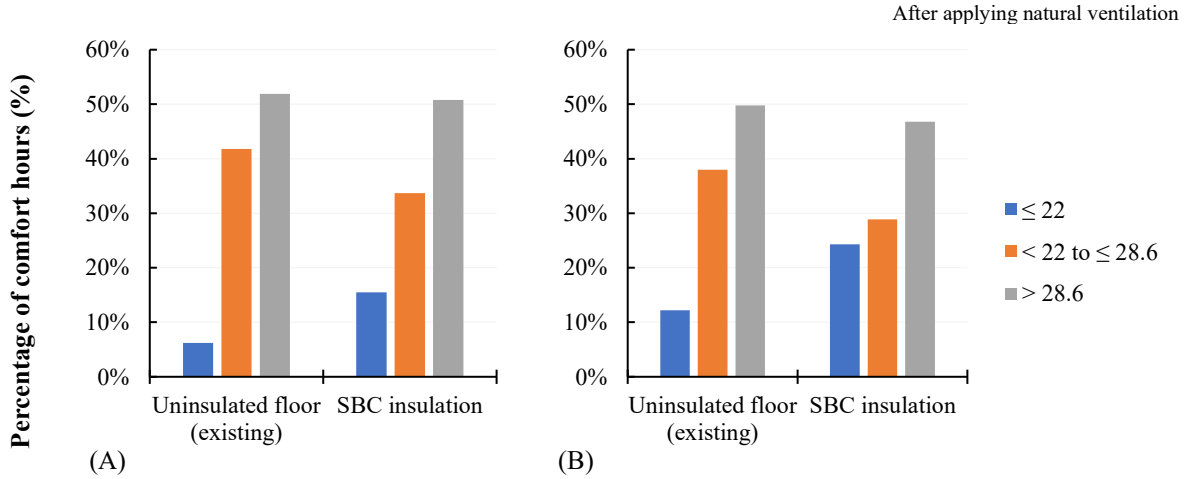


Figure 9-21 Indoor thermal comfort analysis before and after applying SBC ground floor insulation requirements with proposed NV strategy: (A) Case 1 (bedroom); (B) Case 2 (ground floor dining room)

9.4.2 Cooling load

The next step involved estimating the total cooling load for the selected rooms after the implementation of ground floor insulation, as per SBC requirements. As part of this analysis, cooling load savings were calculated to identify the ground floor option that can best improve the overall thermal performance and energy efficiency of the selected case study buildings (see Figure 9-22). The results revealed that the application of ground floor insulation had a considerable impact on improving the energy performance of the buildings. Applying the SBC ground floor insulation requirement (e.g. 60 mm EPS insulation) made it possible to reduce the cooling load by up to 31.3% and 50.6% all year-round for Case 1 and Case 2, respectively.

These results align with Alaboud and Gadi (2022), who reported potential savings in annual cooling load of approximately 10% in a residential building in Makkah, KSA, which has climate conditions similar to those of Riyadh. However, the saving percentage achieved in their study is lower than that achieved in the current thesis, which could be attributed to the higher U-values of the baseline models investigated in this thesis (as demonstrated in Chapter 7) compared to the 0.93 W/m^2·K of Alaboud and Gadi's model.

In addition, based on cooling load savings and life-cycle cost analysis, Harkouss, Fardoun, and Biwole (2018) found that insulating the ground floor with a U-value of no less than 0.5 W/m^2·K was suitable for the hot and arid climate of Abu Dhabi, which agrees with the maximum ground floor U-value requirement set by the SBC for residential buildings in Riyadh, KSA. This is due to the restrictive role of the thermal insulation, as previously indicated in this section.

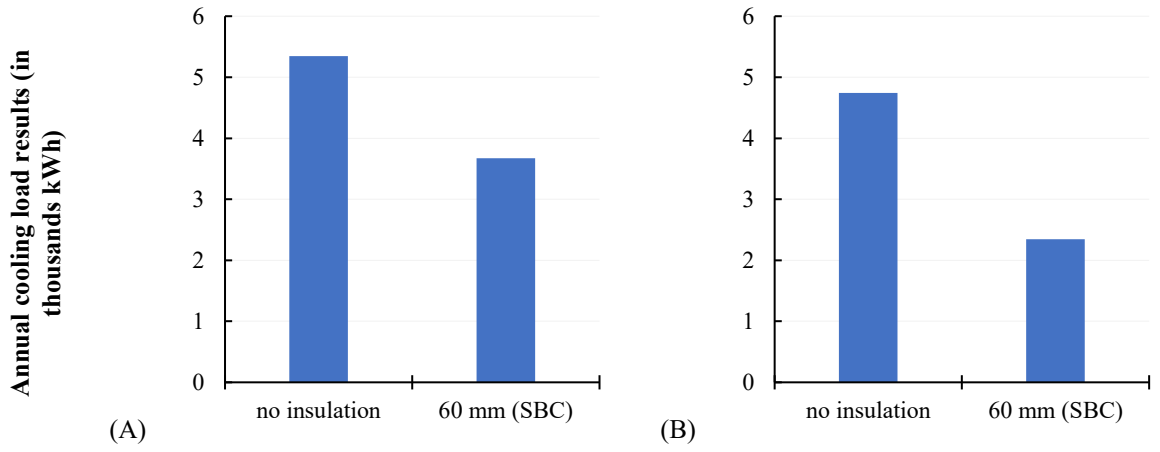


Figure 9-22 Annual cooling load predictions for selected rooms with varying ground floor options: (A) Simulation results for Case 1 (bedroom); (B) Simulation results for Case 2 (ground floor dining room)

To better understand the impact of ground floor insulation, the monthly loads for the tested rooms before and after applying the ground floor thermal insulation are provided in Appendix C-C. The results demonstrate that applying ground floor thermal insulation reduced the rooms' cooling load by 95.9 kWh/m^2 in Case 1 and 130 kWh/m^2 in Case 2; however, it led to an increase in heating load by 3.9 kWh/m^2 and 5.1 kWh/m^2, a negligible detriment when compared to the total cooling savings.

The reduction in cooling load can be explained by the role of ground floor thermal insulation in minimizing thermal exchange between the ground and the controlled indoor thermal environment during the summer season. In winter, the temperature of the ground is slightly higher than the heating setpoint temperatures, which explains the reduced heating load as a result of removing the ground floor insulation. However, the reduction in total and peak cooling demand achieved with ground floor thermal insulation is more significant than the heating load savings achieved without insulation.

9.4.3 Conclusion

The analysis discussed in this section demonstrated how ground floor insulation can affect the thermal performance of residential buildings in Riyadh. It should be noted that ground temperatures were not measured in this study; instead, values were adopted from the literature, as discussed in Chapter 7. While the current uninsulated ground floors can provide a passive cooling effect in the summer, the simulation results suggested that this benefit comes at the cost of a higher cooling load, and consequently higher CO_2 emissions, especially when active cooling is needed the most. For this reason, the SBC-insulated ground floor option was selected for further analysis to improve the overall thermal performance and efficiency of the selected case study buildings. However, uninsulated ground floor options may be more desirable for free-running buildings.

9.5 Air infiltration

As previously stated, the recently enforced SBC requires an effective envelope airtightness for residential buildings in Saudi Arabia. However, higher air infiltration rates (e.g. above 0.5 ACH) may be beneficial for removing internal built-up heat and cooling the building mass. According to the thermal analysis conducted in Section 8.3, heat loss through air infiltration in both summer and winter is higher than infiltration gain in both houses.

Building upon the previous analysis conducted in Section 7.2, various simulations were conducted for both buildings to evaluate the impact on the indoor thermal environment of

changing the rate of uncontrolled air infiltration in comparison to implementing a controlled ventilation strategy. These analyses aimed to mitigate the risks of undesired convective heat gain or loss—particularly during extreme outdoor conditions—thereby improving the thermal performance and energy efficiency of residential buildings in Riyadh. As part of this analysis, cooling load was estimated for both houses with various uncontrolled infiltration rates, and the potential cooling savings were calculated and discussed.

9.5.1 Air temperature

The results of the sensitivity analysis of air infiltration conducted in Chapter 7 demonstrated the direct impact of uncontrolled airflow on indoor thermal environments. The graphs in Figures 9-23 and 9-24 illustrate the negative relationship between infiltration rate and indoor air temperature for Case 1 and Case 2, respectively. As the infiltration rate increased, the mean indoor temperature decreased. However, higher infiltration rates exhibited more significant fluctuations in indoor temperature (see Section 7.2).

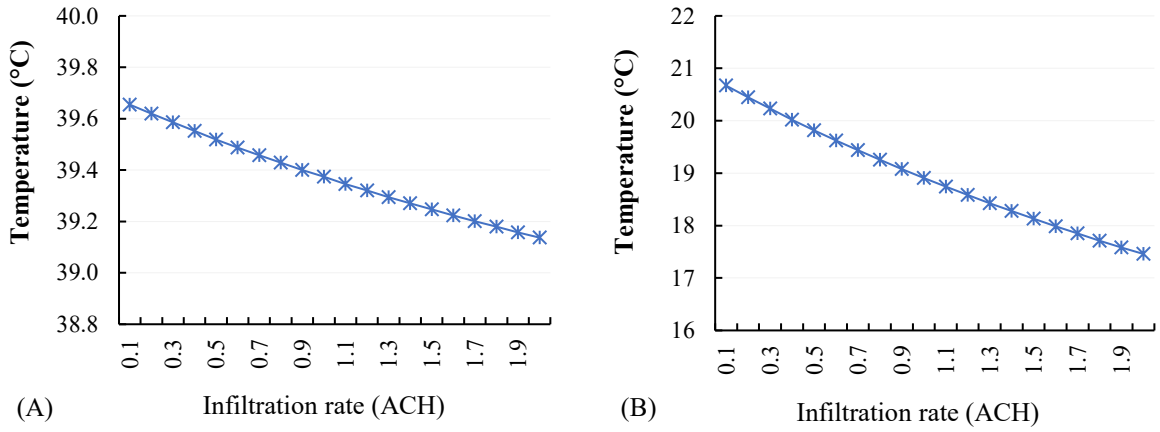


Figure 9-23 Indoor temperature results for Case 1 with various infiltration rates: (A) Simulation results for a typical summer day; (B). Simulation results for a typical winter day

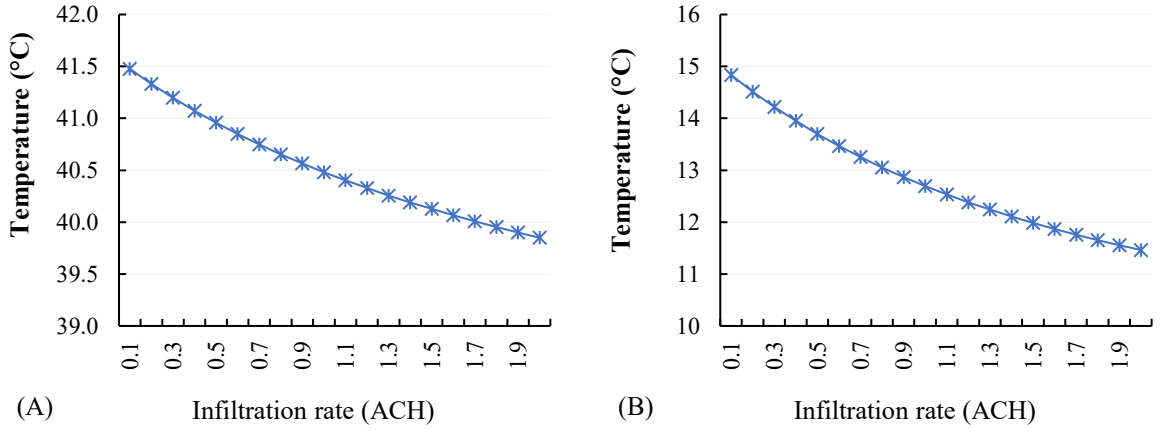


Figure 9-24 Indoor temperature results for Case 2 with various infiltration rates: (A) Simulation results for a typical summer day; (B) Simulation results for a typical winter day

Notably, the results showed that the conventional house (Case 2) was more sensitive to changes in infiltration rates, particularly in the summer, when indoor temperatures would decrease by 1 °C simply by increasing the infiltration rate from 0.1 ACH to 1.0 ACH, compared to only 0.28 °C in the 3D-printed house (Case 1). It was found that the effect of changing infiltration rates on the indoor thermal environment is greater in winter as Tas would drop by 1.7 °C and 2.1 °C, respectively.

To better understand the impact of changing air infiltration rates on indoor thermal environments, the frequency of predicted indoor air temperatures—i.e. the percentage of time temperatures fell within, below, or above the adaptive comfort limits—was reviewed for the selected rooms. The thermal performance of both buildings was assessed throughout the year with and without natural ventilation. See the graphs in Figures 9-25 and 9-26.

The results suggest that increasing the infiltration rate can positively impact the indoor thermal environment by reducing the percentages of overheating hours, as indicated by the grey bars. However, this conflicts with winter thermal comfort requirements as it led to an undesirable increase in the percentage of underheating hours, indicated by the blue bars, which in turn resulted in a reduction in comfort hours throughout the year, represented by the light red bars. Notably, when the proposed controlled natural ventilation strategy was applied, the effect of air infiltration on the percentage of overheating hours became minimal. In this case, lower infiltration rates (e.g. 0.1 ACH) achieved better indoor thermal conditions throughout the year. See Figure 9-26.

The graphs in Figure 9-27 compare indoor thermal conditions for different infiltration rates (without ventilation) against the option with the lower rate (i.e. 0.1 ACH) coupled with the proposed controlled natural ventilation strategy. The results indicate that applying the lower infiltration rate with controlled ventilation reduced the percentage of overheating hours to approximately 52% in the tested rooms. This led to an increase in the percentage of comfort hours to 44.7% (or 3,917 hours) for Case 1 and to nearly 26.7% (or 2,340 hours) for Case 2.

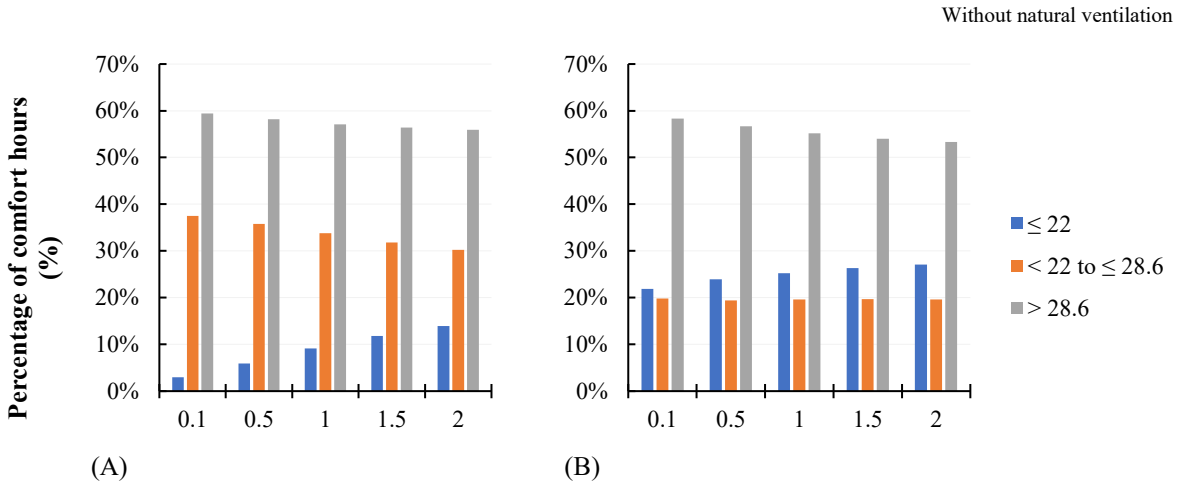


Figure 9-25 Indoor thermal comfort analysis with various air infiltration values: (A) Simulation results for Case 1 (bedroom); (B) Simulation results for Case 2 (upper room)

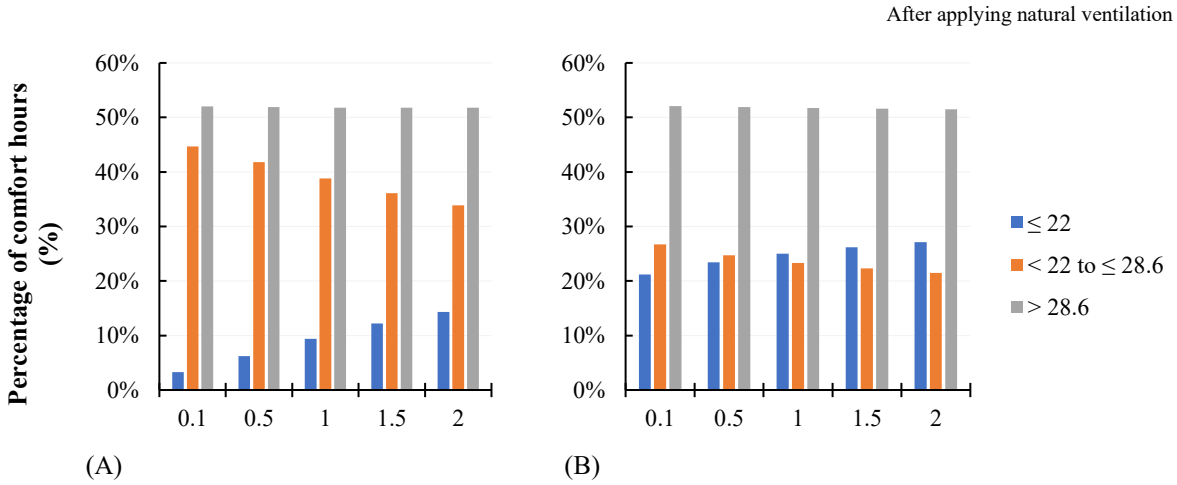


Figure 9-26 Indoor thermal comfort analysis with various air infiltration values after applying natural ventilation strategy: (A) Simulation results for Case 1 (bedroom); (B) Simulation results for Case 2 (upper room). Note that the potential of a free-running period increases when controlled airflow is reduced.

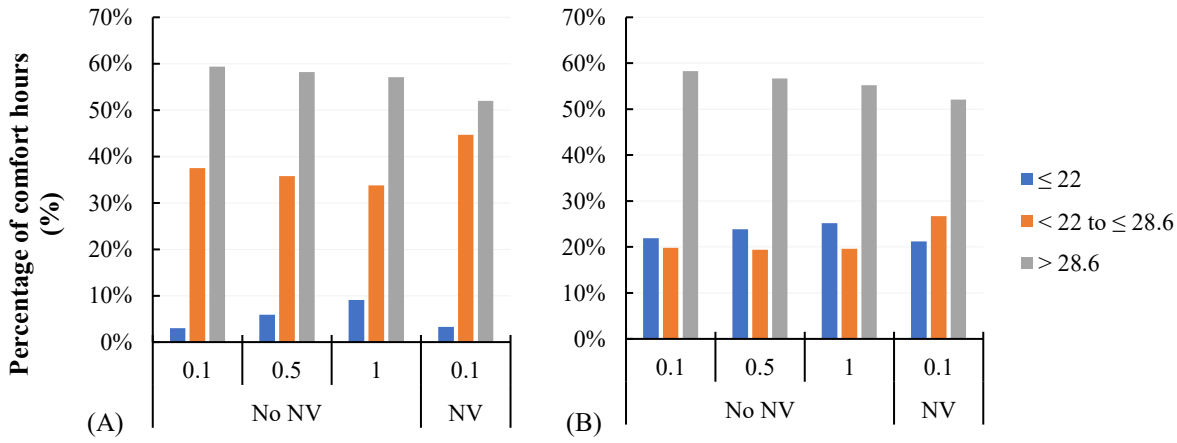


Figure 9-27 A comparison of different air infiltration values versus controlled ventilation for selected rooms: (A) Simulation results for Case 1; (B) Simulation results for Case 2

9.5.2 Cooling load:

To provide a clear indication of the impact of uncontrolled air infiltration rates on the overall energy performance of the selected residential buildings in Riyadh, cooling loads were estimated for both houses with varying infiltration rates (see Figure 9-28). A positive proportional relationship between cooling load predictions and infiltration rates was observed. As the infiltration rate increases, the cooling load increases for both dwellings, and vice versa.

This agrees with Alyami and Omer (2021), Krarti et al. (2020), and Wahl (2017) in Riyadh; Al-Saadi and Al-Jabri (2017) in Muscat, Oman; and Albatayneh (2021) in Amman, Jordan, who reported an improvement in the overall energy performance of residential buildings in the specified locations as a result of improving the airtightness of the building.

The results suggested that by reducing the infiltration rate in Case 1 from 0.5 ACH (baseline) to 0.1 ACH, a potential reduction of approximately 4% in cooling load could be achieved. As for Case 2, increasing the infiltration rate from 0.1 ACH (baseline) to 0.5 ACH and 1.0 ACH would increase cooling loads by 10.7% and 24.4%, respectively. See Appendix C-D.

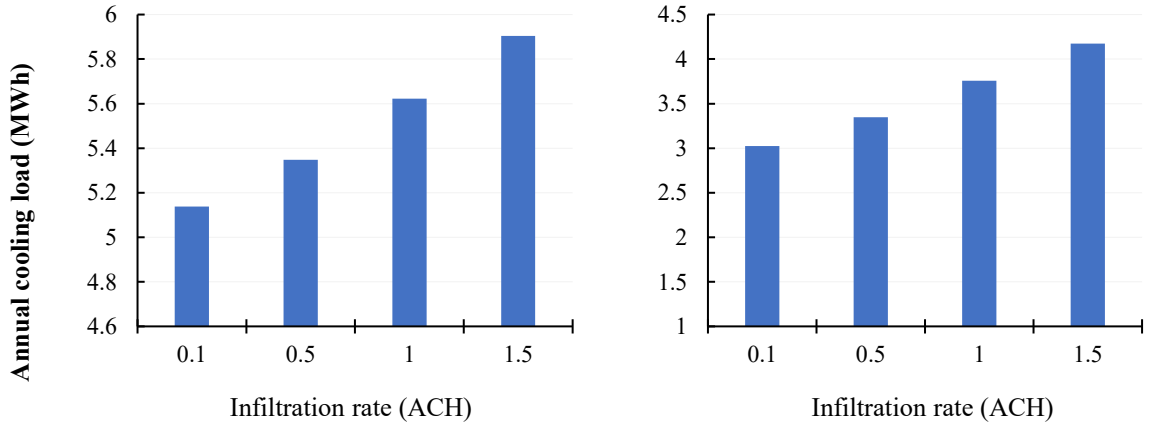


Figure 9-28 Annual cooling load predictions for selected rooms with various uncontrolled infiltration rates: (A) Simulation results for Case 1 (bedroom); (B) Simulation results for Case 2 (upper room). Note that the baseline infiltration rate varies for each house.

9.5.3 Conclusion

The impact of various infiltration rates was analysed for both case study buildings in Riyadh using the IES-VE simulation software. While indoor environments could benefit from higher infiltration rates, this study found that controlled ventilation strategy achieved better indoor thermal conditions. Based on the results discussed in this section, an infiltration rate of 0.1 ACH was selected for further analysis to improve the thermal performance of both buildings

and to maximize savings in energy consumption and CO_2 emissions. The following section explores the impact of window shading options on the thermal performance and energy efficiency of both case study buildings in Riyadh.

9.6 Window shading

As discussed in Chapter 3, heat gain through transparent surfaces in the building envelope differs from heat gain through opaque surfaces. From a thermal performance point of view, controlling solar gain through windows is crucial, especially in hot regions such as Riyadh. As discussed in Chapter 2, the significant role of window shadings in reducing solar gain—and thereby improving building thermal and energy performance—is acknowledged in SBC 602, which permits the use of permanent external overhangs with a projection factor of at least 0.5 to adjust the SHGC requirement for windows. This section investigates the impact of various window shading techniques for residential buildings in Riyadh, Saudi Arabia, using the IES-VE simulation tool.

The simulations covered in this section are divided into two groups. The first set of simulations evaluates three types of shading devices—overhang, egg-crate, and louvers—across different window-orientation scenarios, as discussed in more detail in the following subsections. The second phase applies the most effective shading option, in combination with the proposed glazing types, to both case study buildings to assess potential improvements in indoor thermal environment and energy efficiency.

9.6.1 External shading assessment

The indoor thermal environment can be greatly affected by building orientation due to varying solar gains for different orientations. While the SBC acknowledges the role of applying external shading on reducing solar heat gain, thus improving the thermal performance of residential buildings, it does not take into account the various orientation requirements of shading. As discussed in Section 3.3, the high solar altitude in Riyadh, in addition to the apparent daily movement of the sun, causes both east and west orientations to receive significant solar radiation, particularly during warmer seasons, whereas north and south orientations receive considerably less radiation.

Thus, the following analysis was conducted to assess the impact of applying different external shading devices on reducing summer solar heat gain for various room orientation scenarios. Three different types of shading devices were considered for this analysis: a horizontal overhang with a projection factor of 0.5 as suggested by the SBC, an overhang

with side fins (egg-crate), and louvers. An illustration of the proposed shadings is provided in Figure 9-29.

For the purposes of this analysis, the proposed shading devices were applied to the selected rooms (i.e. the south-facing bedroom in Case 1 and the southwest-facing upper room in Case 2). To gain a better understanding of their performance and to facilitate a comparison in terms of efficiency and effectiveness, each shading type was simulated for eight different orientations. It is worth noting that the models' orientations were adjusted by 45° for each run to allow for this analysis.

Moreover, to better demonstrate the thermal performance of the tested shading devices, the existing unconventional window glazing types in both houses were replaced with a standard typical double-clear window type (W2). The characteristics of the tested window glazing types are illustrated in Table 5-9. The solar gain simulation results were analysed for each orientation before and after the implementation of the proposed shading devices.

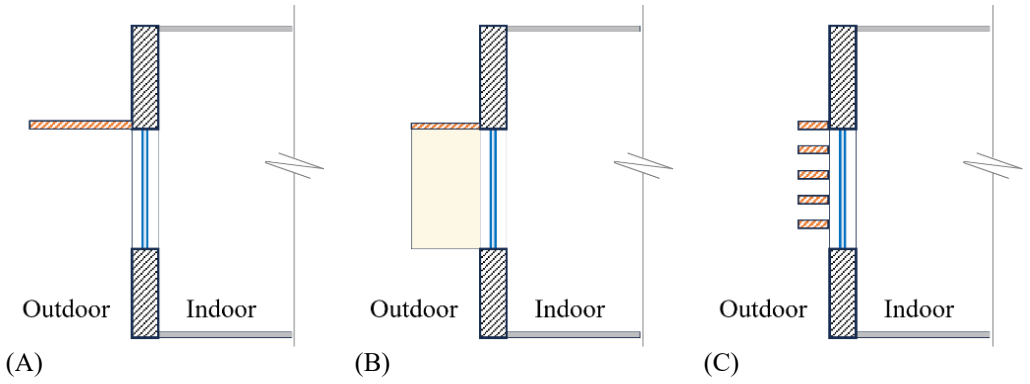


Figure 9-29 Illustrations of the proposed external shading devices: (A) Overhang (PF = 0.50); (B) Egg-crate shadings (PF = 0.5); (C) Louvers (25 cm depth)

Since the aim of this phase was to quantify potential reductions achieved in solar gain, and thus cooling load, after applying the proposed shading devices for different orientations, it was critically important to determine the impact of the orientation of the window on the indoor thermal environment before applying the proposed shading devices. The bar graph in Figure 9-30 compares the solar gain results for the tested rooms under various orientations and shading device scenarios during a typical summer day.

The blue bars show the results before the implementation of the proposed shading devices. Note that the current orientation of the south bedroom in Case Study 1 has changed to become southwest, and so on. Also, the white bold font percentage shows the percentage difference in solar gain for each orientation scenario relative to the existing orientation (i.e.

south for Case 1 and southwest for Case 2). The orange bars represent the results after applying the SBC overhang, the grey bars illustrate the simulation results after the implementation of egg-crate shading, and the yellow bars show the results after applying the proposed louvers. The black font percentages show the percentage improvement in performance after applying shading devices for each particular orientation. The negative percentages indicate improvement in performance (i.e. a reduction in solar gain), while the positive percentages show a decline in performance. The air temperature results are shown in Figure 9-31.

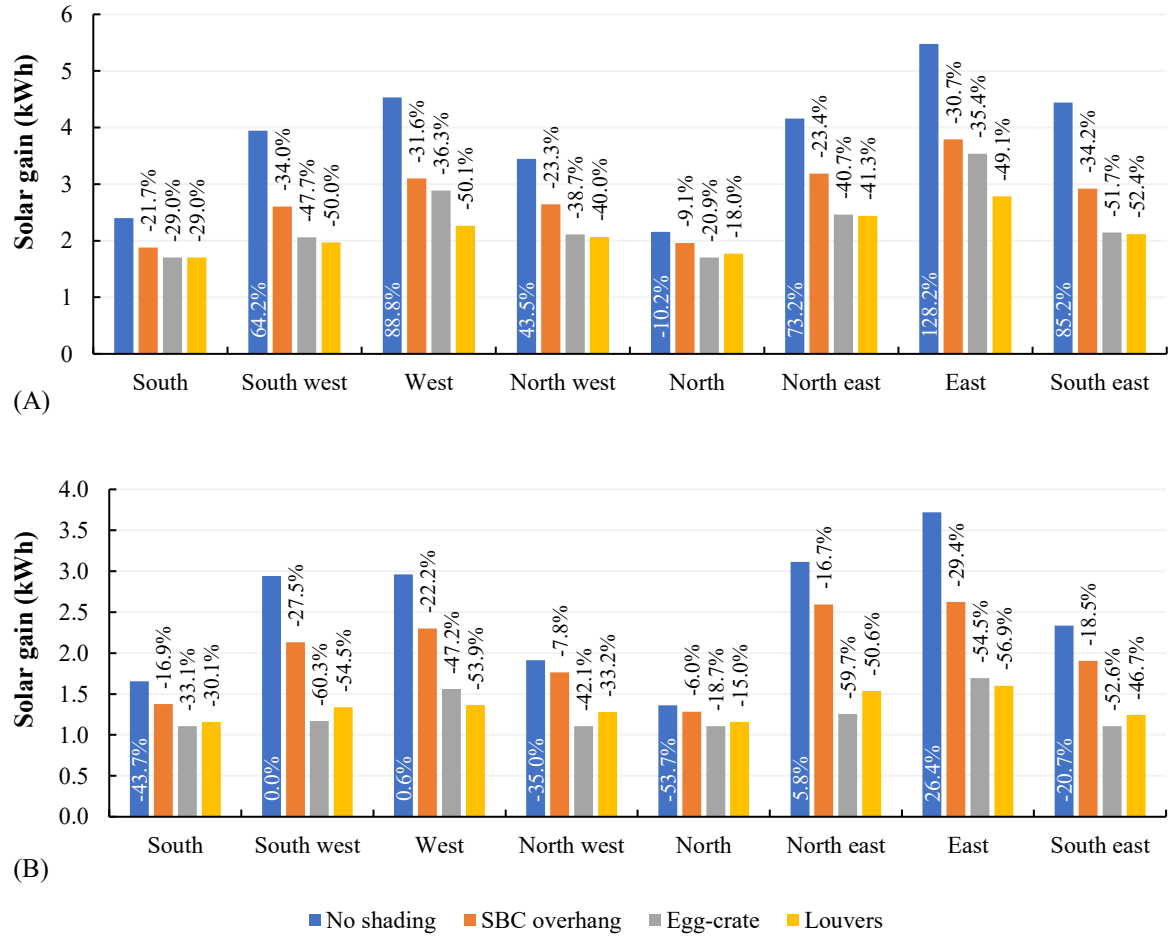


Figure 9-30 Solar gain results for the tested room with various shading techniques under different orientation scenarios during a typical summer day: (A) Simulation results for Case 1; (B) Simulation results for Case 2

Note: Case 2's north-south axis is deviated 30° towards the west

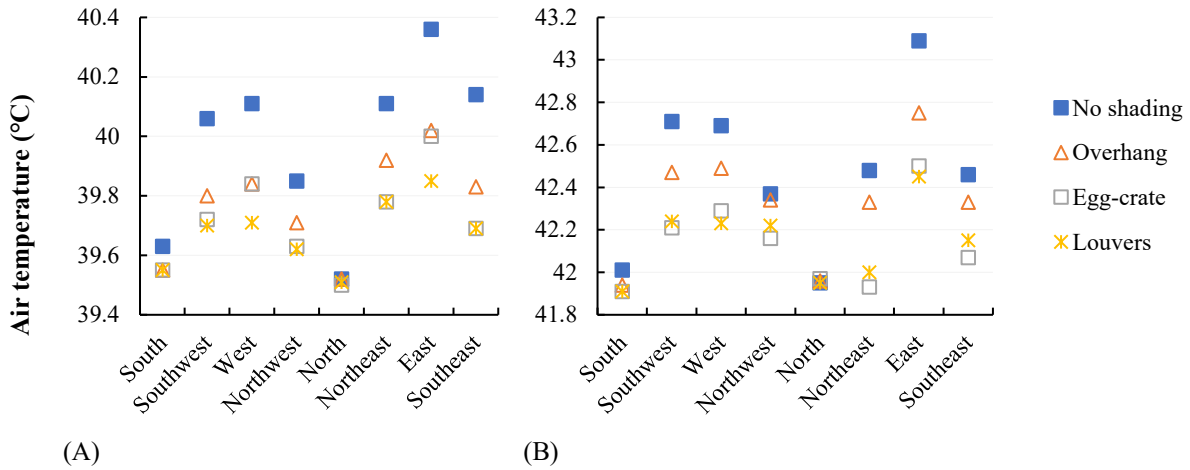


Figure 9-31 Indoor temperature predictions for a typical summer day for both rooms under various orientations and different shading options: (A) Simulation results for bedroom in Case 1; (B) Simulation results for upper room (R2) in Case 2

- **The effect of changing orientation (double-clear window without shading)**:

The results suggested that the orientation of the window had a direct impact on the indoor thermal environment due to the varying amount of solar gain for each orientation. See the graphs in Figure 9-30.

Changing the current orientation of bedroom in Case 1 by 90° to face west and east resulted in increases in solar gain of around 89% and 128%, respectively, for a typical summer day. This resulted in a respective increase in mean indoor temperature of nearly 0.5 °C and 0.73 °C. Turning the building 180° from its north-south axis so that the orientation of the tested south bedroom changed to face north resulted in a reduction in solar gain of around 10%. Consequently, the indoor temperature dropped by 0.12 °C. See Figure 9-31a.

As for Case 2, when the room's orientation was changed from southwest to east, an increase in solar gain of up to 26.4% was observed. As a result, the mean indoor temperature increased by nearly 0.4 °C. Changing the current orientation to south and north orientations led to 43.7% and 53.7% reductions in solar gain, respectively, thus reducing the mean indoor temperatures by at least 0.7 °C during a typical summer day. See Figure 9-31b.

The results indicate that the worst-performing orientations (in terms of solar gain) are, from worst to best, east, southeast, west, and southwest, while the best-performing orientations are, for best to worst, north, south, and northwest. These findings are in agreement with those reported in the literature, such as the work of Alosaimi (2023), Alrashed and Asif (2015a), and Ghabra (2018), who indicated that north is the optimal orientation for residential buildings in KSA. Moreover, the results show that the application of shading devices resulted

in a considerable reduction in solar gain for all orientations, thereby improving indoor thermal performance, particularly during overheating seasons.

- **External shading results for the considered orientations**:

The application of external shading devices contributed significantly to reducing solar gain, thus improving both the indoor thermal environment and energy efficiency. The Ta simulation results for both houses revealed that the effect of the tested shading devices was more significant for the west and east orientations, while the north orientation was the least affected in relation to indoor temperature. Comparing Ta results revealed that the greatest reductions—of 0.51 °C in Case 1 and 0.64 °C in Case 2—were achieved for the east orientation after applying the proposed louvers. This resulted in reductions in the rooms' annual cooling loads of 5.6% and 9.6%, respectively (see Figure 9-32).

These findings are in agreement with those reported in Al-Qahtani and Elgizawi (2020), who evaluated the effectiveness of various passive design strategies for a residential building in Riyadh using DesignBuilder simulation software. Al-Qahtani and her colleague indicated that applying louvers resulted in an indoor temperature reduction of 0.5 °C and cooling load savings of up to 8.9%, which corresponds to the figures reported in this analysis.

Overall, the overhang shading recommended by the SBC performed poorly compared to the proposed egg-crate shading and louvers across all orientation scenarios in both rooms. As discussed in Chapter 3, egg-crate shading has a more complex shadow angle than the horizontal overhang, which explains its greater effectiveness in reducing solar gain.

Notably, the proposed louvers outperformed the egg-crate shading device in Case 1. In Case 2, however, the egg-crate shading performed slightly better for certain orientations, while the louvers remained quite competitive for others. Given the differences in window heights, this conflict was not unexpected.

Although egg-crate shading with a projection factor of 0.5 was tested for both rooms, the varying window heights resulted in different shading depths. As a result, a deeper egg-crate shading device of 1.25 m device depth was applied in Case 2 compared to the 0.75 m depth applied in Case 1. The simulation results for the solar gain of both rooms with varying shading depths are provided in Appendix C-E for information purposes and to illustrate the relationship between the devices' depth and solar gain reduction.

The graphs in Figure 9-32 show the annual cooling load predictions for the tested rooms. It is clear that the SBC does not account for solar geometry, thus neglecting the relationship between window orientation and solar altitude and azimuth angles. This becomes particularly evident in the simulation results for the eastern and western orientations, where shading is needed the most, compared to the northern orientation, where shading may be unnecessary.

It is worth noting that a thermal analysis was conducted based on existing surrounding structures without considering the impact of varying local shielding. Despite the influence of local shielding on solar gain and, consequently, window shading requirements, most studies, such as the work of Alaidroos and Krarti (2015), Almushaikah and Almasri (2020), Ahmed and Asif (2020), and Alosaimi (2023), did not consider this aspect, thus suggesting an opportunity for future research. Based on the discussed results, the proposed louver shading type was selected for further analysis.

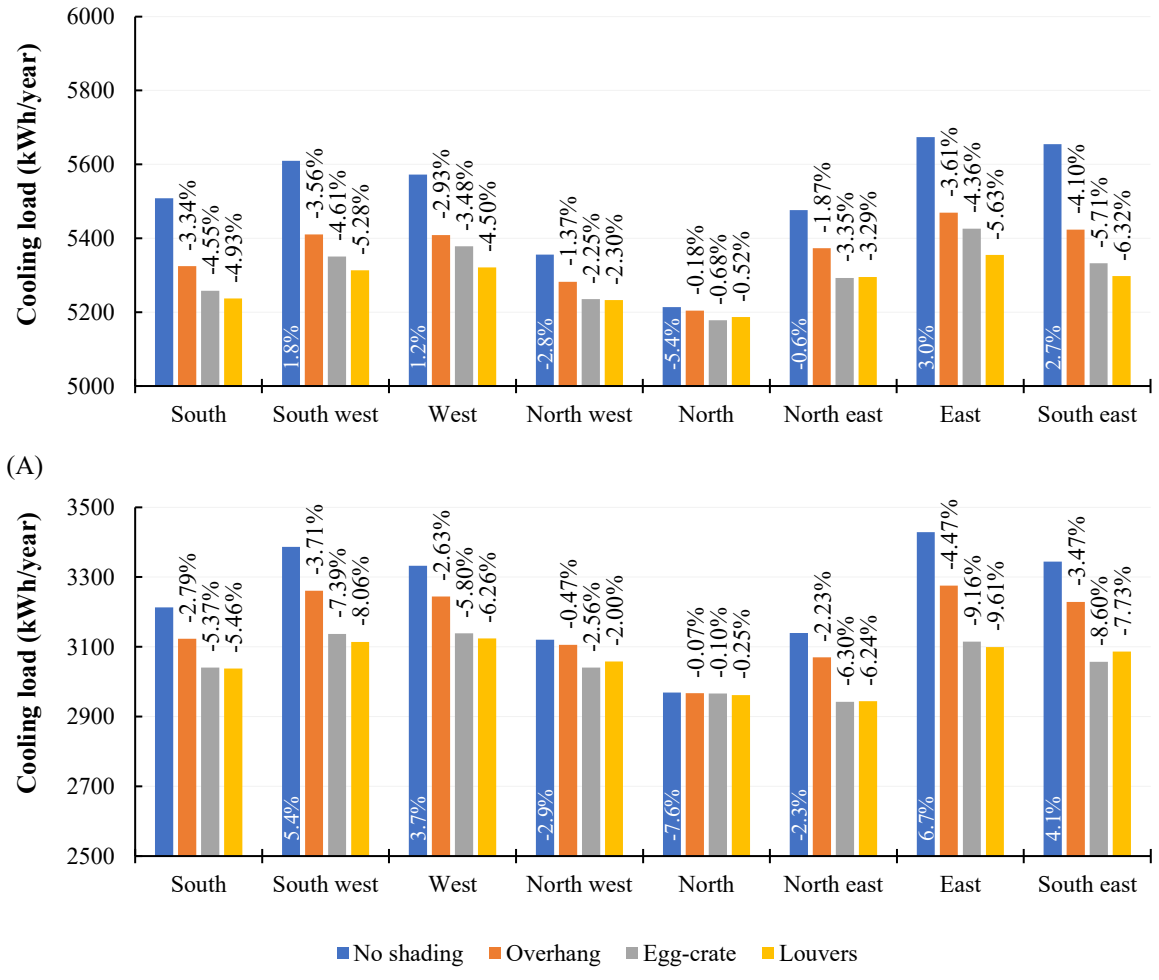


Figure 9-32 Annual cooling load predictions for tested rooms: (A) Simulation results for the bedroom in Case 1; (B) Simulation results for the upper room in Case 2

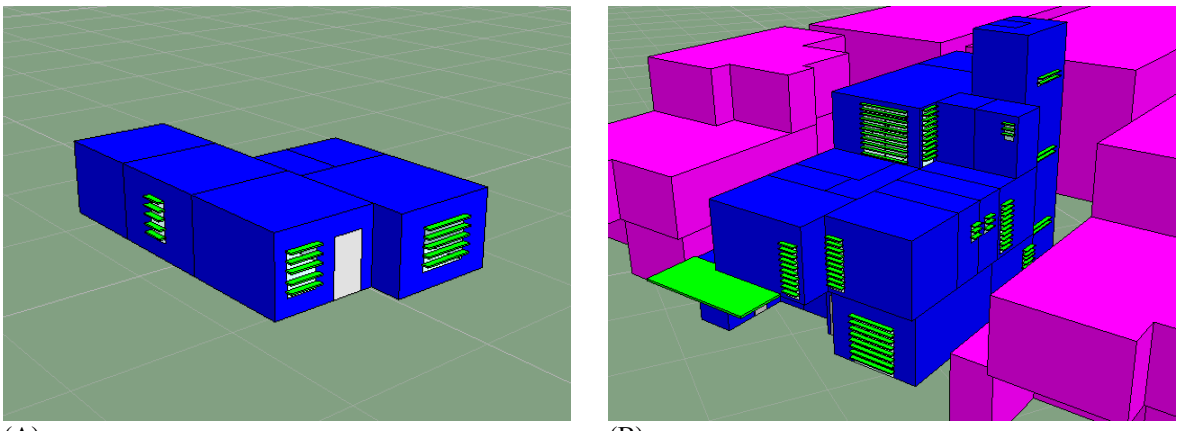
9.6.2 Applying the proposed shading devices to both case study buildings in Riyadh

From the above analysis, it appeared that the proposed louvers achieved better performance than the horizontal overhang with a projection factor of 0.5 recommended by the SBC, particularly during the summer seasons when shading is needed the most. Following this step, a further investigation was conducted to assess the impact of applying the selected shading type integrated with various window glazing types.

The previous analysis suggested that the application of external shading has a positive impact on reducing solar gain, thus improving indoor thermal performance and energy efficiency. Therefore, two different window shading options were proposed and simulated for Case 1 and Case 2 to determine if further improvements could be achieved (see Table 9-4). The simulation results for the selected rooms are presented and discussed below for demonstration purposes. Figure 9-33 shows images of the developed 3D energy model of each house after the implementation of the proposed external shadings.

Table 9-4 Proposed and tested window shading cases

Window cases	Description
Baseline	Existing window glazing and shading
W-shading 2	Standard double-clear window glazing (W2) + proposed louvers
W-shading 3	Double-tinted window glazing (W3) + proposed louvers



(A) (B)

Figure 9-33 Images of the constructed energy models after the implementation of external shading devices: (A) Case Study 1; (B) Case Study 2

9.6.2.1 Air temperature results

To provide a clear indication of the thermal performance of the proposed window shading options, the indoor temperature results for a typical summer day and a typical winter day for the selected rooms were reviewed after applying the selected external shading devices

integrated with various glazing types. The simulation results for indoor air temperature showed that the application of the proposed window shading option (W-sh 3) reduced mean indoor temperatures when compared to the baseline results of each house.

Applying the W-sh 2 window shading option, however, resulted in a minor increase in summer temperatures, particularly in Case 2 (see Figures 9-34 and 9-35). This behaviour can be explained by the relatively high SHGC value of the conventional double-clear window glazing used in W-sh 2 compared to the existing window glazing. In winter, the proposed window shading options led to a reduction in the mean indoor temperatures in both houses. Following this analysis, the frequency of Ta predictions was analysed for the selected rooms before and after the implementation of the proposed window shading options. The results before and after applying natural ventilation are shown in Figures 9-36 and 9-37, respectively.

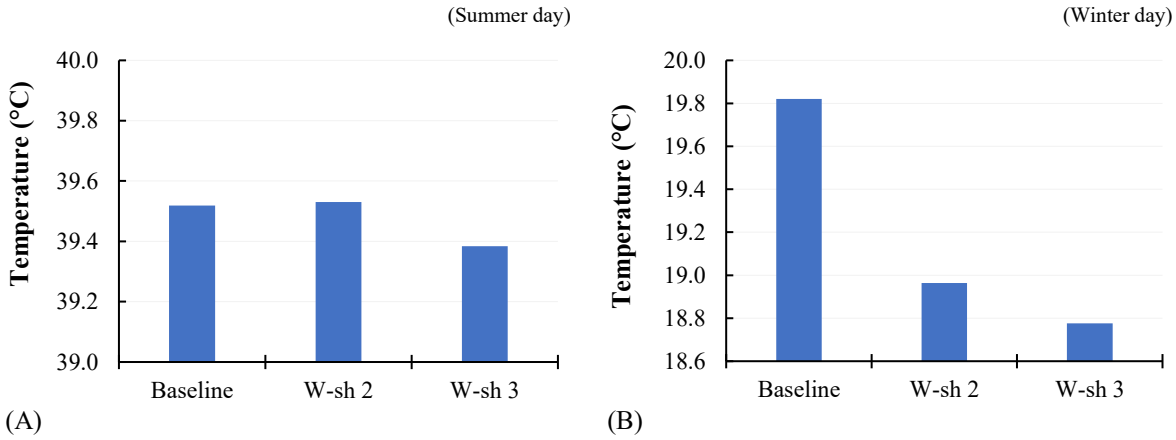


Figure 9-34 Indoor temperature predictions for Case 1 after applying proposed shading devices integrated with different glazing types: (A) Simulation results for a typical summer day; (B) Simulation results for a typical winter day

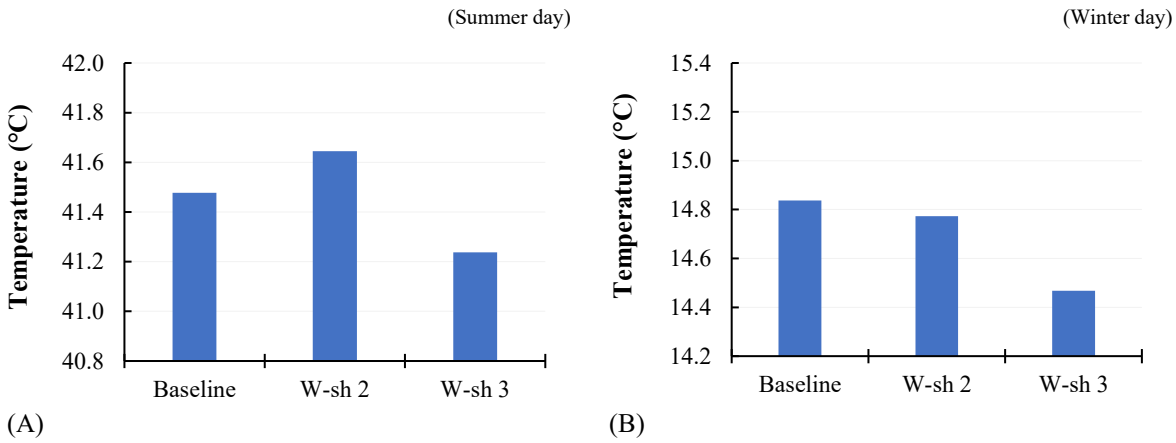


Figure 9-35 Indoor temperature predictions for Case 2 after applying proposed shading devices integrated with different glazing types: (A) Simulation results for a typical summer day; (B) Simulation results for a typical winter day

The analysis revealed that the proposed W-sh 3 decreased annual overheating hour percentages by 1.6% (or 143 hours) in Case 1 and by nearly 1% (or 79 hours) in Case 2 under stable conditions (without NV). When natural ventilation was provided, W-sh 3 reduced overheating hour percentages by 0.6% in both rooms. See Figures 9-36 and 9-37. Notably, an increase in underheating hour percentages (i.e. when indoor Tas were predicted to be lower than 22 °C) of up to 5% (or 440 hours) for Case 1 and 1.3% (or 113 hours) for Case 2 was observed due to reducing solar gain as a result of applying W-sh 3, which could risk increasing heating demands. Consequently, the impact of the proposed window shading options on the thermal load were estimated and analysed for both houses in Riyadh. These are discussed in the following sub section.

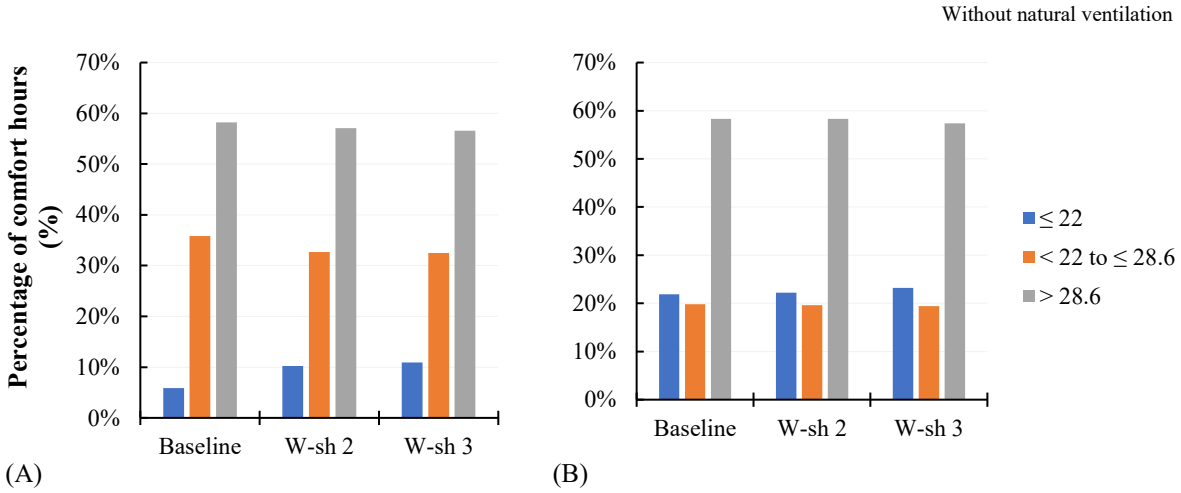


Figure 9-36 Indoor thermal comfort analysis with various window shading cases: (A) Simulation results for Case 1 (bedroom); (B) Simulation results for Case 2 (upper room)

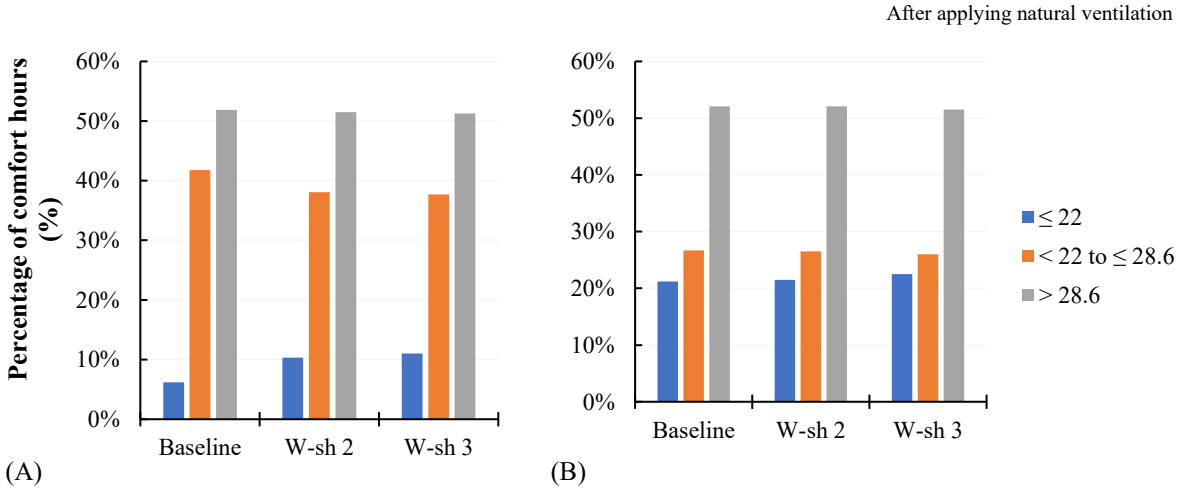


Figure 9-37 Indoor thermal comfort analysis with various window shading cases after applying natural ventilation: (A) Simulation results for Case 1 (bedroom); (B) Simulation results for Case 2 (Room 2)

9.6.2.2 Cooling load

To quantify cooling load savings and improve the overall performance of the selected houses, cooling loads for the selected rooms were estimated with the implementation of various window shading options (see Figure 9-38).

For Case 1, applying W-sh 2 resulted in a slight reduction in the room's total annual cooling load (from 5,347 kWh to 5,225 kWh). However, by applying the double-tinted glazing type along with the proposed louvers (i.e. the W-sh 3 option), the room's cooling load dropped further, to 5,131 kWh, resulting in up to 4% savings compared to the baseline model.

For Case 2, applying W-sh 2 led to a minor increase in the room's total cooling load (from 3,024 kWh to 3,043 kWh). By applying the W-sh 3 option, however, the annual cooling load decreased by 2.8% (to 2,938 kWh/year). This cooling load savings percentage was lower than that achieved in Case 1, which could be due to the relatively lower SHGC assigned to Case 2's baseline model, as previously indicated.

While the proposed W-sh 3 reduced cooling loads in both rooms, it resulted in increased heating loads by 0.48 kWh/m^2 for Case 1 and 1.39 kWh/m^2 for Case 2, a negligible drawback when compared to the total annual rooms' cooling load reductions of 12.38 kWh/m^2 and 3.89 kWh/m^2, respectively. See Appendix C-E for more information.

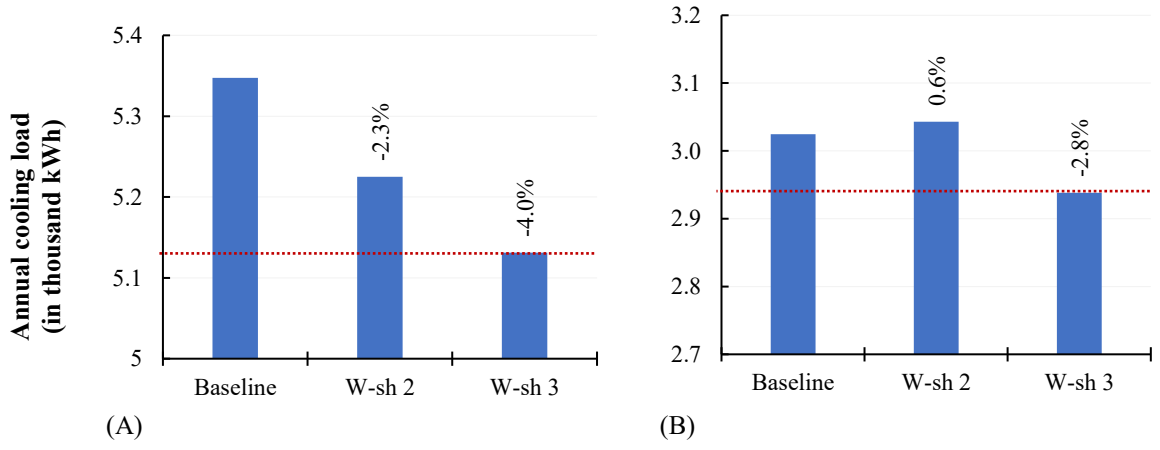


Figure 9-38 Annual cooling load predictions for selected rooms with the integration of various window shading options: (A) Simulation results for Case 1 (bedroom); (B) Simulation results for Case 2 (upper room)

As previously indicated, minimizing solar heat gain in Riyadh's hot and arid climate is a higher priority than heating requirements. However, future studies could investigate the impact of the proposed window shading options on daylight and artificial lighting consumption as increased reliance on artificial lighting could risk offsetting the cooling load

savings achieved through shading. Additionally, exploring the use of movable louvers that adjust based on seasonal solar gain requirements could offer further energy efficiency improvements.

9.6.2.3 Conclusion

Various window shading options were proposed and evaluated in this study. It was found that while the recently developed SBC acknowledges the role of external shading devices on improving the thermal performance and energy efficiency of residential buildings in Riyadh's climate, it does not take into account the various orientation needs of shading. The results discussed in this section suggest that while applying shading devices has a direct impact on improving the indoor thermal environment, further improvement can be achieved by changing the window glazing properties (i.e. SHGC). From this analysis, the proposed W-sh 3 window shading option was selected to improve the indoor thermal environment due to its savings potential regarding solar gain and cooling load in both houses in Riyadh.

9.7 Proposed combination of best building fabric alternatives

This section attempts to compare the thermal performance of the baseline models with the improved energy models. As previously mentioned, the baseline models were constructed based on the existing conditions of each house, which may make improving thermal performance a somewhat challenging task. For example, unconventional double-glazed windows with low SHGC values were applied to the baseline models or thermal insulation was applied to the external walls and roofs. In this section, the proposed building fabric alternatives (from previous sections) were applied to the baseline model of each house to construct the improved building fabric model of each house. Since the previous analysis dealt with each alternative individually, this was done to examine the proposed alternatives in their totality.

The selected building fabric options, discussed earlier in this chapter, were 80 mm EPS insulation applied on the external layer of the external walls, the SBC roof type integrated with white coating, SBC ground floor insulation, a 0.1 ACH air infiltration rate, and a tinted double-glazing window type integrated with external louvers.

9.7.1 Indoor temperatures

To provide a clear indication of the indoor thermal behaviour of the improved energy models, the indoor temperatures were analysed for a typical summer day and a typical winter day for both houses in comparison to the baseline models under no ventilation and natural ventilation

mode. Overall, the indoor thermal conditions of the improved models were more stable and demonstrated less variance during both seasons compared to the baseline models (see Figures 9-39 and 9-40).

The difference between the minimum and maximum temperatures for the considered rooms for a typical summer day was reduced by approximately 0.8 °C in both rooms (from 1.58 °C to 0.83 °C in Case 1, and from 1.9 °C to 1.06 °C in Case 2). When natural ventilation was introduced, the indoor temperature predictions for the summer showed that the improved models consistently remained lower temperatures than those of the baseline models, with a daily mean temperature reduction of around 1.7 °C for both rooms (see Figure 9-41).

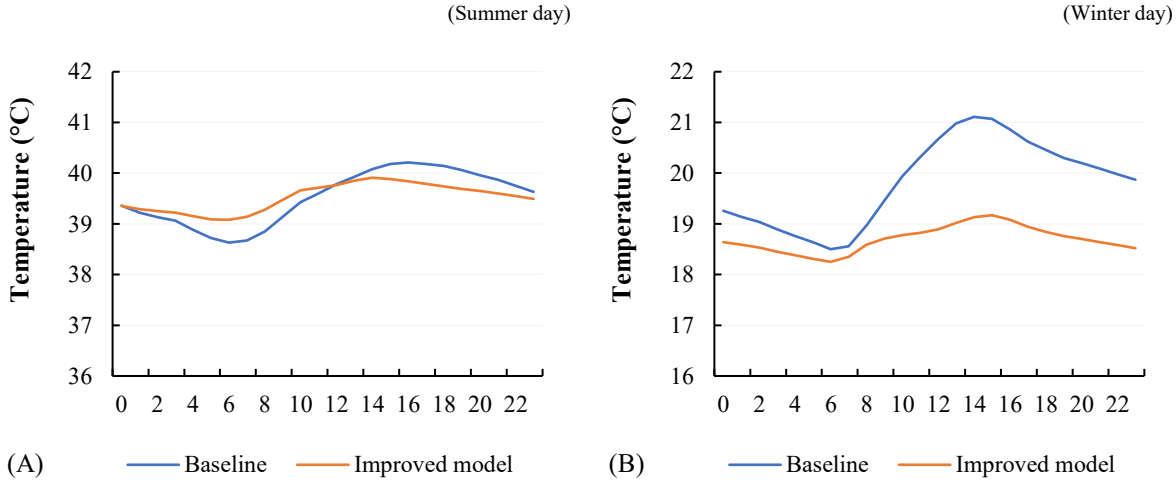


Figure 9-39 Indoor air temperature predictions for Case 1 (bedroom) after the implementation of the proposed building fabric alternatives: (A) Simulation results for a typical summer day; (B) Simulation results for a typical winter day

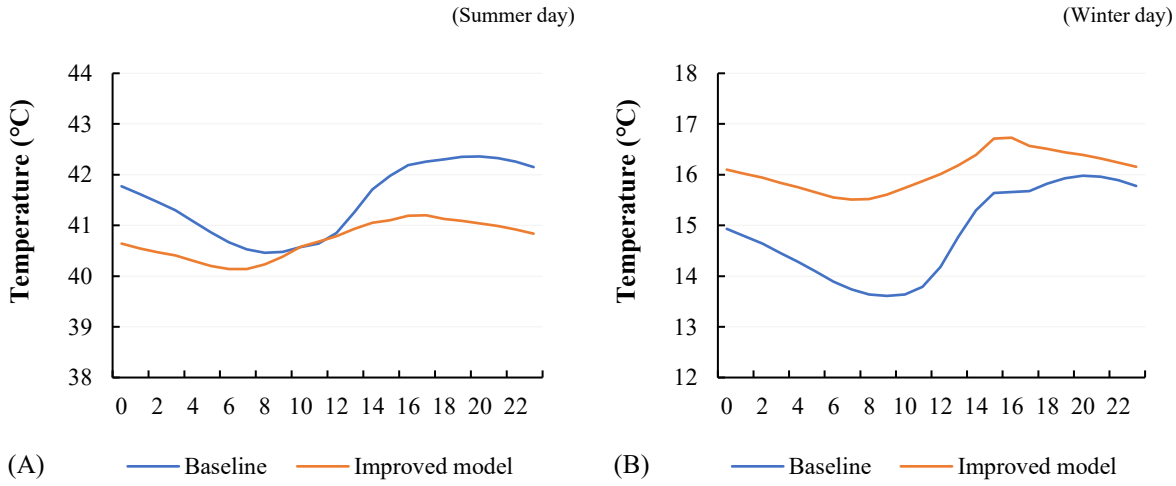


Figure 9-40 Indoor air temperature predictions for Case 2 (upper room) after the implementation of the proposed building fabric alternatives: (A) Simulation results for a typical summer day; (B) Simulation results for a typical winter day

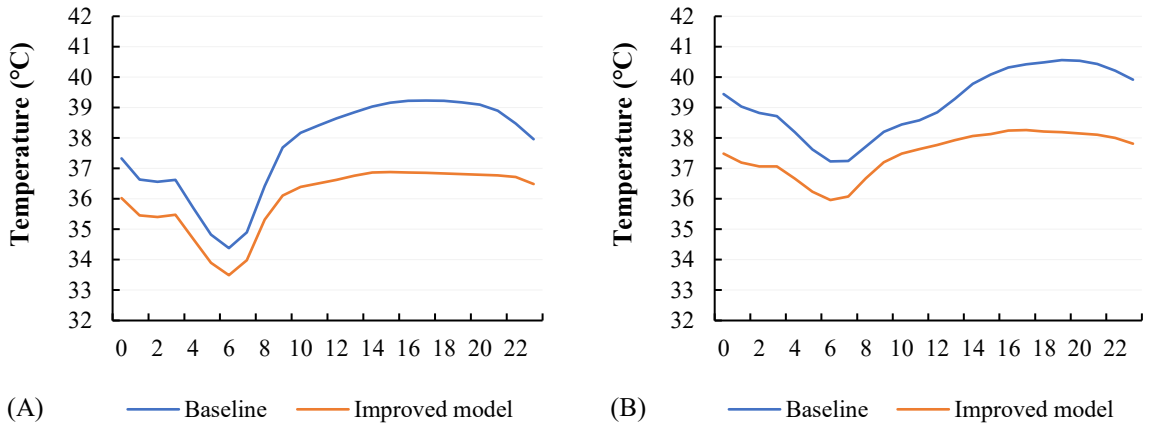


Figure 9-41 Indoor air temperature predictions for selected rooms after applying natural ventilation during a typical summer day: (A) Simulation results for Case 1 (bedroom); (B) Simulation results for Case 2 (upper room)

In winter, the variance in Tas was reduced by 1.7 °C in Case 1 (from 2.6 °C to 0.9 °C) and by 1.15 °C in Case 2 (from 2.37 °C to 1.22 °C). An increase in mean Ta of around 1.2 °C was observed in Case 2 due to the restricted heat dissipation in the improved models that occurred as a result of improving the envelope's resistance to heat flow. Consequently, the built-up heat inside the room caused the indoor temperature to increase. In contrast, the mean Ta decreased in the tested south-facing room in Case 1 compared to the baseline results. For more information, see Appendix D-A.

In addition, the frequency of indoor thermal conditions was reviewed and analysed for both houses before and after the implementation of the selected building fabric alternatives (see Figure 9-42). Compared to the baseline models, an increase in the percentage of underheating hours was observed in both houses as a result of applying these alternatives. This resulted in a reduction in the percentage of comfort hours, particularly in Case 1, in which the percentage of comfort hours (annual) decreased by up to 9.1% (from 35.8% to 26.7%, as seen in Figure 9-42a) compared to the baseline model. This could be attributed to the applied measures, such as ground insulation and window shading, which reduced desired heat gain in winter.

As indicated in the graphs in Figures 9-42 and 9-43, the applied building fabric enhancement strategies contributed to a reduction in overheating hours, and thus the cooling load, in both houses. Under natural ventilation mode, the results shown in Figure 9-43 indicate that applying the proposed building fabric alternatives contributed positively to reducing the percentages of overheating periods from 51.9% (or 4,550 hours) to 46.3% (or 4,055 hours) for Case 1 and from 52.1% (or 4,567 hours) to 48.1% (or 4,210 hours) for Case 2 compared with the baseline results of each house.

Given the previously discussed role of the proposed ventilation strategy in cooling down the indoor thermal mass and flushing out internal built-up heat, the reduction in overheating hours achieved by allowing natural ventilation was not unexpected. These results have motivated the author of this thesis to conduct further analysis to assess the impact of a hybrid cooling mode (i.e. applying natural ventilation when outdoor conditions are favourable and below indoor temperatures for air-conditioned models) when the proposed fabric enhancement strategies are not sufficient to satisfy indoor thermal comfort requirements. The results of these simulations are presented later in this chapter.

An analysis of heat gain through the building fabric after the implementation of the proposed alternatives is discussed in the following section. Subsequent sections will address the simulation results of cooling load, energy consumption, and carbon emissions for both the 3D-printed house and the conventional house.

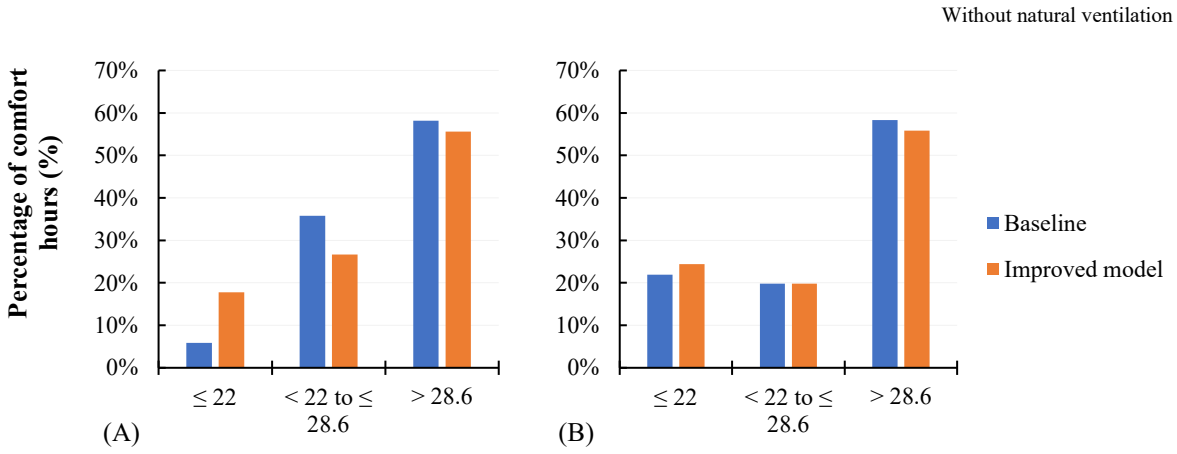


Figure 9-42 Indoor thermal comfort analysis before and after applying the proposed building enhancement alternatives: (A) Case 1 (bedroom); (B) Case 2 (upper room)

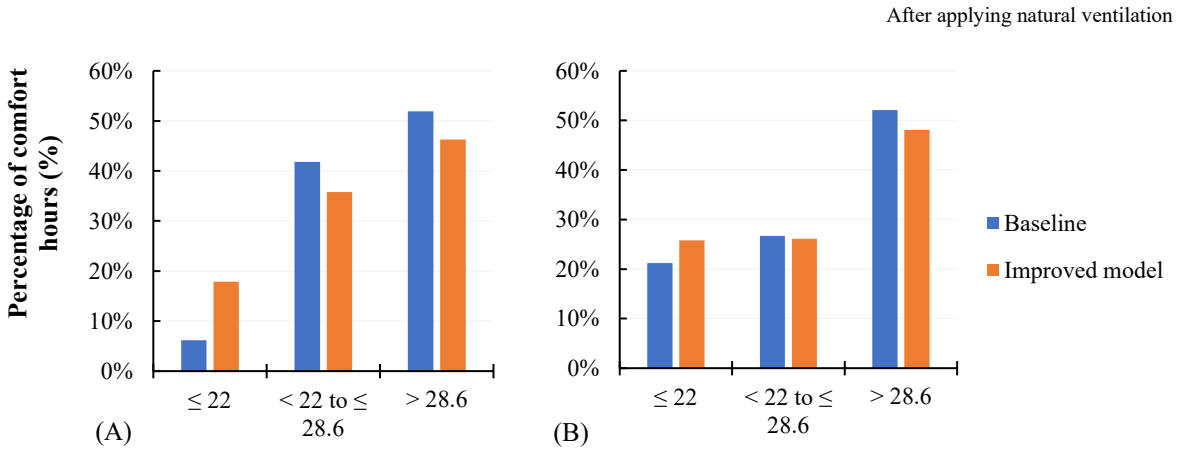


Figure 9-43 Indoor thermal comfort analysis before and after applying the proposed building enhancement alternatives with the implementation of natural ventilation: (A) Case 1 (bedroom); (B) Case 2 (upper room)

9.7.2 Heat gain

This section presents and compares the simulation results of heat gains and losses through the building fabric components for the improved energy model of the selected case study buildings to the corresponding baseline models during a typical summer day and a typical winter day (see Figure 9-44). The results indicate that applying the proposed building fabric alternatives reduced the total summer heat gain by 64.4% for Case 1 and by 41.6% for Case 2, thereby reducing cooling demands (discussed in more detail in the following section). According to the results, the net heat gain/loss through the building fabric components was reduced in Case 1 from 0.56 kWh to 0.11 kWh, and in Case 2 from 9 kWh to 5.6 kWh. This reduction is attributed to decreased conduction gain through the external walls, roof, and windows, as well as reduced solar and infiltration gains. Refer to Appendix D-B for more information.

Additionally, the graphs in Figure 9-44 demonstrate that while applying these alternatives contributed to reducing heat loss by up to 74.7% for Case 1 and 55.1% for Case 2 during a typical winter day, they led to a reduction in winter heat gain, which could slightly increase heating requirements. Net heat gain/loss through the building fabric components was reduced in Case 1 from 2.3 kWh to −0.02 kWh, and in Case 2 from −5.86 kWh to −15.85 kWh. This explains the increased underheating hours discussed in the previous section. Nevertheless, given the significant share of cooling in total energy consumption and CO_2 emissions (see Section 8.5), reducing the cooling load is more beneficial in this climate.

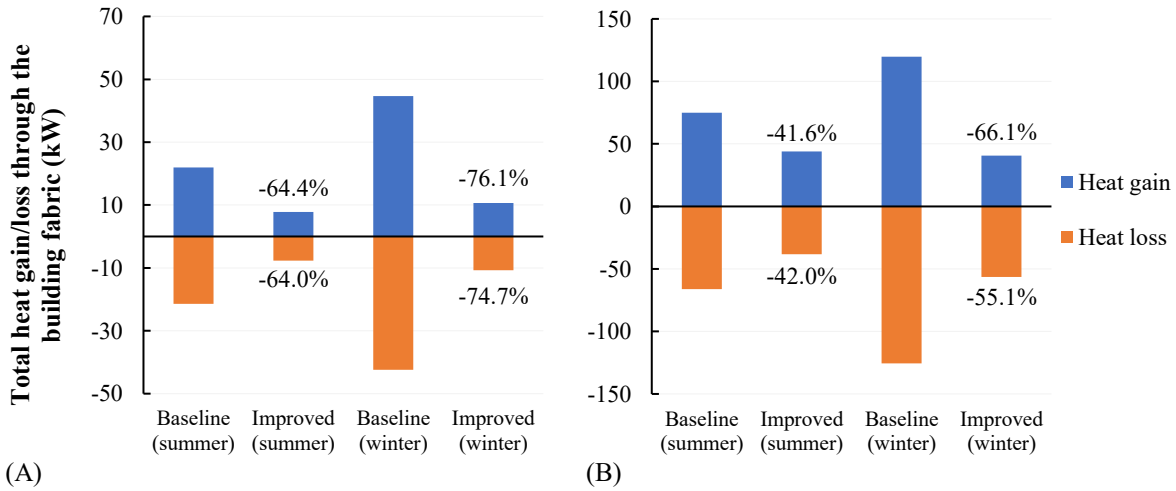


Figure 9-44 A comparison of external heat gain (external walls, roof, ground, infiltration, and windows) between baseline and improved model for a typical summer and a typical winter day (in kW): (A) Simulation results for Case Study 1 (3D-printed house); (B) Simulation results for Case Study 2 (conventional house)

9.7.3 Cooling load

The graphs in Figure 9-45 illustrate the individual and integrated application of the proposed alternatives for the 3D-printed house (Case 1) and the conventional house (Case 2) in Riyadh. For Case 1, the proposed external wall construction, roof type, ground floor insulation, and window shading resulted in a total cooling load savings of approximately 2.4%, 18.9%, 33.6%, and 2.7%, respectively. For Case 2, the savings were about 10.9%, 9.4%, 32.9%, and 0.9%, respectively.

Integrating all design alternatives led to considerable savings in cooling consumption, reducing the total annual cooling load by up to 68.5% for the 3D-printed house (from 17,778.7 kWh in the baseline model to 5,606.2 kWh in the improved model) and by up to 57.7% for the conventional house (from 61,901.1 kWh for the baseline model to 26,186.1 kWh for the improved model). This was due to reducing the total external heat gain from 17,737 kWh (or 227 kWh/m^2) to 5,434 kWh (or 69 kWh/m^2) for Case 1 and from 59,664 kWh (or 134 kWh/m^2) to 24,524 kWh (or 55 kWh/m^2) for Case 2.

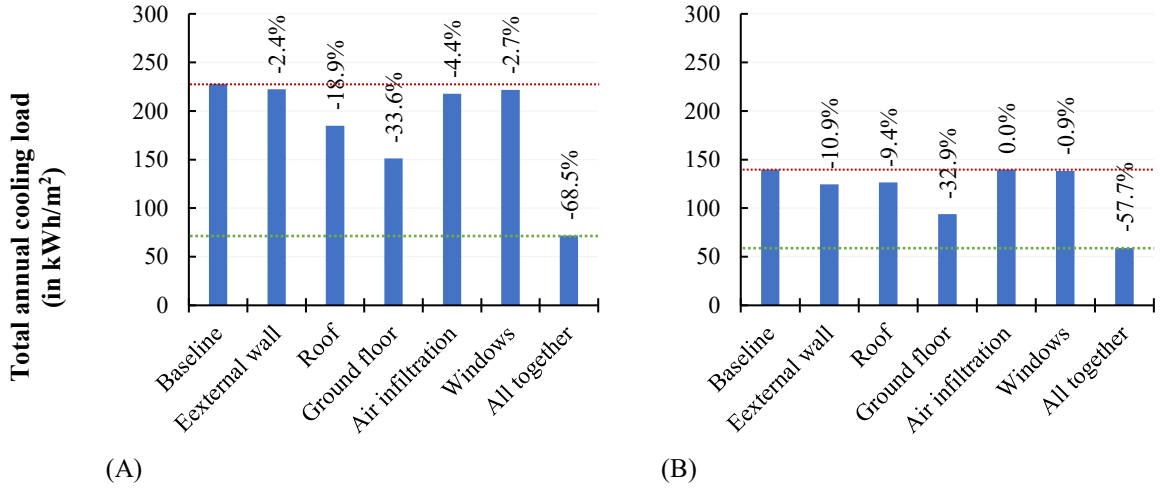


Figure 9-45 Total annual cooling load predictions for residential buildings in Riyadh: (A) Case 1 (3D-printed house); (B) Case 2 (conventional house)

The graphs in Figure 9-46 compare the total monthly cooling load predictions for Case 1 and Case 2 before and after applying the proposed building fabric enhancement measures for each house. The analysis reveals that the greatest reductions in cooling load were achieved during the overheating seasons (i.e. during peak load demand).

According to the graph, the maximum savings occurred in August, with cooling load reductions of 67.2% (−2,235 kWh) for Case 1 and 57.2% (−6,780 kWh) for Case 2. This can be attributed to the effectiveness of the proposed building fabric alternatives in reducing

thermal transmission between indoor and outdoor environments under the extreme outdoor conditions.

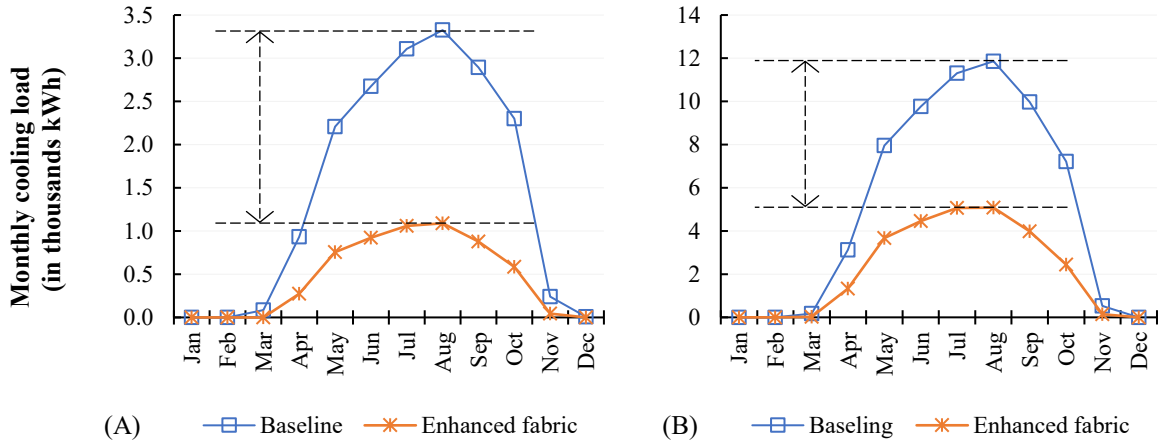


Figure 9-46 A comparison of monthly cooling loads between baseline and improved models for both houses in Riyadh: (A) Case 1 (3D-printed house); (B) Case 2 (conventional house)

Following this analysis, the next step was to estimate the potential for further cooling load savings by applying natural ventilation, whenever possible, along with the implementation of the selected building fabric alternatives.

The mixed-mode ventilation strategy adopted in this study followed the control scheme discussed earlier in Section 5.9. In summary, natural ventilation was enabled when outdoor temperature fell below the indoor temperature and remained lower than 28.6 °C—the upper comfort limit identified for Riyadh—allowing windows to be opened to provide cooling. When indoor thermal comfort could not be maintained by passive means, the mechanical cooling system was activated.

This control scheme was implemented in the models using the window-opening and AC operation profiles described in Figure 5-18. The cooling load was predicted for both houses after applying the proposed mixed-mode ventilation strategy along with the implementation of the selected building fabric alternatives.

The results suggest that applying natural ventilation positively contributed to further enhancing the thermal performance of the buildings. As demonstrated in Table 9-5, an additional reduction in cooling load of approximately 10% for both houses was achieved by applying the proposed mixed-mode ventilation strategy. This reduced the total annual cooling load to 3,995.9 kWh (or 51.2 kWh/m^2) for Case 1 and to 20,207.8 kWh (or 45.6 kWh/m^2) for Case 2, resulting in total reductions of up to 77.5% and 67.4%, respectively, in comparison with the corresponding baseline models.

To better understand the effect of the proposed mixed-mode ventilation strategy, the graphs in Appendix D-C show that the greatest savings occurred during moderate seasons (especially between October and April), which was expected due to the extremely high temperatures during summer (between May and September). For the subsequent analysis, the final model incorporating the proposed mixed-mode ventilation strategy will be referred to as the 'improved model' and will be compared with the baseline results of each house.

Table 9-5 Summary of thermal analysis results of proposed combination of the building fabric and proposed mix-mode ventilation strategy in comparison with baseline models

		Annual cooling load (kWh)	Annual cooling load (kWh/m^2)	Reduction of cooling load (%)
3D-printed house (Case 1)	Baseline	17,778.7	227.9	-
	Enhancing building fabric	5,606.2	71.8	68.5%
	Improved model	3,995.9	51.2	77.5%
Conventional house (Case 2)	Baseline	61,901.1	139.7	-
	Enhancing building fabric	26,186.1	59.1	57.7%
	Improved model	20,207.8	45.6	67.4%

The proposed ventilation strategy contributed to flushing out the accumulated internal heat, thereby reducing overheating hours (i.e. the number of hours throughout the year when the active cooling system is needed to achieve indoor thermal comfort). This, in turn, along with the implementation of the proposed building fabric improvement measures, led to substantial savings in cooling demand.

Figure 9-47 demonstrates that the frequency of total cooling hours was reduced to 3,794 hours for Case 1 and to 4,265 hours for Case 2 compared to the baseline results discussed in Section 8.4. This is mainly due to increasing the frequency of comfort hours from 2,602 hours to 4,105 hours for Case 1 and from 1,012 hours to 2,927 hours for Case 2. Although heating requirements in this climate are minimal, a minor increase in the frequency of heating hours was noticed for Case 1.

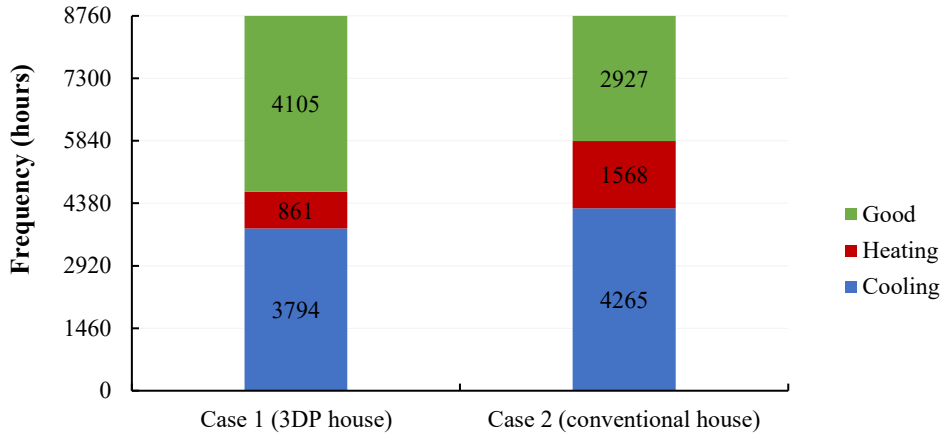


Figure 9-47 Predicted cooling and heating hours for the improved models (after applying proposed building fabric enhancements and mixed-mode ventilation strategy) of both houses in Riyadh

9.7.4 Energy consumption and CO_2 emissions

The IES-VE simulation tool was used to estimate the total energy consumption and CO_2 emissions for the 3D-printed house and the conventional house after applying the proposed building fabric enhancement measures along with the implementation of natural ventilation (i.e. the improved models).

The reductions achieved were calculated and reviewed for both houses in Riyadh. The graphs in Figure 9-48 illustrate the monthly energy consumption and CO_2 emissions in comparison with the baseline model of Case 1 and Case 2. The graphs show that most of the energy savings occurred during the overheating season due to the extreme outdoor conditions.

The predicted energy performance for both houses revealed that total annual energy consumptions were reduced from 14,962 kWh (or 191.8 kWh/m^2) to 8,148.5 kWh (or 104.4 kWh/m^2) for Case 1 and from 54,768.5 kWh (or 123.6 kWh/m^2) to 36,099.6 kWh (or 81.4 kWh/m^2) for Case 2. This resulted in a total reduction in CO_2 emissions from 9,187 kgCO_2 (or 117.78 kgCO_2/m^2) to 5,004 kgCO_2 (or 64.1 kgCO_2/m^2) for Case 1 and from 33,628 kgCO_2 (or 75.9 kgCO_2/m^2) to 22,165 kgCO_2 (or 50 kgCO_2/m^2) for Case 2.

Accordingly, the annual savings in energy consumption, and consequently CO_2 emissions, were 45.5% for Case 1 and nearly 34% for Case 2 compared with the baseline model of each house. Table 9-6 summarizes the total energy consumption and carbon emissions for both houses before and after applying the proposed enhancement measures.

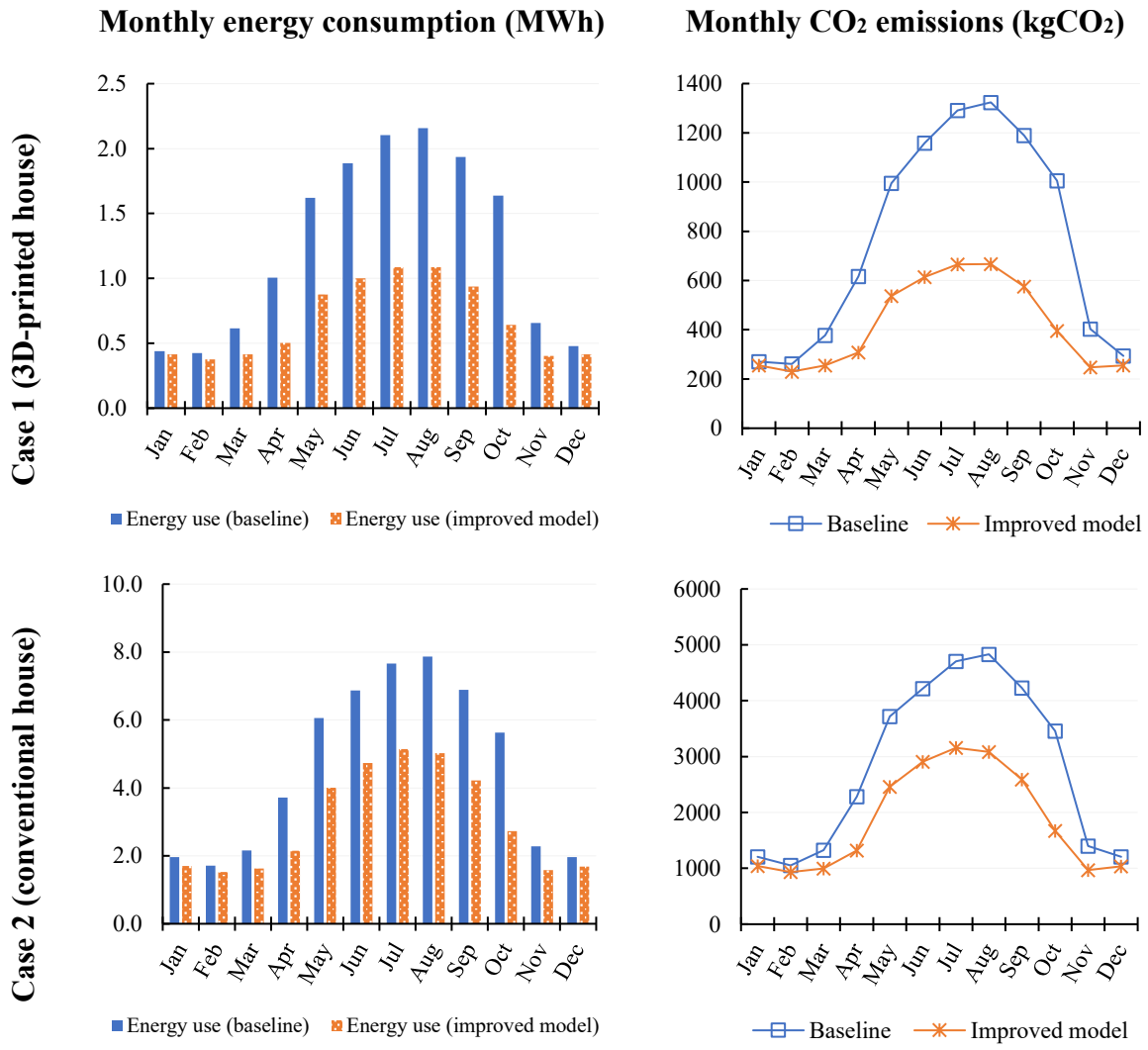


Figure 9-48 Predicted energy consumption and CO_2 emissions for Case Study 1 and Case Study 2

Table 9-6 Summary of baseline, improved model, and the proposed ventilation strategy

		Baseline	Improved model	% reduction
Case 1	Energy (kWh/m^2)	191.82	104.47	45.5%
	CO_2 emissions (kgCO_2/m^2)	117.78	64.15	45.5%
Case 2	Energy (kWh/m^2)	123.63	81.49	34.1%
	CO_2 emissions (kgCO_2/m^2)	75.91	50.03	34.1%

Overall, Case 2 achieved lower energy savings (34% or 42 kWh/m^2) than Case 1 (45.5% or 87.3 kWh/m^2) due to the relatively lower external heat gain sources per unit volume in Case 2 compared to Case 1 (see Section 8.3), which minimized the effect of the applied improvement measures. However, Case 2 yielded more efficiency than Case 1. This could be attributed to a number of factors, including the surrounding environment, the building's design, and differences in the construction material properties of the two construction methods.

These findings agree with Alaidroos and Krarti (2015), Almushaikah and Almasri (2020), Alosaimi (2023), Alrashed (2015), Alyami (2022), and Krarti et al. (2017), who indicated a possible reduction in energy consumption ranging between 37% and 62% for residential buildings in Riyadh City. However, the savings achieved in the current study are slightly lower than the mean savings reported in the literature (see Figure 9-49).

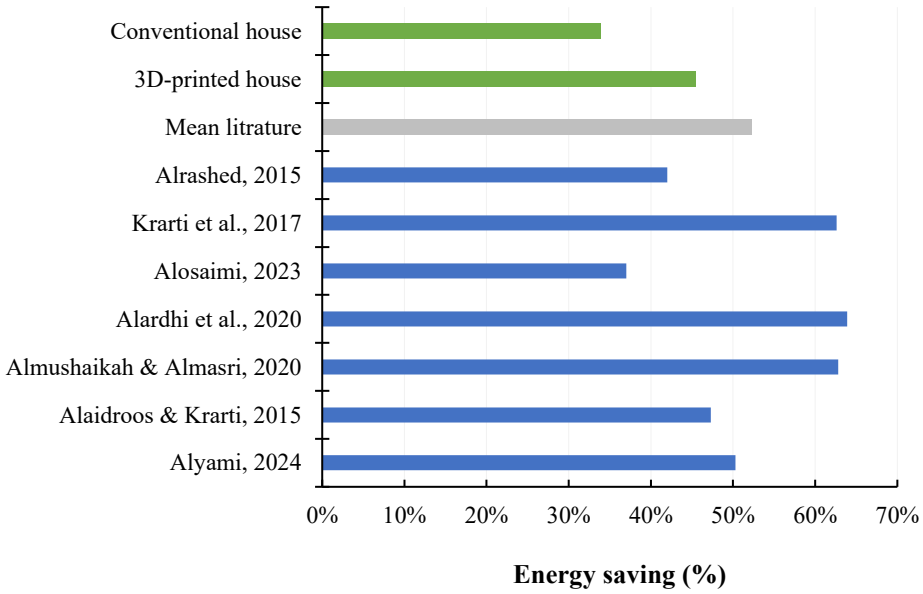


Figure 9-49 Potential energy savings for residential buildings in Riyadh, KSA, in comparison with the estimated savings in this study

This could be attributed to the more efficient baseline models investigated in the current thesis compared to previous research. For example, Almushaikah and Almasri (2020)'s and Alaidroos and Krarti (2015)'s models lacked thermal insulation and applied conventional window types with higher SHGC, Alardhi et al. (2020) applied a significantly lower cooling setpoint temperature of 18 °C, and Alyami and Omer (2021) assumed high air infiltration rates of 1.0ACH for their baseline models.

Moreover, this study focused mainly on assessing the impact of improving the buildings' thermal performance by applying passive cooling techniques learned from vernacular architecture and modern building technology. Thus, investigating the role of improving the efficiency of household appliances, lighting, and HVAC systems, as in the studies carried out by Almushaikah and Almasri (2020) and Krarti et al. (2017), was outside the scope for this thesis. According to Almushaikah and Almasri (2020), more than 30% energy savings can be achieved by improving the efficiency of the HVAC system only. This explains the high savings achieved in the aforementioned studies.

9.8 Summary

In this chapter, potential improvements to the indoor thermal performance were investigated using the IES-VE energy simulation software. Various proposed building fabric alternatives, including external walls, roofs, ground floors, and windows, were simulated for the selected case study buildings in Riyadh.

Indoor air temperatures for a typical summer day and a typical winter day, along with the annual cooling loads, were estimated by applying each improvement measure separately. According to the IES-VE simulation results, the best-performing cases of proposed building fabric alternatives were selected and simulated for each house to evaluate their thermal performance and to determine improvements in overall energy efficiency and carbon emissions.

Applying the proposed combinations of building fabric alternatives could achieve potential cooling load reductions of 68.5% for Case 1 and 57.7% for Case 2. As a result, estimated annual cooling demand intensity dropped to 71.8 kWh/m^2 for Case 1 and to nearly 59.4 kWh/m^2 for Case 2.

Moreover, the study also assessed the impact of applying a natural ventilation strategy to enhance the indoor thermal environment and achieve a further reduction in cooling load. The simulation results indicated that allowing natural ventilation, when desirable, further reduced the cooling load by about 10% for both houses (equivalent to 20.6 kWh/m^2/year for Case 1 and 13.5 kWh/m^2/year for Case 2), thus achieving total savings of 77.5% for Case 1 and 67.4% for Case 2 when compared to the baseline models.

The cooling reduction achieved in this study satisfied the research objective of improving the thermal performance of modern residential buildings in Saudi Arabia built with different construction methods (3D concrete printing and conventional construction). This final total reduction in cooling demand contributed to total energy conservation and CO_2 reductions of up to 45.5% in Case Study 1 and nearly 34% in Case Study 2.

CHAPTER 10

CONCLUSION

- Introduction
- Research conclusions
- Research contributions
- Research limitations
- Recommendations for future research

Chapter 10: CONCLUSION

10.1 Introduction

The Kingdom of Saudi Arabia faces severe energy and environmental challenges; it is among the world's highest-ranked countries for per capita energy consumption and CO_2 emissions, and domestic energy demand is on a steep rise due to rapid population growth. To fulfil the national reform plan, Saudi Vision 2030, and meet international obligations under the 2015 Paris Agreement, reducing national energy demand has become a major priority. The building sector is a major contributor, consuming about 75% of the country's entire electricity production, with residential buildings alone being responsible for a significant share of this consumption.

The energy demands of buildings are highly impacted by local climate conditions. Due to the extreme climate of Saudi Arabia, particularly during the overheating season, contemporary buildings rely heavily on energy-intensive active cooling systems to meet indoor thermal comfort requirements, accounting for approximately 70% of total household energy consumption.

Moreover, the rapidly increasing housing demand in Saudi Arabia, driven by factors such as significant population growth, has necessitated the adoption of advanced, modern construction methods—most notably, three-dimensional concrete printing (3DCP) technology—within the Saudi construction industry to enable the rapid delivery of a larger number of homes. However, the thermal performance of such constructions under the country's severe hot and arid climate conditions remains largely untested.

Given the high energy consumption of Saudi dwellings, particularly for space cooling, this thesis has aimed to learn from vernacular architecture and modern building technology to propose and test more sustainable solutions for residential buildings (through computer simulations) to foster a sustainable future in Saudi Arabia. For the purpose of this research, Riyadh City was selected as the study location. It is noteworthy that Riyadh is located in Zone 1, the country's largest and most representative climate zone.

The limitations of contemporary construction materials and methods in addressing rapidly growing housing demand led to the selection of two existing residential buildings, constructed with different construction methods, to carry out this research. As a result, a 3D-

printed house and a representative conventional house were identified within the city of Riyadh to act as case study buildings investigated in this research.

Field monitoring of environmental parameters in both case study buildings was carried out during the summer of 2022. The collected data were analysed and used to validate the constructed IES models for more in-depth analysis. The following conclusions summarize the key findings of the research to achieve the research objectives and satisfy the research aim.

10.2 Research conclusions

This study aimed to evaluate the indoor thermal performance of residential buildings in KSA constructed with different construction methods (i.e. 3D concrete printing and conventional construction methods) and to propose various solutions for improvements. It focused primarily on reducing demands for active cooling systems. Existing design strategies and construction materials were reviewed for each house to evaluate their current performance and identify suitable improvement measures. The following conclusions provide a summary of the research outcomes, addressing the research questions and demonstrating how the objectives were met.

10.2.1 How can the performance of the selected cases be effectively simulated while ensuring that the predicted outcomes accurately reflect the actual physical conditions?

Modelling the two selected case studies for simulations necessitated the use of IES-VE simulation software as the study's main investigation method. As discussed in Chapter 7, a three-dimensional energy model was constructed for each case study building according to their existing conditions and characteristics. To increase confidence in the constructed models and ensure that predicted performance mimicked actual performance, the simulation results for indoor air temperatures were compared against actual field measurements at hourly intervals. Analysis of the produced errors between simulation predictions and monitored data indicated that the simulations were relatively satisfactory in reflecting the actual thermal behaviour of the houses. Hence, it was safe to conclude that the constructed IES-VE models could satisfactorily simulate the selected houses in Riyadh, KSA.

10.2.2 What are the current thermal performance and energy consumption rates for a 3D concrete house and a conventionally constructed house in the hot climate of Riyadh, KSA?

Upon validating the two IES-VE energy models (by comparing field measurements with predicted results), a whole-year simulation was conducted for each model according to its existing characteristics. To provide insight into the thermal performance of both

constructions, simulations were conducted in free-running mode as this approach allows for the investigation of the building itself without the influence of external interventions.

As discussed in Chapter 8, it was predicted that the indoor temperatures from the selected rooms would fall above the identified cooling setpoint temperatures for more than 60% of the year. This indicates high cooling requirements in both houses, whereas heating requirements were relatively low, particularly for the 3D-printed house (see Section 8.2).

While both houses demonstrated stable indoor thermal conditions compared to the highly fluctuating outdoor temperatures, the 3D-printed house showed a higher percentage of comfort hours, reaching up to nearly 36%, compared to the conventional house, which had a maximum of 23% comfort hours. The greater comfort hours percentages in the 3D-printed house were due to its relatively low underheating hours (i.e. the high temperatures in the winter) compared to the conventional house. A potential justification for this behaviour is the exposure of the tested rooms in the 3D-printed house to the ground, while the tested rooms in Case 2 were located on higher levels with limited heat gain sources in the winter. Nevertheless, both houses had nearly similar cooling hours frequency: 5,940 hours for Case 1 and 5,921 hours for Case 2.

Further simulations were conducted to predict the annual energy consumption of the baseline models in airconditioned mode. To ensure the consistency of the results, a typical occupancy profile was adopted from the relevant literature. The setpoint temperatures for summer and winter were specified in the two models as 26 °C and 20 °C, respectively.

The simulation results indicate that the baseline total energy consumptions were 14,962 kWh (191 kWh/m^2) for the 3D-printed house and 54,769 kWh (123 kWh/m^2) for the conventionally constructed house. The largest share of total consumed energy in both houses, a rate of more than 60%, is attributed to their cooling requirements. The baseline EUI results suggest that the conventionally constructed house was more efficient than the 3D-printed house by approximately 35%. Considering variations in building design, construction methods, and material properties, this finding could also be attributed to the fact that the 3D-printed house had poor insulation levels for the roof, a high form-to-floor ratio, and a lack of surrounding buildings, all of which contributed to the high energy demand for space cooling per square meter.

10.2.3 What is the role of the building envelope in improving the thermal behaviour of KSA's modern houses?

As the primary barrier between indoor and outdoor environments, the building envelope plays a crucial role in determining the indoor thermal conditions and overall thermal performance of a building. In this study, a heat transfer analysis through the building envelope components was conducted for both houses using the developed energy model. For demonstration purposes, the results were reviewed and discussed for a typical summer day and a typical winter day.

The analysis provided insight into the thermal performance of the baseline envelope of each house (i.e. 3D-printed and conventional house) and its role in affecting indoor thermal environments, while also facilitating a comparison between the two distinct building fabrics. It also enabled the identification of major contributors to heat gain/loss through various components of the building envelope for each house (see Section 8.3).

Following this analysis, the inner surface temperatures of the external walls were predicted with and without existing insulation. The results revealed that the existing insulation contributed significantly to stabilizing the inner surface temperatures of the walls, thereby reducing indoor temperature fluctuation. Building on these findings, the simulation results indicated that over 70% of the total predicted cooling load was attributed to external heat gain sources (e.g. external conduction, solar, and infiltration gain), highlighting the critical role of the building envelope in influencing the dynamic interaction between indoor and outdoor environments.

The results suggest that improving the characteristics of the building envelope (e.g. mitigating heat gain/loss through the building envelope components) is crucial to ensure indoor thermal comfort, improve energy efficiency, and minimize the environmental impact of building operations, particularly in hot arid climates. The outcome of this analysis contributed to the development of various strategies to regulate the indoor environment and improve the thermal performance of both case study buildings.

10.2.4 How can design strategies learned from vernacular architecture and modern sustainable building technology improve the thermal performance of residential buildings in Riyadh, KSA?

As indicated earlier, a significant share of the total energy consumption and associated CO_2 emissions is attributed to the indoor cooling requirements needed in severe outdoor climate

conditions, particularly in the overheating month. This research examined how thermal performance of residential buildings in Riyadh can be improved by integrating design strategies and measures learned from vernacular architecture and modern sustainable building technology.

The Saudi Arabia context was discussed at various levels, including a background review, typical building construction, vernacular buildings, and recent initiatives and building standards that were developed to improve the energy efficiency of the building sector. This was followed by a review of applicable passive cooling strategies in hot arid regions and an analysis of the climate features of Riyadh, the study location.

Focusing on the selected case study buildings, the simulation results of the baseline models (discussed in Chapter 8) revealed significant challenges related to thermal performance and energy consumption rates of the baseline models in the climate of Riyadh, which assisted in identifying sources of heat gain through the building envelope components for potential improvement. After identifying the key parameters contributing to the buildings' thermal performance, it was possible to develop various solutions to improve indoor thermal conditions and reduce the cooling consumption for the selected cases in the climate context of Riyadh.

This research identified and tested various passive cooling techniques derived from local building standards, modern applications and trends, and basic vernacular solutions. The selected strategies are briefly discussed in Section 5.9 and are evaluated in Sections 9.2 to 9.6.

The simulation results showed that improving the external walls, roof, ground floor, air infiltration, and window shading of the 3D-printed house can result in up to 2.4%, 18.2%, 33.6%, 4.4%, and 2.7% savings, respectively, in the total annual cooling load of the house. The savings for the conventional house were 10.9%, 8.9%, 32.9%, 0%, and 0.9%, respectively.

Notably, for both houses, the greatest savings were achieved by applying ground floor thermal insulation. This is due to existing insulations and shading techniques, which reduced the impact of improving other areas. However, it should be noted that while ground floor insulation offered the greatest potential for energy savings, it increased the room's mean indoor temperature by up to 4.4% during a typical summer day in free-running mode. When

the proposed ventilation was implemented, the effect of ground floor insulation was negligible.

The selected options for walls, roofs, infiltration rate, and window shading led to a respective reduction in the mean indoor temperature of the tested rooms during a typical summer day of up to 0.3%, 2.5%, 0.08%, and 0.2% in the 3D-printed house, and up to 1.3%, 1.8%, 0%, and 0.4% in the conventional house under natural ventilation mode. The greatest reductions in mean indoor temperature were achieved by applying the roof improvements, which reduced the impact of the high levels of solar radiation received by the roof components.

10.2.5 To what extent can applying the proposed passive strategies reduce cooling load (and associated energy consumption and CO_2 emissions) in a 3D-printed house and a conventionally constructed house in KSA?

Applying passive cooling strategies is crucial to improving the building thermal performance, consequently reducing energy consumption and associated carbon emissions. Various improvement measures were proposed, such as upgrading the insulation (walls, roofs, and ground floors), using thermal mass, improving airtightness, and applying window shading techniques. These strategies can reduce the buildings' heat gain, reduce overheating hours, and reduce reliance on active cooling systems.

The effectiveness of applying these strategies was evaluated for both houses using the validated IES models. The performance of each parameter was assessed by modifying one variable at a time while keeping the other parameters the same. This allowed for identification of the option for each parameter that could best improve indoor thermal conditions and achieve the greatest savings in cooling load (refer to Sections 9.2 to 9.6). Based on these simulations, a combination of the best building fabric options was proposed and simulated for each house (see Section 9.7).

The simulation results revealed that applying the proposed building envelope strategies could reduce total annual energy consumption and associated CO_2 emissions by up to 36.9% for the 3D-printed house and up to 28.4% for the conventional house. This is due to reducing the cooling load by up to 68.5% and 57.7%, respectively. The greatest savings were achieved during the overheating season, particularly in August (peak consumption), with total cooling load reductions of up to 67.2% for the 3D-printed house and 57.2% for the conventional house.

The study also explored the potential for achieving further reductions by employing a controlled ventilation strategy. The window and AC operational control scheme profile is discussed in Section 5.9. The results indicate that applying the proposed mixed-mode ventilation strategy could reduce the cooling load by an additional 10% for both cases, thus reducing the total annual cooling load to about 51.2 kWh/m^2 and 45.6 kWh/m^2 for the 3D-printed and conventional houses, respectively. This contributed to additional savings in annual energy consumption and carbon emissions, achieving a total reduction of up to 45.5% for Case 1 and 34.1% for Case 2 compared to the baseline models.

In conclusion, the thermal performance of residential buildings located in Riyadh, KSA, can be significantly improved by applying passive cooling strategies and solutions. Improving thermal performance can result in a considerable reduction in energy consumption and associated CO_2 emissions, particularly during periods of peak demand. The evaluated strategies can achieve energy savings of up to 45.5% and 34.1% for the 3D-printed house and the conventional house, respectively. Further research is required to evaluate the cost benefits of applying these strategies in the specific context of Riyadh and to evaluate the effectiveness of different strategies for current and future climate scenarios.

10.3 Research key findings and implementation

This research evaluated the thermal performance and energy efficiency of two residential buildings in Riyadh—one constructed using 3D printing and the other using conventional construction methods—while examining a suite of passive design strategies aimed at reducing cooling loads in KSA's hot and arid climate. This section summarizes the key findings of the study and outlines their implications for building development practices and regulatory improvement in the country.

As learned in Chapter 2, the severity of KSA's hot and arid climate underscores the necessity for energy-efficient and climatically responsive buildings. The analysis presented in this thesis demonstrated that the 3D-printed house (Case 1) holds promise in this regard, particularly when its thermal performance is enhanced through passive design measures and controlled ventilation to reduce unwanted heat gain. When compared to the conventionally constructed house (Case 2), however, notable differences in performance were observed between the two constructions.

The simulation results (covered in Chapter 8) demonstrated the superior thermal behaviour of the 3D-printed house in the hot and arid climate of Riyadh compared to the conventional

house. This was evident in the IST analysis (presented in Figures 8-12 and 8-13), which revealed that the 3D-printed walls maintained more stable and generally lower IST values than the conventional walls in Case 1, particularly during the cooling season. This was also reflected in the indoor thermal comfort assessment (Figure 5-8), where both tested rooms in the 3D-printed house recorded higher percentages of comfort hours (31.6% in the dining room and 35.8% in the bedroom, compared with 19.8% in R2 and 23% in R1 in the conventional house), meaning they required less frequent operation of active cooling systems. The presented analysis indicated that Case 1 responded better to the climate conditions of Riyadh than Case 2 in terms of indoor thermal environment.

Despite these thermal advantages, the conventional house demonstrated superior energy performance. A comparison of energy consumption per unit area (summarized in Table 9-6) revealed that Case 2 consumed approximately 35.5% less energy than Case 1 in the baseline models, and 22% less in the improved models following the application of the proposed measures. This difference in energy efficiency highlighted the crucial influence of construction details, design parameters and urban context—including building orientation, external surface-to-floor area ratio (form factor), envelope tightness, and local shading—all of which differed significantly between the two case study buildings.

Although the 3D-printed case study building did not achieve lower energy consumption per square meter, the findings nonetheless indicated that 3D concrete printing—especially when integrated with appropriate improvement measures and passive strategies—can still deliver competitive, energy-efficient buildings in hot and arid climates such as Riyadh, highlighting its promising potential for future development.

Furthermore, the advantages of 3D printing extend beyond building thermal performance and energy efficiency. Given KSA's urgent need for rapid residential development (Section 2.5), large-scale 3D concrete printing remains a highly promising construction technology, offering important advantages over conventional construction methods (as discussed in Chapter 4), even though further optimization is required for 3D-printed buildings to match—or potentially exceed—conventional buildings in terms of operational energy performance.

The findings of this research offer valuable insights for building developers and policymakers for improving the thermal performance and energy efficiency of residential buildings in Saudi Arabia, especially in Climate Zone 1. Across both case study buildings, the application of

passive design strategies led to substantial improvements in indoor thermal conditions reductions in energy demand.

For the 3D-printed house, the combined improvement measures reduced total annual energy consumption from 14,962 kWh (or 191 kWh/m^2) to 8,148 kWh (or 104 kWh/m^2), achieving a total saving of 45%. For the conventionally constructed house, annual energy consumption decreased from 54,768 kWh (or 123 kWh/m^2) to 36,099 kWh (or 81 kWh/m^2), achieving a 34% reduction. These savings demonstrated that applying passive design strategies can significantly reduce reliance on mechanical cooling systems and enhance buildings energy efficiency, regardless of construction method.

The investigation provided a set of evidence-based design principles that can directly benefit building designers, policy makers, and construction professionals in Saudi Arabia, with specific focus on Climate Zone 1:

Building Fabric Improvement

- Improving wall and roof insulation substantially reduces unwanted heat transfer under both free-running and mechanically cooled conditions.
- Increasing insulation thickness beyond SBC 602 minimum requirements could produce diminishing returns, suggesting limited benefit relative to a possible increase in material cost.
- Combining insulation with high-solar-reflectance roofing achieved performance similar to that of significantly thicker insulation layers, indicating that cool roofs offer a cost-effective alternative to excessive insulation.
- Exposing indoor environments to externally insulated thermal mass is an effective cooling strategy, especially when combined with controlled ventilation strategy.

Ground Floor Insulation

- Ground floor heat transfer was found to be a major contributor to cooling load in both buildings.
- The application of EPS insulation led to substantial cooling load reductions, demonstrating that ground-floor insulation is a critical yet often overlooked parameter for residential buildings in Riyadh.

Natural Ventilation and Infiltration

- Natural ventilation is effective in reducing indoor temperatures and improving energy performance in hot and arid regions; however, it must be carefully controlled and avoided during peak summer conditions when outdoor temperatures exceed indoor levels.
- Infiltration rates have a direct impact on indoor thermal environment and overall building energy performance. Thus, improving building airtightness though better sealing and regular inspection is required to enhance energy efficiency.

Soar Heat Gain Control

- Solar heat gain through glazing was identified a major source of heat gain, contributing to overheating in both houses. It should be mitigated through appropriate orientation, external shading devices, and low-SHGC glazing.
- Shading requirements vary significantly by window orientation, and therefore, orientation-specific shading design should be encouraged to ensure adequate solar control.
- Local shading form adjacent structures and site context must be considered, as it can reduce or eliminate the need for additional external shading.

Energy Modelling and Design Decision Support

- Energy simulation tools proved effective for understanding building performance under various scenarios; however, users must remain aware of limitations and uncertainties associated with model assumptions.
- Building developers should be encouraged to incorporate energy modelling tools as a standard practice during the design process for both new and retrofit projects, enabling more accurate performance predictions and supporting the delivery of more energy-efficient, climate-responsive residential buildings in KSA.

10.4 Contributions to knowledge

This thesis addressed the critical challenges facing the sustainability of the Saudi residential sector, responding to the continuously growing pressure on housing demand and energy consumption driven by swift population growth, the national reform plan (Saudi Vision 2030), and the country's international commitment to reducing carbon emissions. The contributions of this research to the body of knowledge can be summarized as follows:

- Providing insight into the thermal behaviour and energy performance of existing contemporary dwellings that were recently constructed using different techniques: 3D concrete printing and conventional construction methods. To the best of the author's knowledge, this thesis is the first study to evaluate the thermal performance of an existing 3D concrete-printed house in the severe climate context of Saudi Arabia using field measurements and computer energy simulation methodologies.
- Proposing and testing various strategies (inspired by sustainable modern techniques, local building regulations, and adaptive strategies) to improve thermal performance and reduce energy consumption and associated carbon emissions for contemporary residential buildings within the climate context of Riyadh.
- Demonstrating the possibility of reducing energy consumption in Saudi dwellings, particularly during peak periods, while maintaining indoor thermal comfort requirements. This is applicable to both 3D-printed and conventionally constructed houses located within climate Zone 1.
- Assessing the sensitivity of modern KSA dwellings (3D-printed and conventionally constructed) to infiltration rates and ground temperatures through computer energy simulations, as well as evaluating the SBC requirements for ground floor insulation and airtightness.
- Assisting building developers and decision-makers in the building sector in KSA to develop current building regulations and standards to construct highly efficient buildings within the investigated climate features.

10.5 Research limitations

While the work of this research successfully achieved the study's primary purpose and objectives through the specified methods, this study, like any research, has its limitations. The scope of this study was limited to the assessment of the thermal performance of existing dwellings in the hot and arid climate of Saudi Arabia. The research investigated the impact of applying passive design strategies learned from vernacular architecture and modern building technology to improve indoor thermal conditions and energy efficiency, with a focus on two types of construction: 3D concrete printing and conventional construction methods.

The selection of the case study buildings was limited to those that allowed access for field measurements, those for which construction details and architectural drawings were available, and buildings that were recently constructed. While the author was permitted access to various potential cases, it was not possible to obtain their construction details and

material specifications, particularly for 3D concrete printed buildings, due to the fact that such data is kept confidential for market competition reasons. When construction data for some buildings were available, it was not possible to obtain access for field monitoring. Thus, only two unique cases that met the research criteria were used in this study. It is also important to note that these two buildings were situated in different urban contexts within Riyadh, which may have influenced their microclimate exposure and, consequently, the comparative results.

Although Saudi Arabia is a vast country with various climatic conditions, this study focused on Climate Zone 1, represented by Riyadh. This limitation was mostly due to limited available resources, funding, and access for field observation and data collection. In addition, only one 3D-printed house was available for study in the country at the time, which contributed to the selection of Riyadh (Zone 1) as the study location of this research. Since Zone 1 represents more than 70% of the KSA's climatic context, it was suggested that the outcomes of this research are widely applicable.

However, the findings may differ in Climate Zones 2 and 3 due to variations in temperature, humidity, diurnal ranges, and seasonal comfort patterns. In cooler and more humid regions, for instance, the effectiveness of key measures—such as natural ventilation, shading requirements, and thermal comfort thresholds—may shift significantly. Therefore, additional studies across different climate zones would be required to expand our understanding and provide holistic details and more accurate results for all regions.

Considering the inherent complexity of the research, time constraints, and the available tools and resources, this study is bounded by several limitations in the applied research methodologies, some of which have been explained in previous chapters. Due to the nature of the selected cases, field measurements and observations were limited to environmental parameters only. It was not possible to cover actual occupancy profiles or collect utility bills as both buildings were uninhabited.

In addition, field measurements were limited to August, which provided valuable insight into the buildings' performance under Riyadh's peak summer conditions but did not capture seasonal variation. Logistical challenges also arose as the reviewed case study buildings were located in KSA while the author was residing in the UK, which contributed to the relatively short field data collection period. Further work is needed to examine performance across different seasons and under actual occupancy conditions.

It would be highly beneficial to conduct further field-based investigations into the thermal performance of Saudi modern residential buildings, particularly those constructed using 3D concrete printing methods, and to capture data across different seasons. An analysis of actual energy bills, for example, could provide more comparison options that would improve accuracy and validation.

In energy simulation work, several limitations arise from the inherent nature of simulation tools and the reliance on multiple input assumptions—such as occupancy profiles, household appliances, system performance, infiltration rates, and ground temperatures. These assumptions, often necessitated by a lack of detailed information in some areas, result in a realistic approximation of the real building but may not fully capture actual performance. As these parameters could not be collected directly from the site, detailed data were adopted from the literature and, where possible, supported by sensitivity analysis.

In addition, the as-built 3D-printed wall structure in Case Study 1 was simplified during the modelling process (as discussed in Chapter 5) due to software limitations, which introduced additional uncertainty in the results. Consequently, the use of a three-dimensional heat transfer model may be more feasible compared to a simplified homogeneous and one-dimensional heat transfer model. The scope of this study is also limited to current climate conditions, and the use of historical weather data may not necessarily reflect future changes in the thermal behaviour of the buildings.

10.6 Recommendations for future research

This section describes further investigation opportunities that were not addressed in the current study. Future research could expand the assessment of residential buildings by incorporating additional strategies that were excluded from this study, such as direct or indirect evaporative cooling, the use of alternative construction materials (e.g. conventional and 3D printing applications), and analysis of different window-to-wall ratios combined with appropriate shading solutions across different orientations.

Further research could also explore the use of roof-mounted photovoltaic systems, which can provide effective roof shading while simultaneously generating on-site renewable energy. These measures could be combined with other envelope improvements to explore their interactive effects.

The scope of this work was restricted to variables related to indoor thermal performance. Other critical factors—such as indoor environmental quality, daylighting performance,

systems efficiency, and occupancy levels—were not considered in the current research. These aspects could be covered in future studies. Moreover, this study focused on only Climate Zone 1 (Riyadh); extending the work to Zones 2 and 3 would offer a broader understanding of how climatic variation influences the effectiveness of the proposed measures.

Given the observed urban-context differences between the two case study buildings, future research should consider comparisons between buildings located in similar urban conditions or incorporate microclimate modelling to account for urban heat-island effects and variations in local shading.

The findings of this thesis could be strengthened by conducing multi-season field measurements, ideally under occupied conditions, supported by real utility data for validation. In this study, the sensitivity analysis (conducted in Chapter 7) revealed that the 3D-printed house had higher infiltration rates than the conventionally constructed house. To validate and refine these findings, future work should incorporate physical measurements of infiltration rates (e.g. using the blower door testing) to more accurately capture infiltration performance across different construction methods applied in KSA's housing projects.

Another important area of consideration is the methodological framework for assessing 3D-printed walls. Owing to the necessary simplification of the 3D-printed wall structure during the modelling process (as noted previously), future research should incorporate laboratory testing, in-situ measurements of material thermal properties, or detailed numerical tools—such as 2D/3D heat-transfer modelling using COMSOL or ANSYS—to more accurately capture heat transfer through the wall and account for the influence of cavity geometry and layer configuration, thereby providing more reliable inputs for whole-building energy simulation.

Future studies should also consider the economic, environmental, and practical feasibility of the proposed measures. Conducting a cost analysis—for example, comparing a cool roof with a thicker insulation alternative—could offer valuable insights to support more informed design decisions and policy development. In addition, incorporating Life Cycle Assessment (LCA) of both conventional construction and 3D printing would enable a more comprehensive evaluation of the two construction methods across their life cycle.

Finally, the research could be extended using parametric analysis tools to explore a wide range of possible building fabric configurations and identify optimal combinations. Further

investigation into emerging construction techniques and alternative building methods may also help advance sustainable and energy-efficient building development in Saudi Arabia.

10.7 Summary

This chapter concluded the research by comprehensively discussing the study's research outcomes and demonstrating how they address the research questions and fulfil the study's objectives. The study highlighted the critical role of the building envelope in improving thermal performance and energy efficiency in 3D-printed and conventional constructions, with a particular focus on reducing total overheating hours and cooling energy demands through the implementation of various design measures and systems (summarized in Section 5.9). The study found that improving the building fabric, combined with the implementation of natural ventilation, can substantially reduce cooling load and increase energy savings for both constructions. The contributions to knowledge made in this thesis were identified, and the study limitations were acknowledged. The chapter ended with suggested recommendations for future research on energy-efficient residential buildings based on questions and issues that arose from this research.

REFERENCES

REFERENCES

Abdel-Ghany, A. M., Al-Helal, I. M., Alsadon, A., Ibrahim, A., & Shady, M. (2022). Measuring and Predicting the In-Ground Temperature Profile for Geothermal Energy Systems in the Desert of Arid Regions. *Energies, 15*(19). doi:10.3390/en15197268

Abdulmajeed, A., Agkathidis, A., Dounas, T., & Lombardi, D. (2022). *Developing a Design Framework for the Mass Customisation of Housing in Saudi Arabia: A Critical Review*. Paper presented at the 10th International Conference of the Arab Society for Computation in Architecture, Art and Design (ASCAAD 2022), Lebanon.

Abergel, T., Dean, B., & Dulac, J. (2017). *Global Status Report 2017, Towards a zero-emission, efficient, and resilient buildings and constrcution sectro*. Retrieved from https://www.worldgbc.org/news-media/global-status-report-2017

Abuhussain, M. (2020). *An Assessment of the Saudi Residential Buildings Envelope Code Under the Current and Future Climate Change Scenarios: the Case for Jeddah in the Hot and Humid Climate Region.* (PhD). The University of Liverpool,

Aerts, M. (2025). C3PO. Retrieved from https://www.kampc.be/en/projects/c3po

Ahmad, A. (2004). Energy Simulation for a Typical House Built with Different Types of Masonry Building Materials. *Arabian Journal for Science & Engineering (Springer Science & Business Media BV), 29*.

Ahmed, W., & Asif, M. (2020). BIM-based techno-economic assessment of energy retrofitting residential buildings in hot humid climate. *Energy and Buildings, 227*, 110406. doi:https://doi.org/10.1016/j.enbuild.2020.110406

Ahmed, W., Asif, M., & Alrashed, F. (2019). Application of Building Performance Simulation to Design Energy-Efficient Homes: Case Study from Saudi Arabia. *Sustainability, 11*(21), 6048. doi:http://dx.doi.org/10.3390/su11216048

Al-Ahmadi, K., & Al-Ahmadi, S. (2013). Rainfall-Altitude Relationship in Saudi Arabia. *Advances in Meteorology, 2013*, 363029. doi:10.1155/2013/363029

Al-Azri, N., Zurigat, Y., & Al-Rawahi, N. (2012). *Development of bioclimatic chart for passive building design in Muscat-Oman.* Paper presented at the International Conference on Renewable Energies and Power Quality (ICREPQ'12), Santiago de Compostela, Spain.

Al-Hathloul, S. (1996). *The Arab-Muslim city: tradition, continuity, and change in the physical environment*. Riyadh: Dar Al Sahan.

Al-Hathloul, S. (2017). Riyadh Development Plans in the Past Fifty Years (1967-2016). *Current Urban Studies, 05*(01), 97-120. doi:10.4236/cus.2017.51007

Al-Homoud, M. S., & Krarti, M. (2021). Energy efficiency of residential buildings in the kingdom of Saudi Arabia: Review of status and future roadmap. *Journal of Building Engineering, 36*, 102143. doi:https://doi.org/10.1016/j.jobe.2020.102143

Al-Naim, M. (2008). Identity in transitional context: open-ended local architecture in Saudi Arabia. *International Journal of Architectural Research, 2*(2), 125-146.

Al-Oraier, F. (2005). *The Thermal Analysis of Traditional Adobe Dwellings in Riyadh City, Saudi Arabia* (PhD). The University of Wales, Cardiff,

Al-Qahtani, L. A. H., & Elgizawi, L. S. E. (2020). Building envelope and energy saving case study: a residential building in Al-Riyadh, Saudi Arabia. *International Journal of Low-Carbon Technologies, 15*(4), 555-564. doi:10.1093/ijlct/ctaa024

Al-Saadi, S., & Al-Jabri, K. (2017, 2017). *Energy-efficient envelope design for residential buildings: A case study in Oman.* Paper presented at the Smart Cities Symposium Prague (SCSP 2017), Czech Republic.

Al-Saadi, S., & Budaiwi, I. (2007). *Performance-based envelope design for residential buildings in hot climates.* Paper presented at the Proceedings of building simulation (2007).

Al-Sanea, S. A., Zedan, M. F., & Al-Hussain, S. N. (2012). Effect of thermal mass on performance of insulated building walls and the concept of energy savings potential. *Applied Energy, 89*(1), 430-442. doi:https://doi.org/10.1016/j.apenergy.2011.08.009

Al-Tamimi, N. (2017). A state-of-the-art review of the sustainability and energy efficiency of buildings in Saudi Arabia. *Energy Efficiency (1570646X), 10*(5), 1129-1141. doi:10.1007/s12053-017-9507-6

Al Dubyan, M., & Gasim, A. (2020). What Happened to Residential Electricity Consumption in Saudi Arabia Between 2015 and 2018? *King Abdullah Petroleum Studies and Research Center (KAPSARC)*.

Al Harbi, F., & Csala, D. (2019). *Saudi Arabia's electricity: Energy supply and demand future challenges.* Paper presented at the 1st Global Power, Energy and Communication Conference (GPECOM-2019).

Al Rasbi, H., & Gadi, M. (2021). Energy Modelling of Traditional and Contemporary Mosque Buildings in Oman. *Buildings, 11*(7). doi:10.3390/buildings11070314

Al Surf, M. S., & Mostafa, L. A. (2017). Will the Saudi's 2030 vision raise the public awareness of sustainable practices? *Procedia Environmental Sciences, 37*, 514-527.

Alabbasi, M. (2021). *Robotic Fabrication of Concrete Building Components for Efficient Housing Construction in Saudi Arabia.* (PhD). University of Liverpool,

Alabbasi, M., Chen, H.-M., & Agkathidis, A. (2021). *Assessing the effectivity of additive manufacturing techniques for the production of building components: Implementing innovation for housing construction in Saudi Arabia*. Paper presented at the 9th International Conference of the Arab Society for Computer Aided Architectural Deisgn (ASCAAD 2021), Cairo.

Alaboud, M. (2021). *Evaluation and improvement of thermal performance of residential buildings in hot and dry climate with reference to Saudi Arabia.* (PhD). University of Nottingham,

Alaboud, M., & Gadi, M. (2019). *Indoor environmental monitoring of residential buildings in Saudi Arabia, Makkah: a case study.* Paper presented at the IOP Conference Series: Materials Science and Engineering.

Alaboud, M., & Gadi, M. (2020). The Effect of Thermal Insulation on Cooling Load in Residential Buildings in Makkah, Saudi Arabia. *Future Cities and Environment, 6*(1). doi:10.5334/fce.87

Alaboud, M., & Gadi, M. (2022). Evaluation of Indoor Thermal Environmental Conditions of Residential Buildings in Saudi Arabia. *Energies, 15*(5), 1603.

Alaidroos, A., & Krarti, M. (2015). Optimal design of residential building envelope systems in the Kingdom of Saudi Arabia. *Energy and Buildings, 86*, 104-117. doi:10.1016/j.enbuild.2014.09.083

Alaidroos, A., & Krarti, M. (2016). Evaluation of passive cooling systems for residential buildings in the Kingdom of Saudi Arabia. *Journal of Solar Energy Engineering, 138*(3), 031011.

Alangari, N. K., & Alzamil, W. S. (2020). Evaluating the building technology stimulus initiative offered by ministry of housing within the kingdom's vision 2030. *Journal of Sustainable Development, 13*, 115-128.

Alardhi, A., S Alaboodi, A., & Almasri, R. (2020). Impact of the new Saudi energy conservation code on Saudi Arabia residential buildings. *Australian Journal of Mechanical Engineering*, 1-15. doi:10.1080/14484846.2020.1802919

Alayed, E., Bensaid, D., O'Hegarty, R., & Kinnane, O. (2022). Thermal mass impact on energy consumption for buildings in hot climates: A novel finite element modelling study comparing building constructions for arid climates in Saudi Arabia. *Energy and Buildings, 271*, 112324. doi:https://doi.org/10.1016/j.enbuild.2022.112324

Alayed, E., O'Hegarty, R., & Kinnane, O. (2021). Thermal envelope analysis for new code compliance of Saudi Arabian dwellings. *Energy and Buildings, 243*, 110997. doi:https://doi.org/10.1016/j.enbuild.2021.110997

Albatayneh, A. (2021). Optimisation of building envelope parameters in a semi-arid and warm Mediterranean climate zone. *Energy Reports, 7*, 2081-2093. doi:https://doi.org/10.1016/j.egyr.2021.04.011

Albatayneh, A., Alterman, D., Page, A., & Moghtaderi, B. (2016). Assessment of the Thermal Performance of Complete Buildings Using Adaptive Thermal Comfort. *Procedia - Social and Behavioral Sciences, 216*, 655-661. doi:10.1016/j.sbspro.2015.12.051

Albayyaa, H., Hagare, D., & Saha, S. (2019). Energy conservation in residential buildings by incorporating Passive Solar and Energy Efficiency Design Strategies and higher thermal mass. *Energy and Buildings, 182*, 205-213. doi:https://doi.org/10.1016/j.enbuild.2018.09.036

Albogami, S. M., & Boukhanouf, R. (2019). *Residential building energy performance evaluation for different climate zones.* Paper presented at the IOP Conference Series: Earth and Environmental Science.

Aldossary, N. A., Rezgui, Y., & Kwan, A. (2014). Domestic energy consumption patterns in a hot and arid climate: A multiple-case study analysis. *Renewable Energy, 62*, 369-378. doi:https://doi.org/10.1016/j.renene.2013.07.042

Aldossary, N. A., Rezgui, Y., & Kwan, A. (2017). Establishing domestic low energy consumption reference levels for Saudi Arabia and the Wider Middle Eastern Region. *Sustainable Cities and Society, 28*, 265-276. doi:https://doi.org/10.1016/j.scs.2016.09.015

AlFaraidy, F., & Azzam, S. (2019). Residential buildings thermal performance to comply with the energy conservation code of Saudi Arabia. *Eng. Technol. Appl. Sci. Res, 9*, 3949-3954.

Algarni, S. (2018). Potential for cooling load reduction in residential buildings using cool roofs in the harsh climate of Saudi Arabia. *Energy & Environment, 30*(2), 235-253. doi:10.1177/0958305X18787340

AlGhamdi, A. (2019). *Data Insight: Electricity Tariff Changes in Saudi Arabia*. Retrieved from Riyadh: https://www.kapsarc.org/research/publications/electricity-tariff-changes-in-saudi-arabia/

Alkelani, A. A. (2025). *Evaluation of Prefabricated Construction Systems and Materials' Thermal Performance with Reference to Housing Construction in Saudi Arabia.* (PhD). University of Nottingham,

Alkhalidi, A., & Hatuqay, D. (2020). Energy efficient 3D printed buildings: Material and techniques selection worldwide study. *Journal of Building Engineering, 30*, 101286. doi:https://doi.org/10.1016/j.jobe.2020.101286

Alkhalifah, E. (2024). *Holistic energy-efficient retrofit strategies in support of Saudi building code: a path towards sustainable residential building.* (PhD). University of Nottingham,

Almasoud, A. H., & Gandayh, H. M. (2015). Future of solar energy in Saudi Arabia. *Journal of King Saud University - Engineering Sciences, 27*(2), 153-157. doi:https://doi.org/10.1016/j.jksues.2014.03.007

Almehrej, M. I. (2015). *A Design Guide for Contemporary Saudi Arabian Homes in Riyadh.* (PhD). University of Northumbria,

Almushaikah, A. S., & Almasri, R. A. (2020). Evaluating the potential energy savings of residential buildings and utilizing solar energy in the middle region of Saudi Arabia – Case study. *Energy Exploration & Exploitation, 39*(5), 1457-1490. doi:10.1177/0144598720975144

Alobailan, L., & Alawad, A. (2022). Architectural Values Behind the Formation of Heritage Houses as a Tool for Promoting Cultural Identity in Saudi Arabia. *WIT Transactions on The Built Environment, 211*, 29-50.

Alosaimi, A. H. (2023). *Optimising the Energy Performance of the Residential Stock of the Kingdom of Saudi Arabia by Retrofit Measures.* (PhD). University of Nottingham,

Alrashed, F. (2015). *Design and Application of Zero-energy Homes in Saudi Arabia.* (PhD). Glasgow Caledonian University,

Alrashed, F., & Asif, M. (2015a). Analysis of critical climate related factors for the application of zero-energy homes in Saudi Arabia. *Renewable and Sustainable Energy Reviews, 41*, 1395-1403. doi:10.1016/j.rser.2014.09.031

Alrashed, F., & Asif, M. (2015b). Climatic Classifications of Saudi Arabia for Building Energy Modelling. *Energy Procedia, 75*, 1425-1430. doi:10.1016/j.egypro.2015.07.245

Alshahrani, J. (2018). *Smart Solutions to Manage Peak Electricity Demand in Saudi Arabia.* (PhD). De Montfort University,

Alyami, M. (2022). *An Approach to Enhancing Energy Performance in Residential Buildings in Hot Climate Regions (The Case of Saudi Arabia).* (PhD). University of Nottingham,

Alyami, M., & Omer, S. (2021). Building energy performance simulation: a case study of modelling an existing residential building in Saudi Arabia. *Environmental Research: Infrastructure and Sustainability, 1*(3), 035001. doi:10.1088/2634-4505/ac241e

AlZahrani, A. A., Alghamdi, A. A., & Basalah, A. A. (2022). Computational Optimization of 3D-Printed Concrete Walls for Improved Building Thermal Performance. *Buildings, 12*(12), 2267.

Aouf, R. S. (2018). ETH Zurich makes lightweight concrete ceiling using 3D sand-printing. Retrieved from https://www.dezeen.com/2018/08/03/eth-zurich-makes-light-concrete-ceiling-using-3d-sand-printing/#/

APICORP. (2018). *Saudi Energy Price Reform Getting Serious*. Retrieved from https://www.apicorp.org/publication/saudi-energy-price-reform-getting-serious/

Arab News. (2022). Saudi Arabia leads GCC construction sector with 63% share of region's future projects. Retrieved from https://arab.news/gkdwr

Arabian Business. (2022). Saudi Arabia needs 1.2m new homes to meet 2030 demand. Retrieved from https://www.arabianbusiness.com/industries/real-estate/saudi-arabia-needs-1-2m-new-homes-to-meet-2030-demand

Asfour, O. S. (2018). Solar and Shading Potential of Different Configurations of Building Integrated Photovoltaics Used as Shading Devices Considering Hot Climatic Conditions. *Sustainability, 10*(12). doi:10.3390/su10124373

ASHRAE. (2002). ASHRAE Guideline 14-2002. In *Measurement of Energy and Demand Savings*: American Society of Heating, Refrigerating and Air-Conditioning Engineers.

ASHRAE. (2013a). ANSI/ASHRAE/IES Standard 90.1-2013. In *Energy Standard for Buildings Except Low-Rise Residential Buildings (SI Edition)*: American Society of Heating, Refrigerating and Air-Conditioning Engineers.

ASHRAE. (2013b). ASHRAE Handbook - Fundamentals (I-P Edition). In: American Society of Heating, Refrigerating and Air-Conditioning Engineers, Inc. (ASHRAE).

ASHRAE. (2014). ASHRAE Guideline 14-2014. In *Measurement of energy, demand, and water savings*: American Society of Heating, Refrigerating and Air-Conditioning Engineers.

ASHRAE. (2017). ANSI/ASHRAE Standard 55-2017. In *Thermal Environmental Conditions for Human Occupancy*. Atlanta, GA: American Society of Heating, Refrigerating and Air-Conditioning Engineers.

Asif, M. (2016). Growth and sustainability trends in the buildings sector in the GCC region with particular reference to the KSA and UAE. *Renewable and Sustainable Energy Reviews, 55*, 1267-1273. doi:https://doi.org/10.1016/j.rser.2015.05.042

Asimakopoulos, D. (1996). *Passive Cooling of Buildings* (1 ed.). United Kingdom: United Kingdom: Routledge.

Auliciems, A., & Szokolay, S. V. (2007). *Thermal Comfort*: Passive and Low Energy Architecture International in association with Department of Architecture, the University of Queensland.

Ayegba, B. O., Egbe, K.-J. I., Matin Nazar, A., Huang, M., & Hariri-Ardebili, M. A. (2022). Resource Efficiency and Thermal Comfort of 3D Printable Concrete Building Envelopes Optimized by Performance Enhancing Insulation: A Numerical Study. *Energies, 15*(3). doi:10.3390/en15031069

Bagasi, A. A. (2022). *Investigation of The Ventilation and Thermal Performance of Mashrabiya for Residential Buildings in the Hot-Humid Climate of Saudi Arabia.* (PhD). University of Nottingham,

Bagasi, A. A., & Calautit, J. K. (2020). Experimental field study of the integration of passive and evaporative cooling techniques with Mashrabiya in hot climates. *Energy and Buildings, 225*, 110325. doi:10.1016/j.enbuild.2020.110325

Baig, H., Sellami, N., Bahaidarah, H., & Mallick, T. (2013). *OPTICAL ANALYSIS OF A CPC BASED CPV/T SYSTEM FOR APPLICATION IN THE KINGDOM OF SAUDI ARABIA*.

Baker, N., & Steemers, K. (2000). *Energy and Environment in Architecture : A Technical Design Guide*. London: London : E. & FN. Spon.

Balabel, A., & Alwetaishi, M. (2021). Towards Sustainable Residential Buildings in Saudi Arabia According to the Conceptual Framework of "Mostadam" Rating System and Vision 2030. *Sustainability, 13*(2), 793. doi:http://dx.doi.org/10.3390/su13020793

Belaid, F., & Al Dubyan, M. (2021). The Role of Building Energy Efficiency in Shaping the Energy Transition in Saudi Arabia: Key challenges and initiatives. *King Abdullah Petroleum Studies and Research Center (KAPSARC)*.

Block, I. (2019). World's largest 3D-printed building completes in Dubai. Retrieved from https://www.dezeen.com/2019/12/22/apis-cor-worlds-largest-3d-printed-building-dubai/

Bos, F., Wolfs, R., Ahmed, Z., & Salet, T. (2016). Additive manufacturing of concrete in construction: potentials and challenges of 3D concrete printing. *Virtual and Physical Prototyping, 11*(3), 209-225. doi:10.1080/17452759.2016.1209867

BP-p.l.c. (2021). *bp Statistical Review of World Energy*. Retrieved from

Brager, G. S., & de Dear, R. J. (1998). Thermal adaptation in the built environment: a literature review. *Energy and Buildings, 27*(1), 83-96.

Camacho, D. D., Clayton, P., O'Brien, W. J., Seepersad, C., Juenger, M., Ferron, R., & Salamone, S. (2018). Applications of additive manufacturing in the construction industry – A forward-looking review. *Automation in Construction, 89*, 110-119. doi:https://doi.org/10.1016/j.autcon.2017.12.031

Carratt, A., Kokogiannakis, G., & Daly, D. (2020). A critical review of methods for the performance evaluation of passive thermal retrofits in residential buildings. *Journal of Cleaner Production, 263*, 121408. doi:https://doi.org/10.1016/j.jclepro.2020.121408
CIBSE Guide F. (2012). *Energy efficiency in buildings*. Retrieved from London:
CIBSE TM63. (2020). *Operational performacne: Building performance modelling and calibration for evaluation of energy in-use*. Retrieved from London:
Clarke, J. A. (2001). *Energy simulation in building design*: Routledge.
Climate Transparency. (2022). Country Profile Saudi Arabia Retrieved from https://www.climate-transparency.org/
COBOD. (2022). The Tallest 3D Printed Building in the World is Now in Saudi Arabia. Retrieved from https://cobod.com/the-worlds-tallest-3d-printed-building-is-now-in-saudia-arabia/
Consolidated Contractors Group. (2018). *3D Printing Project Utilizing CYBE Robot Printing Story*. Unpublished Report.
CyBe Construction. (2023). 3D Studio 2030. Retrieved from https://cybe.eu/
d'Ambrosio Alfano, F. R., Ficco, G., Frattolillo, A., Palella, B. I., & Riccio, G. (2021). Mean radiant temperature measurements through small black globes under forced convection conditions. *Atmosphere, 12*(5), 621.
Dabaieh, M. (2011). *A Future for the Past of Desert Vernacular Architecture.* (PhD). Lund University, Sweden.
DC HUB. (2022). Construction sector and the GCC project awards data. Retrieved from https://dchub.me/digital-construction/construction-sector-continues-as-projects-mainstay-in-latest-gcc-awards-data/
de Dear, R., Brager, G., & Cooper, D. (1997). *Developing an Adaptive Model of Thermal Comfort and Preference - Final Report on RP-884*. Retrieved from
de Dear, R., & Brager, G. S. (1998). Developing an adaptive model of thermal comfort and preference.
de Dear, R., & Brager, G. S. (2002). Thermal comfort in naturally ventilated buildings: revisions to ASHRAE Standard 55. *Energy and Buildings, 34*(6), 549-561.
de Rubeis, T. (2022). 3D-printed blocks: Thermal performance analysis and opportunities for insulating materials. *Sustainability, 14*(3), 1077.
de Rubeis, T., Ciccozzi, A., Giusti, L., & Ambrosini, D. (2024). On the use of 3D printing to enhance the thermal performance of building envelope – A review. *Journal of Building Engineering, 95*, 110284. doi:https://doi.org/10.1016/j.jobe.2024.110284
DeKay, M., & Brown, G. (2014). *SUN, WIND & LIGHT: Architectural Design Strategies, 3rd edition*. Hoboken, New Jersey, USA: John Wiley & Sons, Inc.
Dey, D., & Panda, B. (2023). An experimental study of thermal performance of 3D printed concrete slabs. *Materials Letters, 330*, 133273. doi:https://doi.org/10.1016/j.matlet.2022.133273
Dwidar, S. (2019). BIOCLIMATIC ARCHITECTURE FOR HERITAGE RESIDENTIAL BUILDINGS IN THE KINGDOM OF SAUDI ARABIA.
E.Construct. (2016). Office of the Future. Retrieved from https://www.econstruct.ae/projects/office-of-the-future
Ebrahimi, M., Mohseni, M., Aslani, A., & Zahedi, R. (2022). Investigation of thermal performance and life-cycle assessment of a 3D printed building. *Energy and Buildings, 272*, 112341. doi:https://doi.org/10.1016/j.enbuild.2022.112341
Edie. (2021). Global fossil fuel use not yet in decline, despite renewable energy pledges. Retrieved from https://www.edie.net/report-global-fossil-fuel-use-not-yet-in-decline-despite-renewable-energy-pledges/?register=success

EIA. (2021). Country Analysis Executive Summary: Saudi Arabia. Retrieved from https://www.eia.gov/international/analysis/country/SAU

El-Bakkush, A. F. M. (2016). *Improving Solar Gain Control Strategies in Residential Buildings Located in a Hot Climate (Tripoli-Liby).* (PhD). Heriot-Watt University,

El-Sayegh, S., Romdhane, L., & Manjikian, S. (2020). A critical review of 3D printing in construction: benefits, challenges, and risks. *Archives of Civil and Mechanical Engineering, 20*(2). doi:10.1007/s43452-020-00038-w

Elnabawi, M. H., & Saber, E. (2022). Reducing carbon footprint and cooling demand in arid climates using an integrated hybrid ventilation and photovoltaic approach. *Environment, Development and Sustainability, 24*. doi:10.1007/s10668-021-01571-1

Elnabawi, M. H., Saber, E., & Bande, L. (2024). Passive Building Energy Saving: Building Envelope Retrofitting Measures to Reduce Cooling Requirements for a Residential Building in an Arid Climate. *Sustainability, 16*(2). doi:10.3390/su16020626

Elseragy, A. A. (2003). *Architectural and solar potential of curved and flat roofs in hot arid regions (with reference to Egypt).* (PhD). University of Nottingham,

Facey, W. (2015). *Back to earth: adobe building in Saudi Arabia*. Riyadh: Al-Turath.

Fanger, P. O. (1970). *Thermal comfort. Analysis and applications in environmental engineering*. Copenhagen: Danish Technical Press.

Fathy, H. (1986). Natural energy and vernacular architecture.

Friess, W. A., & Rakhshan, K. (2017). A review of passive envelope measures for improved building energy efficiency in the UAE. *Renewable and Sustainable Energy Reviews, 72*, 485-496. doi:https://doi.org/10.1016/j.rser.2017.01.026

GAISMA. (2023). Retrieved from https://www.gaisma.com/en/

GAS. (2023). Retrieved from https://www.stats.gov.sa/

Ghabra, N. (2018). *Energy efficient strategies for the building envelope of residential tall buildings in Saudi Arabia.* (PhD). University of Nottingham., University of Nottingham.

Ghaffar, S. H., Corker, J., & Fan, M. (2018). Additive manufacturing technology and its implementation in construction as an eco-innovative solution. *Automation in Construction, 93*, 1-11. doi:https://doi.org/10.1016/j.autcon.2018.05.005

Ghoreishi, A. (2019). The Effects of Exterior Thermal Mass (eTM) on Energy Consumption in Residential Buildings. *ARCHive-SR, 3*(1), 14 - 26. doi:10.21625/archive.v3i1.427

Givoni, B. (1998). *Climate Considerations in Building and Urban Design*: John Wiley & Sons, Inc.

Glew, D., Farmer, D., Miles-Shenton, D., Thomas, F., Fletcher, M., Hardy, A., & Gorse, C. (2021). Thin Internal Wall Insulation (TIWI) Measuring Energy Performance Improvements in Dwellings Using Thin Internal Wall Insulation Annex B; TIWI Field Trials Building Performance Evaluation (BPE).

Guo, H., Aviv, D., Loyola, M., Teitelbaum, E., Houchois, N., & Meggers, F. (2020). On the understanding of the mean radiant temperature within both the indoor and outdoor environment, a critical review. *Renewable and Sustainable Energy Reviews, 117*, 109207. doi:https://doi.org/10.1016/j.rser.2019.06.014

Hariri-Rifai, W., & Hariri-Rifai, M. (1990). *The heritage of the Kingdom of Saudi Arabia*. Washington: GDG Exhibits Trust.

Harkouss, F., Fardoun, F., & Biwole, P. H. (2018). Passive design optimization of low energy buildings in different climates. *Energy, 165*, 591-613. doi:https://doi.org/10.1016/j.energy.2018.09.019

Harrouk, C. (2019). Dubai Municipality to Become the World's Largest 3D-Printed Building. Retrieved from https://www.archdaily.com/930857/dubai-municipality-to-become-the-worlds-largest-3d-printed-building

Hawkins, W. J., Herrmann, M., Ibell, T. J., Kromoser, B., Michaelski, A., Orr, J. J., . . . West, M. (2016). Flexible formwork technologies - a state of the art review. *Structural concrete : journal of the FIB, 17*(6), 911-935. doi:10.1002/suco.201600117

HCDR. (2023). *Riyadh The City & The Life*. Riyadg: High Commission for the Development of Ar-Riyadh.

He, Y., Zhang, Y., Zhang, C., & Zhou, H. (2020). Energy-saving potential of 3D printed concrete building with integrated living wall. *Energy and Buildings, 222*, 110110. doi:https://doi.org/10.1016/j.enbuild.2020.110110

Hijazi, J. F. J. (2018). *Towards Displacing Domestic Air Conditioning in KSA*

An Assessment of Hybrid Cooling Strategies Integrated with 'Fabric First' Passive Design Measures. (PhD). University of Strathclyde Engineering,

Hong, T., Chou, S. K., & Bong, T. Y. (2000). Building simulation: an overview of developments and information sources. *Building and Environment, 35*(4), 347-361. doi:https://doi.org/10.1016/S0360-1323(99)00023-2

Hu, M., Zhang, K., Nguyen, Q., & Tasdizen, T. (2023). The effects of passive design on indoor thermal comfort and energy savings for residential buildings in hot climates: A systematic review. *Urban climate, 49*, 101466. doi:https://doi.org/10.1016/j.uclim.2023.101466

Humphreys, M. (1978). Outdoor temperatures and comfort indoors. *Batiment International, Building Research and Practice, 6*(2), 92-92. doi:10.1080/09613217808550656

Hyde, R. (2008). *Bioclimatic Housing: Innovative Designs for Warm Climates*: Earthscan.

Ibrahim, I., Eltarabishi, F., Abdalla, H., & Abdallah, M. (2022). 3D Printing in Sustainable Buildings: Systematic Review and Applications in the United Arab Emirates. *Buildings, 12*(10). doi:10.3390/buildings12101703

IEA. (2019). *Global Status Report for Buildings and Construction 2019*. Retrieved from Paris: https://www.iea.org/reports/global-status-report-for-buildings-and-construction-2019

IEA. (2021). Saudi Arabia. Retrieved from https://www.eia.gov/international/analysis/country/SAU

IEA. (2023). *Net Zero Roadmap: A Global Pathway to Keep the 1.5°C Goal in Reach*. Retrieved from https://www.iea.org/reports/space-cooling-2#dashboard

IEA. (2024). Electricity 2024 Analysis and forecast to 2026. Retrieved from https://www.iea.org/reports/electricity-2024

IES-VE. (2023). Retrieved from https://www.iesve.com/

Illampas, R., Ioannou, I., & Charmpis, D. (2009). *Adobe: an environmentally friendly construction material*.

ISO-7730. (2005). Ergonomics of the thermal environment: Analytical determination and interpretation of thermal comfort using calculation of the PMV and PPD indices and local thermal comfort criteria. In: British Standards Institute.

John, G. R., Owen, L. J., & Theo, S. C. (1992). *Energy in Architecture-The European Passive Solar Handbook*. London: B.T. Batsford Limited, 4 Fitzhardinge Street.

Kamel, E., & Kazemian, A. (2023). BIM-integrated thermal analysis and building energy modeling in 3D-printed residential buildings. *Energy and Buildings, 279*, 112670. doi:https://doi.org/10.1016/j.enbuild.2022.112670

Kaszynka, M., Olczyk, N., Techman, M., Skibicki, S., Zielinski, A., Filipowicz, K., . . . Hoffmann, M. (2019). Thermal-Humidity Parameters of 3D Printed Wall. *IOP Conference Series: Materials Science and Engineering, 471*(8), 082018. doi:10.1088/1757-899X/471/8/082018

Keating, S. (2016). *From Bacteria to Buildings: Additive Manufacturing Outside the Box.* (PhD). Massachusetts Institute of Technology,

Kelly, G. (2025). See how Australia's first 3D-printed multistorey house is being built: four bedrooms in five weeks. Retrieved from https://www.theguardian.com/international

Khalili Tari, M., Reza Faraji, A., Aslani, A., & Zahedi, R. (2023). Energy simulation and life cycle assessment of a 3D printable building. *Cleaner Materials, 7*, 100168. doi:https://doi.org/10.1016/j.clema.2023.100168

Khoshnevis, B. (2004). Automated construction by contour crafting—related robotics and information technologies. *Automation in Construction, 13*(1), 5-19. doi:https://doi.org/10.1016/j.autcon.2003.08.012

Kiamba, L. N. (2016). *Optimising environmental design strategies to improve thermal performance in office buildings in Kenya.* (PhD). University of Nottingham,

Koch-Nielsen, H. (2013). *Stay cool: A design guide for the built environment in hot climates*: Routledge.

Kolarevic, B. (2005). *Architecture in the Digital Age: Design and Manufacturing*. Abingdon: Taylor & Francis.

Kottek, M., Grieser, J., Beck, C., Rudolf, B., & Rubel, F. (2006). World map of the Köppen-Geiger climate classification updated.

Krarti, M., Aldubyan, M., & Williams, E. (2020). Residential building stock model for evaluating energy retrofit programs in Saudi Arabia. *Energy, 195*, 116980.

Krarti, M., Dubey, K., & Howarth, N. (2017). Evaluation of building energy efficiency investment options for the Kingdom of Saudi Arabia. *Energy, 134*, 595-610. doi:10.1016/j.energy.2017.05.084

Lasker, W. J. (2016). *The Impact of Construction and Building Materials on Energy Consumption on Saudi Residential Buildings.* (PhD). University of Heriot-Watt,

Lawrie, L. K., & Crawley, D. B. (2022). Development of Global Typical Meteorological Years (TMYx). *Climate.OneBuilding.Org.* Retrieved from https://climate.onebuilding.org/sources/default.html

Lechner, N. (2014). *Heating, cooling, lighting: Sustainable design methods for architects*: John wiley & sons.

Lim, S., Buswell, R. A., Le, T. T., Austin, S. A., Gibb, A. G. F., & Thorpe, T. (2012). Developments in construction-scale additive manufacturing processes. *Automation in Construction, 21*, 262-268. doi:https://doi.org/10.1016/j.autcon.2011.06.010

Lloret-Fritschi, E. (2016). *Smart Dynamic Casting - A digital fabrication method for non-standard concrete structures.* (PhD). ETH Zürich, Retrieved from http://hdl.handle.net/20.500.11850/123830

Lotfabadi, P., & Hançer, P. (2019). A comparative study of traditional and contemporary building envelope construction techniques in terms of thermal comfort and energy efficiency in hot and humid climates. *Sustainability (Switzerland), 11*(13). doi:10.3390/su11133582

Mahadevan, M., Francis, A., & Thomas, A. (2020). A simulation-based investigation of sustainability aspects of 3D printed structures. *Journal of Building Engineering, 32*, 101735. doi:https://doi.org/10.1016/j.jobe.2020.101735

Mahgoub, M., & Saber, E. (2022). Reducing carbon footprint and cooling demand in arid climates using an integrated hybrid ventilation and photovoltaic approach. *Environment, Development and Sustainability, 24*. doi:10.1007/s10668-021-01571-1

Mahmoud, S., & Ismaeel, W. S. E. (2019). Developing sustainable design guidelines for roof design in a hot arid climate. *Architectural Science Review, 62*(6), 507-519. doi:10.1080/00038628.2019.1665984

Marais, H., Christen, H., Cho, S., De Villiers, W., & Van Zijl, G. (2021). Computational assessment of thermal performance of 3D printed concrete wall structures with cavities. *Journal of Building Engineering, 41*, 102431. doi:https://doi.org/10.1016/j.jobe.2021.102431

Marzoq, A. (2010). *The Art of Vernacular Architecture of Asir*. Riyadh: Saudi Heritage Commission.

Meibodi, M. A., Jipa, A., Giesecke, R., Shammas, D., Bernhard, M., Leschok, M., . . . Dillenburger, B. (2018). *Smart Slab: Computational Design and Digital Fabrication of a Lightweight Concrete Slab*. Paper presented at the 38th Annual Conference of the Association for Computer Aided Design in Architecture (ACADIA 2018), Mexico City, Mexico. http://hdl.handle.net/20.500.11850/315758

Ministry of Municipal Rural Affairs and Housing. (2022). Modern Construction Initiative. Retrieved from https://momrah.gov.sa/ar

Ministry of Municipal Rural Affairs and Housing. (2023). Retrieved from

Mirrahimi, S., Mohamed, M. F., Haw, L. C., Ibrahim, N. L. N., Yusoff, W. F. M., & Aflaki, A. (2016). The effect of building envelope on the thermal comfort and energy saving for high-rise buildings in hot–humid climate. *Renewable and Sustainable Energy Reviews, 53*, 1508-1519. doi:10.1016/j.rser.2015.09.055

Mohamed, M. (2010). *Traditional ways of dealing with climate in Egypt.* Paper presented at the The Seventh International Conference of Sustainable Architecture and Urban Development (SAUD 2010). S. Lehmann, HA Waer and J. Al-Qawasmi. Amman, Jordan, The Center for the Study of Architecture in Arab Region (CSAAR Press).

Monawar, A. H. (2001). *A study of energy conservation in the existing apartment buildings in Makkah Region, Saudi Arabia.* (PhD). Newcastle University,

NASA. (2021). Global Temperature Anomalies from 1880 to 2020. Retrieved from https://svs.gsfc.nasa.gov/4882

National Center for Meteorology. (2023). Retrieved from https://ncm.gov.sa/ar/Pages/default.aspx

Nicol, J. F., & Humphreys, M. A. (2002). Adaptive thermal comfort and sustainable thermal standards for buildings. *34*(6), 563-572. doi:10.1016/S0378-7788(02)00006-3

Nicol, J. F., Raja, I. A., Allaudin, A., & Jamy, G. N. (1999). Climatic variations in comfortable temperatures: the Pakistan projects. *Energy and Buildings, 30*(3), 261-279. doi:https://doi.org/10.1016/S0378-7788(99)00011-0

Nithesh, N. (2018). *Development of concrete 3D printing.* (Master of Science in Building Technology). Aalto University,

O'Neill, A. (2021). Saudi Arabia: Total population from 2016 to 2026. Retrieved from https://www.statista.com/statistics/262467/total-population-of-saudi-arabia/

Obaid, R. R., & Mufti, A. H. (2008). *Present state, challenges, and future of power generation in Saudi Arabia.* Paper presented at the 2008 IEEE Energy 2030 Conference.

Olgyay, V. (2015). *Design with climate: bioclimatic approach to architectural regionalism-new and expanded edition*: Princeton university press.

Pachano, J. E., & Bandera, C. F. (2021). Multi-step building energy model calibration process based on measured data. *Energy and Buildings, 252*, 111380. doi:https://doi.org/10.1016/j.enbuild.2021.111380

Parsons, K. C. (2014). *Human thermal environments : the effects of hot, moderate, and cold environments on human health, comfort, and performance* (3rd edition ed.). Boca Raton ;: CRC Press.

Peeters, L., Dear, R. d., Hensen, J., & D'haeseleer, W. (2009). Thermal comfort in residential buildings: Comfort values and scales for building energy simulation. *Applied Energy, 86*(5), 772-780.

Pérez-Lombard, L., Ortiz, J., & Pout, C. (2008). A review on buildings energy consumption information. *Energy and Buildings, 40*(3), 394-398. doi:https://doi.org/10.1016/j.enbuild.2007.03.007

Pessoa, S., Guimarães, A. S., Lucas, S. S., & Simões, N. (2021). 3D printing in the construction industry - A systematic review of the thermal performance in buildings. *Renewable and Sustainable Energy Reviews, 141*, 110794. doi:https://doi.org/10.1016/j.rser.2021.110794

Prieto, A., Knaack, U., Klein, T., & Auer, T. (2017). 25 Years of cooling research in office buildings: Review for the integration of cooling strategies into the building façade (1990–2014). *Renewable and Sustainable Energy Reviews, 71*, 89-102. doi:10.1016/j.rser.2017.01.012

Ralegaonkar, R. V., & Gupta, R. (2010). Review of intelligent building construction: A passive solar architecture approach. *Renewable and Sustainable Energy Reviews, 14*(8), 2238-2242. doi:https://doi.org/10.1016/j.rser.2010.04.016

Ritchie, H., Roser, M., & Rosado, P. (2020). CO_2 and Greenhouse Gas Emissions. Retrieved from https://ourworldindata.org/co2-and-greenhouse-gas-emissions

Riyadh Urban Observatory. (2022). Retrieved from http://www.ruo.gov.sa/EN/

Royal Commission for Riyadh City. (2016). *Population Study of Riyadh City (143H)*. Retrieved from

Royal Commission for Riyadh City. (2018). *Arriyadh Urban Observatory Indicators*. Retrieved from http://www.ruo.gov.sa/EN/

Saber, H. H., & Maref, W. (2019). Energy performance of cool roofs followed by development of practical design tool. *Frontiers in Energy Research, 7*, 122.

Salandin, A., Quintana-Gallardo, A., Gómez-Lozano, V., & Guillén-Guillamón, I. (2022). The First 3D-Printed Building in Spain: A Study on Its Acoustic, Thermal and Environmental Performance. *Sustainability, 14*(20). doi:10.3390/su142013204

Saleh, M. A. E. (1990). Adobe as a thermal regulating material. *Solar & Wind Technology, 7*(4), 407-416. doi:https://doi.org/10.1016/0741-983X(90)90025-W

Saudi Central Bank. (2023). Retrieved from https://www.sama.gov.sa/en-US/EconomicReports/Pages/AnnualReport.aspx

Saudi Electricity Company. (2023). Retrieved from https://www.se.com.sa/

Saudi Infrastructure EXPO. Invest in Saudi Arabia. Retrieved from https://www.saudiinfrastructureexpo.com/invest-in-saudi-arabia/

Saulles, T. d. (2019). *Thermal Mass Explained*. London: The Concrete Centre.

SBC 602. (2018). *Saudi Energy Conservation Code - Low Rise (SBC 602)*. Retrieved from

SEEC. (2023). Saudi Energy Efficiency Center. Retrieved from https://www.seec.gov.sa/en/

Shahrouri, I., Moghazy, N., & Awad, S. (2022). *Transforming the Housing Sector in Saudi Arabia*. Retrieved from pwc.com/me/housingsector-ksa

Shehata, A., & Waheeb, S. (2018). Thermal Performance of Contemporary Residential Buildings in Hot-Arid Climates. *Journal of Advanced Research in Dynamical and Control Systems, special*, 1295-1303.

Sitnikov, V. (2020). *The Rationale and Potential of Ice-Based Moulding Systems for the Production of Complex-Geometry Precast Concrete.* (PHD). KTH Royal Institute of Technology,

Solmaz, A. S. (2019). A critical review on building performance simulation tools. *Alam Cipta, 12*(2), 7-21.

Sovetova, M., & Kaiser Calautit, J. (2024). Thermal and energy efficiency in 3D-printed buildings: Review of geometric design, materials and printing processes. *Energy and Buildings, 323*, 114731. doi:https://doi.org/10.1016/j.enbuild.2024.114731

Staszczuk, A., Wojciech, M., & Kuczyński, T. (2017). The effect of floor insulation on indoor air temperature and energy consumption of residential buildings in moderate climates. *Energy, 138*, 139-146. doi:https://doi.org/10.1016/j.energy.2017.07.060

Statista. (2022). Electricity consumption in Saudi Arabia in 2020, by sector. Retrieved from https://www.statista.com/statistics/975288/saudi-arabia-electricity-consumption-by-sector/

Statista. (2023). Construction industry in the GCC - statistics & facts. Retrieved from https://www-statista-com.nottingham.idm.oclc.org/topics/7193/construction-industry-in-the-gcc/#topicOverview

Statista. (2024). Net electricity consumption worldwide in select years from 1980 to 2022. Retrieved from https://www.statista.com/statistics/280704/world-power-consumption/

Stouhi, D. (2018). ETH Zurich Fabricated the World's First Full-Scale Architectural Project Using 3-D Sand Printing. Retrieved from https://www.archdaily.com/899392/eth-zurich-fabricated-the-worlds-first-full-scale-architectural-project-using-3-d-sand-printing

Sun, J., Xiao, J., Li, Z., & Feng, X. (2021). Experimental study on the thermal performance of a 3D printed concrete prototype building. *Energy and Buildings, 241*, 110965. doi:https://doi.org/10.1016/j.enbuild.2021.110965

Suntharalingam, T., Upasiri, I., Gatheeshgar, P., Poologanathan, K., Nagaratnam, B., Santos, P., & Rajanayagam, H. (2021). Energy Performance of 3D-Printed Concrete Walls: A Numerical Study. *Buildings, 11*(10). doi:10.3390/buildings11100432

Szokolay, S. V. (2004). *Introduction to Architectural Science: The Basis of Sustainable Design*.

Taleb, H. M. (2011). *Towards Sustainable Residential Buildings in the Kingdom of Saudi Arabia.* (PhD). The University of Sheffield,

Taleb, H. M. (2014). Using passive cooling strategies to improve thermal performance and reduce energy consumption of residential buildings in U.A.E. buildings. *Frontiers of Architectural Research, 3*(2), 154-165. doi:10.1016/j.foar.2014.01.002

Taleb, H. M., & Sharples, S. (2011). Developing sustainable residential buildings in Saudi Arabia: A case study. *Applied Energy, 88*(1), 383-391. doi:10.1016/j.apenergy.2010.07.029

Talib, K. (1984). *Shelter in Saudi Arabia*. London: Academy Editions.

The World Bank Group. (2022a). Electric power consumption (kWh per capita). Retrieved from https://data.worldbank.org/indicator/EG.USE.ELEC.KH.PC?end=2019&start=1960

The World Bank Group. (2022b). Surface area (sq. km). Retrieved from https://data.worldbank.org/indicator/AG.SRF.TOTL.K2?locations=1A

The World Bank Group. (2023). CO2 emissions (metric tons per capita). Retrieved from https://data.worldbank.org/indicator/EN.ATM.CO2E.PC

Time and Data AS. (2022). Riyadh, Saudi Arabia — Sunrise, Sunset, and Daylength. Retrieved from https://www.timeanddate.com/

Urbanist. (2023). Made in China: World's First 3D-Printed Apartment Complex. Retrieved from https://weburbanist.com/2015/01/20/made-in-china-worlds-first-3d-printed-apartment-complex/

Vision 2030. (2022a).

Vision 2030. (2022b). *Housing Program Delivery Plan (2021-2025)*. Retrieved from https://www.vision2030.gov.sa/v2030/vrps/housing/

Vu, H. (2014). Contour Crafting earns Khoshnevis top design prize. Retrieved from https://news.usc.edu/69544/contour-crafting-earns-professor-top-design-prize/

Wahl, E. (2017). Buildings in arid desert climate: Improving energy efficiency with measures on the building envelope. In.

Watkin, H. (2018). ETH Zurich Uses 3D Sand Printed Formwork to Build Concrete Smart Slab. Retrieved from https://all3dp.com/4/eth-zurich-researchers-use-3d-sand-printed-formwork-build-concrete-smart-slab/

Weather Atlas. (2022). Monthly weather forecast and climate (Riyadh, Saudi Arabia). Retrieved from https://www.weather-atlas.com/

Weather Spark. (2022). Retrieved from https://weatherspark.com/

Weatherbase. (2022). Riyadh, Saudi Arabia. Retrieved from https://www.weatherbase.com/

Winsun. (2016). *Demonstrating the Viability of 3D Printing at Construction Scale.* Paper presented at the World Economic Forum.

World Meteorological Organization. (2022). World Weather Information Services. Retrieved from https://worldweather.wmo.int/en/home.html

WorldData.info. (2023). The climate in Saudi Arabia. Retrieved from https://www.worlddata.info/asia/saudi-arabia/climate.php

Wu, P., Wang, J., & Wang, X. (2016). A critical review of the use of 3-D printing in the construction industry. *Automation in Construction, 68*, 21-31. doi:https://doi.org/10.1016/j.autcon.2016.04.005

Yau, Y. H., & Chew, B. T. (2012). A review on predicted mean vote and adaptive thermal comfort models. *Building Services Engineering Research and Technology, 35*(1), 23-35. doi:10.1177/0143624412465200

Yin, H., Qu, M., Zhang, H., & Lim, Y. (2018). 3D Printing and Buildings: A Technology Review and Future Outlook. *Technology|Architecture + Design, 2*(1), 94-111. doi:10.1080/24751448.2018.1420968

Zawya. (2022). Housing demand in Saudi Arabia to surge 50% by 2030 – PwC. Retrieved from https://www.zawya.com/en/projects/construction/housing-demand-in-saudi-arabia-to-surge-50-by-2030-pwc-tl0qfqud

Zhang, S., & Lin, Z. (2020). Standard effective temperature based adaptive-rational thermal comfort model. *Applied Energy, 264*, 114723.

APPENDICES

- Appendix A
- Appendix B
- Appendix C
- Appendix D

APPENDICES

Appendix A

A-A: Research validation of energy simulation software for residential buildings in Riyadh

To assess the uncertainty of IES-VE tool and the adopted simulation process, this study seeks to compare IES-VE output with studies examining energy consumption and thermal performance of residential buildings in Riyadh, withing data such as:

- Constructing the model accurately,
- Inputting construction material properties correctly,
- Inputting the weather data, site settings, and data inputs correctly,
- Running the simulation and obtaining results correctly.

The primary objective was to determine the IES model's position among other developed models, particularly those representing typical dwellings in Riyad, KSA.

Alaidroos and Krarti (2015) conducted a comprehensive study to investigate and improve the energy performance of typical Saudi dwellings by optimizing the building envelope components. The researchers employed DesignBuilder simulation software to carry out their analysis. The construction materials and configurations for walls, windows, roof, and ground floor—summarized in the table below—represent conventional KSA's dwellings and provide a foundation for evaluating the energy performance of the building envelope.

Since the aforementioned study was carried out using DesignBuilder, the same model was recreated in IES-VE, following the simulation workflow and modelling steps described in this thesis, with the aim of reproducing the published results. It should be noted that the developed IES model employed identical inputs for construction material, occupancy profile, lighting and appliances power consumptions, and HVAC system to that identified in original study. These data are summarized in the tables below.

The annual electricity consumptions for Aladiroos and his colleague's model (published) and the replicated IES model (reproduced) were 119,700 kWh (or 228 kWh/m^2) and 121,143 kWh (or 230 kWh/m^2), respectively, indicating that the replicated model consumes about 2 kWh/m^2 more electricity annually.

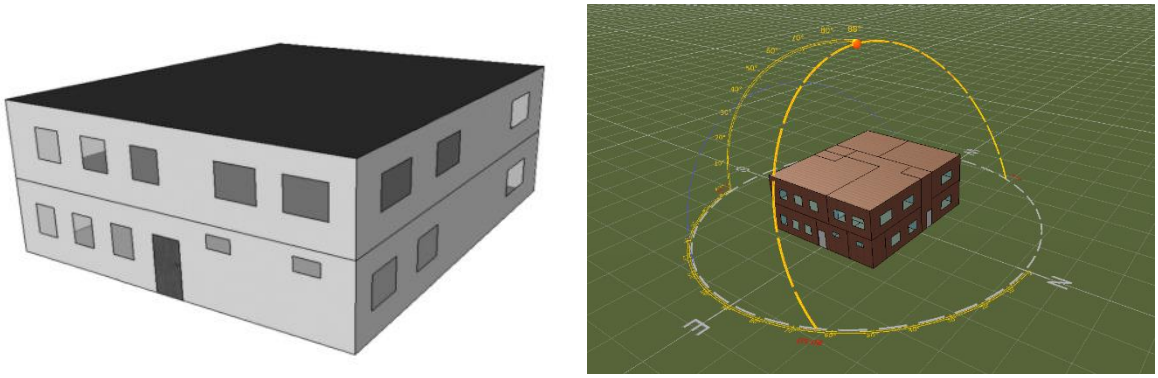
Building construction specifications

Location	Riyadh
Orientation	Front elevation facing east
Number of stories	2
Total height	7.0 m
Floor dimension	15.0 m × 17.5 m
Gross floor area	525.0 m^2
Gross wall area	455.0 m^2 (including windows)
Window area	13.29% of gross wall area
Type of glass	Single pane window
External walls	20 mm plaster outside + 200 mm concrete hollow block + 20 mm plaster inside
Roof	10 mm built-up roofing + 150 mm concrete slab + 12.7 mm plaster inside
Floor	150 mm slab on grade
Number of occupants	6
Lighting	3.0 kW (lower level), 2.0 kW (upper level)
Appliances	2.0 kW (lower level), 1.0 kW (upper level)

Total annual energy consumption	Published:	119,700 kWh (equivalent to 228 kWh/m^2)
	Reproduced:	121,143 kWh (equivalent to about 230 kWh/m^2)

HVAC system specification

Characteristics	Description
System type	Constant-Volume DX air-cooled A/C system with electric heating
Thermostat type	Two-position with dual (heating and cooling) set point
Thermostat setting	72°F for heating and 76°F for cooling
Heating and cooling	Available throughout the year
COP	2.17
Ventilation	None
Infiltration	Assumed 0.7 ACH for the replicated model in IES-VE based on reviewed literature



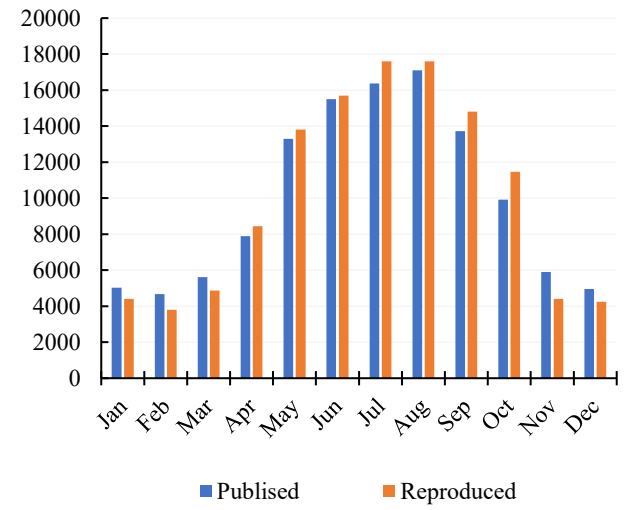
(A) (B)

Constructed energy model: (A) DesignBuilder model (published); (B) IES-VE model (reproduced)

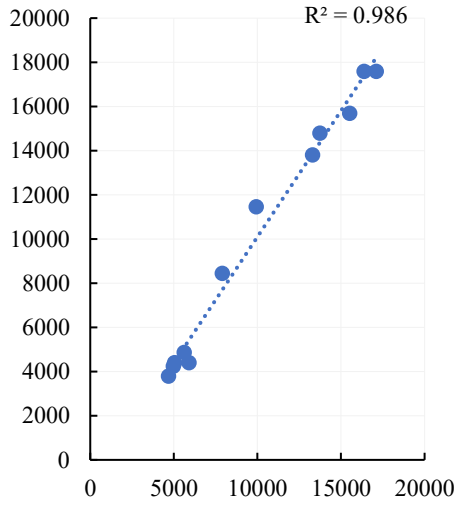
The study was conducted in Riyadh, KSA; thus, the same weather file employed in this thesis—obtained from Climate.onebuilding.org—was utilized for the developed IES model. The purpose of this analysis was to validate the reliability of the employed simulation tool (IES-VE), along with the simulation process, settings, and data inputs used in this thesis, including ground temperatures.

Despite the high level of agreement between the published reproduced data, the variance could be due to variation in weather data, default settings of simulation software, and some assumptions that were not included in Alaidroos and Krarti's study, such as ground temperature input, infiltration rate, site settings, and sensible and latent heat gain. It was demonstrated in this thesis that ground temperature settings and data input showed clear data variance, especially when they are not involved in the simulation process, thus impacting the simulation outputs. Nevertheless, the difference in electricity consumption between the published and replicated models is not significantly greater than 2 kWh/m^2/year.

Analysis of the monthly consumptions between the two models demonstrated a high correlation between published and reproduced results, with mean absolute error (MAE) of 8.3% and root mean square error (RMSE) of 9.2%, thereby encouraging the reliability of the selected simulation tool and simulation process adopted in this thesis.



Monthly consumptions (in kWh)

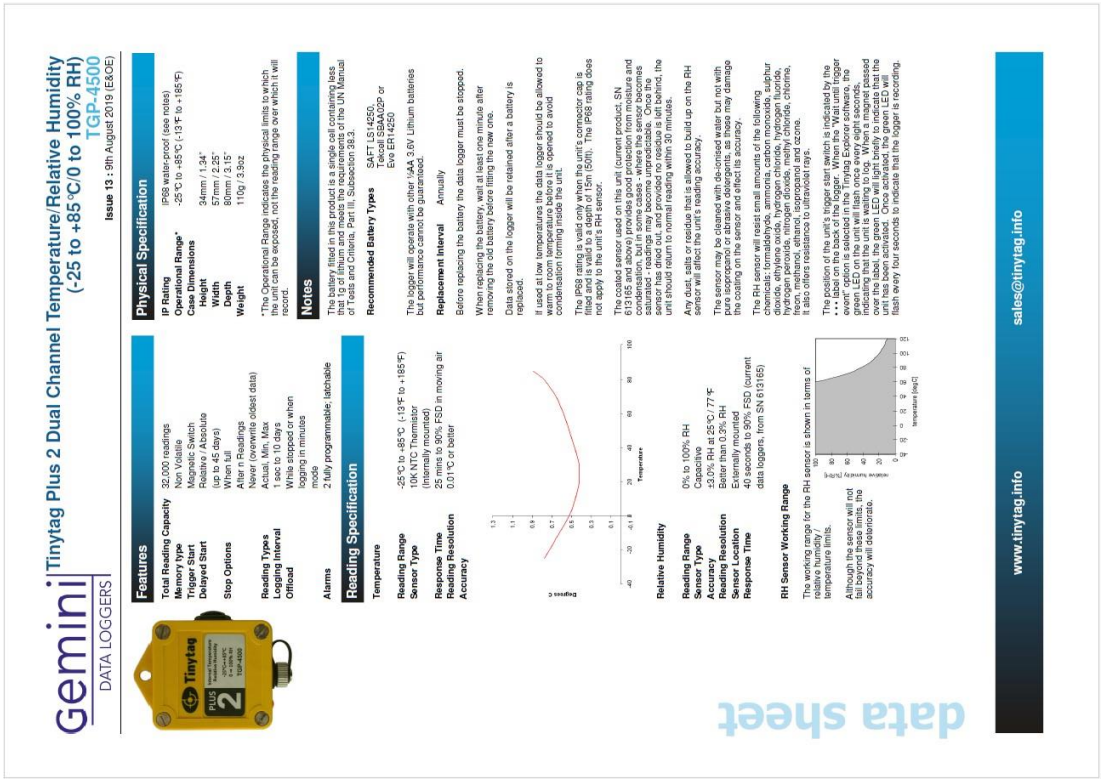


The trend between the two sets of data

A comparison between published and reproduced results in terms of energy consumptions (kWh) shows high correlation between the two sets of data.

A-B: Specification sheet of data loggers

Tinytag Plus 2 (TGP-4500): outdoor



gemini DATA LOGGERS

Tinytag Plus 2 Dual Channel Temperature/Relative Humidity (-25 to +85°C/0 to 100% RH)

TGP-4500

Issue 13 : 9th August 2019 (E&OE)

Features

Total Reading Capacity	32,000 readings
Memory type	Non Volatile
Trigger Start	Magnetic Switch
Delayed Start	Relative / Absolute (up to 45 days)
Stop Options	When full After n Readings Never (overwrite oldest data)
Reading Types	Actual, Min, Max
Logging Interval	1 sec to 10 days
Offload	While stopped or when logging in minutes mode
Alarms	2 fully programmable, latchable

Physical Specification

IP Rating	IP68 water-proof (see notes)
Operational Range*	-25°C to +85°C (-13°F to +185°F)
Case Dimensions	
Height	34mm / 1.34"
Width	57mm / 2.25"
Depth	80mm / 3.15"
Weight	110g / 3.9oz

*The Operational Range indicates the physical limits to which the unit can be exposed, not the reading range over which it will record.

Reading Specification

Temperature	
Reading Range	-25°C to +85°C (-13°F to +185°F)
Sensor Type	10K NTC Thermistor (Internally mounted)
Response Time	25 mins to 90% FSD in moving air
Reading Resolution	0.01°C or better
Accuracy	

Relative Humidity	
Reading Range	0% to 100% RH
Sensor Type	Capacitive
Accuracy	±3.0% RH at 25°C / 77°F
Reading Resolution	Better than 0.3% RH
Sensor Location	Externally mounted
Response Time	40 seconds to 90% FSD (current data loggers, from SN 613165)

RH Sensor Working Range

The working range for the RH sensor is shown in terms of relative humidity / temperature limits.

Although the sensor will not fail beyond these limits, the accuracy will deteriorate.

Notes

The battery fitted in this product is a single cell containing less that 1g of lithium and meets the requirements of the UN Manual of Tests and Criteria, Part III, Subsection 38.3.

Recommended Battery Types	SAFT LS14250, Tekcell SB-AA02P or Eve ER14250

The logger will operate with other 1xAA 3.6V Lithium batteries but performance cannot be guaranteed.

Replacement Interval	Annually

Before replacing the battery, the data logger must be stopped.

When replacing the battery, wait at least one minute after removing the old battery before fitting the new one.

Data stored on the logger will be retained after a battery is replaced.

It used at low temperatures the data logger should be allowed to warm to room temperature before it is opened to avoid condensation forming inside the unit.

The IP68 rating is valid only when the unit's connector cap is fitted and the battery compartment lid is sealed (both). The IP68 rating does not apply to the unit's RH sensor.

The coated sensor used on this unit (current product, SN 613165 and above) provides good protection from moisture and condensation, but in some cases - where the sensor becomes saturated - readings may become unpredictable. Once the sensor dries out (which may take several days), and the unit should return to normal reading within 30 minutes.

Any dust, salts or residue that is allowed to build up on the RH sensor will affect the unit's reading accuracy.

The sensor may be cleaned with de-ionised water but not with cleaning fluids or detergents as these may damage the coating on the sensor and affect its accuracy.

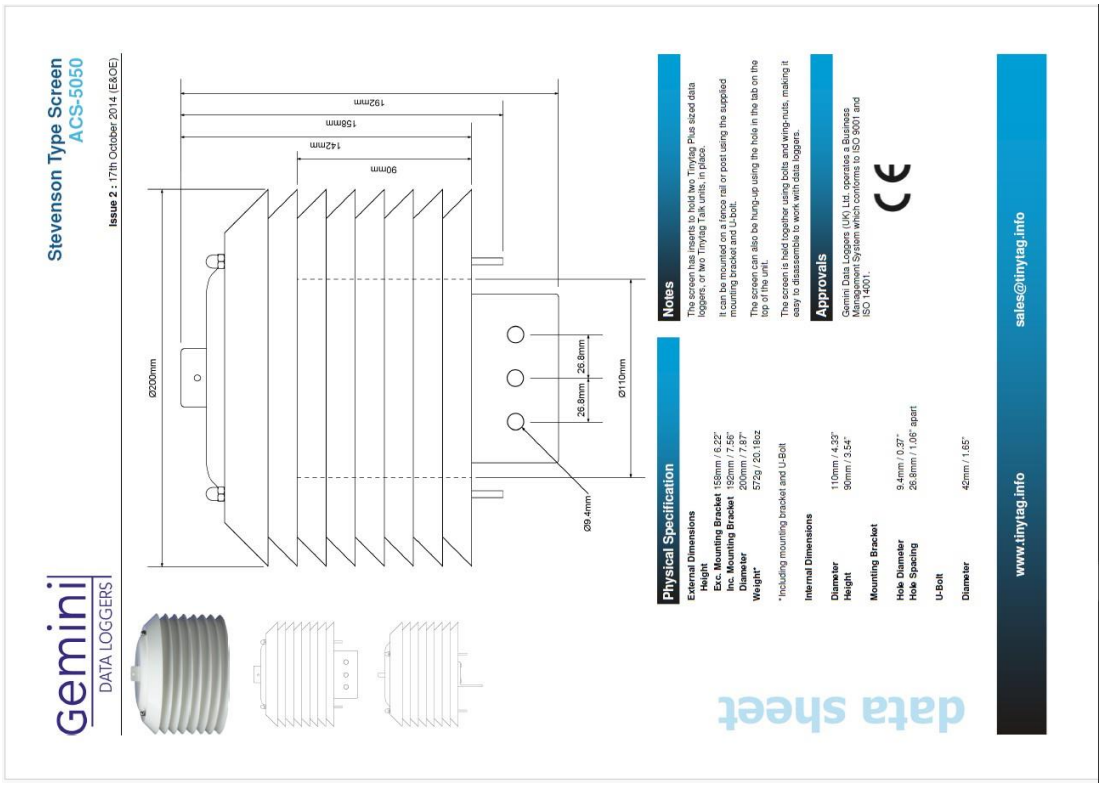
The RH sensor will resist small amounts of the following chemicals: formaldehyde, ammonia, carbon monoxide, sulphur dioxide, ethylene oxide, hydrogen chloride, hydrogen fluoride, hydrogen peroxide, nitrogen dioxide, methyl chloride, chlorine. It also offers resistance to ultraviolet rays.

The position of the unit's trigger start switch is indicated by the "• •" label on the back of the logger. When the "Wait until trigger event" option is selected in the Tinytag Explorer software, the green LED on the unit will flash once every eight seconds. Pressing the switch for 1 second will start the logger. Once passed over the label, the green LED will light briefly to indicate that the unit has been activated. Once activated, the green LED will flash every four seconds to indicate that the logger is recording.

data sheet

www.tinytag.info sales@tinytag.info

Stevenson Type Screen



Stevenson Type Screen ACS-5050

Issue 2 : 17th October 2014 (E&OE)

gemini DATA LOGGERS

Physical Specification

External Dimensions	
Height	
Exc. Mounting Bracket	158mm / 6.22"
Inc. Mounting Bracket	192mm / 7.56"
Diameter	200mm / 7.87"
Weight*	572g / 20.18oz

*Including mounting bracket and U-Bolt

Internal Dimensions	
Diameter	110mm / 4.33"
Height	90mm / 3.54"
Mounting Bracket	
Hole Diameter	9.4mm / 0.37"
Hole Spacing	26.8mm / 1.05" apart
U-Bolt	
Diameter	42mm / 1.65"

Notes

The screen has inserts to hold two Tinytag Plus sized data loggers, or two Tinytag Talk units, in place.

It can be mounted on a fence rail or post using the supplied mounting bracket and U-bolt.

The screen can also be hung-up using the hole in the tab on the top of the unit.

The screen is held together using bolts and wing-nuts, making it easy to disassemble to work with data loggers.

Approvals

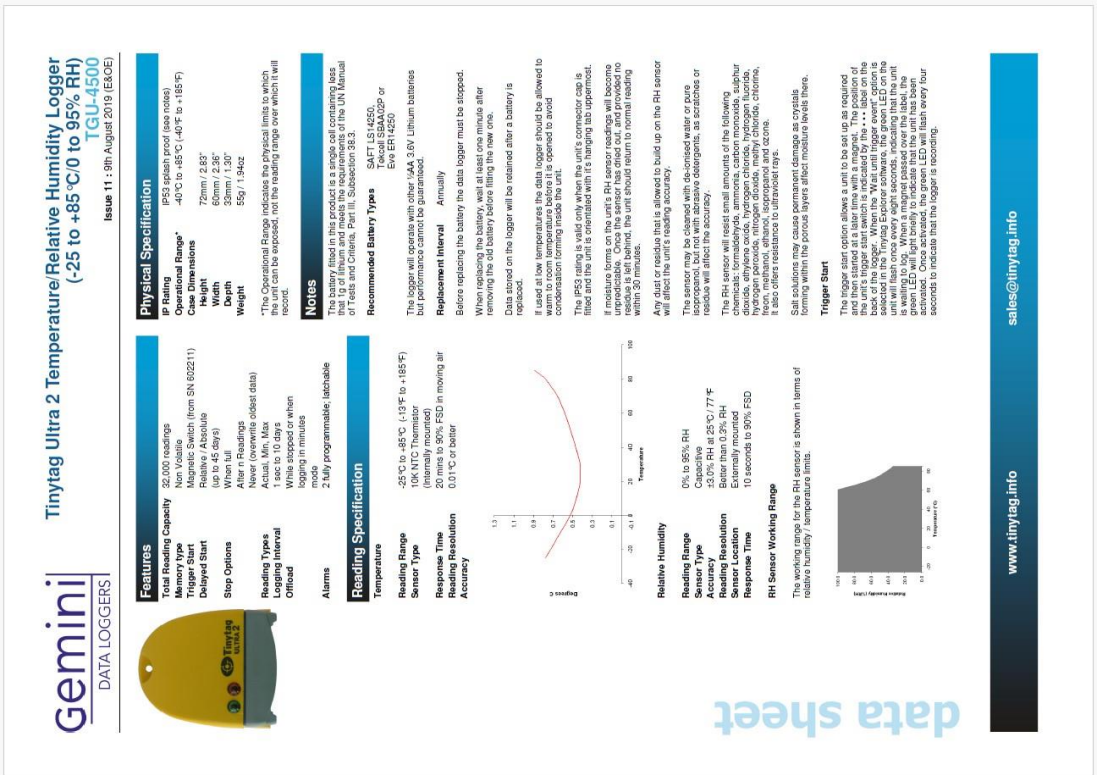
Gemini Data Loggers (UK) Ltd. operates a Business Management System which conforms to ISO 9001 and ISO 14001.

CE

data sheet

www.tinytag.info sales@tinytag.info

Tinytag Ultra-2 (TGU-4500): indoor



gemini DATA LOGGERS

Tinytag Ultra 2 Temperature/Relative Humidity Logger (-25 to +85 °C/0 to 95% RH) TGU-4500

Issue 11 : 9th August 2019 (E&OE)



Features

Total Reading Capacity	32,000 readings
Memory type	Non Volatile
Trigger Start	Magnetic Switch (from SN 602211)
Delayed Start	Relative / Absolute (up to 45 days)
Stop Options	When full After n Readings Never (overwrite oldest data)
Reading Types	Actual, Min, Max
Logging Interval	1 sec to 10 days
Offload	While stopped or when logging in minutes mode
Alarms	2 fully programmable; latchable

Reading Specification

Temperature

Reading Range	-25°C to +85°C (-13°F to +185°F)
Sensor Type	10K NTC Thermistor (Internally mounted)
Response Time	20 mins to 90% FSD in moving air
Reading Resolution	0.01°C or better
Accuracy	

Relative Humidity

Reading Range	0% to 95% RH
Sensor Type	Capacitive
Accuracy	±3.0% RH at 25°C / 77°F
Reading Resolution	Better than 0.3% RH
Sensor Location	Externally mounted
Response Time	10 seconds to 90% FSD

RH Sensor Working Range

The working range for the RH sensor is shown in terms of relative humidity / temperature limits.

Physical Specification

IP Rating	IP53 splash proof (see notes)
Operational Range*	-40°C to +85°C (-40°F to +185°F)
Case Dimensions	
Height	72mm / 2.83"
Width	60mm / 2.36"
Depth	33mm / 1.30"
Weight	55g / 1.94oz

*The Operational Range indicates the physical limits to which the unit can be exposed, not the reading range over which it will record.

Notes

The battery fitted in this product is a single cell containing less that 1g of lithium and meets the requirements of the UN Manual of Tests and Criteria, Part III, Subsection 38.3.

Recommended Battery Types	SAFT LS14250; Tekcell SB-AA02P or Eve ER14250

This logger will operate with other ½AA 3.6V Lithium batteries but performance cannot be guaranteed.

Replacement Interval	Annually

Before replacing the battery the data logger must be stopped.

When replacing the battery, wait at least one minute after removing the old battery before fitting the new one.

Data stored on the logger will be retained after a battery is replaced.

If used at low temperatures the data logger should be allowed to warm to room temperature before it is opened to avoid condensation forming inside the unit.

The IP53 rating is valid only when the unit's connector cap is fitted and the unit is orientated with it's hanging tab uppermost.

If moisture forms on the unit's RH sensor readings will become unreliable. Should this occur, drying the unit for 24 hours with no residue is left behind, the unit should return to normal reading within 30 minutes.

Any dust or residue that is allowed to build up on the RH sensor will affect the unit's reading accuracy.

The sensor may be cleaned with de-ionised water or pure isopropanol, but not with abrasive detergents, as scratches or residue will affect the accuracy.

This RH sensor will resist small amounts of the following chemicals: formaldehyde, ammonia, carbon monoxide, sulphur dioxide, ethylene oxide, hydrogen chloride, hydrogen fluoride, hydrogen peroxide, nitrogen dioxide, methyl chloride, chlorine, freon, methanol, ethanol, isopropanol and ozone.
It also offers resistance to ultraviolet rays.

Salt solutions may cause permanent damage as crystals forming within the porous layers affect moisture levels there.

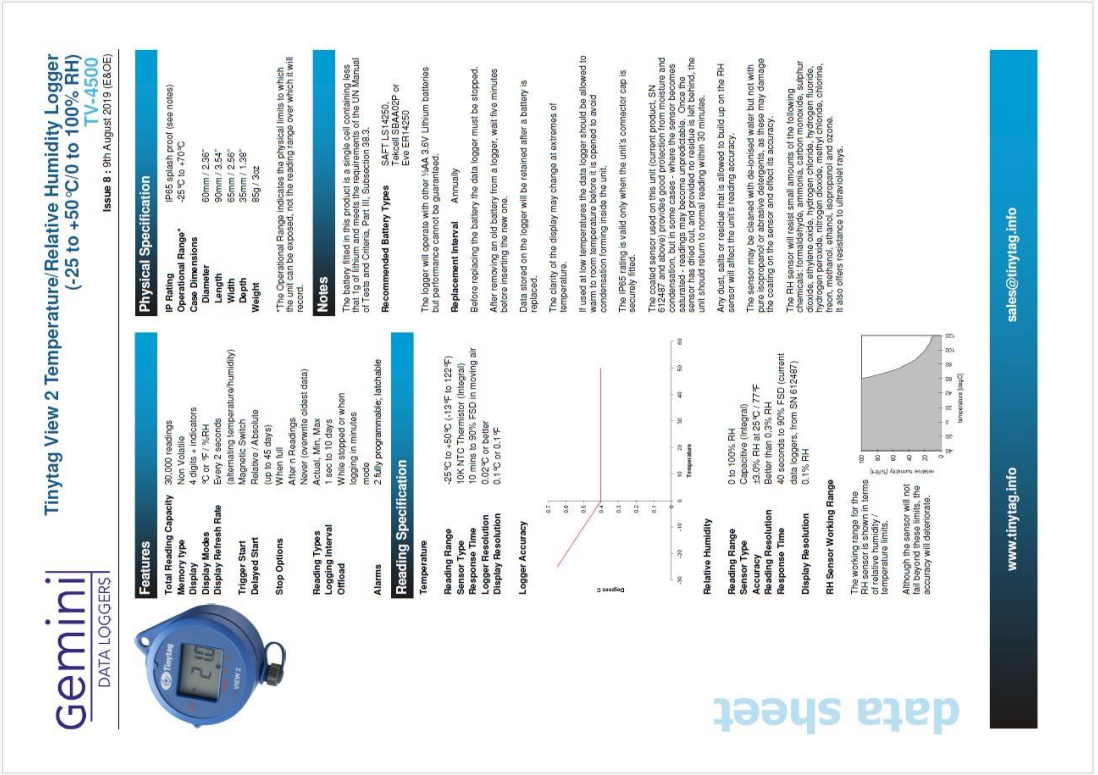
Trigger Start

The trigger start option allows a unit to be set up as required (stopped or logging) and then started by the operation of the unit's trigger start switch is indicated by the • • • label on the back of the logger. When the 'Wait until trigger event' option is selected, the green LED will flash once every 8 seconds. Once the unit will flash once every eight seconds, indicating that the unit is waiting to log. When a magnet passed over the label, the green LED will light briefly to indicate that the unit has been triggered. The LED will then flash every 4 seconds to indicate that the logger is recording.

data sheet

www.tinytag.info sales@tinytag.info

Tinytag View-2 (TV-4500): indoor



gemini DATA LOGGERS

Tinytag View 2 Temperature/Relative Humidity Logger (-25 to +50 °C/0 to 100% RH) TV-4500

Issue 8 : 9th August 2019 (E&OE)

Features

Total Reading Capacity	30,000 readings
Memory type	Non Volatile
Display	4 digits + indicators
Display Modes	°C or °F / %RH
Display Refresh Rate	Every 2 seconds (alternating temperature/humidity)
Trigger Start	Magnetic Switch
Delayed Start	Relative / Absolute (up to 45 days)
Stop Options	When full After n Readings Never (overwrite oldest data)
Reading Types	Actual, Min, Max
Logging Interval	1 sec to 10 days
Offload	While stopped or when logging in minutes mode
Alarms	2 fully programmable; latchable

Reading Specification

Temperature

Reading Range	-25°C to +50°C (-13°F to 122°F)
Sensor Type	10K NTC Thermistor (Integral)
Response Time	10 mins to 90% FSD in moving air
Logger Resolution	0.02°C or better
Display Resolution	0.1°C or 0.1°F

Logger Accuracy

Relative Humidity

Reading Range	0 to 100% RH
Sensor Type	Capacitive (integral)
Accuracy	±3.0% RH at 25°C / 77°F
Reading Resolution	Better than 0.3% RH
Response Time	40 seconds to 90% FSD (current data loggers, from SN 612487)
Display Resolution	0.1% RH

RH Sensor Working Range

The working range for the RH sensor is shown in terms of relative humidity / temperature limits.

Although the sensor will not fail beyond these limits, the accuracy will deteriorate.

Physical Specification

IP Rating	IP65 splash proof (see notes)
Operational Range*	-25°C to +70°C
Case Dimensions	
Diameter	80mm / 3.26"
Length	90mm / 3.54"
Width	65mm / 2.56"
Depth	35mm / 1.38"
Weight	85g / 3oz

*The Operational Range indicates the physical limits to which the unit can be exposed, not the reading range over which it will record.

Notes

The battery fitted in this product is a single cell containing less that 1g of lithium and meets the requirements of the UN Manual of Tests and Criteria, Part III, Subsection 38.3.

Recommended Battery Types	SAFT LS14250; Tekcell SB-AA02P or Eve ER14250

This logger will operate with other ½AA 3.6V Lithium batteries but performance cannot be guaranteed.

Replacement Interval	Annually

Before replacing the battery the data logger must be stopped.

After removing an old battery from a logger, wait five minutes before inserting the new one.

Data stored on the logger will be retained after a battery is replaced.

The clarity of the display may change at extremes of temperature.

If used at low temperatures the data logger should be allowed to warm to room temperature before it is opened to avoid condensation forming inside the unit.

This IP65 rating is valid only when the unit's connector cap is securely fitted.

The coated sensor used on this unit (current product, SN 612487 and above) provides good protection from moisture and condensation, however, should the sensor become saturated - readings may become unpredictable. Once the sensor has dried out, and provided no residue is left behind, the unit should return to normal reading within 30 minutes.

Any dust, salts or residue that is allowed to build up on the RH sensor will affect the unit's reading accuracy.

The sensor may be cleaned with de-ionised water but not with pure isopropanol or abrasive detergents, as these may damage the coating on the sensor and affect its accuracy.

This RH sensor will resist small amounts of the following chemicals: formaldehyde, ammonia, carbon monoxide, sulphur dioxide, ethylene oxide, hydrogen chloride, hydrogen fluoride, hydrogen peroxide, nitrogen dioxide, methyl chloride, chlorine, freon, methanol, ethanol, isopropanol and ozone.
It also offers resistance to ultraviolet rays.

data sheet

www.tinytag.info sales@tinytag.info

PCE-WB 20SD

DATA SHEET

Technical specifications

Wet Bulb Globe Temperature (WBGT)

Measurement range	Indoors: 0 ... +59 °C (32 ... 138 °F) Outdoors: 0 ... +56 °C (32 ... 132 °F)
Accuracy indoors	± 1 °C (± 1.5 °F) from +15 ... +59 °C (59 ... 138 °F) ± 1.5 °C (± 2.7 °F) other temperature ranges
Accuracy outdoors	± 1.5 °C (± 2.7 °F) from +15 ... +56 °C (59 ... 132 °F) ± 2 °C (± 3.6 °F) other temperature ranges

Air Temperature (TA)

Measurement range	0 ... +50 °C
Resolution	0.1 °C
Accuracy	± 0.6 °C

Black-Globe Temperature

Measuring range	0 ... +80 °C
Resolution	0.1 °C
Accuracy	± 0.6 °C

Humidity

Measurement range	5 ... 95 % R.H.
Resolution	0.1 % R.H.
Accuracy	>70 % RH: ± (3 % read value + 1 % RH) < 70 % RH: ± 3 % RH

Dew Point Temperature

Measuring range	-25.3 ... +48.9 °C
Resolution	0.1 °C

Wet Bulb Temperature

Measuring range	-21.6 ... +50 °C
Resolution	0.1 °C

General Technical Specifications

WBGT formula	Inside /outdoors and no sun: WBGT= (0.7 x WB) + (0.3 x TG) Outdoors and sun: WBGT=(0.7 x WB) + (0.2 x TG) + (0.1 x TA)
Data storage intervals	Automatically: every 1 ... 3600 seconds Manually: with every key press
Memory Card	SD memory card 1 ... 16 GB
Interface	RS232 / USB
Display	LCD with background lights (52 x 38 mm)
Operation Temperature	0 ... +50 °C
Environmental Humidity	<85 % R.H.
Voltage Supply	6 x 1.5 V AA batteries or 9 V Adapter
Power Consumption	DC 14 mA at standard operation DC 37 mA with data storage and without Display lights on
Weight	489 g
Dimensions	Device: 177 x 68 x 445 mm Bulb: Ø 75 mm

Delivery content

1 x PCE-WB 20 SD environmental meter
1 x SD card memory
1 x SD card reader
1 x user manual
1 x carrying case

© PCE Instruments

EXTECH SDL350

EXTECH INSTRUMENTS

Experience the Extech Advantage

PRODUCT DATASHEET

Hot Wire CFM Thermo-Anemometer/Datalogger

Records data on an SD card in Excel® format
For easy transfer to a PC for analysis



Features:

- Air Velocity/Air Flow meter with telescoping probe designed to fit into HVAC ducts and other small openings
- Datalogger date/time stamps and stores readings on an SD card in Excel® format for easy transfer to a PC
- Probe extends up to 7.05ft (215cm) maximum length with cable
- Adjustable data sampling rate: 1 to 3600 seconds
- Stores 99 readings manually and 20M readings via SD card included
- Type K/J Thermocouple input for high temperature measurements
- Large (9999 count) LCD displays Air Velocity or Air Flow and Temperature simultaneously
- Record/Recall MIN, MAX readings
- Data Hold plus Auto power off with disable function
- Complete with 6 x AA batteries, SD card, 3.1ft (95cm) fully extended telescoping probe with 3.9ft (120cm) cable, and hard carrying case

Specifications	Range	Resolution	Basic Accuracy
Air Velocity			
m/s	0.2 to 25m/s	0.01 m/s	±5%rdg
ft/min	40 to 3940ft/min	1ft/min	±5%rdg
MPH	0.5 to 45MPH	0.01MPH	±5%rdg
knots	1 to 31knots	0.01knots	±5%rdg
km/h	0.7 to 72km/h	0.01km/h	±5%rdg
CFM (feet³/min)	0 to 1,907,000 CFM	0.001 to 100 CFM	
CMM (meter³/min)	0 to 54,000 CMM	0.001 to 1 CMM	
Temperature	32 to 122°F (0 to 50°C)	0.1°	±1.5°F (±0.8°C)
Type K Temperature	-148 to 2372°F (-100 to 1300°C)	0.1°	±(0.4% + 1.8°F/1°C)
Type J Temperature	-148 to 2192°F (-100 to 1200°C)	0.1°	±(0.4% + 1.8°F/1°C)
Memory	20 Million data records using 2G SD card		
Dimensions	7.2 x 2.9 x 1.9" (182 x 73 x 47.5mm)		
Weight	23.1oz (655g)		

Ordering Information:

SDL350 .....Hot Wire CFM Thermo-Anemometer
SDL350-NIST .....SDL350 with Certificate Traceable to NIST

872502 .....Type J Bead Wire Probe (-328 to 392°F/-200 to 200°C)
TP870 .....Type K Bead Wire Probe (-40 to 482°F/-40 to 250°C)
TP200 .....Type K Clamp Probe (-4 to 200°F/-20 to 93°F)
TP400 .....Type K Clamp Probe (-4 to 450°F/-20 to 232°C)
153117 .....117V AC Adaptor
UA100-240 .....100-240V AC Adaptor with 4 plugs (US, EU, UK, AU)

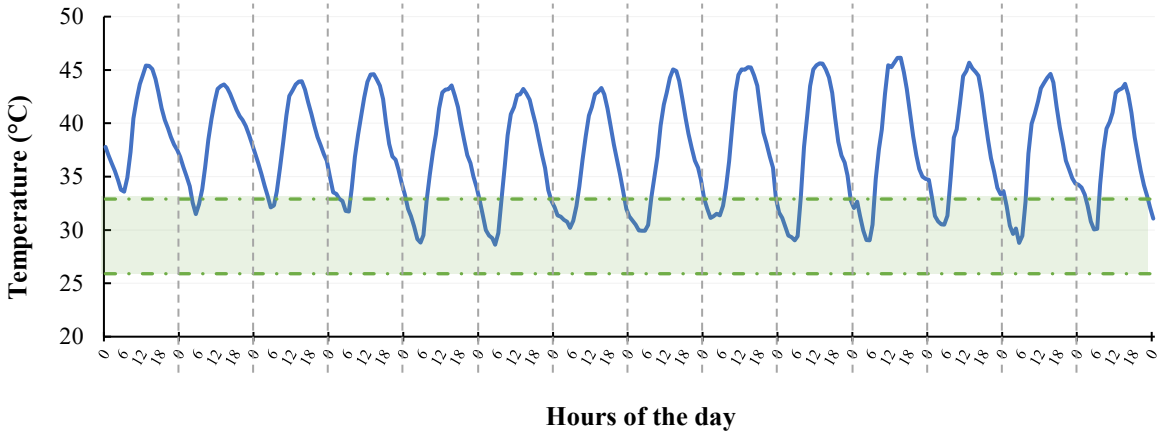
CE 3 YEAR WARRANTY

www.extech.com

Specifications subject to change without notice.
Copyright © 2010-2016 FLIR Systems, Inc. All rights reserved including the right of reproduction in whole or in part in any form.

8/22/16 - R1

A-C: Hourly Tout in relation to comfort identified limits



A-D: Example of hourly air temperature measurements

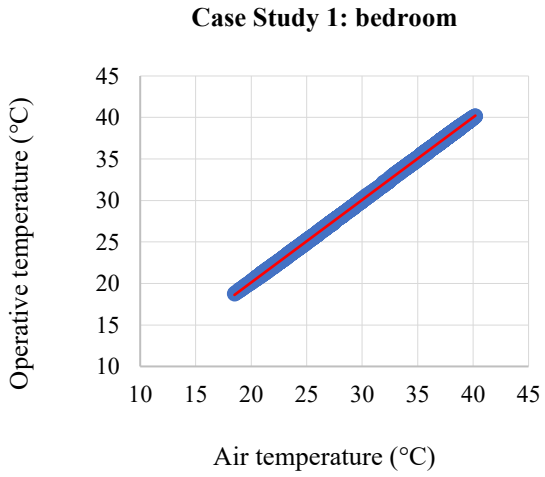
	3D-printed house (Case Study 1)			Conventional house (Case Study 2)	
Hour	**Bedroom**	**Living room**	**Dining room**	**Room 1**	**Room 2**
00:00	40.49	40.08	40.06	41.08	43.08
01:00	40.39	39.97	39.98	41.07	42.99
02:00	40.26	39.84	39.87	41.03	42.89
03:00	40.10	37.67	39.72	40.98	42.77
04:00	39.94	39.48	39.55	40.93	42.64
05:00	39.77	39.28	39.35	40.86	42.52
06:00	39.60	39.12	39.19	40.79	42.38
07:00	39.52	39.09	39.15	40.74	42.26
08:00	39.57	39.22	39.22	40.69	42.16
09:00	39.67	39.41	39.36	40.68	42.08
10:00	39.75	39.58	39.47	40.67	42.06
11:00	39.87	39.79	39.63	40.67	42.08
12:00	40.01	40.00	39.80	40.68	42.16
13:00	40.15	40.18	39.98	40.74	42.29
14:00	40.24	40.27	40.13	40.79	42.42
15:00	40.24	40.24	40.17	40.81	42.53
16:00	40.22	40.18	40.16	40.83	42.61
17:00	40.18	40.09	40.10	40.84	42.67
18:00	40.14	40.00	40.03	40.85	42.70
19:00	40.12	39.93	39.96	40.85	42.72
20:00	40.12	39.90	39.92	40.86	42.72
21:00	40.12	39.86	39.86	40.85	42.69
22:00	40.09	39.79	39.77	40.83	42.65
23:00	40.05	39.71	39.67	40.81	42.59
24:00	39.98	39.61	39.59	40.77	42.52
Max	40.49	40.27	40.17	41.08	43.08
Min	39.52	39.09	39.15	40.67	42.06
Mean	40.02	39.77	39.75	40.83	42.53
RNG	0.97	1.18	1.02	0.42	1.02
SD	0.26	0.35	0.32	0.12	0.29

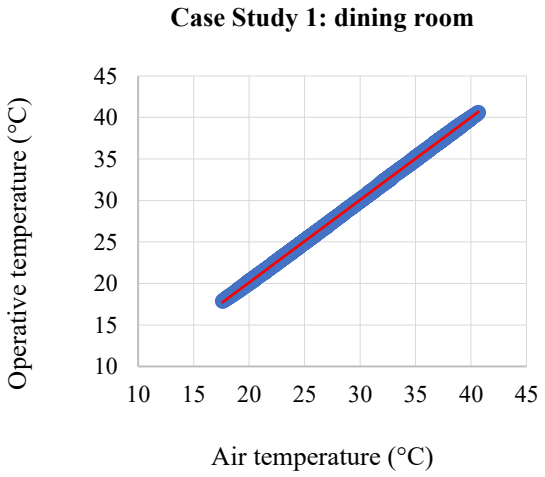
Note: presented data are calculated from sub-hourly measurements.

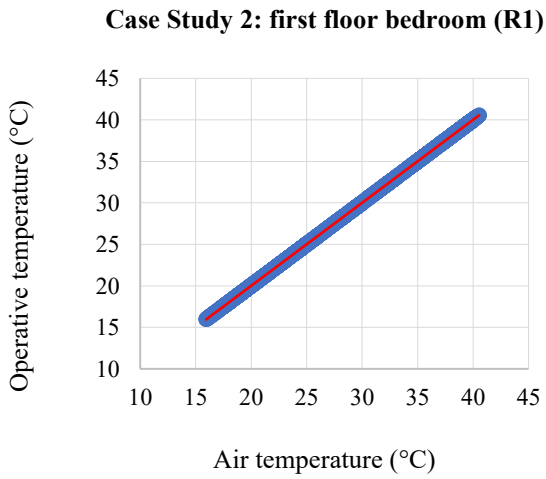
Appendix B

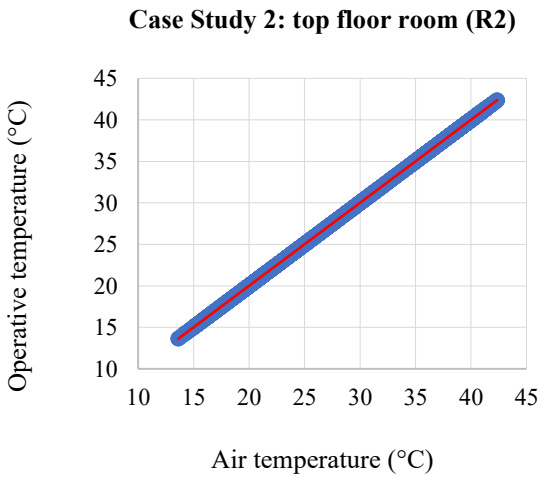
B-A: Correlation between Ta and To in tested rooms

Note that the X-axis shows indoor air temperature predictions (Ta) in °C, while the Y-axis shows operative temperature results (To) in °C. The results are presented for the entire year and for selected rooms in both houses.









B-B: Summary of indoor air temperature predictions for selected zones in both case studies in Riyadh

Hourly Ta predictions for a typical summer day:

	12 August	3D-printed house (Case 1)		Conventional house (Case 2)	
Hour	**Tout**	**Bedroom**	**Dining room**	**Room 1**	**Room 2**
00:00	35	39.36	39.43	40.03	41.77
01:00	33.5	39.22	39.26	39.96	41.62
02:00	32	39.13	39.13	39.91	41.46
03:00	34	39.06	39.04	39.86	41.3
04:00	32.2	38.88	38.85	39.76	41.08
05:00	30	38.72	38.65	39.66	40.86
06:00	29	38.63	38.54	39.6	40.67
07:00	28.6	38.67	38.59	39.59	40.53
08:00	32	38.85	38.82	39.63	40.46
09:00	36	39.14	39.13	39.72	40.48
10:00	40.8	39.43	39.44	39.82	40.57
11:00	41	39.6	39.64	39.82	40.64
12:00	42	39.78	39.79	39.91	40.85
13:00	42.2	39.93	40.01	40.16	41.26
14:00	43	40.08	40.34	40.44	41.71
15:00	44	40.18	40.58	40.54	41.98
16:00	43.7	40.21	40.66	40.55	42.19
17:00	43	40.18	40.56	40.42	42.26
18:00	43	40.14	40.4	40.39	42.3
19:00	41.9	40.06	40.26	40.4	42.35
20:00	40	39.96	40.13	40.4	42.36
21:00	39	39.87	40.01	40.39	42.33
22:00	37.6	39.75	39.87	40.35	42.26
23:00	36	39.63	39.71	40.3	42.15
Max	44.00	40.21	40.66	40.55	42.36
Min	28.60	38.63	38.54	39.59	40.46
Mean	37.48	39.52	39.62	40.07	41.48
RNG	15.40	1.58	2.12	0.96	1.90
SD	5.11	0.54	0.68	0.33	0.71

Hourly Ta predictions for a typical winter day:

	31 January	3D-printed house (Case 1)		Conventional house (Case 2)	
Hour	**Tout**	**Bedroom**	**Dining room**	**Room 1**	**Room 2**
00:00	6	19.26	18.37	16.5	14.93
01:00	4.9	19.14	18.27	16.44	14.79
02:00	5	19.04	18.18	16.38	14.64
03:00	4	18.89	18.05	16.29	14.46
04:00	3.1	18.76	17.93	16.21	14.28
05:00	3	18.64	17.82	16.12	14.09
06:00	2	18.5	17.69	16.04	13.89
07:00	0.9	18.56	17.62	15.99	13.74
08:00	1	18.97	17.69	15.99	13.64
09:00	4	19.46	17.95	16.03	13.61
10:00	9.6	19.94	18.28	16.09	13.64
11:00	12	20.32	18.52	16.18	13.79
12:00	12	20.67	18.72	16.39	14.18
13:00	13.5	20.98	19	16.49	14.77
14:00	15	21.11	19.39	16.4	15.3
15:00	16	21.07	19.7	16.42	15.64
16:00	17.3	20.86	19.77	16.45	15.66
17:00	16	20.62	19.63	16.47	15.68
18:00	15	20.46	19.5	16.5	15.82
19:00	11.9	20.3	19.37	16.49	15.93
20:00	10.8	20.2	19.28	16.49	15.98
21:00	9.8	20.09	19.19	16.47	15.96
22:00	8.5	19.98	19.08	16.44	15.89
23:00	7.5	19.87	18.99	16.4	15.78
Max	17.30	21.11	19.77	16.50	15.98
Min	0.90	18.50	17.62	15.99	13.61
Mean	8.70	19.82	18.67	16.32	14.84
RNG	16.40	2.61	2.15	0.51	2.37
SD	5.24	0.86	0.72	0.18	0.89

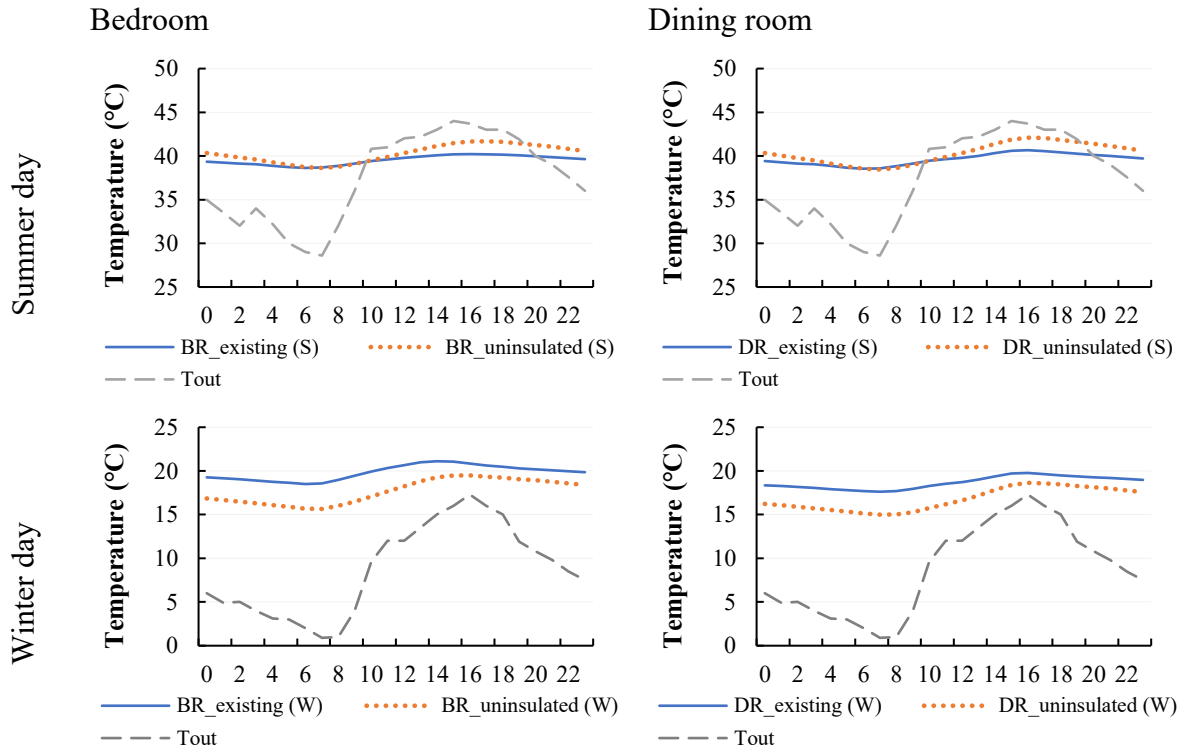
Note:

- *Results are shown under current conditions of each house (baseline models).*
- *RNG in tables above = Max – Min.*

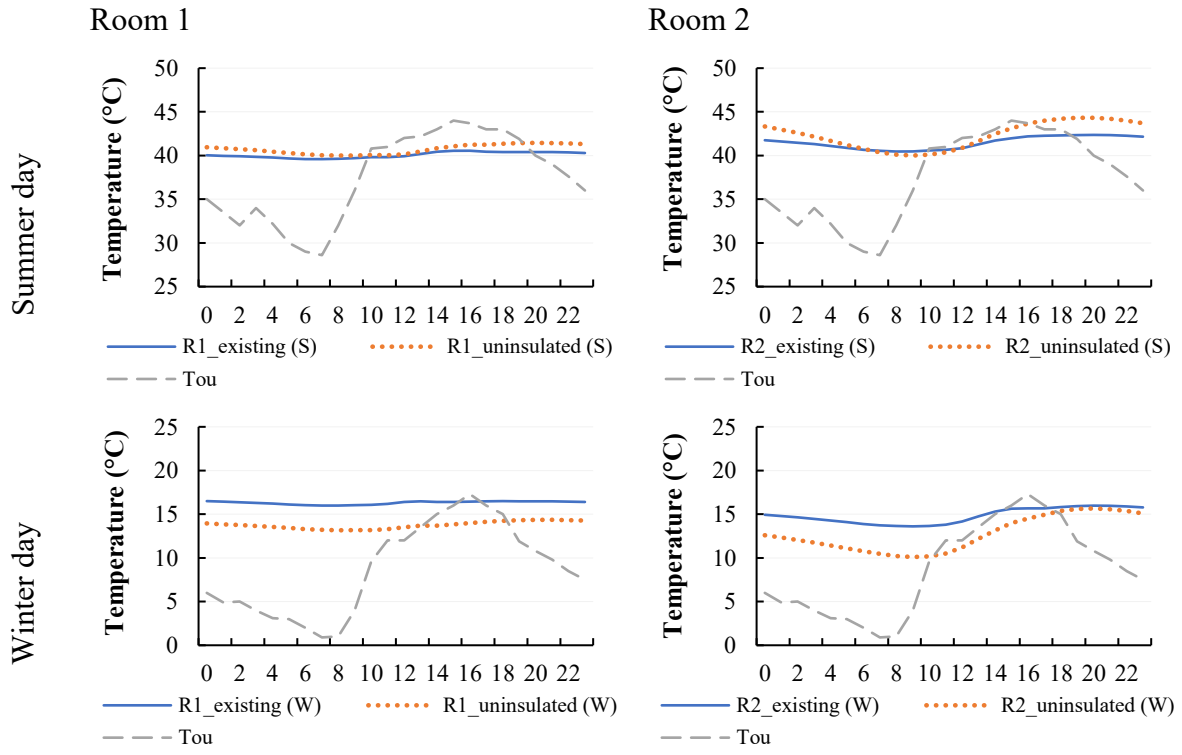
B-C: A comparison between existing construction and uninsulated models

Ta predictions with and without current thermal insulation in relation to Tout:

- **Case 1 (3D-printed house):**

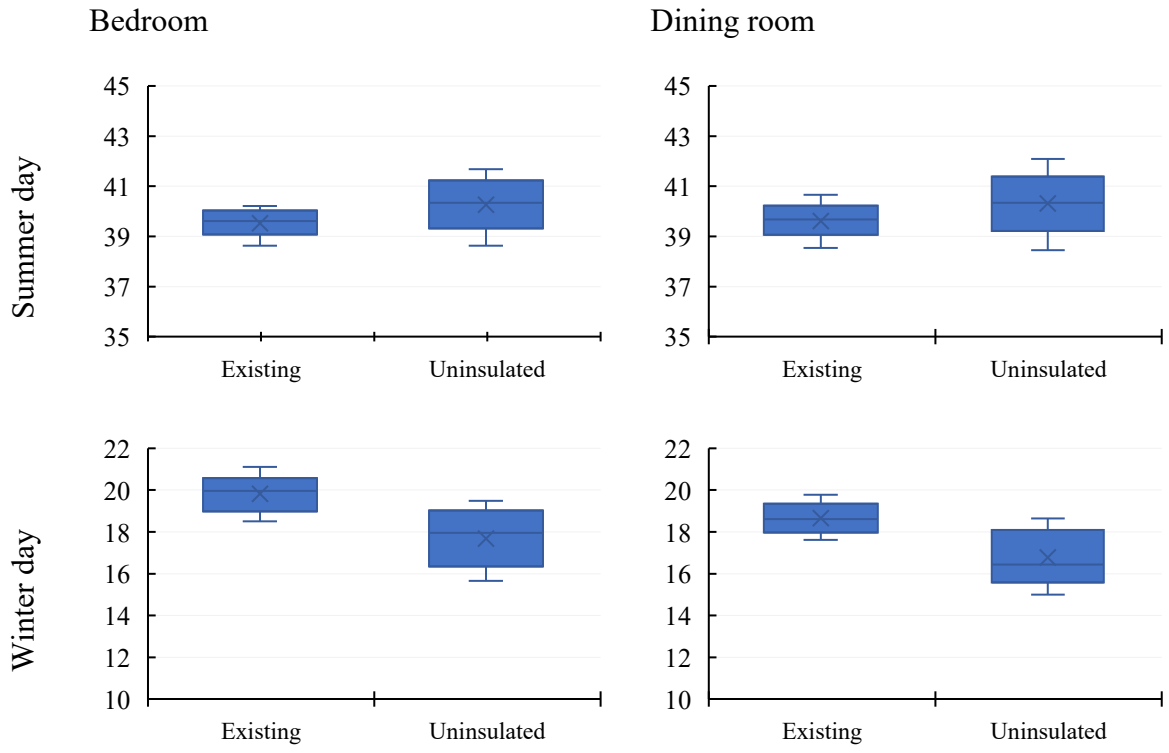


- **Case 2 (Conventional house):**

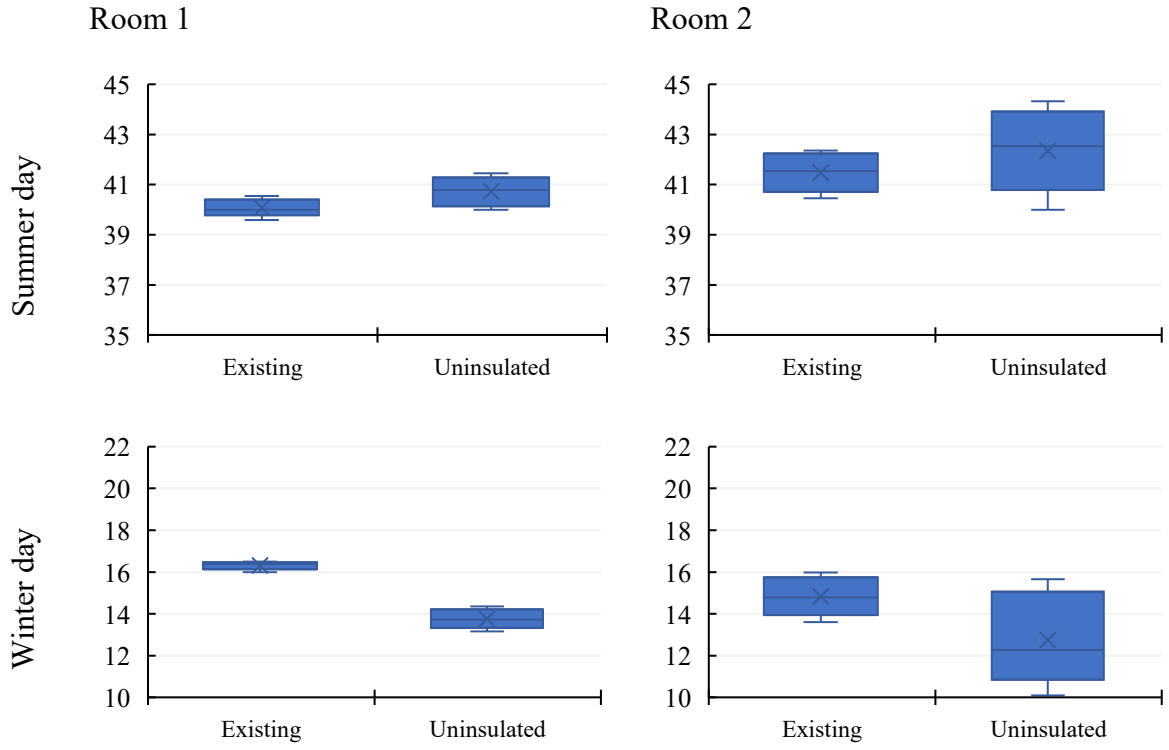


Box diagram summarizes Ta results (with current insulation and without insulation):

- **Case 1 (3D-printed house):**



- **Case 2 (Conventional house):**

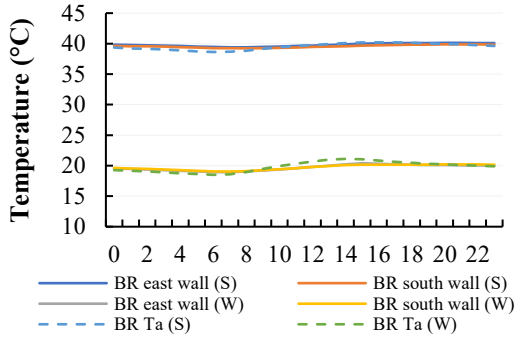


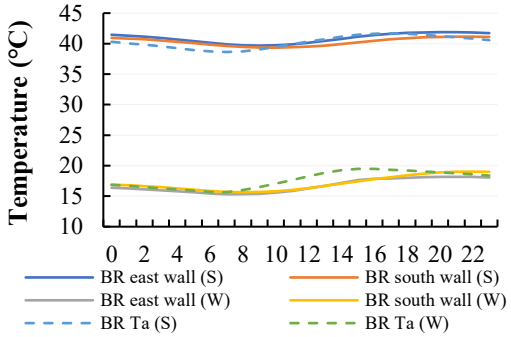
Correlation between Ta and IST for selected zones in both houses (with insulation and without insulation) for a typical summer day (S) and a typical winter day (W):

- **Case 1 (3D-printed house):**

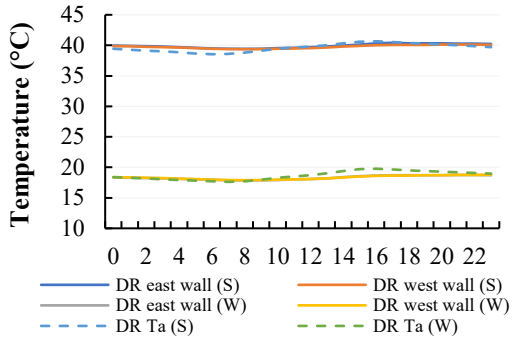
Existing construction | Uninsulated model

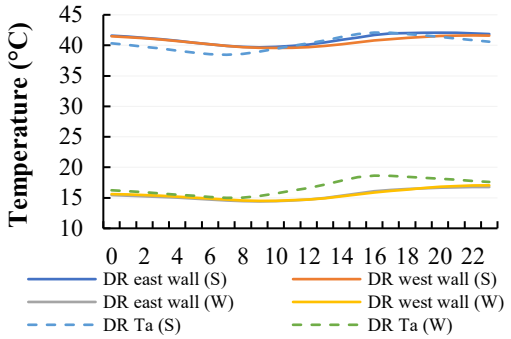
South-facing bedroom





West-facing dining room

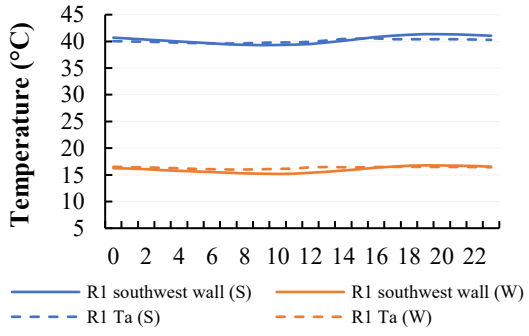


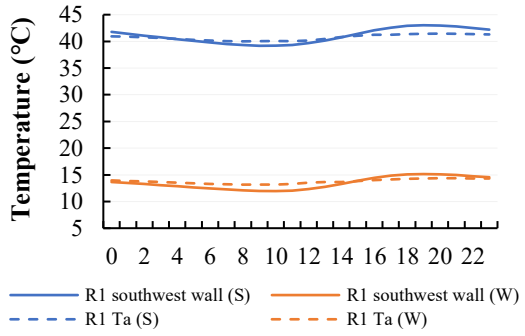


- **Case 2 (conventional house):**

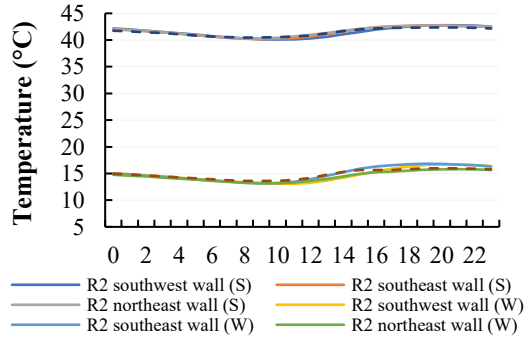
Existing construction | Uninsulated model

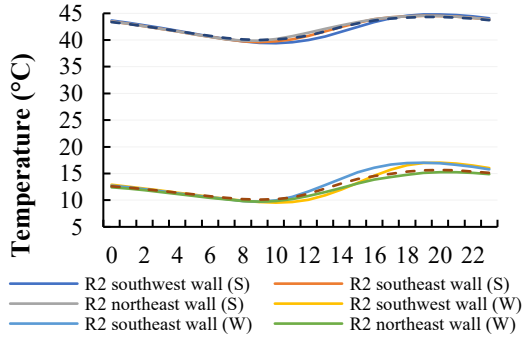
First-floor bedroom (R1)



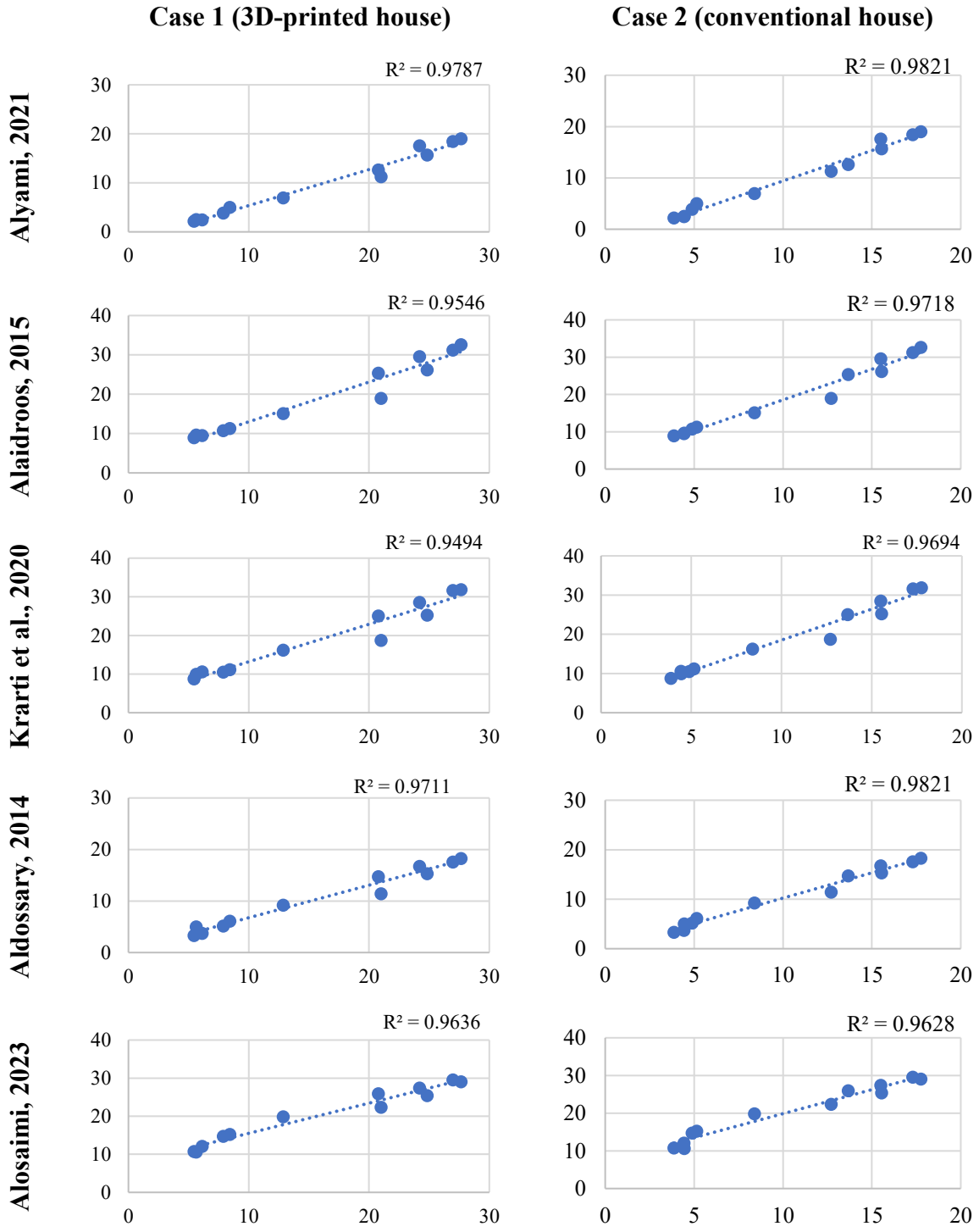


Top-floor room (R2)





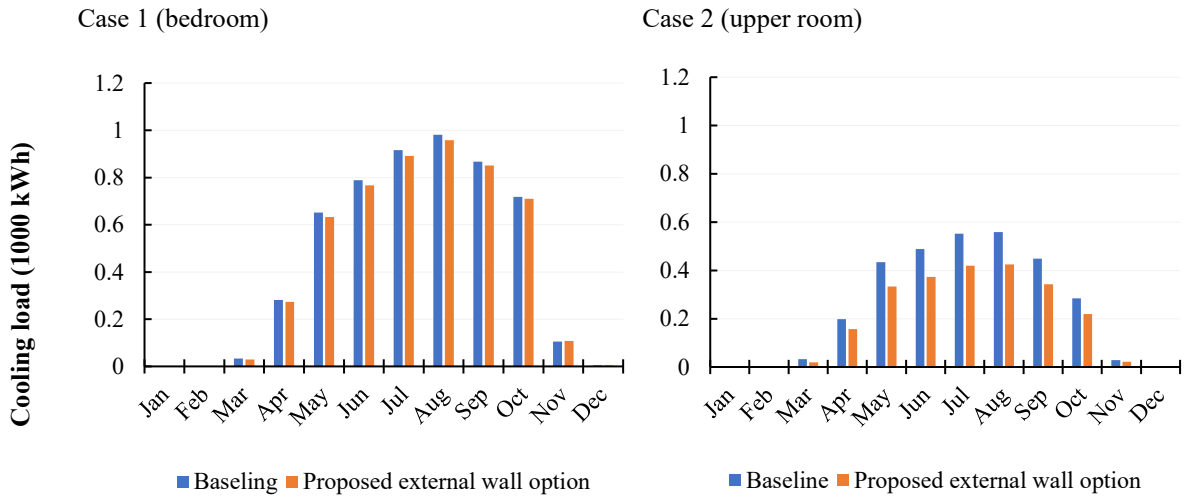
B-D: A comparison between predicted energy consumptions (EUI) and consumption reported consumptions in relevant literature



Appendix C

C-A: External wall options

Cooling load results for selected rooms in both houses with the proposed external wall options:



Comparison of monthly cooling load between the baseline model and the proposed external wall option with outside insulation for each house

Summary of total load for tested room in Case 1 (bedroom) with various external wall options

		Baseline	Proposed inside insulation	Proposed outside insulation
Cooling load	kWh	5,347	5,248	5,225
	kWh/m^2	305.9	300.2	298.9
Heating load	kWh	4.7	6.4	2.2
	kWh/m^2	0.26	0.36	0.12

Note: tested room area is 17.48m^2

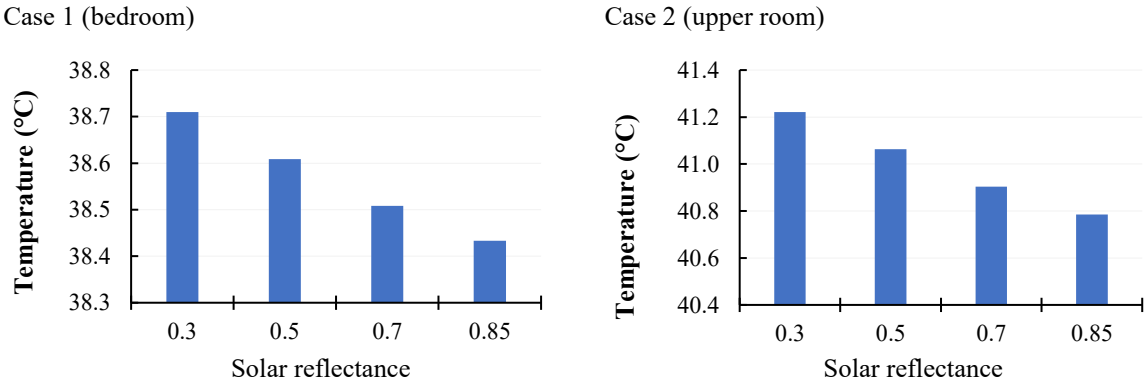
Summary of total load for tested room in Case 2 (upper room) with various external wall options

		Baseline	Proposed inside insulation	Proposed outside insulation
Cooling load	kWh	3,024	2,316	2,309
	kWh/m^2	136.6	104.6	104.3
Heating load	kWh	172.2	110.3	99.4
	kWh/m^2	7.7	4.9	4.4

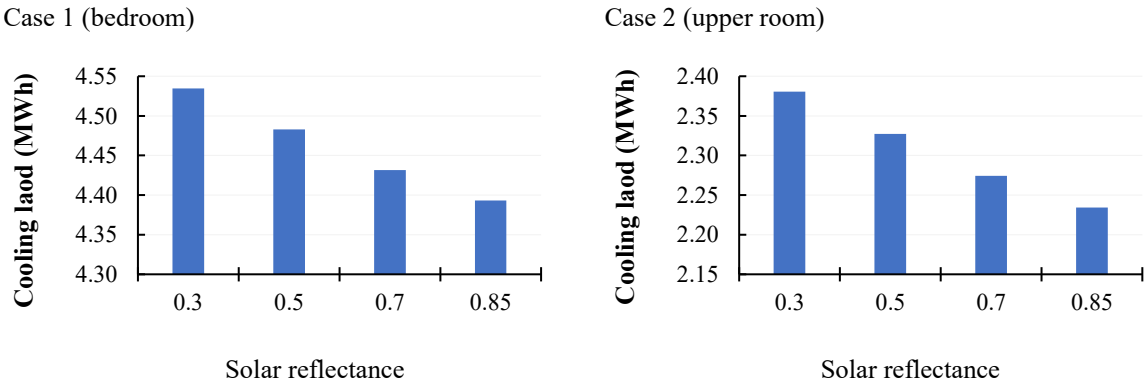
Note: tested room area is 22.14 m^2

C-B: Roof options

The impact of varying roof solar reflectance while maintaining the same U-value of the proposed SBC roof type for both houses:



Mean Ta predictions for the selected rooms with different solar reflectance values of the SBC roof type



Room's annual load with different solar reflectance values of the SBC roof type

Summary of total load for tested room in Case 1 (bedroom) with various proposed roof options

		Baseline	SBC roof (R1-2)	SBC + reflective (R1-3)
Cooling load	kWh	5,347	4,534	4,393
	kWh/m^2	305.9	259.4	251.3
Heating load	kWh	4.7	0	0
	kWh/m^2	0.26	0	0

Room area: 17.48 m^2

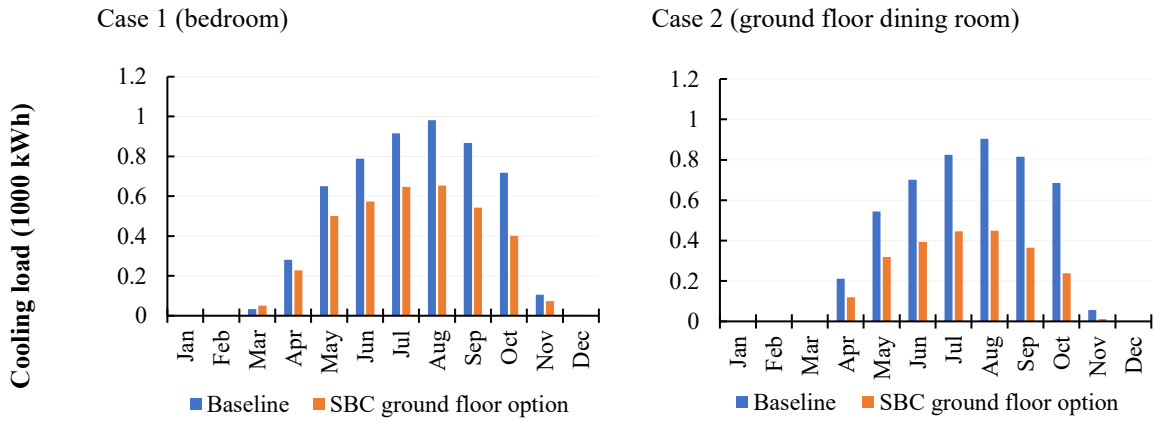
Summary of total annual load for tested room in Case 2 (upper room) with various proposed roof options

		Baseline	SBC roof (R2-2)	SBC + reflective (R2-3)
Cooling load	kWh	3,024	2,380	2,234
	kWh/m^2	136.6	107.5	100.9
Heating load	kWh	172.2	104.2	122.2
	kWh/m^2	7.7	4.7	5.5

Room area: 22.14 m^2

C-C: Ground floor options

The impact of applying SBC ground floor insulation requirements for both houses:



Monthly cooling load with and without SBC ground floor insulation

Summary of total load for tested room in Case 1 (bedroom) with and without proposed SBC ground floor insulation

		Baseline	SBC ground floor insulation	Reduction (−) / increase (+)
Cooling load	kWh	5,347	3,671	−1,676
	kWh/m^2	305.9	210	−95.9
Heating load	kWh	4.7	73.3	+68.5
	kWh/m^2	0.26	4.1	+3.8

Room area: 17.48 m^2

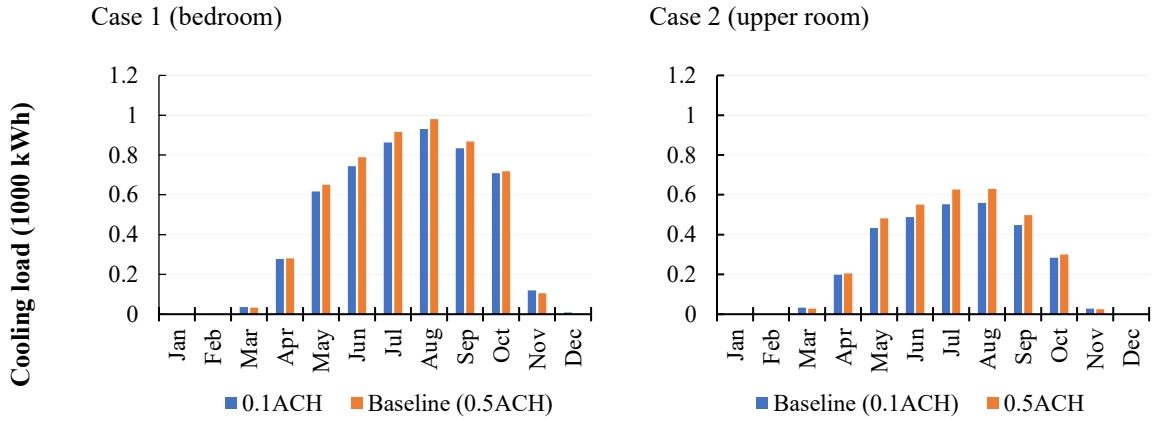
Summary of total load for tested room in Case 2 (ground floor dining room) with and without proposed SBC ground floor insulation

		Baseline	SBC ground floor insulation	Reduction (−) / increase (+)
Cooling load	kWh	4,743	2,343	−2,400
	kWh/m^2	257	127	−130
Heating load	kWh	0	94.4	+94.4
	kWh/m^2	0	5.1	+5.1

Room area: 18.45 m^2

C-D: Air infiltration

The impact of changing infiltration rates (from 0.5 ACH in Case 1's baseline model to 0.1 ACH and from 0.1 ACH in Case 2's baseline model to 0.5 ACH)



Monthly cooling load with various infiltration rates

Summary of total load for tested room in Case 1 (bedroom) with various infiltration rates

	Infiltration rate	1.0 (ACH)	Baseline: 0.5 (ACH)	0.1 (ACH)
Cooling load	kWh	5,622	5,347	5,138
	kWh/m^2	321.6	305.9	293.9
Heating load	kWh	17.5	4.7	0.4
	kWh/m^2	1.0	0.26	0.02

Room area: 17.48 m^2

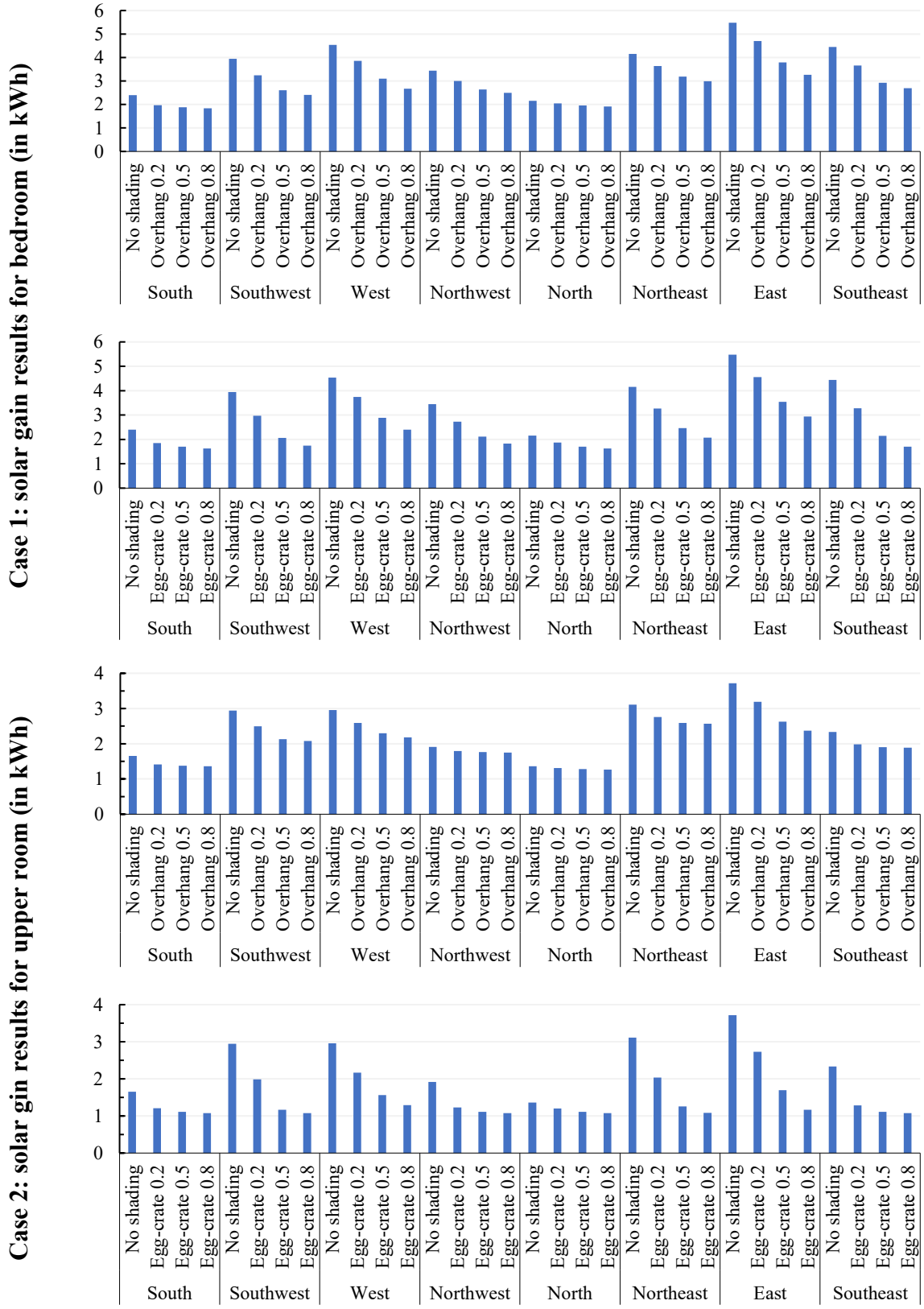
Summary of total load for tested room in Case 2 (upper room) with various infiltration rates

	Infiltration rate	1.0 (ACH)	0.5 (ACH)	Baseline: 0.1 (ACH)
Cooling load	kWh	3,757	3,347	3,025
	kWh/m^2	169.7	151.16	136.6
Heating load	kWh	393.5	268.1	172.2
	kWh/m^2	17.7	12.1	7.7

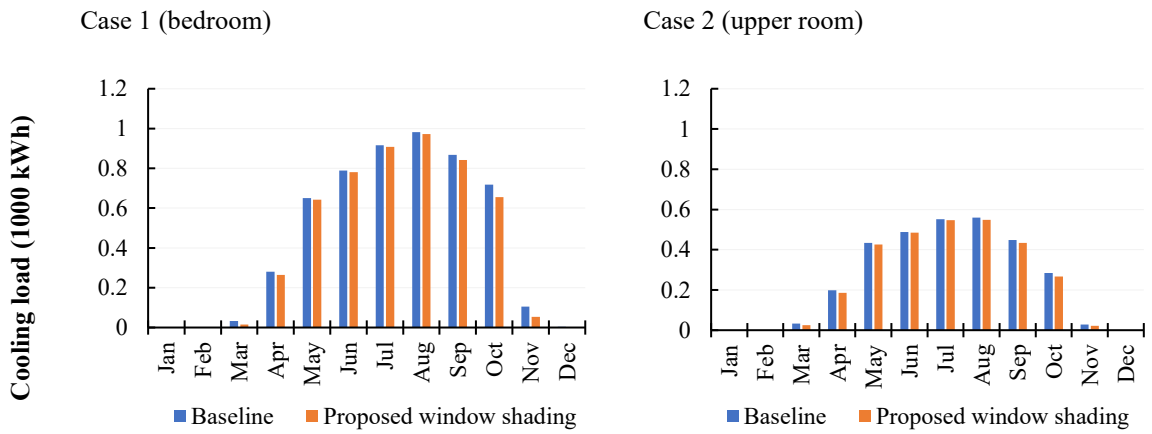
Room area: 22.14 m^2

C-E: External shading analysis

Solar gain results for a typical summer day after applying external shading devices (overhang & eggcrate shadings) with various projection factor (PF: 0.0, 0.2, 0.5, and 0.8).



- **Cooling and heating loads after applying the proposed window shading options:**



Monthly cooling load before (baseline) and after applying the proposed window shading option (W-sh 3: louvers integrated with double-tinted glazing)

Summary of total thermal loads for the tested room in Case 1 (bedroom) before and after applying the proposed (W-sh 3) window shading option (louvers: 25 cm depth and glazing with SHGC = 0.46).

		Baseline	Proposed W-sh3	Reduction (−) / Increase (+)
Cooling load	kWh	5,347.6	5,131.2	−216.4
	kWh/m^2	305.9	293.5	−12.38
Heating load	kWh	4.7	13.1	+8.4
	kWh/m^2	0.26	0.74	+0.48

Room area: 17.48 m^2

Summary of total thermal loads for the tested room in Case 2 (upper room) before and after applying the proposed (W-sh 3) window shading option (louvers: 25 cm depth and glazing with SHGC = 0.46).

		Baseline	Proposed W-sh3	Reduction (−) / Increase (+)
Cooling load	kWh	3,024.6	2,938.4	−86.2
	kWh/m^2	136.6	132.7	−3.89
Heating load	kWh	172.2	203.0	+30.8
	kWh/m^2	7.7	9.1	+1.4

Room area: 22.14 m^2

Note: during this analysis, selected shading type was applied to all windows, but results were only showed for selected rooms for demonstration purposes.

C-F: Summary of tested improvement measures of the building fabric components

- **Case 1: 3D-printed house (bedroom)**

Variables	Descriptions	Season / Parameter	Typical summer day 12 Aug (Indoor air temperature (Ta))	Typical summer day 12 Aug, NV (Indoor air temperature (Ta))	Winter day 31 Jan (Indoor air temperature (Ta))	Annual overheating Hours percentage	Annual Cooling load
	Bedroom	**Baseline**	39.52°C	37.69°C	19.82°C	51.9%	5.348MWh
Walls insulation	Cavity	W1-1	-0.1%	-0.2%	1.1%	**51.8%**	**-2.3%**
	Inn	W1-2	0.2%	0.4%	0.7%	52.4%	-1.9%
	Out	W1-3	**-0.3%**	**-0.3%**	**2.7%**	**51.8%**	**-2.3%**
Roof options	SBC	R1-2	-2.0%	-2.0%	**10.4%**	50.7%	-15.2%
	SBC + reflective	R1-3	**-2.7%**	**-2.5%**	9.5%	**50.5%**	**-17.8%**
Ground floor	Uninsulated	GF1-1	**0.0%**	**0.0%**	**0.0%**	51.9%	0.0%
	SBC insulation	GF1-2	4.4%	0.8%	-16.2%	**50.8%**	**-31.3%**
Infiltration	Reduced	0.1ACH	0.3%	**-0.08%**	**4.3%**	52.0%	**-3.9%**
	Existing	0.5ACH	0.0%	0.00%	0.0%	51.9%	0.0%
	Increased	1.0ACH	**-0.4%**	0.09%	-4.6%	**51.8%**	5.1%
Window shading and glazing	Louvers + single clear	W-sh-1	0.1%	0.3%	-6.3%	51.6%	1.0%
	Louvers + double clear	W-sh-2	0.0%	0.0%	-4.3%	51.5%	-2.3%
	Louvers + double tented	W-sh-3	**-0.3%**	**-0.2%**	-5.3%	**51.3%**	**-4.0%**

- **Case 2: conventionally constructed house (upper room and ground floor dining room)**

Variables	Descriptions	Season / Parameter	Typical summer day 12 Aug (Indoor air temperature (Ta))	Typical summer day 12 Aug, NV (Indoor air temperature (Ta))	Winter day 31 Jan (Indoor air temperature (Ta))	Annual overheating Hours percentage	Annual Cooling load
	Upper room (R2)	**Baseline**	41.48°C	39.17°C	14.84°C	52.1%	3.025MWh
Walls insulation	Cavity	W2-1	-0.4%	-1.21%	7.8%	**51.5%**	**-23.7%**
	Inn	W2-2	-0.1%	-0.7%	6.2%	52.0%	-23.4%
	Out	W2-3	**-0.6%**	**-1.30%**	**10.1%**	**51.5%**	**-23.7%**
Roof options	SBC	R2-2	-0.6%	-1.1%	**9.3%**	51.7%	-21.3%
	SBC + reflective	R2-3	**-1.7%**	**-1.8%**	7.5%	**51.1%**	**-26.1%**
Ground floor: dining room	Uninsulated (baseline)	GF2-1	**38.81°C**	36.64°C	**20.23°C**	49.8%	4.743MWh
	SBC insulation	GF2-2	4.3%	**-0.2%**	-21.2%	**46.8%**	**-50.6%**
Infiltration	Existing	0.1ACH	0.0%	0.0%	**0.0%**	52.1%	**0.0%**
	Increased	0.5ACH	-1.2%	-0.2%	-7.7%	51.9%	10.7%
	Increased	1.0ACH	**-2.4%**	**-0.4%**	-14.4%	**51.7%**	24.2%
Window shading and glazing	Louvers + single clear	W-sh-1	0.4%	0.6%	-4.1%	52.3%	7.6%
	Louvers + double clear	W-sh-2	0.4%	0.2%	-0.4%	52.1%	0.6%
	Louvers + double tented	W-sh-3	**-0.6%**	**-0.4%**	-2.5%	**51.5%**	**-2.8%**

Note: bold figures indicate the best performance.

Improvement in performance Worsening in performance

Appendix D

D-A: Air temperature results (baseline versus improved building fabric)

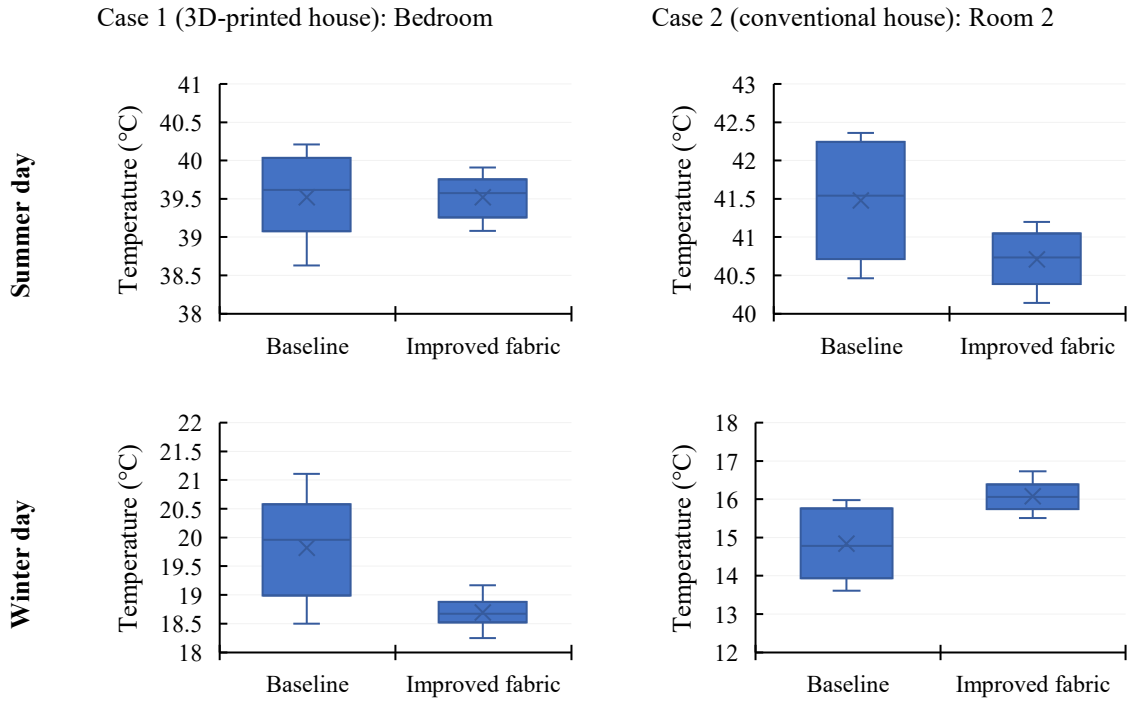
Comparison of indoor temperatures before and after applying fabric improvement measures

Air temperature results (in °C) for a typical summer day (12 August)

		Max	Min	Mean	RNG	SD
Case 1 (3D-printed house): Bedroom	Baseline	40.21	38.63	39.52	1.58	0.54
	Improved fabric	39.91	39.08	39.52	0.83	0.28
Case 2 (conventional house): Room-2	Baseline	42.36	40.46	41.48	1.9	0.71
	Improved fabric	41.20	40.14	40.71	1.06	0.36

Air temperature results (in °C) for a typical winter day (31 January)

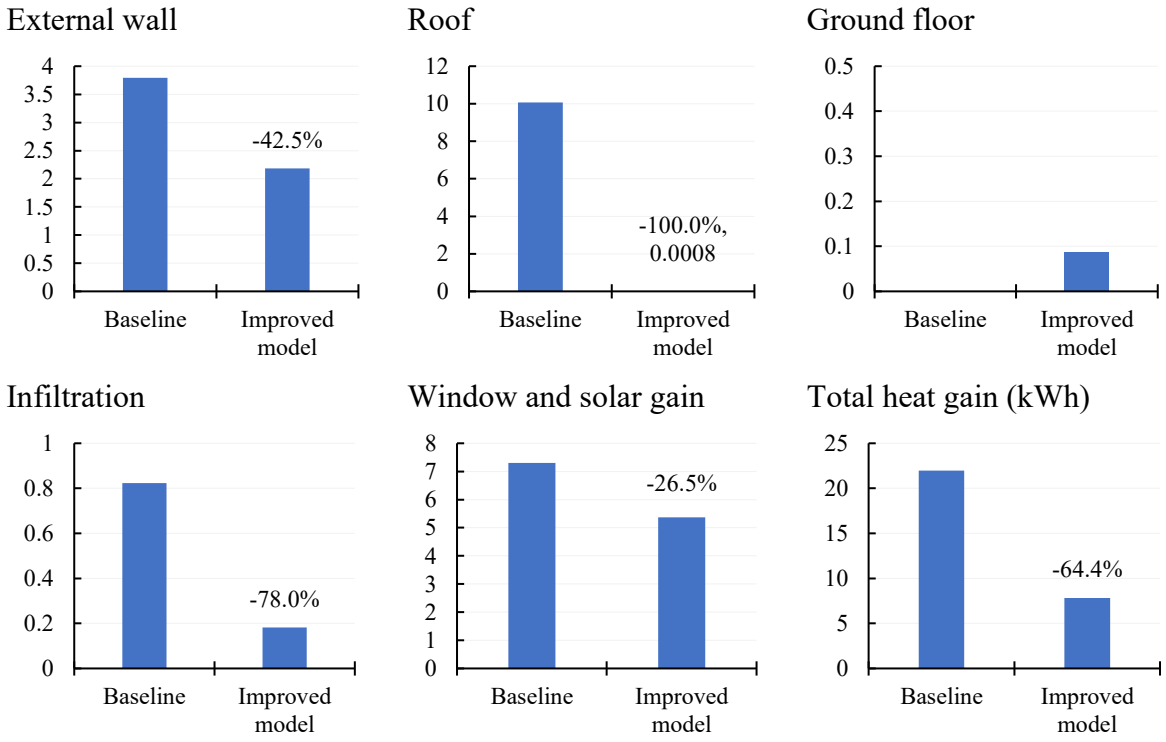
		Max	Min	Mean	RNG	SD
Case 1 (3D-printed house): Bedroom	Baseline	21.11	18.50	19.82	2.61	0.86
	Improved fabric	19.17	18.25	18.69	0.92	0.26
Case 2 (conventional house): Room-2	Baseline	15.98	13.61	14.84	2.37	0.89
	Improved fabric	16.73	15.51	16.07	1.22	0.38



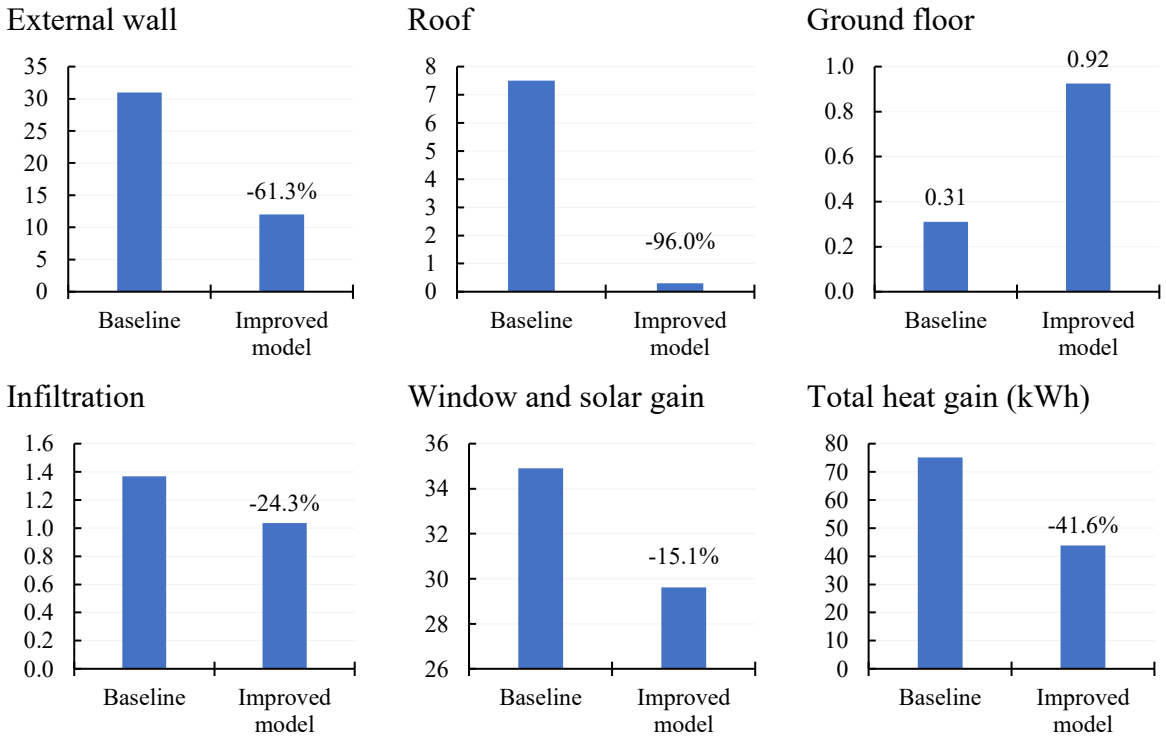
Graphical comparison of indoor temperatures before (baseline) and after applying building fabric improvement measures

D-B: Heat gain analysis: Improved models VS Baselines

- **Total external heat gain results for Case 1 (3D-printed house)**



- **Total external heat gain results for Case 2 (conventional house)**

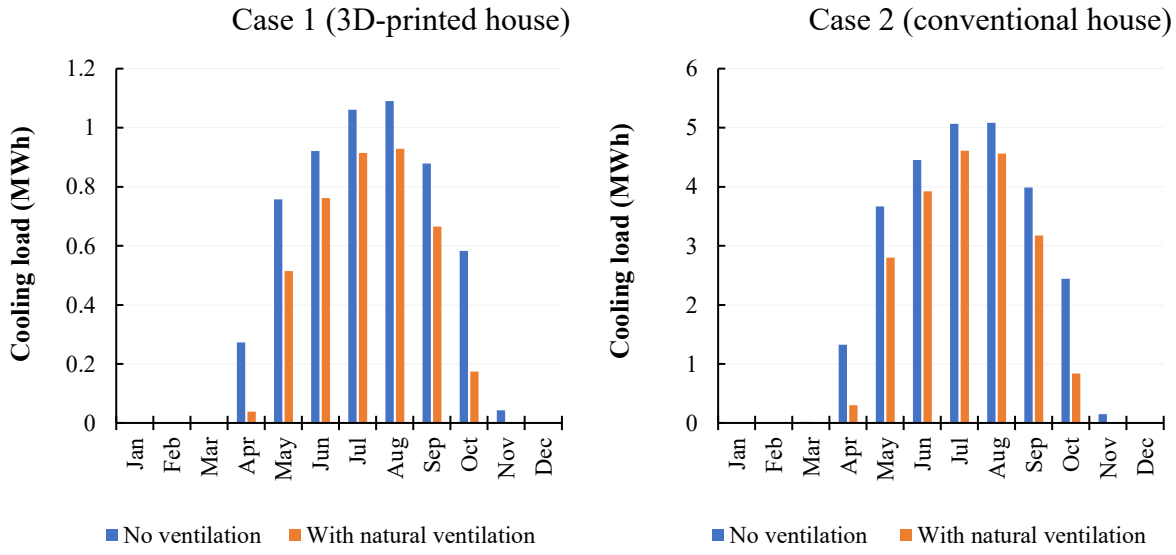


Total heat gain (+) and heat loss (−) results for Case 1 and Case 2 before and after applying proposed alternatives. Results are shown for a typical summer and a winter day (in kWh).

		External walls		Roof		Ground		Infiltration		Window/solar	
	(kWh)	Gain	Loss	Gain	Loss	Gain	Loss	Gain	Loss	Gain	Loss
Case 1 (3D-printed house)	▪ **Summer day**										
	Baseline	3.79	−2.46	10.06	−0.28	0	−14.65	0.82	−2.46	7.30	−1.55
	Improved	2.18	−1.39	0	−2.15	0.08	−2.06	0.18	−0.49	5.36	−1.59
	▪ **Winter day**										
	Baseline	0.23	−11.55	0	−18.24	33.36	−0.2	0	−8.29	11.01	−4.23
	Improved	0.76	−2.98	0.02	−2.09	6.06	−0.2	0	−1.5	3.82	−4.10
Case 2 (conventional house)	▪ **Summer day**										
	Baseline	30.99	−12.68	7.50	−1.91	0.31	−35.79	1.37	−4.27	34.90	−11.37
	Improved	11.99	−6.56	0.30	−7.52	0.92	−9.01	1.04	−4.59	29.62	−10.58
	▪ **Winter day**										
	Baseline	3.77	−62.60	0.52	−21.12	91.81	−6.58	0.13	−11.08	23.42	−24.12
	Improved	1.10	−22.02	3.55	−1.28	19.53	−2.21	0.02	−10.26	16.37	−20.64

D-C: Monthly cooling load

Total monthly cooling load predictions for the improved building fabric models before and after applying the proposed mixed-ventilation mode.



Note that most cooling savings were achieved during the moderate months (i.e., April and October).

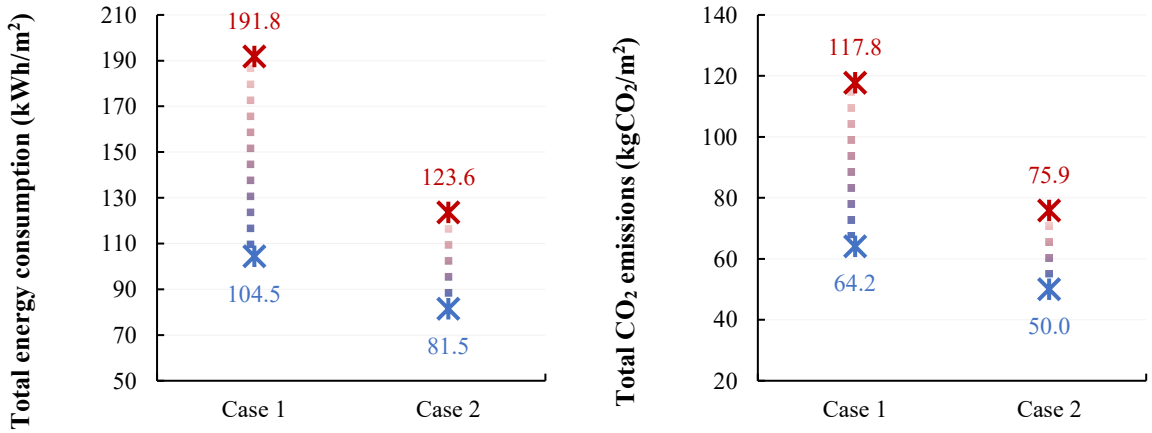
Total monthly cooling load by parameter for the selected cases in Riyadh in kWh/m^2

	Month	1	2	3	4	5	6	7	8	9	10	11	12	AV	SD
Case Study 1 (3D-printed house)	Baseline	0.00	0.00	1.08	11.99	28.32	34.32	39.87	42.63	37.08	29.49	3.07	0.07	18.99	17.73
	External walls	0.00	0.00	0.93	11.64	27.47	33.34	38.77	41.56	36.32	29.13	3.15	0.09	18.53	17.29
	Roof	0.00	0.00	0.28	8.23	21.24	27.10	32.07	34.88	31.16	26.18	3.32	0.31	15.4	14.53
	Ground floor	0.00	0.02	1.59	9.44	21.29	24.43	27.57	27.82	22.36	15.03	1.78	0.01	12.61	11.66
	Air infiltration	0.00	0.00	1.13	11.8	26.79	32.29	37.45	40.33	35.51	28.99	3.48	0.15	18.16	16.75
	Window shading	0.00	0.00	0.66	11.37	27.86	33.9	39.45	42.2	36.36	28.0	1.95	0.00	18.48	17.59
	All together	0.00	0.00	0.00	3.49	9.71	11.81	13.6	13.97	11.27	7.48	0.55	0.00	5.99	5.87
	All together + NV	0.00	0.00	0.00	0.49	6.59	9.76	11.72	11.91	8.53	2.22	0.00	0.00	4.27	5.02
Case Study 2 (conventional house)	Baseline	0.00	0.00	0.4	7.04	17.96	22.04	25.51	26.77	22.51	16.3	1.19	0.00	11.64	11.17
	External walls	0.00	0.00	0.28	6.19	15.62	19.32	22.43	23.78	20.33	15.29	1.31	0.01	10.38	9.91
	Roof	0.00	0.02	0.25	6.02	15.86	19.77	23.05	24.37	20.69	15.36	1.26	0.00	10.55	10.15
	Ground floor	0.00	0.00	0.39	5.37	13.47	15.89	17.94	17.93	14.0	8.27	0.48	0.00	7.81	7.62
	Air infiltration	0.00	0.00	0.4	7.04	17.96	22.04	25.51	26.77	22.51	16.3	1.19	0.00	11.64	11.17
	Window shading	0.00	0.00	0.29	6.83	17.83	21.99	25.45	26.65	22.32	16.05	1.05	0.00	11.54	11.14
	All together	0.00	0.00	0.04	2.99	8.27	10.06	11.43	11.47	9.0	5.51	0.34	0.00	4.93	4.87
	All together + NV	0.00	0.00	0.00	0.68	6.32	8.85	10.4	10.3	7.17	1.89	0.00	0.00	3.8	4.42

D-D: Energy consumption predictions

Predicted total annual energy consumption by parameter for the selected case study buildings in Riyadh, Saudi Arabia

	Parameter	kWh	kWh/m²	Reduction %
Case Study 1 (3D-printed house)	Baseline	14,962	191.82	–
	External wall	14,778	189.46	1.2%
	Roof	13,530	173.46	9.6%
	Ground floor	12,420	159.23	17%
	Air infiltration	14,478	185.61	3.2%
	Window shading	14,211	182.19	5.0%
	All together	9,444	121.08	36.9%
	All together + NV (**improved model**)	8,148	104.47	45.5%
Case Study 2 (conventional house)	Baseline	54,769	123.63	–
	External wall	51,735	116.78	5.5%
	Roof	52,157	117.74	4.8%
	Ground floor	46,096	104.05	15.8%
	Air infiltration	54,769	123.63	0.0%
	Window shading	54,496	123.01	0.5%
	All together	39,196	88.48	28.4%
	All together + NV (**improved model**)	36,099	81.49	34.1%



Graphical comparison of the total annual energy consumption and operational CO_2 emissions of the baseline and the improved energy models (i.e., improved building fabric + the proposed mixed-ventilation mode).



In conclusion, all praise is due to Allah, Lord of all worlds, and may peace and blessings be upon the Prophet Muhammad.